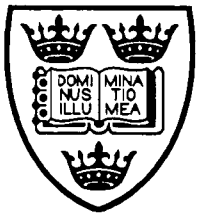
MODEL TESTING AND ANALYSIS

OF INTERACTIONS BETWEEN TUNNELS IN CLAY

by

Sang-Hwan Kim



A Thesis submitted for the degree
of Doctor of Philosophy
at the
University of Oxford

Brasenose College

Trinity Term, 1996.

ABSTRACT

Model Testing and Analysis of Interactions Between Tunnels in Clay

S.H. Kim
Brasenose College, University of Oxford

A Thesis submitted for the Degree of Doctor of Philosophy
Trinity Term 1996

This dissertation describes a study of the interaction between closely spaced tunnels during shield tunnel construction, concentrating on the study of the short-term incremental behaviour of the liner. Carefully controlled physical model tests were carried out and the test results were complemented by a limited amount of numerical analysis.

In the physical model tests described in this dissertation, two groups of tests were carried out at laboratory scale; one set of tests studied closely spaced parallel tunnels and the other set investigated perpendicular tunnels. An important feature of the study was that a novel model tunnelling machine was designed and developed as part of the research. Thin steel tubes were used to model the tunnel linings.

The experimental technique adopted in the preparation of clay samples (which is a well-established procedure) was found to produce high quality samples. Good repeatability was achieved in preparing the kaolin samples. The tunnelling machine allowed tunnel liners to be installed using similar procedures to those adopted in the construction of full scale shield tunnels using an earth pressure balance approach.

The instrumentation system used in this experimental programme are shown to produce reliable data. During the model tests measurements were made of liner strains, pore water pressures and total stresses acting on the liner. Errors in the data logging system were shown to be very small (of the order of less than 2% of peak values).

The mechanisms governing the structural interaction between closely spaced tunnels are highly complex. The tunnel installation was shown to modify the stresses acting on the liner of an adjacent tunnel. These stress increments led, in turn, to liner deformations and induced bending moments. The nature of the interaction mechanisms depends on the geometric configuration of the tunnels, the liner properties, and overconsolidation ratio.

For the parallel tunnel, the pillar width ratio (W/D) is an important parameter governing the magnitude of the interaction effects. The interaction effects increase as the pillar width ratio is reduced. Increasing the liner flexibility was found to reduce the induced bending moments but to increase the induced displacements. The interaction effects were larger in overconsolidated clay than normally consolidated clay. The worst case for interaction effects occurs when the pillar width is small, the liner is flexible and the value of OCR is large.

Three-dimensional considerations suggest that interaction between parallel tunnels may be more severe than those measured in the corresponding perpendicular tunnel tests. However, the different nature of the mechanisms in the two cases appear to be more significant than this geometric effect.

CONTENTS

ABSTRACT

CONTENTS

ACKNOWLEDGEMENTS

LIST OF SYMBOLS

1. INTRODUCTION

1.1 Introduction 1.1

1.2 Outline of the Dissertation 1.2

1.3 Objectives of the Research 1.4

2. LITERATURE REVIEW

2.1 Introduction 2.1

2.2 Tunnelling in Clay 2.1

2.2.1 Shield Tunnelling Methods 2.1

2.2.2 Heading and Face Stability 2.3

2.2.3 Displacements and Dtresses Around Tunnels 2.5

2.2.4 Liner Behaviour 2.9

2.3 Interactions Between Closely Spaced Tunnels 2.11

2.3.1 General 2.11

2.3.2 Analytical and Numerical Studies 2.12

2.3.3 Field Measurements 2.15

2.3.4 Laboratory Studies 2.18

2.4 Summary of Relevance of Previous Work to the Research Programme 2.18

3. DESIGN OF APPARATUS

3.1 Introduction 3.1

3.2 Specification of Model Tests 3.1

3.3 Test Tanks 3.3

3.3.1 Plane Strain Tank 3.4

3.3.2 Cylindrical Tank 3.5

3.3.3 Pressure System 3.6

3.4 Soil Specimens 3.7

3.4.1 Speswhite Kaolin 3.7

3.4.2 Specification of the Consolidated Sample 3.9

3.4.3 Shear Modulus of Clay 3.13

3.5 Tunnel Liners 3.17

3.6 Tunnelling Machine 3.19

3.6.1 Rotary Cutting Head 3.19

3.6.2 Water Jet System 3.20

3.6.3 Jacking Systems 3.20

3.6.4 Reference Frame 3.20

3.7 Instrumentation 3.21

3.7.1 Instrumentation Systems 3.21

3.7.2 Instrumentation on Test Tanks 3.22

3.7.3 Instrumentation on Tunnel Liners 3.23

3.7.4 Instrumentation for Tunnel Installation 3.25

3.7.5 Radial Displacement Measuring Device 3.25

3.7.6 Surface Settlement Measuring Device 3.26

3.8 Accuracy of Measurement Systems 3.26

3.8.1 Datalogger 3.27

3.8.2 Instruments 3.28

3.9 Vane Test Apparatus 3.30

4. EXPERIMENTAL PROCEDURE

4.1 Introduction 4.1

4.2 Sample Preparation 4.1

4.2.1 Preparing the Test Tanks 4.1

4.2.2 Preparation of Speswhite Kaolin Slurry 4.2

4.2.3 Consolidation of the Clay 4.3

4.2.4 Surcharge on the Samples 4.4

4.3 Model Test Procedures 4.5

4.3.1 Introduction 4.5

4.3.2 Model Tunnel Installation 4.6

4.3.3 Connection of Pore Water Pressure Transducers 4.8

4.3.4 Installation of Radial Displacement Measuring Device 4.9

4.4 Model Test 4.9

4.5 Jacking Pressure and Tunnel Advance Speed 4.11

4.6 Site Investigation on Clay Samples 4.13

4.6.1 Introduction 4.13

4.6.2 Shear Vane and Water Content Tests 4.14

4.6.3 Measured Undrained Shear Strength and Water Content 4.15

4.6.4 Theoretical Variation of Undrained Shear Strength Profile 4.16

5. RESULTS OF MODEL TESTS

5.1 Introduction 5.1

5.2 Boundary Stresses 5.1

5.3 Parallel Tunnel Model Tests 5.2

5.3.1 Introduction 5.2

5.3.2 Measurements of Single Tunnel Behaviour 5.3

5.3.3 Measurements of Interaction Between Parallel Tunnels 5.6

5.4 Perpendicular Tunnel Model Tests 5.12

5.4.1 Introduction 5.12

5.4.2 Measurements of Single Tunnel Behaviour 5.12

5.4.3 Measurements of Interaction Between Perpendicular Tunnels 5.14
5.5 Repeatability 5.18
5.6 Measurements of Total Stress, Pore Pressure and Liner Strain 5.20

6. ANALYSIS OF INTERACTIONS BETWEEN CLOSELY SPACED TUNNELS

6.1 Introduction 6.1
6.2 Application of Elastic Beam Theory 6.2
6.3 Interaction Between Parallel Tunnels 6.4
6.3.1 Radial Stresses Acting on the Liner 6.4
6.3.2 Bending Moments in the Liner 6.7
6.3.3 Liner Displacements 6.11
6.4 Interaction Between Perpendicular Tunnels 6.12
6.4.1 Radial Stresses Acting on the Liner 6.13
6.4.2 Bending Moments in the Liner 6.15
6.4.3 Liner Displacements 6.16
6.5 Comparison Between Parallel and Perpendicular Tunnel Tests 6.18
6.6 Virtual Work Analysis 6.19

7. NUMERICAL ANALYSIS AND COMPARISON WITH MODEL TESTS

7.1 Introduction 7.1
7.2 Specification of Analysis 7.2
7.2.1 Numerical Modelling 7.2
7.2.2 Specification of Parameters 7.4
7.3 Results of Back-Analyses 7.6
7.3.1 Displacements and Diameter Changes 7.7
7.3.2 Bending Moments 7.8
7.3.3 Conclusions 7.9
7.4 Additional Results 7.9

8. CONCLUDING REMARKS

8.1 Introduction 8.1

8.2 Experimental Procedures 8.1

8.2.1 Preparation of Clay Samples 8.1

8.2.2 Design of Tunnelling Machine 8.2

8.2.3 Measurement Systems 8.3

8.3 Interaction Between Tunnels 8.3

8.3.1 Parallel Tunnels 8.3

8.3.2 Perpendicular Tunnels 8.5

8.4 Mechanisms of Interaction 8.6

8.5 Practical Applications 8.7

8.6 Future Research 8.10

REFERENCES

FIGURES

ACKNOWLEDGEMENTS

I have enjoyed being a member of the Oxford Soil Mechanics Group, and I should like to express gratitude to my fellow workers in the group for their advice and encouragement.

I wish particularly to express sincere gratitude to my supervisor Dr. Harvey Burd. He has shown tremendous patience, unfailing guidance, and enthusiasm for my work. Without his unstinted help this research could not have been completed. I am also greatly indebted to my joint supervisor Dr. George Milligan for his thoughtful guidance and useful advice.

The funding for the experimental programme, provide by EPSRC is gratefully acknowledged. I am also grateful to Dong-Ah Engineering Co. Ltd. and ORS Award for their financial support.

I would like to thank Mr. CE Augarde for his valuable assistance in my finite element analysis work, and Mr. Bob Earl for his technical assistance in my experimental work.

Appreciation is extended to Prof. B.H. Kang, who is chairman of Korean Geotechnical Society, for his continuous encouragement while pursuing the research.

A very special debt of deep gratitude is offered to my parents and mother-in-law for their unceasing prayers and encouragement.

Finally I would also like to express sincere gratitude to my wife, Moon-Sook, for her tremendous prayers, encouragement and many sacrifices, and to my beloved two sons, Kiseok and Kiuk.

LIST OF SYMBOLS

γ'	submerged unit weight
γ_t	unit weight of clay
γ_w	unit weight of water.
δ_{vmax}	maximum settlement at the tunnel centre-line
δ_v	settlement at distance x from the tunnel axis
δ_g	specified gap for overcutting
$\Delta\varepsilon$	incremental liner strain
$\Delta\phi$	angle between two plane cross sections of the beam
$\Delta A/A$	over-cutting ratio
$\Delta D/D$	horizontal diameter change of tunnel
ΔM_m	maximum incremental bending moment
ΔM	incremental bending moment
Δp	change in total radial stresses
Δr	incremental radial displacement
Δu	change in pore water pressure
ε	longitudinal strain
ε_c, ε_t	compressive and tensile strain
ε_l	liner strain corresponding to long-term stresses (p_l)
κ	slope of unloading-reloading line in υ:lnp' plane
λ	slope of normal compression line in υ:lnp' plane
Λ	plastic volumetric strain ratio ($(\lambda-\kappa)/\lambda$)
ν_l, ν	Poisson's ratio of the liner and soil
σ'_{vi}	effective vertical stress at a depth z
σ_{vo}, σ'_{vo}	total and effective vertical stress
σ_i	internal pressure of the tunnel
σ_{ic}	value of σ_i at which collapse would occur.
σ_y	yield stress of steel
A	cross sectional area of tunnel
A_a	cross sectional area of the cutting head
A_t	cross sectional area of test tank
C	compressibility ratio

C/D	tunnel depth ratio
D	tunnel diameter
D_v	vane blade diameter
e_{1D}	void ratio corresponding to N_{1D}
E_l	Young's modulus of the liner
E_s	Young's modulus of the soil
F	flexibility ratio
F_a	measured jacking force during the tunnel is advanced
F_{hu}	hydrostatic suction
G	shear modulus of clay
G_s	specific gravity
H	tunnel depth
H_f	final height at the end of consolidation
H_i	initial height of saturated kaolin slurry
H_v	vane blade height
i	abscissa of the inflexion point
I	moment of inertia of the cross-section per unit length along the axis of the tunnel ($t^3/12$)
K_o	earth pressure coefficient at rest
$K_{o(nc)}$	coefficient of earth pressure for normally consolidated clay.
LF	load factor
LI	the liquidity index
$M/\gamma HR^2$	moment coefficient
M	bending moment or shape factor for Cam clay ellipse/slope of critical
M^*	bending moments created from the virtual work system
M_{max}	initial maximum bending moment
N	stability ratio
N_{1D}	location of one dimensional normal compression line in υ:ln$p$' plane
n_p	isotropic overconsolidation ratio(p'_o/p'_i)
OCR	overconsolidation ratio
p	total stresses acting on the tunnel
p_a	jacking pressure
p_{amax}	maximum jacking pressure

p_i	initial stresses corresponding to the stresses after tunnel 1 is installed
p_i, p'_i	total and effective internal pressure ($p_i=p'_i+u_o$)
PI	plasticity index (LL - PL)
p_l	long-term stresses acting on the tunnel
PL, LL	plastic limit and liquid limit
p_{max}	maximum consolidation pressures
p_o	overburden pressure
p_{oil}	oil pressure
p_s	short-term stresses acting on the tunnel
p_{sur}	surcharge pressure
r	Cam-Clay spacing ratio
R	tunnel radius or radius of curvature of the neutral axis of the beam
R'_p	the radius of the plastic region in the drained ($c'=0$)
R_p	the radius of the plastic region in the undrained ($\phi=0$)
R_v	reading value from vane test apparatus.
S	tunnel spacing (vertically)
S/D	clearance ratio
s_u/σ'_{vo}	ratio of undrained shear strength to effective stress
s_u	undrained shear strength
$s_{u(sur)}$	undrained shear strength under the surcharge pressure (p_{sur})
t	thickness of the liner
$T/\gamma HR$	thrust coefficient
T_q	applied torque
u_i , U_i	calculated and measured displacements at node i at time step n.
V_o	ground loss
V_s	volume of Speswhite kaolin powder, volume of settlement trough
V_w	water volume
W/D	pillar width ratio
W	pillar width
w_f	final water content
w_i	initial water content of the slurry
W_s	Kaolin powder weight

y	distance from the neutral axis of the beam
y'	distance between the neutral and centroidal axes of the beam.
z	depth below the surface of the sample

CHAPTER 1

INTRODUCTION

1.1 Introduction

The use of tunnels in major transportation schemes has increased considerably during the last decade especially in urban areas. The state of stress and the displacements in a zone around a tunnel will be modified by the construction of a tunnel. The size of this influence zone depends on the type and properties of subsoil, in situ stresses, tunnel depth and size, the tunnel support system, and tunnelling method.

In recent years many new tunnels have been also designed and constructed nearby existing tunnels in order to develop and extend underground transportation systems (e.g. CrossRail and the Jubilee line extension in London). In the design of new tunnels, it is important to ensure that any existing underground transportation systems in close proximity to the proposed tunnelling activities can continue to operate safely both during, and after construction. If the existing tunnel is influenced by the construction of a new tunnel, it may be serious because the repair of any damage is both time-consuming and expensive. Therefore, it is necessary to understand the interaction mechanisms between tunnels due to the construction of new tunnels. In general, this interaction may be strongly dependent on the spacing between tunnels. If the new tunnel is constructed at a large distance from the existing tunnel so that their influence zones do not overlap, the individual tunnels can be considered separately as single tunnels and analyzed as such. However, if the influence zones of the two

tunnels do overlap, some degree of interaction between tunnels will take place. Therefore, an ability to predict interactions of this kind is necessary in order to assess the possibility of damage to existing tunnels caused by new, nearby, tunnelling activities. Interaction between tunnels will affect the state of stress and the displacements around the tunnels, the ground surface displacements and the support loads.

1.2 Outline of the Dissertation

The main purpose of the present research programme is to study the influence of shield tunnel construction on the stresses, moments and displacements induced in the liners of nearby tunnels.

This research programme consists of the study of the effects of tunnel proximity and alignment, liner stiffness and soil overconsolidation ratio on the nature of the interactions between tunnels that are closely spaced in clay. A total of seven sets of carefully controlled physical model tests were carried out and the test results were complemented by a limited amount of two-dimensional finite element analysis.

The physical model tests consist of two main interaction test series:

i) parallel tunnel model;

ii) perpendicular tunnel model.

Two different test tanks were developed and used to produce clay samples of Speswhite kaolin:

i) plane strain tank for parallel tunnels;

ii) cylindrical tank for perpendicular tunnels.

Three model tunnels were installed in each of the tests in order to carry out two

interaction experiments in one clay sample. In the case of the parallel tunnel tests, one of these experiments was for a 'distant' tunnel (centre-line spacing of 2.0 D) and the other was for a 'close' tunnel (centre-line spacing of 1.4 D) where D is the tunnel diameter. In the case of the perpendicular model tunnel tests, one for a 'lower' tunnel (centre-line spacing of 2.0 D) and the other for an 'upper' tunnel (centre-line spacing of 1.4 D).

The clay samples used in the model tests were either normally consolidated or overconsolidated with a value of OCR of approximately 3. All samples had approximately the same shear strength (about 20 kPa). The upper boundary of the samples was stress controlled in order to simulate the behaviour of a tunnel that is distant from the ground surface.

Two different types of model tunnel were used:

i) instrumented tunnel for modelling an existing tunnel;

ii) non-instrumented tunnel for modelling a new tunnel.

The tunnel liners consisted of plain steel tubes of diameter 69.85mm. Two thicknesses of liner were used in the tests to model liners of different stiffness. All tunnel liners were installed using a model tunnelling machine that was designed and developed to simulate the construction of a full scale shield tunnel.

Various measurements were carried out to investigate the existing tunnel liner behaviour due to the installation of each of the new tunnels.

In this chapter, the present research programme is outlined. In Chapter 2, the current state of the art of soft ground tunnelling is presented, and previous research relating to interactions between closely spaced tunnels is then briefly reviewed. In the next two chapters (Chapter 3 and 4), the details of the apparatus design and testing procedures are described. The results of the model tests are discussed and interpreted in Chapters 5 and 6 respectively. In Chapter 7, details of the numerical back-analysis of the plane strain tests are described.

Finally, the main conclusions from the model tests and numerical analysis are set out in Chapter 8, where recommendations for future research are made.

1.3 Objectives of the Research

The objectives of the research can be summarized as follows:

i) to investigate the behaviour of an existing tunnel both during and after installation of nearby new tunnels.

ii) to design and develop equipment and instrumentation systems relevant to parallel and perpendicular model tests. This includes the development of a model tunnelling machine to simulate the construction of a full scale shield tunnel.

iii) to conduct parallel tunnel model test series in a plane strain tank with various values of pillar width, liner stiffness and overconsolidation ratio, and to monitor total radial stresses, pore water pressures, moments, and radial displacements.

iv) to perform numerical back-analyses of the parallel tunnel model tests.

v) to conduct perpendicular tunnel model tests in a cylindrical tank with various values of pillar width and liner stiffness, and to monitor total radial stresses, moments, and radial displacements.

vi) to interpret and compare interaction mechanisms between parallel and perpendicular tunnel systems.

vii) to evaluate the measured liner displacements by comparing them with values of estimated bending moments using a virtual work analysis.

CHAPTER 2

LITERATURE REVIEW

2.1 Introduction

This chapter gives a general survey of previous research relevant to the study of interactions between closely spaced tunnels. The chapter also contains a brief review of previous research on more general aspects of tunnelling in soft ground. This is important background material although some of the work is not directly relevant to this research.

2.2 Tunnelling in Clay

This section contains a brief review of the following aspects of the construction and behaviour of single tunnels in clay: i) shield tunnelling methods, ii) heading and face stability; iii) ground movement; and iv) lining behaviour.

2.2.1 Shield Tunnelling Methods

The stresses and displacements developed around tunnels constructed in clay are significantly influenced by the method of tunnelling. The excavation of tunnels in clay is often carried out in practice using a shield which provides a safe working space during excavation and liner installation. This section presents a summary of the main features of the

shield tunnelling technique.

The conventional shield is open-faced and the excavation is achieved by hand or a mechanical digger. This technique may be used in both good ground conditions, or soils where obstructions are encountered. In the past decade, construction equipment manufacturers have introduced a number of advanced new shield machines and there has been a trend towards the use of shields which excavate using a rotating cutter head. In soils with adequate standup time, and where soils are dry or impervious, the new shields may only differ from the conventional open shield in that the soil excavation process is performed using the rotating cutterhead rather than by hand. It is sometime necessary to support the tunnel face during excavation to prevent collapse or excessive ground loss. A variety of systems have been developed to provide suitable support during shield tunnelling, these include earth pressure balance, water pressure balance, and slurry, mud or slime shields (Clough, 1981 & 1983; Murayama, 1979; Matsushita, 1979). An extensive overview of shield tunnel technology is given by Kitamura *et al* (1981). The earth pressure balance (EPB) shield consists of a rotating cutter with slots through which excavated spoil passes into a closed chamber (see Figure 2.1). This type of installation procedure was adopted in the research described in this thesis.

Miniature tunnelling machines have been constructed in the past in order to carry out laboratory-based tunnelling research. Mori *et al* (1991), for example, designed a miniature shield machine to study the effect of slurry pressure in slurry-type shield tunnelling in the laboratory. In more recent work (Nomoto *et al.*, 1994 and Imamura *et al.*, 1996), progress has been on the development of a miniature shield tunnelling machine for use in a centrifuge.

2.2.2 Heading and Face Stability

It is often necessary to apply a suitable pressure to the face of a tunnel during collapse in order to prevent failure and to reduce soil deformations in front of the tunnel heading. This is particularly the case when the soil is soft. This section gives a brief review of some of the previous research on face stability.

Broms and Bennermark (1967) carried out a simple experimental study of this problem, and suggested that the stability of a tunnel face may be characterized using the 'stability ratio' which is defined as:-

$$N = \frac{\sigma_{vo} - \sigma_i}{s_u} \tag{2.1}$$

where σ_{vo} and σ_i are the overburden pressure and the pressure acting on the tunnel face, respectively. For undrained behaviour, they suggested a tunnel face will be stable provide that N is less than about six.

An extensive study of the stability of tunnels in cohesive soil was presented by Davis *et al* (1980). These results consist of upper and lower bound solutions for two important cases: i) the face stability of a circular lined tunnel, and ii) for a long unlined circular tunnel. As expected, the value of stability ratio at collapse for an unlined tunnel is shown to be less than the value for the corresponding lined tunnel (i.e. the unlined tunnel is less stable). Davis *et al* (1980) also discussed the critical value of stability ratio and show that for tunnels with small cover to diameter ratios the limiting value of 6 proposed by Broms and Bennermark (1967) is unsafe. This finding was confirmed by Uriel and Sagaseta (1989).

A detailed set of analyses of the stability of shallow square tunnels and shallow circular tunnels is given by Assadi and Sloan (1991) and Assadi and Sloan (1993). These

analyses were based on the use of a finite element formulation of the limit theorems. The results obtained for a homogeneous soil were very similar to those obtained by Davis *et al* (1980). However, these solutions have the advantage that they also deal with soils for which strength increases with depth.

Atkinson and Mair (1981) introduced the general concept of dimensionless tunnel stability numbers T_c, T_s, and T_γ which are analogous to the bearing capacity factors for foundations N_c, N_q, and N_γ, respectively. These values depend on the geometry of the tunnel and the soil strength. Theoretical values of T_c were obtained by Davis *et al* (1980) and model tests were used by Kimura and Mair (1981) to obtain experimental values. Atkinson and Potts (1977) discussed the values of T_s, and T_γ based on theoretical analysis and model test results.

Mair (1983) introduced the load factor (*LF*) which is the ratio between the stability ratio at working condition and that at collapse and is the reciprocal of the safety factor against collapse:-

$$LF = \frac{(\sigma_{vo} - \sigma_i)}{(\sigma_{vo} - \sigma_{ic})} \qquad (2.2)$$

where σ_{ic} is the value of σ_i at which collapse would occur. The load factor is a convenient way to express the safety against collapse of the heading of a tunnel and has important implications regarding the magnitude of ground movements induced by the excavation of shallow tunnels.

2.2.3 Displacements and Stresses Around Tunnels

2.2.3.1 Ground Loss and Surface Settlements

Tunnel construction inevitably leads to displacements in the soil, and this may lead to damage to any nearby structures. These ground movements are associated with two separate mechanisms; i) radial movements of the soil as a result of overcutting during tunnel construction and ii) ground movements associated with incomplete support at the tunnel face. The magnitude of the movements generally depend on soil type, ground water conditions, construction method, rate of tunnel advance, tunnel size and location, support system, and construction quality. The movements associated with incomplete support of the tunnel face are sensitive to the tunnel face pressure and are related to the face stability (Mair, 1987).

Ground loss (V_o) is a useful parameter to characterise displacements around tunnels. The ground loss is defined as the volume enclosed between the initial and the deformed excavation lines of the tunnel. Attempts have been made by many authors to estimate the ground loss associated with the tunnel face by correlating experimental values with either the stability ratio or the load factor for cohesive soils. Glossop (1977) for example suggested a simple linear relationship, and Clough and Schmidt (1981), Mitchell (1983), and Uriel and Sagaseta (1989) suggested expressions in which V_o is related exponentially to the stability ratio. Attewell and Yeates (1984) and Attewell *et al* (1986) collected together a large set of experimental data relating to ground loss. On the basis of this data, a graphical relationship is proposed between ground loss and stability ratio. This relationship is shown to be comparable with that proposed earlier by Glossop (1977). It is important to note that these empirical approaches do not include the effects of tunnel size and depth, and soil stiffness.

Mair (1979), however, described a set of results obtained from centrifuge tests under plane strain conditions with two different tunnel depth to diameter ratios (*H/D*). These results indicated that ground loss may increase as the ratio of *H/D* decreases. The studies described above deal, in general, with the component of ground loss due to incomplete support at the tunnel face. Other mechanism of ground loss are more directly related to construction procedures and so are difficult to quantify.

Ground movements around tunnels lead to surface settlements. The magnitude and distribution of these settlements has been studied extensively by previous researchers (e.g. Schmidt, 1969; Peck, 1969; Clough & Schmidt, 1980; O'Reilly & New, 1982; Rankin, 1988; Mair *et al,* 1993). The settlement profile of the ground surface has generally two symmetrical points of inflexion, where its maximum slope occurs. Structures built in between the inflexion points are subjected to sagging whereas structures lying outside them are subjected to hogging.

It is well accepted that the shape of the surface settlement troughs developed during tunnel construction may be reasonably well approximated by a Gaussian distribution of the form:-

$$\delta_v = \delta_{v\,max} \exp\left(\frac{-x^2}{2i^2}\right) \tag{2.3}$$

where, δ_v is the surface settlement at distance x from the tunnel axis and δ_{vmax} is the maximum settlement at the tunnel centre-line. The width of the settlement profile is defined by the important parameter i, which is the distance from the tunnel centre line to the point of inflexion. By integrating Equation 2.3, the volume of the settlement trough (V_s) for a unit length of tunnel can be expressed by:-

$$V_s = \sqrt{(2\pi)}\ i\ \delta_{max} \tag{2.4}$$

For undrained soil, the volume of the settlement trough would be expected to be equal to the ground loss (V_o).

A number of empirical correlation have been proposed to relate i to the tunnel depth to diameter ratio and soil type (e.g. Schmidt, 1969; Cording and Hansmire, 1975; Attewell, 1977; Clough and Schmidt, 1981; O'Reilly and New, 1982; Attewell *et al*, 1986; Rankin, 1988; Schmidt, 1988; Mair *et al*, 1993). For practical purposes, it is often assumed that the parameter i varies with tunnel depth, z_o :-

$$i = K\ z_o \tag{2.5}$$

where K is a constant. Mair *et al* (1993) suggested that a value of K of 0.5 is reasonably representative of tunnels in clay. In order to estimate subsurface ground movements more complex empirical expression are needed. This is discussed in detail by Mair *et al* (1993).

Recently, Grant and Taylor (1996) investigated the ground movement caused by tunnelling in two layered strata using a geotechnical centrifuge model tests. The results suggest that the selection of a suitable value of i in this case is not straightforward and cannot be based on a simple superposition of the values of K appropriate for the two soils. These model test results were also examined by Stallebrass *et al* (1996) using a plane strain finite element analyses performed using a three-surface kinematic hardening model (Stallebrass, 1990).

2.2.3.2 Stress and Strain Behaviour around Tunnels

Deere *et al* (1969) presented theoretical results for a one-dimensional analysis of

radial and tangential stress in the elastic and plastic region developed by tunnel excavation, for both the short term (total stress, undrained condition) and long term (effective stress, drained condition) conditions. Deere *et al* (1969) showed that the radius of the plastic region, R_p, in the undrained state and R'_p, in the drained state were given by:-

$$R_p = a \exp\left(\frac{\sigma_{vo} - p_i - s_u}{2 s_u}\right) \tag{2.6}$$

$$R'_p = a \left[(1-\sin\phi')\frac{\sigma'_{vo}}{p'_i}\right]^{\frac{1-\sin\phi'}{2\sin\phi'}} \tag{2.7}$$

where σ_{vo}, σ'_{vo} are total and effective stress at the tunnel depth; p_i and p'_i are total and effective internal pressure ($p_i'=p_i-u_o$), a is the tunnel radius, s_u is undrained shear strength, and ϕ' is effect angle of friction. These results suggest that the size of the plastic zone around the tunnel generally tends to reduce with time as consolidation takes place.

Ng and Lo (1985) described the stress paths for three typical soil elements around a tunnel. Near the crown, excavation produces a reduction of the radial stress (initially the major principal stress) and a small increase in the tangential stress (initially the minor principal stress). The tangential stress becomes the major principal stress, and so the principal stresses are rotated by 90°. At the springline, excavation brings about an increase in the tangential (*i.e.* vertical) major principal stress and a reduction in the radial (i.e. horizontal) minor principal stress. The principal stresses are not rotated at the springline. At the shoulder, of the tunnel, the major principal stress varies slightly and rotates in direction by about 45°. In addition, the shear strength mobilization increases monotonically at the springline and shoulder, however, at the crown it first decreases and then increases.

Details of finite element analysis of the stresses around tunnels are described by

Fernández-Moya *et al* (1981), Oteo and Sagaseta (1982), and Lee and Rowe (1989). In particular, Oteo and Sagaseta (1982) discussed the influence of the boundary locations in numerical analysis. They suggested that the influence of the lateral boundary can be neglected if it is at a distance from the centreline equal to or greater than $9D$ where D is tunnel diameter. This information allows rational decisions to be taken about the size of test chamber necessary for laboratory studies of tunnelling to ensure that the boundaries do not affect the results.

2.2.4. Lining Behaviour

Soil movements immediately adjacent to the tunnel are influenced by the stiffness of the liner. Peck *et al* (1972) suggested that tunnel liners may be classified as either flexible or stiff. It is clear, however, that a tunnel liner which is stiff with respect to a soft clay may behave as a flexible liner in a very stiff clay. To characterise the stiffness of a liner, therefore, it is necessary to adopt suitable ratios of liner to soil stiffness.

A flexible liner supports the soil stresses applied to it primarily by ring compression. The normal stresses acting on the liner would be expected to be approximately uniform and any bending moments will be relatively small. A stiff liner, however, will tend to support the soil stresses by bending action although hoop stresses will also be present.

Peck *et al.* (1972) suggested the use of the compressibility and flexibility ratios as a means of defining tunnel liner stiffness, based on the analytical work by Burns and Richards (1964) and Höeg (1968) in soil-structure interaction. The compressibility ratio, C, is the ratio of a measure of the compressive stiffness of the soil relative to the hoop stiffness of the liner, and the flexibility ratio, F, is defined as the ratio of a measure of the shear stiffness of the

soil relative to that the flexural stiffness of the liner. These ratios are expressed by:-

$$C = \frac{E_s R (1 - \nu_l^2)}{E_l t (1 + \nu) (1 - 2\nu)} \tag{2.10}$$

$$F = \frac{E_s R^3 (1 - \nu_l^2)}{6 E_l I (1 + \nu)} \tag{2.11}$$

where E_l, ν_l, R, and t are respectively the Young's modulus, Poisson's ratio, radius and thickness of the liner, and E_s and ν are the Young's modulus and Poisson's ratio of the soil. The moment of inertia of the cross-section per unit length along the axis of the tunnel is I. Peck *et al* (1972) suggested that tunnel liners may be classified as flexible if F is greater than about 10. Typical values of F for real tunnels lie in the range of about 5 to 300; however tunnels with a substantial concrete secondary lining may be stiffer than this. Segmental linings with articulated joints between segments are difficult to characterise using this approach, however. The linings themselves may behave in a highly flexible manner even when the segments themselves are relatively stiff. The compressibility ratio is less useful than the flexibility ratio in characterising tunnel behaviour. For tunnels constructed in soil, values of C, for drained conditions, are typically less than 1, while for rock tunnels C generally exceeds 1 (Sinha, 1989). However for short-term undrained behaviour of clay, with ν equal to 0.5, C becomes infinite and the liner hoop stiffness of no consequence.

A further complexity is the nature of the interaction between liner and ground when NATM procedures are adopted. This construction method is essentially a shieldless tunnel procedure and the philosophy behind the method is that stresses and displacements of the tunnel depend on installation method as well as liner stiffness. Some attempts to analyze this difficult soil-structure interaction problem have been published (e.g. Eisenstein and

Branco,1985; Gesta,1986; Duffaut and Panet,1989) but further discussion of this topic is beyond the scope of this thesis.

2.3 Interactions Between Closely Spaced Tunnels

2.3.1 General

When a new tunnel is installed close to an existing tunnel, this may lead to important interaction effects. For example, new tunnel construction may lead to unacceptable distortions or bending moments in the existing tunnel liner. The nature of these interactions depends significantly on the tunnel spacing, size of both tunnels, the liner stiffness, and the method used to install the tunnel. In a real design problem where interaction effects are important, empirical methods developed from field measurements and two-dimensional numerical methods are usually used. Although three-dimensional effects may often be important, it is not generally feasible to carry out detailed three-dimensional finite element analysis during routine design.

Interaction between closely spaced tunnels has been studied in the past using a variety of approaches. Much of the published work is based on measurements made during the construction of full scale tunnels. Some work is also reported in which finite element analysis and other analytical procedures were used to study the problem. Little research, however, seems to have been carried out using reduced scale laboratory testing. It is noticeable that although an extensive amount of research literature is available on this subject much of it was written 10 to 30 years ago. Very few good studies have been published in recent years.

2.3.2 Analytical and Numerical Studies

Few purely analytical studies of the twin tunnel problem appear to have been carried out. One study of this sort, however, is described by Fotieva and Sheinin (1966). This study was based on the assumption of an elastic soil and used a Laplace Transformation technique. The analysis was applied to an example problem of a lined tunnel of 6 m diameter at a depth of 36 m. The soil and the liner were assigned material properties of rock and concrete respectively. A second tunnel of the same diameter is excavated adjacent to this existing tunnel at a central distance of 8 m which gives a pillar width (W) to tunnel diameter (D) ratio of W/D=0.33. The driving of the second tunnel caused additional stresses in the liner of the existing tunnel leading to a maximum thrust coefficient of $T/\gamma HR$ = 0.24 and a maximum moment coefficient of $M/\gamma HR^2$ = 0.0053, where H and a are tunnel depth and radius respectively. This example indicates that the induced thrusts and bending moments do not have a substantial effect on the total thrust and bending moment in the liner. It should be noted, however, that this analytical approach does not allow ground loss to be specified and so will, in general, tend to underestimate the magnitude of any interaction effects. The inability to include the effects of ground loss is a major shortcoming. It is unfortunate that in much of the later theoretical work published on this subject this important limitation still applies.

Peck *et al* (1969) discussed the problem of two parallel or intersecting tunnels of different diameters at adjacent, crossed or stacked relative positions. A semi-empirical approach was used to develop some general guidelines for the liner distortions that occur due to the construction of a new nearby tunnel (see Figure 2.2). They suggested that when the tunnel spacing is greater than about $2D$, where D is diameter of larger tunnel, displacement

interaction effects may be neglected. However, these rules are highly simplified; they do not account for variations in tunnel liner stiffness and are only given for certain, specified, values of tunnel spacing.

Barla and Ottoviani (1974) used a finite element method to study the case of two shallow parallel unlined tunnels excavated simultaneously. These analyses were based on linear elastic and non-linear variable moduli material properties. They reported the results of a parametric study which covered a range of geometric parameters such as depth to diameter ratios of 0.75 to 3; pillar width to diameter ratios of 0.25 to 1.0; and two tunnel diameter values of 6 m and 12 m. This study was concerned primarily with the stresses developed in the pillar (i.e. the zone of soil between the two tunnels). The results suggest that, in some cases, the compressive and shear stresses in this region may become excessive. Since the analyses were for unlined tunnel, however, the results are not readily applied to lined tunnels.

An extensive numerical study for a variety of tunnel spacings, liner stiffness and procedures to model tunnel construction has been carried out by Ghaboussi and Ranken (1977). This study was similar to that of Barla and Ottoviani (1974) with the important, exception that the analysis of lined tunnels was included. These numerical analysis were performed using a two-dimensional geometry and an elastic soil model. The results of this study are consistent with earlier suggestions by Peck *et al* (1969) that the computed interaction effects between two parallel tunnels are small when the centre-line spacing exceeds twice the tunnel diameter. Ghaboussi and Ranken (1977) apply their numerical model to the case of lined tunnels with a liner flexibility ratio (F) of 16. A series of analyses were carried out at different values of pillar width (W) and tunnel depth (H). Typical plots of bending moment for parallel tunnels with different pillar widths is shown in Figure 2.3 (Note that the second tunnel is to the left of the plot). This figure illustrates several important features.

Firstly, bending moment interaction effects tend to be confined to the springline adjacent to the second tunnel. Secondly, the magnitude of the interaction effects tend to increase as the pillar width is reduced. These data suggest, however, that the additional moments associated with the construction of the second tunnel do not increase significantly the total bending moments in the liner (this conclusion is similar to that reached by Fotieva and Sheinin (1966)). It should be carefully noted, however, that this analysis did not include the effects of ground loss during tunnel construction. All interaction effects were therefore associated with tunnel liner distortion. The predicted moment interaction effect, therefore, are smaller than would be expected in practice. Typical plots of liner distortions obtained from Ghaboussi and Ranken's study are also shown in Figure 2.4. These results suggest that horizontal diameter reduces as the pillar width is reduced. This is contrary to intuition and also to various measurements made on full-scale tunnels that interaction effects tend to cause on increase in horizontal diameter.

Leca (1989) used a finite element method to study the interaction between two adjacent NATM tunnels. These numerical analysis were carried out using a softening factor and an elastic soil model. The results of this study also led to the conclusion that significant interaction effects can be expected to occur between two adjacent tunnels only when the pillar width ratios (W/D) are smaller than 1.0.

Further two-dimensional finite element studies of this problem are described by Perri (1994), Wang and Chang (1992), and Kanzki *et al* (1992). These analyses were all carried out as part of practical design procedures. In these cases, it was noted, however, that a three-dimensional finite element model was required to model important feature such as: i) driving sequences and rates, ii) changes in initial ground stresses and stiffness, and iii) the type of excavation and lining used. However, the cost of using such models for design can generally

be considered prohibitive. In addition, the merit of such complex analysis is questionable when stiffness parameters for the ground are not known to high accuracy.

Soliman *et al* (1993) reported two and three-dimensional analyses for closely spaced double-tube tunnels for cases where the pillar width ratios (*W/D*) are 0.25 and 0.5.The analyses were carried out using the elastic ground model. They showed the diagrams of the relative changes in stresses, moments, and displacements in comparison with a single tunnel analysis. This study produced results that were generally consistent with those produced by Ghaboussi and Ranken (1977). The Soliman *et al* (1993) study also did not include the effects of ground loss and so this correlation is to be expected.

Addenbrooke and Potts (1996) reported a two-dimensional finite element study of a twin-tunnel problem. This study differed from the earlier finite element work in that it was based on a small strain non-linear soil model. They concluded that the interaction between two tunnels passing at depth depends on relative tunnel position (side by side or vertically above) and on the spacing. Driving a new tunnel above an existing tunnel was shown to have significantly less influence on the existing tunnel lining than was the case for equivalent side-by-side tunnels. This is an important finding. Previous numerical work has characterized the magnitude of tunnel interaction effects in terms of tunnel separation. Addenbrooke and Potts (1996), however, indicate that relative position may also have an important influence on the nature and magnitude of the interaction mechanisms.

2.3.3 Field Measurements

Several researchers have reported the results of measurements made during and following construction of two or more parallel tunnels. These field measurement data are,

however, difficult to correlate because of site specific nature of the projects and the different instrumentation systems that were adopted.

Terzaghi (1942) reported in detail the field measurements observed from tunnels constructed in Chicago Clay. These tunnels had a horseshoe shaped cross-section and were lined with steel ribs and liner plates. The tunnels were 6.1 m in average diameter and were constructed at a distance of 8.7 m centre-to centre, giving a pillar width of 2.6 m (W/D=0.425). Significant movements occurred while the second tunnel was being advanced and both points at the springline of the first tunnel moved outward. The displacement at the springline nearest the second tunnel was much greater than that at the opposite springline as would be expected. This displacement corresponded to a horizontal diameter change (ΔD) of the first tunnel of $\Delta D/D$=0.10%, where D is tunnel diameter. The final horizontal diameter change ratio ($\Delta D/D$) was measured to be about 0.25%. The contact pressures between the soil and the concrete invert of the first tunnel, at the side nearest the second tunnel, increased and thereafter remained greater than those at the opposite side. This is presumably a result of arching in the soil above the second tunnel. Unfortunately, bending moments were not measured during the study.

Ward and Thomas (1965) reported on two parallel tunnels constructed in London Clay. These particular tunnels were lined with precast concrete segments which had a thickness of 23 cm. The tunnels were approximately 4 m in diameter and were separated by a pillar of 2.4 m minimum thickness (i.e. W/D=0.6). Passage of the tunnel caused an additional maximum horizontal diameter change of the first tunnel of $\Delta D/D$=0.12%. In addition, the average radial pressure acting on the first tunnel was increased by about 15% of overburden pressure. After 40 months the total maximum diameter change, $\Delta D/D$, of the first tunnel was 0.32% and the total average radial pressure was estimated to be approximately 65% of overburden pressure.

Deere *et al* (1969) give an excellent summary of the available field data prior to 1969. In most cases, measurements were made as a second tunnel was driven past a test section set up in an existing tunnel or in one whose heading was a considerable distance ahead of the test section.

Sauer and Jonuscheit (1976) reported stress measurements in the pillar separating two parallel tunnels in rock. The two tunnels were driven simultaneously and the stresses were measured as the tunnel headings approached the test section. They concluded that high stress concentrations occurred in the pillar region between two tunnels, presumably as a result of arching over the tunnels.

Hansmire *et al* (1981) reported a set of measurements that were made during the construction of new sewer in close proximity to a pair of existing subway tunnels. In this case, the sewer was perpendicular to, and above, the existing tunnels. Excavation for the sewer caused an increase in the vertical diameter of the subway tunnels in the zone immediately beneath it. This increase in diameter was, presumably, associated with a reduction in vertical stress acting on the existing tunnels. When the shield was advanced during tunnel construction, however, the vertical diameter of the existing tunnels tended to decrease. Hansmire *et al* suggested that this latter effect was associated with shear stresses developed between the shield and soil.

Lo *et al* (1987) reported the behaviour and interaction of four mass rapid transit tunnels of 5.4m internal diameter in close proximity. The measured displacement data were shown to agree reasonably well with Peck's empirical approach (Peck, 1969).

A certain amount of recent research on the behaviour of twin tunnels has focused on the nature of the induced ground surface settlements (e.g. Hisatake, 1994; Fang, *et al.*, 1994 and Kimmance, 1996). Further consideration of this topic, however, is beyond the scope of

this thesis.

2.3.3 Laboratory Studies

Little research has been reported in which this problem has been studied using reduced scale model testing, although the behaviour of single tunnels has been studied extensively using centrifugal modelling (e.g. Cairncross, 1973; Atkinson et al., 1974, Atkinson and Orr, 1976; Potts, 1976; Seneviratne, 1979; Mair, 1979 and Taylor, 1984). In much of this single tunnel research, attempts have not been made to develop realistic methods of incremental tunnel installation. However, as described in Section 2.2.2, Mori *et al* (1991), Nomoto et al (1994) and Imamura et al (1996) give useful information on the design of a model shield tunnelling machine for reduced-scale model testing.

2.4 Summary of Relevance of Previous Work to the Research Programme

The main feature of the previous research described in this chapter that are relevant to this research study are summarized below.

i) An extensive amount of research has been carried out on twin tunnels. Much of this consists of field measurements and is highly site specific. A substantial amount of finite element analysis has also been published. This work all suggests that the mechanisms governing the interaction between adjacent tunnels are highly complex.

ii) Previous finite element studies suggest that interaction effects are important only when pillar width is less than one tunnel diameter ($W<D$). This suggests that tunnel interaction effects are important only for very close tunnels or where new tunnels are

constructed to join with existing tunnels. This information may be used to select suitable values of tunnel spacing for study in the model tests.

iii) For single tunnels, Peck et al (1972) suggests that liner behaviour may be characterized by two non-dimensional numbers; the flexibility ratio and compressibility ratio. Peck suggests that tunnels will behave in a flexible manner if $F>10$. It is further thought that C is not an important parameter. This information allows suitable values of F (and hence liner stiffness) to be selected for study in the model tests.

iv) Field data (e.g. Hansmire, 1981) suggest that interaction effects may depend on tunnel installation procedures. It is, therefore, important to use realistic installation procedures in the laboratory tests. A useful design for a model tunnelling machine is given by Mori *et al* (1991), Nomoto *et al* (1994) and Imamura *et al* (1996) and may be used as the basis of the design of a tunnelling machine for the present research.

v) Addenbrooke and Potts (1996) suggest that the relative position as well as tunnel proximity are important. This information was published after the testing program was complete. With hindsight it is clear that it may have been useful to study this effect in the model tests.

vi) Oteo and Sagaseta (1982) suggest minimum distance for rigid boundaries from a study of the behaviour of single tunnel, using finite element analysis. The results suggest that the influence of the lateral boundary can be neglected if it is at a distance from the centreline equal to or greater than $9D$, where D is tunnel diameter. This information may be used to select suitable dimension the model tests.

vii) Previous finite element analysis results (e.g. Ghaboussi and Ranken, 1977; Soliman *et al.*, 1993) are curious. Incremental horizontal diameter change (ΔD) is negative whereas field data (and intuition) suggest that ΔD is positive. However, Addenbrooke and

Potts (1996) obtained much more realistic results using an approach in which ground loss was explicitly modelled. It is clear, then, that great care needs to be taken in order to obtain realistic finite element solution to this problem.

CHAPTER 3

DESIGN OF APPARATUS

3.1 Introduction

The objectives and nature of the author's research are stated in Chapter 1. The purpose of this chapter is to describe the experimental apparatus used to conduct the small scale model tests. Discussion of the test procedures, and data retrieval methods that were adopted, is given in Chapter 4. It is important to note that it was not the intention of the model tests to simulate in all respects the behaviour of real prototypes; instead the tests were intended to represent simple idealised boundary value problems in which the conditions were close to those in the soil near a real tunnel.

The experimental apparatus was designed so that it was capable of applying a variety of precisely known loadings. Details of the various apparatuses used in the test series are presented in this chapter.

3.2 Specification of Model Tests

This section describes briefly the model test specifications adopted for the design of the apparatus. The specifications of the tests were based on the procedures described below.

The model tests consisted of two interaction tests:

i) for the parallel tunnel model;

ii) for the perpendicular tunnel model.

Two different types of test tanks were used to performed these model tests. The plane strain tank was used for the parallel tunnel model tests, and the cylindrical tank used for the perpendicular tunnel model tests.

Clay samples were produced by consolidation of a slurry of kaolin to provide both normally consolidated and overconsolidated samples. All overconsolidated samples had an *OCR* of approximately 3. All samples used in the tests had approximately the same shear strength (about 20 kPa). Testing was performed using a stress controlled boundary to the top surface of each clay sample. It is accepted that this approach will not reproduce the level of stress experienced in the prototype and that other procedures, for example centrifuge testing, might overcome this difficulty. The additional complexity of performing tests of this sort in a centrifuge, however, is thought to outweigh the possible advantages.

The tunnel liners used in the tests consisted of plain steel tubes. Peck *et al.* (1972) defined two non-dimensional numbers that should be equal for perfect scaling between model and prototype tunnels. The 'compressibility ratio' is the ratio of a measure of the soil stiffness to the hoop stiffness of the liner (see Equation 2.10) and the 'flexibility ratio' is defined as the ratio of a measure of the stiffness of the soil to the bending stiffness of the liner (see Equation 2.11). Since it is only possible to vary one parameter (the thickness of the model tunnel liner) it will only be possible to achieve perfect scaling for one of these numbers. The results presented by Peck *et al.* (1972) suggest that the 'flexibility ratio' is the more important parameter of the two. Therefore, the model tunnels were specified on the basis of flexibility ratio.

Two specifications of tunnel liner were used in the tests. One of these would be

expected to behave in a 'flexible' manner and the other would be expected to behave in a 'stiff' manner. Suitable values of flexibility ratio to achieve this were adopted in the model tests.

All tunnel liners were installed using a specially designed model tunnelling machine. This machine was designed and developed based on the system of Earth Pressure Balance (EPB) shields which has become popular for soft ground tunnelling.

Two different types of tunnels were used in each of the model tests. An 'instrumented' tunnel was used to model an existing tunnel and a 'non-instrumented' tunnel was used to model a new tunnel under construction.

Measurements were made during the installation of each of the tunnels. The radial total stresses, pore water pressures, and radial displacements were measured in the instrumented tunnel due to installation of the tunnels.

In order to ensure the estimation of strength of the clay samples, a miniature site investigation consisting of vane tests and moisture content tests were carried out in each of the clay samples.

3.3 Test Tanks

In this testing programme, plane strain and cylindrical tanks were used to provide the consolidated clay samples. The design and development of these tanks were originally undertaken by Love (1984) for the plane strain tank and May (1987) and Nyirenda (1989) for the cylindrical tank. Some modifications and development were necessary in order to adapt the test tanks to the requirements of this research programme. Both tanks used the same pressure system to pressurise the surface of samples during consolidation and tunnelling.

Details of the modifications of the tanks are described in the following sections.

3.3.1 Plane Strain Tank

The plane strain tank was used to carry out the two-dimensional model testing of the parallel tunnels with different tunnel parameters. The tank consisted of a rectangular box of internal dimensions 1000 mm by 300 mm in plan and 610 mm in height as shown in Figure 3.1. A top-extension piece fitted to the test box for consolidation was also included.

Modifications to the tank were made to install the model tunnels through the side walls of the tank. A tunnel diameter of 70 mm was chosen based on:

i) the efficiency of the tunnelling work in the laboratory, for example, smaller tunnels may be difficult to excavate,

ii) minimising the influence of the lateral boundary.

For the lateral distance of the tank boundaries from the centre-line of the tunnel, a distance of three tunnel diameters has generally been adopted in previous laboratory tests (Seneviratne, 1979; Potts, 1976; Mair, 1979; and Taylor, 1984). However, Oteo and Sagaseta (1982) suggested that, on the basis of numerical analysis, the influence of the lateral boundary can be neglected when the distance from the centre-line of tunnel to the boundary is greater than $9D$. In these model tests, a minimum lateral distance of $5.5D$ was adopted.

The two 25 mm thick perspex walls contained three parallel holes (corresponding to the tunnel positions) in order to perform two interaction tests; one with a distant tunnel and the other with a close tunnel. For the distant tunnel, the centre-line spacing between tunnels was adopted as twice the tunnel diameter (D). This may examine an accurate view of the

interaction behaviour investigated by previous researchers (Ghaboussi and Ranken, 1977; and Leca, 1989). They suggested that the interactions between two parallel tunnels are small when the centre-line spacing is greater than two tunnel diameters . For the close tunnel, a spacing of 1.4*D* was adopted. Hence the side holes were spaced at 140 mm and 98 mm distance from the axis of the centre hole (see Figure 3.1). All of the holes were of 80 mm diameter in size to allow a clearance between the hole and the tunnel liner.

The tank was equipped with ports to allow the measurement of total pressure and pore water pressure at the front tank wall during consolidation and subsequent testing. The positions of the instruments are shown in Figure 3.1.

In order to measure the undrained shear strength using a laboratory vane for the case where surface pressure is applied, two holes of 20 mm diameter were made at each end of the front perspex wall at the same level as the horizontal axis of the tunnels. Both holes were 50 mm distant from the end walls of the tank (see Figure 3.1).

3.3.2 Cylindrical Tank

The cylindrical tank used to perform the model testing of the perpendicular tunnels is shown in Figure 3.2. The tank was circular in plan with a 581 mm internal diameter and 1012 mm height and a base plate connected by bolts with silicone sealant as shown in Figure 3.2. Three pairs of circular holes were made in the tank wall, to perform two interaction tests with perpendicular tunnels; one test with a lower tunnel and the other with an upper tunnel. In order to make the spacing the same as the parallel tunnel case, the vertical distances between perpendicular holes axes were of 140 and 98 mm for the lower and upper tunnels respectively. All of the holes were of 80 mm diameter in size.

The tank height of 1012 mm was enough to allow the initial depth of slurry to produce a block of clay approximately 450 mm thick under the maximum consolidation pressure. Two 6mm wide drainage channels were provided along two diameters in the base of the tank. Drainage holes of 8 mm diameter with taps were placed at the side of the base. A 3.2 mm thick piece of porous Vyon sheet, produced by Porvair Technology Ltd., cut exactly to size, was laid on the base to act as a drainage layer and filter. Flexible plastic hose (6 mm internal diameter) connected to the taps returned the drainage water to the top of the sample to keep a constant head of water.

In order to mount the total pressure and pore water pressure transducers, two M10 holes were made at the side of the tank wall at the same level as the instrumented tunnel axis. Two 18 mm holes were also made to measure the undrained shear strength using a laboratory vane under surface pressure at the tank wall. Details of locations and sections of instruments were shown in Figure 3.2.

3.3.3 Pressure System

The Soil Mechanics Laboratory at Oxford University is equipped with a clay consolidation pressure system designed and built by Love and Gue (1984). Santa Maria (1988) and Martin (1994) used the same equipment to produce soil samples to carry out model footing tests. The design and operation of the system was described in detail by Gue (1984), Love (1984), Santa Maria (1988) and Martin (1994), so only essential details are described below.

Two different reaction frames to consolidate and pressurise the samples in the plane strain tank and cylindrical tank were used as shown in Figure 3.3. Double action hydraulic

rams (three for the plane strain tank, one for the cylindrical tank) were mounted on the top of each reaction frame, with the compressive load applied to the clay surface via a rigid loading platen. These rams were pressurized by a hydraulic oil control system and a pneumatic control system using a compressed air and nitrogen supply. Two different pressure systems were used during the consolidation according to the magnitude of consolidation pressure. A summary of the pressure system control is given below in Table 3.1.

Table 3.1 Pressure System Control

Pressure System	Control System	Remarks
Low (p_{oil} < 100 psi)	Hydraulic (oil) and Pneumatic (air)	p_{oil} = Oil Pressure
High (p_{oil} > 100 psi)	Hydraulic (oil) and Pneumatic (nitrogen gas)	

Pressure gauges were mounted at the top of each reaction frame to measure the applied pressure. Schematic details of the pressure system are shown in Figure 3.4.

3.4 Soil Specimens

Salient features of the behaviour of reconstituted Speswhite kaolin used in this testing programme are presented in this section.

3.4.1 Speswhite Kaolin

Speswhite kaolin has been used in numerous research programmes involving scaled physical model testing as shown in Table 3.2. This table also lists several authors particularly

concerned with work on model tunnels using Spestone kaolin, which has similar engineering properties to Speswhite kaolin (Mair, 1979).

In this research, Speswhite kaolin was used in the model tests since this kaolin is used widely for research and its engineering properties are well established.

Table 3.2 Previous model tests using Speswhite kaolin

Research Areas	Researchers	
	Speswhite kaolin	Spestone kaolin
Tunnel	- Mair (1979) - Kim (1993)	For Tunnel - Cairncross(1973) - Orr (1976) - Casarin (1977) - Seneviratne (1979) - Mair (1979) - Taylor (1984)
Piles	- Randolph *et al.*(1979) - Steenfelt *et al.*(1981) - Martins (1983) - Gue (1984)	
Piezocone	- May (1987) - Nyirenda (1989)	
Dilatometer	- Smith (1993)	
Shallow Foundations	- Santa Maria (1988) - Craig and Chua (1990) - Martin (1994)	
Reinforced Soil	- Love (1984) - Fannin (1986)	

The physical and mechanical properties of Speswhite kaolin have been investigated by many researchers: Steenfelt *et al.*(1981), Clegg (1981), Martins (1983), Airey (1984), Elmes (1985), Al-Tabbaa (1987), Santa Maria (1988), Smith (1993). Based on these investigations, the physical (index) properties of this clay are well established and are, typically, plastic limit PL = 34 %, liquid limit LL = 65 %, and specific gravity G_s = 2.61. However, it was found that properties relating to strength and consolidation behaviour showed

considerable variation as indicated in Table 3.3.

Table 3.3 Mechanical properties of Speswhite kaolin

Parameters	Steenfelt (1981)	Martins (1983)	Fannin (1986)	Al-Tabbaa (1987)	Santa Maria (1988)	Smith (1993)
λ	0.25	0.22 - 0.25	0.25	0.187	0.22	0.174
κ	0.05	0.04	0.04	0.028	0.03	0.05
N_{1D}	3.58	3.52	3.51	3.13	3.34	3.1
M	0.9	0.9	0.88	0.9(ϕ=23°)		0.8
e_{1D}	2.58			2.13		
$K_{o(nc)}$		0.65	0.64	0.69		

In order to formulate and control the preparation procedures for each model test, the Fannin and Al-Tabbaa values given in Table 3.3 have been adopted because they represent the most general and comprehensive study into the properties of Speswhite kaolin and are in broad agreement with values cited by the other researchers.

3.4.2 Specification of the Consolidated Sample

In these model tests, the clay samples were produced by the consolidation of a slurry of Speswhite kaolin to provide both normally consolidated and overconsolidated samples. All overconsolidated samples were prepared at an overconsolidation ratio (*OCR*) of approximately 3. Details of the procedures used to produce the samples are given in Chapter 4.

In order to produce the same shear strength (approximately 20 kPa) and height of the samples under the different surcharge pressure adopted in the tests, both theoretical and empirical approaches were adopted in order to select the consolidation pressure and slurry

volumes required. Firstly, the maximum consolidation pressures (p_{max}) were estimated from the assumed $s_{u(sur)}$ under surcharge pressure and *OCR*. Secondly, a final water content (w_f) was estimated from the $s_{u(sur)}$ values to determine the initial slurry height (H_i). Detailed procedures to satisfy the specification of the clay samples are given below.

3.4.2.1 Determination of Maximum Consolidation and Surcharge Pressure

The maximum consolidation pressure (p_{max}) and surcharge pressure (p_{sur}) were determined to produce consolidated samples with a shear strength of approximately 20 kPa. For the overconsolidated clay, the ratio of undrained shear strength to effective stress is generally related to the same ratio for normally consolidated clay and the *OCR*.

For a Modified Cam-Clay soil (Roscoe and Burland, 1968), Wroth (1984) derived the following relationship between undrained shear strength and *OCR*:-

$$\frac{s_u}{p'_i} = \frac{M}{2}\left(\frac{n_p}{r}\right)^{\Lambda} \tag{3.1}$$

where Λ (= $(\lambda-\kappa)/\lambda$) is the plastic volumetric strain ratio, n_p ($=p'_o/p'_i$) is the isotropic overconsolidation ratio and r is the Cam-Clay spacing ratio (defined in Wroth, 1984). Equation 3.1 may be rewritten in the more convenient form:-

$$\frac{s_u}{p'_i} = \left(\frac{s_u}{p'_i}\right)_{nc} n_p^{\Lambda} \tag{3.2}$$

where $(s_u/p'_i)_{nc}$ is the undrained strength ratio for a normally consolidated sample. For one dimensional consolidation and swelling, there is ample experimental evidence for a similar relationship between undrained shear strength and *OCR* (Ladd *et al.*,1977; Muir Wood,

1990):-

$$\frac{s_u}{\sigma'_{vo}} = \left(\frac{s_u}{\sigma'_{vo}}\right)_{nc} OCR^{\Lambda} \tag{3.3}$$

Typical values of the undrained shear strength ratio for normally consolidated clays, $(s_u/\sigma'_{vo})_{nc}$, and the value of Λ are 0.25 and 0.8 respectively (Houlsby, 1993). These values were adopted in order to specify the consolidation procedures adopted in the tests.

The maximum consolidation pressure (p_{max}) and surcharge pressure (p_{sur}) corresponding to the *OCR* to be adopted in each sample were estimated from Equation 3.3. Firstly, the surcharge pressure was estimated from the estimated s_u values, and the maximum consolidation pressure was then calculated by:-

$$p_{max} = OCR \cdot p_{sur} \tag{3.4}$$

Table 3.4 summarizes the estimated pressures of p_{max} and p_{sur} for each of the normally consolidated and overconsolidated samples.

Table 3.4 Maximum consolidation pressure and surcharge pressure

Pressures	NC-clay	OC-clay (OCR=3)	Remarks
p_{max}	4 s_u	4.984 s_u	s_u is the estimated value under the surcharge pressure (p_{sur}).
p_{sur}	4 s_u	1.661 s_u	

3.4.2.2 Relationship Between Water Content and Undrained Shear Strength

The water content (w) of clay can be expressed in term of the liquidity index (LI) by the expression:-

$$LI = \frac{w - PL}{PI} \tag{3.5}$$

where PI (= LL - PL) is the plasticity index. For a soil with a liquidity index of less than 1, the relationship between the liquidity index and undrained strength can be expressed as follows: Mitchell (1976); Muir Wood (1990); and Atkinson (1993).

$$LI = a \log(s_u) + b \tag{3.6}$$

where a and b are constants (typically, $a \approx -0.5$ and $b \approx 1.09$ to 1.15).

By combining Equation 3.5 and 3.6, the water content can be estimated using the following expression:-

$$w = (a \log s_u + b) PI + PL \tag{3.7}$$

3.4.2.3 Derivation of the Initial Height of Speswhite Kaolin Slurry

Accurate estimation of initial slurry height was important to ensure that the height of the consolidated sample was as required. The mechanical properties obtained by Al-Tabbaa (1987) were used to estimate the initial slurry height.

The initial height (H_i) of saturated kaolin slurry is given by :-

$$H_i = \frac{V_s}{A_t} (1 + w_i G_s) \tag{3.8}$$

where V_s is a volume of Speswhite kaolin powder, and A_t is a cross section area of test tank (0.3 m^2 for plane strain tank, 0.265 m^2 for cylindrical tank), and w_i is the initial water content of the slurry. In these tests, w_i was set to 120 %.

The ratio of initial to final height of the sample (H_i/H_f) can be obtained from the following

expression:-

$$\frac{H_i}{H_f} = \frac{1 + w_i G_s}{1 + w_f G_s} \tag{3.9}$$

where H_f and w_f are final height and water content at the end of consolidation. Based on the equations 3.3 and 3.4, the initial height of slurry was calculated. Also, the required water volume (V_w) and Kaolin powder weight (W_s) to produce the initial height of the slurry were estimated using the following equations:-

$$w_s = \gamma_w G_s V_s \tag{3.10}$$

$$V_w = H_w A_t = w_i G_s V_s \tag{3.11}$$

3.4.3 Shear Modulus of Clay

In order to express the values of liner stiffness used in the model tests in a non-dimensional form and also to perform elastic finite element analysis for comparison with the test results, it was necessary to estimate appropriate values of clay stiffness. These estimated values of clay shear modulus were then used to calculate the flexibility ratio (F) which is a non-dimensional number defined as the ratio of a measure of stiffness of the soil to the bending stiffness of the liner (refer to Equations 2.11 or 3.16).

The shear modulus of clay is known to be highly dependent on the magnitude of the strain, as well as being influenced by previous stress history (Syallebrass, 1990). The selection of an appropriate value of shear modulus to characterise the stiffness of a clay, therefore, is far from straightforward. A typical plot of shear modulus against strain level is shown in Figure 3.4.1. It is clear that three regions exist: i) very small strain (less than 0.001 %) where

shear modulus is independent of strain, ii) small strain (intermediate) where shear modulus reduces significantly with strain, and iii) large strain (greater than 1%) where the shear modulus is low. The selection of the clay shear modulus must therefore take account of the magnitudes of shear strain developed in the model tests.

Much of the early data on soil stiffness appears to have been based on measurements at soil strains corresponding to region (ii) although precise details of the strain levels at which the data were obtained are generally not given. Duncan and Buchigani (1976), for example, presented a plot of the undrained modulus ratio (E_u/s_u) against overconsolidation ratio (OCR) and plasticity index (PI). Ladd, *et al.* (1977) also presented the range of the undrained modulus ratio (E_u/s_u) as a function of stress level and OCR based on the data obtained from direct simple shear tests. In addition, Wroth and Houlsby (1985) suggested the relationship between undrained shear modulus ratio (G/s_u) and overconsolidation ratio (OCR) by combining the empirical relationships (Equation 3.12) and the modified Cam clay relationship (Equation 3.13) to give Equation 3.14:-

$$(G/\sigma_{vo'})_{oc} = (G/\sigma_{vo'})_{nc} (1 + C \ln OCR) \tag{3.12}$$

$$(s_u/\sigma_{vo'})_{oc} = (s_u/\sigma_{vo'})_{nc} OCR^{-\Lambda} \tag{3.13}$$

$$\frac{(G/s_u)_{oc}}{(G/s_u)_{nc}} = (1 + C \ln OCR) OCR^{-\Lambda} \tag{3.14}$$

in which C is an experimentally determined constant that is expected to be between 0 and 2. These correlations were based on the results of monotonic tests conduced in the triaxial or

direct shear apparatus. A value of C=1 appears to be representative of the trends observed in laboratory test data (Fred *et al*, 1990). Equation 3.14 relates the value of shear modulus, undrained shear strength and overconsolidation ratio. From these equations, it is clear that the ratio of G/σ'_{vo} increases with OCR, whereas the ratio of G/s_u decreases with OCR.

More recent work has concentrated on the variation of shear modulus with strain level. Jardine *et al* (1986), for example, studied the influence of non-linear stress-strain characteristics on the results of soil-structure interaction analyses. They concluded that although linear elasticity remains a convenient tool for expressing measurements of soil stiffness, unless the non-linear nature of soils is taken into account, soil-structure interaction computations and the interpretation of field measurements can sometimes be misleading. Recently, Viggiani (1992) and Viggiani and Atkinson (1995) investigated the variation of the shear modulus of fine-grained soil with state (i.e. current stress and overconsolidation ratio) and strain. They suggested that the shear modulus at small strain (G_o) is a useful parameter for characterizing the non-linear stress-strain behaviour of soil for monotonic loading. They also proposed the following expressions for G_o :-

$$\frac{G_o}{p_r} = A \left(\frac{p'}{p_r}\right)^n OCR^m \tag{3.15}$$

where A, m and n are non-dimensional parameters and p_r is a reference pressure.

For the speswhite kaolin used in these model tests, Davidson (1980), Al-Tabbaa (1987) and Smith (1993) proposed a linear relationship between the shear modulus and the mean stress. The results showed that a shear modulus ratio (G/s_u) depended on a mean effective stress and the values were highly scattered. Smith (1993) observed that the values of the shear modulus ratio (G/s_u) ranged from 100 to 250 for the kaolin samples. This range was

obtained from two sets of tests using the Marchetti Dilatometer, one where the samples were normally consolidated to a mean effective stress of 200 kPa, the second set to a mean effective stress of 450 kPa. The results also indicated that the values of G/s_u were highly scattered at a low mean effective stress of 200kPa. These results suggest that the value of G/s_u tend to increase with decreasing mean effective stress.

Recently, Viggiani and Atkinson (1995) also provided the data of shear modulus (G) for kaolin clay. Figure 3.4.2 shows stiffness-strain curves for a set of constant mean effective stress (p') drained triaxial compression tests carried out on normally consolidated samples of kaolin. These data clearly show that the values of G decrease with increasing strain and the effects of p' appear to decrease with increasing strain.

To select suitable values of shear modulus, it is necessary to develop an understanding of the levels of strains that are developed around the tunnels. In order to obtain some preliminary results, an elastic cavity contraction analysis was carried out in order to model the displacements caused by the installation of a single tunnel. This simple model suggested that when a contraction corresponding to 6% ground loss was applied (i.e. the value adopted in the model tests) then this led to a shear strain of about 1% at a distance of $2D$ from the tunnel axis (where D is tunnel diameter). The interaction tests were carried out at spacings of this order and so a strain value of 1% is thought to be reasonably representative. This would suggest that suitable values of soil stiffness may be derived from data given by Duncan and Buchigani (1976), Ladd et al (1971) and Wroth and Houlsby (1985) rather than from the more recent research on small strain stiffness.

A value of G/s_u of 200 for normally consolidated clay was chosen based on the chart proposed by Duncan and Buchigani (1976). This value was reasonably consistent with the data given by Smith (1993) and Viggiani and Atkinson (1995). The value of G/s_u for

overconsolidated clay was estimated using Equation 3.14 taking the constant C to be 1. The shear modulus of each clay samples estimated in this way are listed in Table 4.1 and 4.2.

A further assessment of the strains developed in the soil is provided by the results of the finite element analyses described in Chapter 7. These analyses were all based on the use of the values of shear modulus listed in Table 4.1 and 4.2. Typical values of incremental shear strain developed after the installation of a new tunnel are plotted in Figure 7.9 and 7.10 (Chapter 7) and discussed in Section 7.4. The results indicate that the local maximum shear strains developed around the existing tunnel liner (tunnel 1) are of the order 0.5% to 1.0% and similar to the results obtained from the cavity contraction analysis. It is clear that the strains decrease with distance. It is, however, interesting to note that at the boundary of sample shear strains are still greater than 0.001%. This suggests that beyond a distance from the tunnels of about $6D$, clay behaviour might be expected to be determined by its very small strain response.

3.5 Tunnel Liners

Stainless steel tubes, produced by Oxford Instruments (UK) Ltd. and Labertec Ltd., were used for the tunnel liners. Liners with two different stiffnesses were investigated (0.254 mm and 0.3556 mm). These thicknesses were selected on the basis of flexibility ratio (F) as described below.

The flexibility ratio (F) is a measure of the flexural stiffness of the soil relative to that of the liner. This ratio is expressed by:

$$F = \frac{2 E_s R^3 (1 - \nu_l^2)}{E_l t^3 (1 + \nu)} \qquad (3.16)$$

where E_l, ν_l, and R are respectively the Young's modulus (210 kN/mm^2), Poisson's ratio (0.3), and radius of the liner, and E_s and ν, are the undrained Young's modulus (see Section 3.4.3, Table 4.1 and 4.2) and Poisson's ratio (0.49) of the soil. The thickness of the tunnel liner is t (note that this equation is identical to Equation 2.11 except that I is replaced by $t^3/12$).

The flexibility ratios (F) of the two liners were about 200 and 70. Both liners would behave flexibly since the liner behaves relatively flexibly with respect to the ground for $F > 10$ (Peck *et al.*, 1972). Flexible liners interact fully with the soil. It is, therefore, expected that the use of flexible liners will lead to clearer indications of interaction mechanism in the model tests. Typical values of F for real tunnels lie in the range of about 5 to 300 although tunnels with a substantial concrete secondary lining may be less flexible than this. Segmental lining with articulated joints between segments are difficult to characterise using this approach, however. The linings themselves are relatively stiff.

The length of liners were 350 mm for parallel tunnels and 600 mm for perpendicular tunnels. For the perpendicular tunnels, two 125 mm liner segments were connected to each end of the liner (350 mm long) used in the parallel tunnel tests by soldering in order to use for cylindrical tests. The outer diameter of all of the liner was 69.85 mm. The same liner thickness was used for the instrumented and non-instrumented tunnels in each test. Details of the instrumented tunnel liner are given later in Section 3.7.

3.6 Tunnelling Machine

The model tunnelling machine used in these tests was designed based on the mechanism of the earth pressure balance (EPB) shield (Kitamura *et al.* 1981; Clough 1981) and hydro- or hydrojet shield (Stein, 1989) which is used for constructing mansize tunnels. Two main tunnelling mechanisms were considered in the development of this machine:

i) The machine provides an overcut in order to model the ground loss that occurs on tunnel installation,

ii) The full face cutting head supports the earth to minimise the ground deformations in front of the tunnel face.

A general view of the model tunnelling machine used in the tests is shown in Figure 3.5. Details of the mechanisms of this machine are described below.

3.6.1 Rotary cutting head

The rotary cutting head was designed as a full flat-faced plate type as shown in Figure 3.6. The diameter of head is 72 mm to produce the over-cutting ratio ($\Delta A/A$) of 6 percent, which is defined as the ratio of overcutting area (ΔA) to cross-sectional area of tunnel (A). Two blades are mounted on the cutting face to excavate the soil. The cutting head is rotated through a central shaft by a 24 Volts-DC geared servo motor. This power is provided by DC Servo Amplifiers. The maximum torque is about 800 N cm. The rotation speed may be varied from 0 to 9 rpm in either direction. The excavation can proceed at the rate of 4 mm per rotation of the cutting head. A maximum tunnelling speed of 36 mm/min can be, therefore,

made.

3.6.2 Water jet system

The water jet system was designed to break up and remove horizontally the soil excavated by the rotary cutting head (see Figure 3.6). Three stationary nozzle units which have several orifices of 1.0 mm diameter are mounted just behind the rotary cutting head with a polar angle of 120°. The water pressure at the nozzle orifice is set within a range of 200 to 300 kPa, which is enough to crush and separate quickly the excavated soil. The crushed and separated soil is automatically removed from the tunnel face by gravity water flow.

3.6.3 Jacking systems

As shown in Figure 3.5, the main jack is located at the end of the machine body at which the load transformer unit and motor are also mounted. The jacking force is produced manually by rotating a 10 mm diameter threaded bar. This force is transmitted simultaneously to the central shaft and to the two side shafts. The central shaft pushes the rotary cutting head, and the side shafts push the liner. The water jet pressure was controlled by an adjustable valve.

3.6.4 Reference Frame

The reference frame is the steel structure to which the tunnelling machine was attached. It also provides support for any additional accessories needed during tunnelling. It

mainly consists of an adjustable guide lane to maintain the alignment of the tunnelling machine, a levelling plate to adjust the tunnel axis, and a holding frame to fix to the test tanks as shown in Figure 3.7.

3.7 Instrumentation

3.7.1 Instrumentation Systems

Instrumentation systems were used to carry out the measurement of the following:-

i) clay behaviour during consolidation,

ii) tunnel liner behaviour,

iii) tunnel position during installation,

iv) radial displacements of tunnel,

v) surface settlements.

During the model tests, data acquisition was accomplished using an E500 Translog datalogger, manufactured by RDP Electronics Ltd. The datalogger consisted of four main modules. Each module has eight channels capacity. Details are given in Section 3.8.

The instrumentation systems are schematically shown in Figure 3.8 [a]. A total of thirty one channels were used in the instrumentation systems. Each channel was connected to one of the modules in the datalogger, which was controlled by an IBM AT personal computer. Figure 3.8 [b] shows a photograph of the datalogger with computer. Software supplied by RDP Electronics Ltd. was used to record the test data at set intervals of time, to convert it into engineering units and to format it for analysis using a spreadsheet. The

recording time intervals indicated in Table 3.5 were generally adopted in each test stage.

Table 3.5 Recording Time Intervals

Test Stage	Sample Preparation	During Tunnelling	After Tunnelling
Time Intervals (sec)	60 to 900 sec	20 sec	60 to 900 sec

3.7.2 Instrumentation on Test Tanks

In order to monitor the consolidation processes in each model test, total pressure and pore water pressure, settlement, and consolidation pressure were measured in each test tank. One total pressure and one pore pressure transducer was installed in the front of the wall of each test tank to measure the horizontal earth pressure and pore water pressure at the same level as the instrumented tunnel axis (see Figure 3.1 and 3.2). The total pressure transducers were the Kyowa miniature pressure transducer (PS-2KB) for the plane strain tank and a Druck pressure transducer for the cylindrical tank. The pore pressure transducers were the Druck PDCR 81 for both test tanks.

During consolidation of each sample, a 400 mm stroke LVDT manufactured by Sangamo Transducers was used to monitor the descent of the platen. The consolidation pressure was also monitored using pressure gauges.

The instruments installed on each of the test tanks (PS and CY tanks) are summarized in Table 3.6.

Table 3.6 Summary of the Instrumentation on each test tank

Instruments	No.(ea)	Measurements
Oil Pressure Gauge	1	Consolidation Pressure
Pressure Transducer	1	Total horizontal Pressure
Pore Water Pressure Transducer	1	Pore water pressure
LVDT	2	Settlement

3.7.3 Instrumentation on Tunnel Liners

The instrumented liner was installed with eight strain gauges on the outside of the tube for evaluating the bending moments, four miniature pressure transducers for observing the total pressure on the liner, and two pore pressure transducers. These instruments were located around the mid length cross-section of the liner in positions indicated in Figure 3.9[a]. The connecting wires were protected by steel pipes of 2 mm diameter installed along the inside of the liner. Figure 3.9[b] shows a photograph of an instrumented liner illustrating each instrument position and connecting wires.

Strain gauges manufactured by Measurements Group, Inc., were installed on the outside of the liner. Each of these strain gauges had a 350 ohm resistance and a gauge factor of 2.105, and formed one arm of its own Wheatstone bridge circuit. The excitation was 3 volts incorporated in the datalogger (see Section 3.7.1). Due to the nature of the strain gauge recording system incorporated into the datalogger no direct calibration of the liner strain gauges was required. Only a calibration of the strain gauges was performed. Details of the calibration procedures are given in Section 3.8.

Two types of miniature pressure transducer (PS-2KA, PS-2KB) (which were 5 mm in

diameter, 0.2 mm thick and manufactured by Kyowa Co., Ltd.) were used with a securing flange (Figure 3.9 [a] and [b]). The maximum range of the pressure transducer was 200 kPa, with a rated output of 0.839 mV/V and 0.856 mV/V, and the excitation was also 3 Volts.

In order to measure the pore water pressure, a 10 mm diameter and 3 mm thick porous filter tip was installed on the liner with a 2 mm thin steel tube as shown in Figure 3.9 [a] and [b]. During tests, a pore water pressure transducer (Druck PDCR) was connected to the tube. Details of the connection procedures are given in Chapter 4. The size of porous filter tip was designed based on the hydrodynamic time lag which is the time required for water to flow into or out of the piezometer to effect equalization (Penman,1960; Brand and Premchitt,1982). The transducers were powered by a stabilized 5 Volts supply and had a sensitivity of 0.011 mV/V/kPa.

The calibration of all pressure transducers installed on the liner was performed using a special calibration device. This device consisted of a rubber sheet surrounding the liner and a pressure system as shown in Figure 3.10 [a]. The uniform hydrostatic pressures applied in each step were measured by a digital pressure indicator (DPI). Figure 3.10 [b] shows a view of this calibration setup.

All instruments installed on the liner are listed in Table 3.7.

Table 3.7 Summary of the Instrumentation on the liner

Instruments	No.(ea)	Measurements
Strain Gauges	8	Strain of outer liner surface
Pressure Transducer	4	Total radial pressure acting on the liner
Pore Water Pressure Transducer	2	Pore water pressure acting on the liner

3.7.4 Instrumentation of Tunnel Installation

As described in section 3.6, the jacking force and the tunnel advance were monitored during the installation of each model tunnel. A D95 load transducer was used to measure the jacking force, which is necessary to evaluate the tunnel face pressure and liner friction during tunnelling. The load transducer has a maximum range of 2.5kN and a sensitivity of 2.7 mV/V.

A 500 mm long stroke Linear Variable Differential Transformer (LVDT), was used to evaluate the tunnelling speed for each model test. The LVDT was calibrated against a steel ruler.

3.7.5 Radial Displacement Measuring Device (RDMD)

The two different types of radial displacement measuring devices, namely RDMD1 and RDMD2, were developed and used to monitor the radial displacement of the liner.

The RDMD1, similar to those used by Britto (1979) and Taylor (1984), consisted of four strain gauged cantilevers made from stainless steel as shown in Figure 3.11[a]. The properties of this material are Young's modulus (E) of 210 kN/mm^2 and yield stress (σ_y) of 1600 N/mm^2. These cantilevers were mounted on a specially machined aluminium block to measure radial displacements of the crown, invert and both springlines of the tunnel liner. The maximum range of each cantilever was 20 mm corresponding to the maximum elastic deflection. Each cantilever was 70 mm long, 5 mm wide, 0.25 mm thick and inclined to the horizontal at 40°. A dome type tip was attached to the free end of each cantilever to ensure good contact with the measuring points.

The RDMD2 was specially designed to confirm the radial displacements of the liner

measured by RDMD1 since the RDMD1 was sensitive for changing the temperature. Although this device was similar to RDMD1, the measurement mechanism was quite different. This device monitored the radial displacements by means of converting the displacement direction from the radial to axial. Figure 3.11 [b] shows the mechanism of this device. It consisted of four arms connected with small bars to corresponding LVDTs. A small roller was mounted at the end of each arm to move smoothly in the liner. The middle of each arm was fixed to a mounting block with a pin to allow rotation to occur. Two end points of the small bars were also connected with a pin to the arms and LVDTs. The LVDTs had a maximum working range of 10 mm.

Both RDMDs were calibrated against a micrometer.

3.7.6 Surface Settlement Measurement Device (SSMD)

The Surface Settlement Measurement Device (SSMD) was designed and developed to measure the surface settlement as shown in Figure 3.12. Although the settlements were obtained for zero surcharge pressure, they were useful for evaluating the trend of the ground loss and shape of the settlement trough. However, the measured data were not presented in this dissertation. The SSMD consisted of a LVDT, mounted on a horizontal bar. The LVDT was calibrated against a micrometer.

3.8 Accuracy of Measurement Systems

In general, the accuracy of measurements is related to the datalogger capacity and transducers quality in the instrumentation system. Figure 3.8 shows schematically the

instrumentation system adopted in thes model tests. Sources of measurement errors may be an electronic interface (noise) both internal and external to the system, temperature effects and long-term drift. This section describes the accuracy of measurement systems used in the model tests.

3.8.1 Datalogger

Data were collected automatically using a translog 500 datalogger. This is a general purpose, medium speed, data acquisition system, designed for use with a personal computer. The base unit (E505) comprises a power supply, computer module (E504) and 8 slots for signal conditioning modules. The E504 computer module is an intelligent instrumentation front end, designed to turn any personal computer with an RS232 serial port into a powerful data acquisition system. Logging facilities provided by E504 computer module are as follows;-

i) up to 256 channels per second data acquisition in the same mode.

ii) Digital filtering (average between 1 and 255 A/D conversions).

iii) On-board data storage, up to 8192 reading values can be stored.

iv) ±15 bit accuracy (1 in 32768) of analogue to digital conversion (A/D conversion).

In addition, this module controls the operation of the signal conditioning modules, and performs a variety of data logging tasks. Details of the signal conditioning modules used in this instrumentation system are given in section 3.8.2.

The E504 computer module included two modes of A/D conversion; i) normal mode and ii) ratiometric mode. For the normal mode, the transducer signal for the selected channel

is converted directly to a 16-bit digital value and stored in RAM. For the ratiometric mode, the transducer signal input and transducer excitation voltage input (ratiometric inputs) are converted to 16-bit values. The ratiometric value is then used as a reference to measure any drift in the transducer excitation voltage, and the transducer value is automatically adjusted accordingly. This mode was adopted in this measurement system in order to improve the stability of long term data-logging.

3.8.2 Instruments

Two different signal conditioning modules were used in this instrumentation system; i) LVDT scanner (E510) and ii) strain gauge scanner (E511). Each module is a complete signal conditioning unit, capable of providing amplification and excitation for LVDTs, strain gauges (quarter bridge configuration), and pressure transducers (full bridge configuration).

For the output data measured from each transducer, there are many factors that can influence the signals and therefore the linearity of any data capturing system. Not only is there the linearity of the transducers themselves, but also the linearity of the datalogger as well as electronic interface (noise) both internal and external to the system. Therefore, it was necessary to calibrate the system in the configuration that it would be used during the actual testing programme. This ensured that all the factors likely to affect the linearity of the logging system were included in the PC screen output.

All the transducers were calibrated against very accurate known forces and the screen output was used to produce the calibration constants. This method obviated any need to investigate in great detail the accuracy of any signal component in the system. Linear regression was then performed on the calibration curves to produce figures for the accuracy

of the engineering units produced by the curves. The accuracy of each of the instruments are given below.

3.8.2.1 Strain Gauges on the liner

The strain gauges used to measure liner strain were calibrated using stainless steel cantilevers as shown in Figure 3.13. The gauge factor provided from the manufacture was then checked. Details of the specification of the strain gauge are described in Section 3.7.3. This calibration exercise suggested that the accuracy of measurement is ±10 $\mu\varepsilon$. This corresponds to a possible non-linearity error in measured bending moments of less than ±0.05 Nm assuming no hoop stress. Figure 3.14 also shows long-term stability.

3.8.2.2 Pressure Transducers

Details of calibration procedures are presented in 3.7.3. The possible non-linearity errors in measured total and pore water pressures are ±0.05 and ±0.15 kPa, respectively. It was noticed that the measurement of pore water pressure was less accurate than that of total pressure. This is mostly due to flexible leads which expand under positive water pressures and response time (Section 3.7.3).

3.8.2.3 Radial Displacement Measuring Devices (RDMD)

For the radial displacement measuring devices (RDMD1 and 2), the accuracy of measurement for RDMD1 (strain gauge type) is ±5 $\mu\varepsilon$ and the possible error in measured

radial displacement of the tunnel liner for RDMD1 and 2 are ±0.05 mm and ±0.01mm. Both RDMDs were calibrated against a micrometer.

Figure 3.14 shows the typical results measured from each instrument for about 4 days. The results show that all instruments used in this measurement system were relatively stable over the 4 day period. It was found that the stain gauge type transducers (strain gauges, pressure transducer) show some fluctuation. This may be due to room temperature (i.e. the temperature variations in day and night). However, this model test programme only considered short-term incremental behaviour (about 1 hour which was time taken for tunnel installation) so that the data measured within about 1 hour could not be influenced by long-term drift, noise and temperature.

3.9 Vane Test Apparatus

The vane test apparatus was originally manufactured by Wykeham Farrance Engineering Ltd. Some modifications were made to use it appropriately in the test tanks. The vane tests were performed at various levels to measure the undrained shear strength (s_u) to be used in the evaluation of the real soil strength profile during tunnelling. Details of test procedure and locations are given in Chapter 4. The main elements of the apparatus are shown in Figure 3.15. The vane was 15 mm in diameter and 30 mm long. The rotation speed of the vane was 1 rpm in all tests. The calibration of the shear vane was carefully carried out using existing apparatus in the laboratory (Smith, 1993; Martin, 1994). The undrained shear strength corresponding to a known applied torque was calculated using the standard BS 1377 (1975) relationship given below:-

$$T_q = \frac{1}{2} \pi D_v^2 H_v \left[1 + \frac{D_v}{3H_v}\right] s_u \qquad (3.17)$$

where T_q is the applied torque, D_v and H_v are the vane blade diameter and height respectively, s_u is the undrained shear strength. Based on the dimensions of the vane as mentioned above and the calibration factor, the s_u values were computed from the following relationship:

$$s_u\ (kPa) = 0.06851\ R_v \qquad (3.18)$$

where R_v is the reading value from vane test apparatus.

CHAPTER 4

EXPERIMENTAL PROCEDURE

4.1 Introduction

As outlined in Chapter 1, two types of model tunnel test series were conducted: tests on parallel model tunnels and on perpendicular model tunnels. Different types of tanks, described in Chapter 3, were used in each test series. Both types of model test are represented schematically in Figure 4.1. Details of the sample preparation and test procedures for each of the two types of test are described in this chapter.

4.2 Sample Preparation

4.2.1 Preparing the Test Tanks

Details of the assembly procedure for the plane strain and cylindrical tanks used in the study are given below.

For the plane strain tank, the front and rear perspex walls were fixed in place by lining the inside of the 'O-ring' seat with transparent Superflex silicone sealant, and then bolting to the steel side frame. After assembly of these walls, the bottom drainage lines were checked for blockages. The tank was filled with water and the bottom tap was closed. The total pressure and pore water pressure transducers were installed and fixed to the perspex face at

the relevant ports. The insides of the perspex walls also were coated carefully with Silicone grease.

Three pairs of plugs with O-ring seals were fixed onto the front and rear walls in order to seal the tunnel installation ports. In order to install the guide shaft for aligning the tunnel axis during tunnelling, a removable M12 bolt was mounted at the centre of each of the plugs. PTFE tape was wound around the thread of the bolt to obtain a good seal.

The top surface of the test tank was lined with a sealant, before lowing the top-extension onto it, using the overhead crane. The extension was then bolted down, and bracing-pillars were connected to the outside of the tank to prevent bulging of the walls during consolidation. Finally, a saturated piece of 3.2 mm thick porous Vyon sheet was laid on the bottom of the tank.

For the cylindrical tank, the assembly procedure was essentially the same as for the plane strain tank except that it was not necessary to install a top-extension and outside bracing.

4.2.2 Preparation of Speswhite Kaolin Slurry

A slurry of Speswhite kaolin was formed by mixing the dry clay power with water in a 110 litre ribbon blade mixer. Details of this mixer are given by Gue (1984) and Love (1984). To ensure that the slurry was free of air bubbles, the mixer was operated under a vacuum of about 30 kPa absolute pressure. A higher vacuum would have been desirable but Mair (1979) and Smith (1993) found that problems would have occurred both with kaolin powder being sucked out of the mixer and with obtaining an adequate seal.

With regard to water content of the slurry, Sheeran and Krizek (1971) recommended

that a water content of 120 %, which is approximately twice the liquid limit (*LL*), is suitable for the preparation of uniform clay beds using slurry consolidation. Smith (1993) and Martin (1994) also adopted a water content of twice the liquid limit. Anderson *et al.* (1989), however, used a water content of 1.5 times the liquid limit (*LL*) (to reduce the volume changes required) with no apparent detrimental effect on the uniformity of the final sample. In these model tests, however, to form a pumpable slurry and prevent the formation of fabric features during the pumping stage, a water content of 120 % (± 2%) was adopted.

Three mixer batches were required to fill each of the test tanks (plane strain and cylindrical tanks). A mixing time of approximately three hours was required to form a homogeneous kaolin slurry. After mixing, the slurry was pumped out of the mixer using a diaphragm slurry pump and deposited in the fully assembled test tanks under 200 mm of water to prevent desiccation and air entrainment.

4.2.3 Consolidation of the Clay

When the desired level of slurry in the tank was reached, a piece of 3.2 mm thick porous Vyon sheet was laid on top of the slurry. Pressure was then applied on the top platen to consolidate the kaolin slurry in each of the test tanks. The consolidation pressure was generally applied in five stages, to produce homogeneous test samples, with each stage continuing until the completion of primary consolidation. During the first load increment, the sample was left to drain at both its top and bottom for about 48 hours. Subsequent load increments were applied at intervals of not less than 3 days, each increment being approximately twice the previous increment. The process of consolidation was much the same as followed by other researchers preparing Speswhite kaolin samples of similar dimensions

(e.g. Love,1984; Gue,1984; Martin,1994). The maximum consolidation pressures (final vertical stresses, p_{max}) of approximately 88.5 kPa and 120 kPa were adopted to produce the normally consolidated clay samples and overconsolidated clay samples ($OCR \approx 3$) respectively. These final consolidation pressures were greater than the values required when s_u = 20 kPa (see Table 3.4). Therefore, the shear strengths of the clay samples were slightly greater than 20 kPa. Details of the clay strength are described in Section 4.6. The ratios of initial to final height of the sample (H_i/H_f) for the normally consolidated and overconsolidated clay samples were 1.8 and 1.9 respectively. The consolidation of the clay was monitored with a 0.5 m stoke LVDT measuring the platen movement. In addition, total pressures and pore pressures were also measured during consolidation. Typical results of consolidation curves observed in each of the tanks are presented in Figure 4.2.

4.2.4 Surcharge on the Samples

After the final consolidation increment was completed, the bottom tap was closed and the pressure reduced in stages. No single unloading step was great enough to cause cavitation, and each unloading step was separated by a two hour gap. After unloading and removing the platen top-extension piece, several rubber balloons containing water were placed on the top of the sample and the sample was reloaded to produce a stress controlled boundary on its top surface. After installation of the balloons, the sample was reloaded to the maximum consolidation pressure (p_{max}) for the normally consolidated sample, and one third of the maximum consolidation pressure ($\frac{1}{3}p_{max}$) for the overconsolidated sample. These pressures were maintained for five days to allow excess pore water pressures to dissipate.

The total time required for sample preparation was just over one month. Figure 4.3[a]

and [b] show views of the assembled plane strain tank during consolidation and with the stress controlled top surface respectively.

4.3 Model Test Procedures

4.3.1 Introduction

After the clay sample preparation was complete, the water level was maintained at 5 cm above the top surface of the sample in order to ensure that the clay remained saturated. The pore pressures and horizontal total pressures of each of the samples were carefully monitored until they stabilized. Before the start of each of the tests, all instruments to be monitored during testing, as described in Section 3.7, were warmed up and continuously scanned by the data-logger until the output values stabilized .

At the start of each test, a tunnel liner was installed at position 1 (see Figure 4.1). This liner was instrumented with strain gauges on the outside of the tube to allow estimates of the bending moments in the liner to be made. Total stresses and pore water pressures were also measured using the pressure and pore water pressure transducers mounted on the tube (see Chapter 3).

After swelling and consolidation processes associated with the tunnel installation were complete, a second, non-instrumented, tunnel was installed in position 2 (see Figure 4.1). At this stage, the radial displacements of the instrumented tunnel were measured using the specially developed devices (refer to Section 3.7.5). The RDMD1 was used in the parallel tunnel tests to measure the radial displacement of the instrumented tunnel and both RDMD1 and RDMD2 were used in the perpendicular tunnel tests. After sufficient time had passed for

the pore water pressures to dissipate, a third, non-instrumented, tunnel was installed in position 3. The installation interval for each of the model tunnels was about 10 days. Tunnel installation procedures were the same for the plane strain and cylindrical tanks.

4.3.2 Model Tunnel Installation

All model tunnels were installed using the model tunnelling machine described in Section 3.3. As the excavation proceeded, the tunnel was lined (i.e. the tunnel liner was installed just behind the cutting head of the machine).

In order to model full scale shield tunnelling techniques, the following installation procedures were used:

Step 1 : Fix the reference frame

The reference frame described in Section 3.6.5, was fixed at the front of the test tank to hold the tunnelling machine. The cylindrical tank required extension pieces in order to fix the reference frame to the test tank.

Step 2 : Install the guide shaft

The M10 bolts mounted at centre of the perspex plugs were unscrewed and an auger was inserted carefully into the sample. The guide shaft consisting of a 9.5mm diameter steel bar was installed into the clay sample by auger. The purpose of the guide shaft is to align the tunnel axis during tunnelling.

Step 3 : Adjust the centre-line of the tunnel

The tunnel axis was adjusted carefully using the levelling plate mounted on the reference frame (see Figure 3.7). The guide lane frames were also mounted on the levelling plate.

Step 4 : Assemble the tunnelling machine

The tunnelling machine was assembled on the guide lane.

Step 5 : Check the machine operation and the liner

The operating system of the tunnelling machine including the cutting head, water jet system, jacking system, instruments and so on, was checked. The outside surface of the liner was carefully coated with silicone grease to reduce the friction between liner and clay during the installation. After that, the threaded plug in the front perspex wall was removed and the cutting head was connected to the guide shaft.

Step 6 : Operate the tunnelling machine

After setting up the recording time interval, excavation of the tunnel could begin. A cutting head rotation speed of 9 rpm and tunnel advance speed of about 10 mm/min were normally adopted during tunnelling. To counteract the changing face pressure and to maintain a constant speed, the advance of the tunnel was controlled by hand.

In order to ensure consistency for installation of each of the tunnels, the jacking forces were measured by a load cell mounted on the tunnelling machine. The measurements of tunnel advance speed and pressures are described and discussed later in this chapter.

Step 7 : Dismantle the tunnelling machine

After installation of the model tunnel liner, the tunnelling machine set was carefully dismantled and removed from the test tank.

Step 8 : Sealing the gap between liner and hole

The gap between the liner and the hole at the front and rear tank walls, was sealed with grease in order to prevent drainage.

A summary of the installation steps for the model tunnel is shown schematically in Figure 4.4.

4.3.3 Connection of Pore Water Pressure Transducers

The pore water pressure transducers were connected to plastic tubes which were attached to the end of the liner immediately after installation of tunnel 1. Details of this transducer system are described in Chapter 3.

Before connecting the plastic tubes, they were filled with de-aired water using a

special syringe having a long catheter. Details of this procedure are shown schematically in Figure 4.5.

4.3.4 Installation of Radial Displacement Measuring Device

The radial displacement measuring device (RDMD1 in parallel tunnel tests, RDMD1 and RDMD2 in perpendicular tunnel tests) was installed inside the liner after tunnel 1 was installed. Details of this device are given in Section 3.7.4.

Firstly, the holding plate for the centre-line shaft was fixed to the front of the tank wall by two bolts. After that, the centre-line shaft with the device was carefully inserted inside the liner so as not to touch the mounted instruments until the tips of the cantilevers were positioned at the centre of the liner. Finally, the shaft was held at the rear end by another holding plate, and was gently rotated to place the measuring points accurately at the tunnel crown, two springlines, and invert. Figure 4.6 shows graphically the arrangement used to install this device.

4.4 Model Test

Two separate test series were carried out:

i) parallel tunnels test series;

ii) perpendicular tunnels test series.

The parallel tunnel test series are summarized in Table 4.1. In this table, W is the pillar width defined as the distance between the two tunnels, and C/D^* is the ratio of tunnel

depth to diameter. $PS3^R$ is a repeat test for PS3 to investigate the repeatability of the model tests. The results of tests PS3 and $PS3^R$ were generally in quite good agreement. Details of these results are presented in Chapters 5 and 6.

Table 4.1 Summary of the parallel tunnels test series

Test Series		PS1	PS2	PS3	PS4	$PS3^R$
Test No.	'Instrumented' Tunnel (Single)	**PS1E**	**PS2E**	**PS3E**	**PS4E**	**$PS3E^R$**
	'Distant' Tunnel (W=1.0D)	**PS1D**	**PS2D**	**PS3D**	**PS4D**	**$PS3D^R$**
	'Close' Tunnel (W=0.4D)	**PS1C**	**PS2C**	**PS3C**	**PS4C**	**$PS3C^R$**
Surcharge Pressure, p_{sur} (kPa)		88.5	38.35	88.5	41.3	88.5
Sample Height, H, (m)		0.46	0.49	0.50	0.48	0.49
C/D^*		3.36	3.79	3.94	3.65	3.79
Clay	$s_{u\text{-}avg}$ (kPa)	23.4	24.3	20.7	24.3	21.6
	OCR_{avg}	1	2.93	1	2.81	1
Shear Modulus, G=E_s/3 (kPa)		4680	4270	4140	4330	4320
Flexibility Ratio, F		212	194	68	72	71

The values of average undrained shear strengths, $s_{u\text{-}avg}$, were calculated from the laboratory shear vane values using the theoretical approach (refer to Section 3.8). Details of the shear vane measurements are described later in this chapter. The values of OCR_{avg} were also estimated based on the stress history after the clay sample preparation. Values of shear modulus were estimated using the procedures described in Section 3.4.3.

The perpendicular tunnels test series are summarized in Table 4.2.

Table 4.2 Summary of the perpendicular tunnels test series

Test Series		CY1	CY2	Remarks
Test No.	'Instrumented' Tunnel (Single)	**CY1E**	**CY2E**	S = Clearance between tunnels.
	'Lower' Tunnel (S=1.0D)	**CY1L**	**CY2L**	
	'Upper' Tunnel (S=0.4D)	**CY1U**	**CY2U**	
Surcharge Pressure, p_{sur} (kPa)		89.04	88.2	
Sample Height, H, (m)		0.503	0.488	
C/D*		3.69	3.48	
Clay	$s_{u\text{-}avg}$ (kPa)	23.6	22.7	
	OCR_{avg}	1	1	
Shear Modulus, G=E$_s$/3 (kPa)		4710	4530	
Flexibility Ratio, F		214	75	

In Table 4.2, the values of $s_{u\text{-}avg}$ and OCR_{avg} were also obtained based on the laboratory shear vane tests and the stress history after the clay sample preparation.

Each of the test series took about ten weeks, in which the first four to five weeks were taken up with consolidation of the sample and preparation of the model; the next five to six weeks were spent in model tunnel testing and miniature site investigation. Figure 4.7 shows a typical view of tunnel installation.

4.5 Jacking Pressures and Tunnel Advance Speed

This section is concerned with the jacking pressures and the tunnel advance speed during installation of the model tunnels. The clay around the tunnel face (i.e. the cutting face) was excavated while the pressure of the cutting head supported the tunnel face.

Figure 4.8 [a] shows typical variation of the jacking pressure (p_a) against the tunnel advance. In this figure, the values of p_a were calculated by Equation 4.1.

$$p_a = \frac{F_a}{A_a} \tag{4.1}$$

where, F_a is the measured jacking force during the tunnel is advanced, and A_a is the cross sectional area of the cutting head (note that the p_a values may not be fully acting on the tunnel face).

The results show that the jacking pressures gradually increased as the tunnel moved forward. This jacking pressure increase may be caused by increasing friction between liner and clay as the embedded length of the liner is increased. It was also observed from Figure 4.8 that the jacking pressure was applied consistently during the installation of each of the tunnels.

Table 4.3 gives a summary of the range of maximum jacking pressures (p_{amax}), observed during installation of the tunnels in each test series. In this table, the overburden pressures ($p_o = p_{sur} + \gamma H$, where H is the depth of the instrumented tunnel) at each tunnel axis are also included to compare with the values of p_{amax}.

The results show that the values of p_{amax} , in all test series, were smaller than the corresponding overburden pressures. That is, there was no danger of blow-out arising from excessive tunnel face pressure during the tunnel advance. In addition, backward movements of the tunnel face, caused by insufficient face pressure, can be neglected because the tunnelling machine was designed not to allow backward movements during tunnelling.

Table 4.3 Range of maximum jacking pressures (p_{amax})

Parallel Tunnels Test Series			**Perpendicular Tunnels Test Series**		
Test Series	p_{amax}(kPa)	p_o (kPa)	Test Series	p_{cmax}(kPa)	p_o (kPa)
PS1	20 - 30	92.4	CY1	60 - 65	93.4
PS2	10 - 20	42.8	CY2	40 - 61	92.3
PS3	20 - 44	93.1	$PS3^R$ = Repeat test for PS3 series.		
PS4	10 - 30	45.1			
$PS3^R$	25 - 42	92.9			

For consistent performance of model tunnel installation, a constant speed should be adopted for each tunnel. Figure 4.8 [b] shows typical variation of the tunnel advance speed. The results show that the tunnel advance speed was relatively constant during tunnelling. The average was about 10 mm/min, which was about 30 per cent of maximum tunnelling speed estimated from the cutting head rotation speed (refer to Section 3.6.1).

4.6 Site Investigation of Clay Samples

4.6.1 Introduction

Site investigation is an essential part of any test study, being no less important for reduced scale model tests than for full scale field trials.

This section presents details of the miniature site investigation performed in each of the samples. The purpose of this investigation is to confirm the estimated clay strengths for each of the samples. The investigation results are also interpreted theoretically in this section.

The miniature site investigations consisted of shear vane and water content tests. Details of the procedures and apparatus of shear vane tests are given in Section 3.8.

4.6.2 Shear Vane and Water Content Tests

The shear vane tests and moisture content sampling was carried out in each clay sample of the test series. The vane tests were carried out with two different surface stress conditions:

i) with the surcharge pressure (p_{sur})

ii) without surcharge pressure.

Under the surcharge pressure, the horizontal shear vane tests with the corresponding water content sampling were performed using the two holes, which were located at the same level as the horizontal axis of the instrumented tunnel and are shown in Figure 4.9 and 4.10.

In order to perform the vane tests without surcharge pressure, the pressure was gently released by stages so as not to develop cavitation in the clay sample, until negative pore water pressure was fully dissipated. At least two days were needed to stabilize fully each clay sample. The shear vane tests with corresponding water content sampling were performed at different depths in nine boreholes for the plane strain tank samples (see Figure 4.9), and in four boreholes for the cylindrical tank samples (see Figure 4.10). Figure 4.11[a] and [b] show views of both vertical and horizontal shear vane tests.

Water content specimens (typically of about 40 grams) were taken and weighed to the nearest 0.01 grams as quickly as possible after sampling. Each specimen was then oven dried and re-weighed in accordance with BS 1377 to determine its water content.

Table 4.4 shows a summary of the miniature site investigation for each clay sample.

Table 4.4 Summary of No. of tests in site investigation

Test Tanks	PS tank					CY tank	
Clay Sample	PS1	PS2	PS3	PS4	PS3^R	CY1	CY2
s_u-tests with p_{sur}	2	2	4	4	2	3	2
s_u-tests without p_{sur}	43	52	52	43	52	16	16
Water Content Tests	45	45	45	45	45	19	18

4.6.3 Measured Undrained Shear Strength and Water Content

Figures 4.12 show five sets of the undrained shear strength (s_u) distributions measured after each set of the test series in the plane strain tank was complete (without surcharge pressure). The results show that overall values of s_u increased with depth. It is clear that the clay strength variations were relatively larger around the tunnel, although somewhat erratically. The corresponding water content distributions are shown in Figure 4.13.

Figure 4.14 [a] shows a plot of water content against undrained shear strength. The data plotted in this figure were measured from the plane strain tank and cylindrical tank samples. Even though there is considerable scatter, there appears to be general verification of the expected straight line relationship (Muir Wood, 1990). Figure 4.14[b] shows not only the points from Figure 4.14[a] but also the range of the measured values presented by Smith (1993) and Martin (1994) for Speswhite kaolin samples with different strengths. The results obtained in this study seem to be consistent with these previously proposed correlations.

4.6.4 Theoretical Variation of Undrained Shear Strength Profile

This section is concerned with the interpretation of the observed undrained shear strength profiles.

Based on the relationship between undrained shear strength and *OCR* described in Section 3.4.2.1, the observed variation of s_u for each clay sample can be regressed by a nonlinear fit defined as:-

$$s_u = \left(\frac{s_u}{\sigma'_{vo}}\right)_{nc} \sigma'_{vi}\, OCR^{\Lambda} \qquad (4.2)$$

This equation is identical to Equation 3.3 except that σ'_{vo} is replaced by σ'_{vi} which is the effective vertical stress at a depth z after the compressive load on the sample surface was released.

Figures 4.15 and 4.16 show the best fit to the measured strengths over the depth range considered. In each of these plots, two pairs of s_u profiles are plotted:

i) the measured and calculated s_u values without surcharge pressure;

ii) the measured and calculated s_u values with surcharge pressure.

The best fit was obtained by means of iteration using the different values of $[s_u/\sigma'_{vi}]_{nc}$ and Λ. Consequently, the measured values were in good agreement with the results obtained from the theoretical approach when the values of $[s_u/\sigma'_{vi}]_{nc}$ and Λ were 0.25 and 0.84 respectively. These values were also consistent with the values adopted in the determination of maximum consolidation pressures (see Section 3.4.2.1). In general there are few outlying values in the strength, indicating that good repeatability was achieved in preparing the kaolin samples.

The values of $[s_u/\sigma'_{vi}]_{nc}$ and Λ adopted to find the best fit, also fall within the typical range proposed by previous researches. Seneviratne (1979) suggested that the $[s_u/\sigma'_{vi}]_{nc}$ values were generally ranged from 0.21 to 0.26 for one-dimensional consolidated kaolin. Ladd *et al.* (1977) obtained a good fit to their data by varying Λ from 0.85 to 0.75 with increasing *OCR*. Martin (1994) suggested that an appropriate value of Λ was 0.754.

The following approach was adopted to calculate the values of σ'_{vi} and *OCR*. Consider a soil element at a depth z below the surface of each clay sample with submerged unit weight γ'. During the consolidation procedure described in Section 4.2.3, this element is subjected to a maximum vertical effective stress of:-

$$\sigma'_{vo} = p_{max} + \gamma' z \tag{4.3}$$

Upon some or total removal of the compressive load from the sample surface, and after negative pore water pressures have dissipated, the effective vertical stress becomes:-

$$\sigma'_{vi} = p_{sur} + \gamma' z \tag{4.4}$$

where p_{sur} is the surcharge pressure. Therefore, the *OCR* at depth z is given by:-

$$OCR = \frac{p_{max} + \gamma' z}{p_{sur} + \gamma' z} \tag{4.5}$$

The submerged unit weight of the unloaded clay sample may be estimated from

$$\gamma' = \left(\frac{G_s - 1}{w\, G_s + 1} \right) \gamma_w \tag{4.6}$$

where γ_w is the unit weight of water and w is the water content.

CHAPTER 5

RESULTS OF MODEL TESTS

5.1 Introduction

The model test programme consisted of two main groups: i) interaction between parallel tunnels; and ii) interaction between perpendicular tunnels. The tests that were carried out within each series are defined in Tables 4.1 and 4.2. The clay behaviour during sample preparation prior to tunnel excavation and the experimental procedures adopted for the various test sets are described in Chapter 4.

In this chapter, the results of the various tunnel interaction tests are presented and some of the experimental observations from these tests are discussed. The analysis of these data is given in Chapter 6.

5.2 Boundary Stresses

As described in Chapter 4, the model tests were all carried out with clay of approximately the same strength ($s_u \approx 20$kPa). The value of *OCR* was adjusted by changing the stress applied to the top boundary of the soil. In the preparation of the sample, it was assumed that sidewall friction had a negligible effect on the stresses in the sample. Orr (1976) and Cairncross (1973), for example, carried out measurements of the sidewall friction using load cells. This approach was not successful, however, because the boundary shear stress was

found to be sensitive to the protrusion of the load cell. They measured that about 80% of the vertical stress was transmitted to the base of the sample. With regard to the influence of model height on side friction effects, Mair (1979) found that the stress lost in friction increases with increasing sample height.

In these model tests, total horizontal stresses were measured at the same level as the instrumented tunnel axis by means of pressure transducers. At the end of K_o consolidation, the measured horizontal total stresses were about 80 % (in the plane strain tank) and 90 % (in the cylindrical tank) of the theoretical values calculated using a value of K_o of 0.64 (Fannin, 1986) even though water-pump grease was used on the sidewalls to reduce the sidewall friction. That is, under the same surcharge pressure, the horizontal total stresses were slightly larger in the cylindrical tank than in the plane strain tank. This might be due to the stiffer nature of the cylindrical tank wall. It is thought that the perspex sides of the plane tank may allowed a small amount of side bulging.

5.3 Parallel Tunnel Model Tests

5.3.1 Introduction

This section describes the results obtained from the parallel tunnels test series. A total of five sets of tests, including one repeat test, were carried out in order to investigate the interaction mechanisms for parallel tunnel cases. The main parameters considered were pillar width ratio (*W/D*), flexibility ratio (*F*) and overconsolidation ratio (*OCR*). In each set of tests, three parallel tunnels were individually installed in the same clay sample using the installation procedures described in Chapter 4. In the discussion of the tests, the model tunnels are named

tunnel 1, 2 and 3 according to their installation order.

5.3.2 Measurements of Single Tunnel Behaviour

This section is concerned with the behaviour of tunnel 1 before installation of tunnels 2 and 3. The data used in this section were obtained from the measurements made during the installation of tunnel 1 in each of the tests (PS1E, PS2E, PS3E, PS4E, and $PS3E^R$ see Table 4.1). The total stresses acting on tunnel 1 were measured by pressure transducers installed at the crown, invert and two springlines on the liner. Strains were measured by strain gauges mounted at eight points on the exterior of the liner. Details of these measurements are given below.

5.3.2.1 Total Stresses Acting on the Liner

Figure 5.1 shows the variation of total radial stress on the liner during and immediately after tunnel installation. The pattern of the results was similar for all the measuring points. Initially, the stresses were zero because at this stage the instrumented section had not entered the clay. Approximately 15 minutes after the start of tunnel installation, the instrumented section entered the clay (i.e the tunnel liner advanced about 170 mm) and the total stresses gradually increased as the tunnel liner was advanced. After the liner was installed, the stresses gradually decreased until equilibrium stress conditions were attained.

The stress increase, observed during tunnel advance, may be caused by the swelling of the surrounding clay against the liner, which causes additional shear stresses between liner

and clay. The pressure cells measured some combined stresses of normal and shear stresses acting on the liner.

The stresses on the liner seem to be also influenced by the speed of the tunnel advance. However, the stress was relatively constant when the tunnel was advanced continuously.

This information about variation in stress with tunnel advance speed could be particularly relevant to pipe-jacking. The stresses acting on the liner may be dependent on the liner advance speed during jacking the pipe.

Table 5.1 gives the ranges of total normal stresses acting on the liner, which were measured at two different times after installation of tunnel 1 in each of the tests. The first set of stresses (p_s) were measured immediately after tunnel installation, corresponding to the short-term behaviour (undrained condition), and the second set of stresses (p_l) were measured after the swelling and consolidation processes associated with the tunnel installation were complete.

Table 5.1 The range of the stresses ($p_s$and p_l) acting on the liner for single tunnel

Test No.	p_o(kPa)	p_s(kPa)	p_l(kPa)	Remarks
PS1E (NF)	92.44	23.5 - 34.6	35.4 - 52.8	PS3E^R = Repeat Test for PS3E. NF = NC-clay, Flexible liner. OF = OC-clay, Flexible liner. NS = NC-clay, Stiff liner. OS = OC-clay, Stiff liner. p_o = Overburden pressure at the tunnel axis
PS2E (OF)	42.83	14.7 - 21.9	24.5 - 37.6	
PS3E (NS)	93.07	34.4 - 40.0	37.6 - 59.2	
PS4E (OS)	45.06	25.8 - 37.0	28.1 - 43.2	
PS3E^R(NS)	92.94	48.8 - 58.3	41.1 - 61.4	

The results show that the long-term stresses (p_l) acting on the liner were generally

larger than the short-term stresses (p_s). The magnitudes of p_l were approximately 40 - 70 per cent of overburden pressure (p_o). These results were consistent with the field data obtained by long-term measurements. A large number of measurements was made on a wedge-block lining system (Cooling *et al.*,1953; Tattersall *et al.*,1955; Cooley, 1982) and on an expanded concrete lining in London Clay (Ward *et al.*,1965; Smith, 1970). More recently, Barratt *et al.* (1994) reported the results of long-term monitoring of the pressures developing in instrumented rings of the segmental concrete linings in London Clay and Oxford Clay. They found that, in the long-term, the total stresses on all these liners increased to between 35 and 65 % of the overburden pressure. The results of the long-term stresses (p_l) obtained from model tests therefore fall well within the range of values measured in the field.

5.3.2.2 Liner Strains

Figure 5.2 shows the variations of the strains developed at the crown, invert and springlines in the liner during the installation of tunnel 1, plotted against time. The results show that at the beginning of the liner installation, the strain measurements were erratic. A Possible explanation for this behaviour is that since the strain gauge is generally very sensitive to temperature, it may be affected by temperature changes on entering the sample.

After the instrumented section entered the clay, the strain values gradually increased with the advance of the tunnel liner. After installation of the liner was complete, these values decreased with time. This behaviour was similar to that of the total stresses acting on the liner. The variation of strain values was larger in the flexible liner case than in the stiff liner case as would be expected. In both cases, similar variation patterns were observed at both springlines as well as at crown and invert.

Table 5.2 gives the strain values (ε_l) corresponding to long-term stresses (p_l) developed in the liner after the installation of the tunnel.

Table 5.2 The strains (ε_l) in the liner

Test No.	θ=0°	45°	90°	135°	180°	225°	270°	315°	Remarks
PS1E (NF)	51	3	-51	-46	-14	54	-166	-27	θ = Clockwise angle from the crown. Unit = micro-strain ($\mu\varepsilon$)
PS2E (OF)	-23	-56	-44	-59	-97	17	-135	-57	
PS3E (NS)	25	-6	-134	-73	11	-35	-74	-70	
PS4E (OS)	24	-40	-97	-27	-35	-46	-69	-34	
$PS3E^R$(NS)	56	-72	-137	-50	25	-40	-166	-30	

(NF) = NC-clay, Flexible liner; (OF) = OC-clay, Flexible liner; (NS) = NC-clay, Stiff liner; (OS) = OC-clay, Stiff liner.

The results show that strains were greatest at the springlevels of the liner (θ=90° and 270°) although the data are subject to some scatter.

5.3.3 Measurements of Interaction Between Parallel Tunnels

This section presents the results of the interaction behaviour observed in the installed tunnel 1 during the installation of each of tunnels 2 and 3. A total of ten tests consisting of PS1D, PS2D, PS3D, PS4D and $PS3D^R$ for the 'distant' tunnel (W/D=1.0, where W/D is pillar width ratio), and PS1C, PS2C, PS3C, PS4C $PS3C^R$ for the 'close' tunnel case (W/D=0.4) were performed. During the installation of each tunnel, the total stresses, pore water pressures, strains and displacements were monitored in tunnel 1 (instrumented tunnel).

5.3.3.1 Total Stresses Acting on the Liner

The total stresses acting on tunnel 1 were measured at the crown, invert and two springlines as each of tunnels 2 and 3 was installed.

Figures 5.3 and 5.4 show change in total radial stresses (Δp) acting on tunnel 1 during the installation of each of tunnels 2 and 3, respectively. In this figure, the values of Δp are the difference between total stresses (p) acting on tunnel 1 due to the installation of each of tunnels 2 and 3, and the corresponding total stresses (p_i), which acted on the liner after tunnel 1, alone, had been installed.

The results show that the variations of Δp were different at each of the four points on tunnel 1. Relatively large stress variations were noticed at the crown, invert and tunnelling side springline (defined as pillar springline). It is clear that the largest variation of total stresses occurred at the pillar springline. The typical pattern of stress behaviour was that initially, the stresses acting on tunnel 1 continuously decreased as the new tunnel head approached the measuring points. After passing, the stresses gradually increased with time and then reduced to attain the equilibrium stress conditions on tunnel 1. A possible explanation for this behaviour is that the clay in the vicinity of the pillar springline, crown and invert of tunnel 1 may have swelled toward the excavating tunnel side as each of tunnels 2 and 3 was installed and so the stresses at these points decreased. This stress decrease may also be associated with the decreasing pore water pressure. Especially, at the pillar springline, the variations of changes in stress acting on tunnel 1 were greater during the installation of tunnel 3 ('close' tunnel) than during installation of tunnel 2 ('distant' tunnel).

Table 5.3 gives a summary of the change in total stress (Δp) acting on tunnel 1 after installation of each of tunnels 2 and 3 in each of the model tests. In this table, for tests PS3D

and PS3C, the stresses at the invert were not measured during the tests, because the transducer was not working after tunnel 1 was installed completely.

The results clearly show that the largest decrease in total stress, after installation of each of tunnels 2 and 3, occurred at the pillar springline (SL_{T2} and SL_{T3}) on tunnel 1. The closer tunnel installation led to larger stress interactions.

Table 5.3 Changes in stress (Δp) after installation of tunnels 2 and 3 (kPa)

Tunnel Installation	Test No.	Crown	SL_{T3}	Invert	SL_{T2}	Remarks
		$\theta = 0°$	90°	180°	270°	
'Distant' tunnel Tunnel 2 (*W/D*=1.0)	PS1D (NF)	- 9.8	- 2.1	- 5.5	- 4.0	SL_{T3} = Tunnel 3 side springline. SL_{T2} = Tunnel 2 side springline. θ = Clockwise angle from the crown.
	PS2D (OF)	- 2.9	- 2.0	- 5.8	-10.1	
	PS3D (NS)	- 2.3	1.9	?	- 4.2	
	PS4D (OS)	- 4.3	- 3.8	- 9.0	-10.2	
	$PS3D^R$(NS)	- 1.4	- 0.8	- 2.1	-10.4	
'Close' Tunnel Tunnel 3 (*W/D*=0.4)	PS1C (NF)	-15.5	-19.0	-11.1	- 7.9	
	PS2C (OF)	- 4.7	- 8.7	- 4.1	- 5.9	
	PS3C (NS)	- 8.0	-19.2	?	-1.0	
	PS4C (OS)	- 7.9	-25.4	-15.8	-1.9	
	$PS3C^R$(NS)	4.1	-15.0	- 4.1	2.5	

(NF) = NC-clay, Flexible liner; (OF) = OC-clay, Flexible liner; (NS) = NC-clay, Stiff liner; (OS) = OC-clay, Stiff liner.

5.3.3.2 Pore Water Pressures

The pore water pressures were measured at the two springlines on tunnel 1 during the

installation of each of tunnels 2 and 3. Details of the measurement procedure are given in Chapter 4.

Figure 5.5 and 5.6 show the variation of change in pore water pressure (Δu) on tunnel 1 measured during the installation of each of tunnels 2 and 3, respectively. From both figures, the results clearly show that the pore water pressures at the pillar springline were significantly changed during each tunnel installation. Although the data are subject to some scatter, the variation of the changes in pore water pressure was relatively larger during the installation of tunnel 3 than that of tunnel 2. At the pillar springline, negative pore water pressures were developed as the new tunnel head approached the measuring points. After passing, the negative pore water pressures dissipated with time. The dissipation time was relatively quicker in the normally consolidated clay than the overconsolidated clay.

5.3.3.3 Liner Strains

The strains were measured at eight points on the liner surface of tunnel 1 during the installation of tunnels 2 and 3.

Figures 5.7 and 5.8 show the variation of incremental strains ($\Delta\varepsilon$) in tunnel 1 during the installation of tunnels 2 and 3, respectively. In these figures, negative and positive values correspond to tensile and compressive strains respectively.

The results show that the strain variations mainly occurred at the pillar springline, crown and invert. At these points, the changes in strain increased as the new tunnel was advanced. It is clear that the largest strain variation occurred at the pillar springline, and the smallest variation occurred at the opposite springline. In addition, the strains in the stiff liner are generally greater than those in the flexible liner.

Table 5.4 gives the incremental strains developed on tunnel 1 after installation of each of tunnels 2 and 3. The results clearly show that the incremental strains were considerably large in the vicinity of the pillar springline (SL_{T2} and SL_{T3}). Positive strains corresponding to compression were developed at the crown and invert, and negative strains corresponding to tension at the two springlines. It can be deduced from these results that the pillar springline moved outward and crown and invert moved inward.

Table 5.4 Incremental strains ($\Delta\varepsilon$) after installation of tunnels 2 and 3 (micro-strain, $\mu\varepsilon$)

Tunnel Installation	Test No.	C	S_{T3}	SL_{T3}	H_{T3}	I	H_{T2}	SL_{T2}	S_{T2}
		θ=0°	45°	90°	135°	180°	225°	270°	315°
'Distant' tunnel Tunnel 2 (*W/D*=1.0)	PS1D (NF)	95	-101	-22	-20	11	195	-220	73
	PS2D (OF)	35	-31	-6	-17	3	60	-91	17
	PS3D (NS)	120	-76	-44	-16	116	59	-213	96
	PS4D (OS)	44	-54	-16	-20	68	-32	-129	81
	$PS3D^R$(NS)	121	-117	-23	-10	104	54	-215	-125
'Close' Tunnel Tunnel 3 (*W/D*=0.4)	PS1C (NF)	35	456	-618	396	39	57	-36	-134
	PS2C (OF)	41	282	-476	256	24	-43	-16	-92
	PS3C (NS)	169	98	-281	115	150	-56	-62	-96
	PS4C (OS)	105	173	-354	177	108	-66	-35	-106
	$PS3C^R$(NS)	351	19	-389	194	195	-91	-93	-137

C and I = Crown and Invert; S_{T2} and S_{T3}= Shoulder of tunnel 2 and 3 side;
SL_{T2}, SL_{T3}= Springline of tunnel 2 and 3 side; H_{T2}, H_{T3} = Haunch of tunnel 2 and 3 side;
(NF) = NC-clay, Flexible liner; (OF) = OC-clay, Flexible liner; (NS) = NC-clay, Stiff liner;
(OS) = OC-clay, Stiff liner.

5.3.3.4 Radial Displacement of the Liner

The radial displacements were measured at the crown, invert and two springlines inside tunnel 1 using the specially designed measuring device (see Sections 3.7.5 and 4.3.4).

Figures 5.9 and 5.10 show the variation of incremental radial displacements (Δr) during the installation of each of tunnels 2 and 3, respectively. In these figures, negative and positive values are outward and inward radial displacements, respectively.

The results show that the pattern of variations of Δr was similar to that of the strain variation. Relatively large values of Δr occurred at the pillar springline and crown. The incremental radial displacement continuously increased as the new tunnel was advanced. The crown moved inward and the pillar springline moved outward (toward the new tunnel side). In addition, the amount of distortion of tunnel 1 may be strongly dependent on the displacements allowed during the installation of the new tunnel before the new tunnel liner becomes effective.

Table 5.5 Incremental radial displacements (Δr) after installation of tunnel 2 and 3 (mm)

Tunnel Installation	Test No.	Crown	SL_{T3}	Invert	SL_{T2}	Remarks
		θ=0°	90°	180°	270°	
'Distant' tunnel Tunnel 2 (W/D=1.0)	PS1D (NF)	0.484	0.029	0.077	-0.560	θ = Clockwise angle from the crown.
	PS2D (OF)	0.140	-0.003	0.109	-0.198	
	PS3D (NS)	0.385	0.020	-0.010	-0.390	SL_{T2},SL_{T3} = see Table 5.3
	PS4D (OS)	0.203	-0.018	0.092	-0.201	
	$PS3D^R$(NS)	0.372	-0.041	0.008	-0.331	NF,OF,NS,OS = refer to Table 5.3
'Close' Tunnel Tunnel 3 (W/D=0.4)	PS1C (NF)	0.689	-1.120	0.168	0.153	
	PS2C (OF)	0.428	-0.720	0.164	0.075	
	PS3C (NS)	0.536	-0.800	0.066	0.275	
	PS4C (OS)	0.397	-0.594	0.172	0.123	
	$PS3C^R$(NS)	0.825	-0.938	0.042	0.207	

Table 5.5 gives the incremental radial displacements in tunnel 1 after the installation of each of tunnels 2 and 3 in each of the tests. The results clearly show that at the pillar springline (SL_{T2} and SL_{T3}), the magnitudes of incremental radial displacements were much larger in the case of the installation of tunnel 3 than tunnel 2. That is, the displacements were larger when the tunnel spacing was small.

5.4 Perpendicular Tunnel Model Tests

5.4.1 Introduction

This section describes the results obtained from the perpendicular tunnels test series. A summary of this test programme is given in Table 4.2. Two sets of model tests were carried out in the cylindrical tank in order to compare the interaction mechanisms with the parallel tunnels cases. The experimental procedures for the test are described in Chapter 4. Three model tunnels were individually installed. After tunnel 1 was installed, tunnel 2 and 3 (lower and upper tunnels) were installed under and over tunnel 1, respectively. The main parameters considered in this test series were clearance ratio (*S/D*), corresponding to pillar width ratio (*W/D*) for parallel tunnels cases, and flexibility ratio (*F*).

5.4.2 Measurements of Single Tunnel Behaviour

The single tunnel behaviour in the plane-strain tank is described in Section 5.2.2. This section is concerned with the behaviour of a single tunnel in the cylindrical tank, prior to

installation of other tunnels. The data used in this section were obtained from the measurements made during the installation of tunnel 1 in each of the two sets of model tests (CY1E and CY2E). The total stresses acting on the liner and liner strains were also measured using the same instruments as in the parallel tunnel test case.

Figures 5.11 [a] and [b] show the variation of the total radial stresses (p) and the variation of strains (ε) measured during the installation of tunnel 1 respectively.

The results show that the patterns of variations of total radial stresses were quite similar to those obtained from the plane-strain tank (refer to Figure 5.1 for the normally consolidated clay case) as would be expected. The total radial stresses increased with advancing the tunnel liner and decreased and converged with time. In the test CY1E, it is noteworthy to point out that the total radial stresses decreased when tunnel installation was halted, and the stresses increased again when starting the tunnel advance. This aspect was clearly associated with the fact that frictional shear forces were imposed on the liner during tunnel installation.

The patterns for strain variations were also similar to those obtained from the plane-strain tank although the data show some scatter (refer to Figure 5.2 for the normally consolidated clay case). The patterns differed according to the liner flexibility.

Table 5.6 gives the results of the long-term total radial stresses (p_l) and strains (ε_l), which were measured after the swelling and consolidation processes associated with the tunnel installation were complete. The results show that both p_l and ε_l were slightly greater than those observed in the plain strain tank (refer to Table 5.1 and 5.2 for normally consolidated clay case; PS1E, PS3E and PS3E^R). As mentioned in Section 5.2, this may be because of the boundary stress effects. The magnitudes of long-term stresses (p_l) were approximately 55- 75 per cent of overburden pressure (p_o).

Table 5.6 Total radial stresses (p_l) and strains (ε_l)

Items	Test No.	P_o kPa	C	S_F	SL_F	H_F	I	H_R	SL_R	S_R
			θ=0°	45°	90°	135°	180°	225°	270°	315°
p_l (kPa)	CY1E(NF)	93.4	57.1		52.8		64.5		52.8	
	CY2E(NS)	92.3	63.5		46.9		71.6		70.4	
ε_l (μ)	CY1E(NF)		85	18	-216	15	53	-359	-150	-74
	CY2E(NS)		158	-1	-332	30	166	0	-364	20

C= Crown, I = Invert, S_F, S_R= Shoulder of front and rear side,
SL_F, SL_R= Springline of front and rear side, H_F, H_R = Haunch of front and rear side.
P_o = Overburden pressure at the tunnel axis.
(NF) = Normally consolidated clay, Flexible liner;
(NS) = Normally consolidated clay, Stiff liner.

5.4.3 Measurements of Interaction Between Perpendicular Tunnels

This section presents the results of the interaction behaviour between perpendicular tunnels observed in the installed tunnel 1 during the installation of the new tunnels. The new tunnels were installed under and over tunnel 1 with a clearance of 1.0D and 0.4D between tunnels, where D is the tunnel diameter, respectively (see Chapter 4).

A total of four tests of CY1L and CY2L for 'lower' tunnel tests, and CY1U and CY2U for 'upper' tunnel tests were performed according to the specification given in Table 4.2.

5.4.3.1 Total Stress Acting on the Liner

Figures 5.12 [a] and [b] show the variation of change in total radial stresses (Δp) acting on tunnel 1 during the installation of each of tunnels 2 and 3. Different trends of the stress variations were observed at the measuring points during installation of the new tunnel. The results show that as the tunnel advanced, the stress change response is observed first at the front springline, then at the crown (or invert) and finally at the rear springline. At each point, the stress gradually decreased as the new tunnel approached the measuring point, and after passing, the stress increased until an equilibrium stress condition was developed around the tunnel liner. It is clear that the largest variation occurred at the invert for the installation of tunnel 2, and at the crown for the installation of tunnel 3.

Table 5.7 gives a summary of the change in total stress (Δp) acting on tunnel 1 after installation of each of tunnels 2 and 3.

Table 5.7 Change in total radial stress (Δp) on Tunnel 1 after installation of tunnel 2 and 3

Tunnel Installation	Test No.	Crown	SL_F	Invert	SL_R	Remarks
		$\theta = 0°$	90°	180°	270°	
'Lower' Tunnel 2 (*S/D*=1.0)	CY1L(NF)	3.3	-0.2	-13.9	-1.7	*S/D* = Clearance ratio between tunnels. SL_F = Front springline SL_R = Rear springline. Units = kPa
	CY2L(NS)	9.6	-1.3	-33.3	-5.1	
'Upper' Tunnel 3 (*S/D*=0.4)	CY1U(NF)	-7.1	-8.1	21.9	9.9	
	CY2U(NS)	-40.9	-7.1	-1.3	-12.8	

(NF) = Normally consolidated clay, Flexible liner;
(NS) = Normally consolidated clay, Stiff liner.

5.4.3.2 Liner Strains

Figures 5.13 [a] and [b] show the variations of incremental strains ($\Delta\varepsilon$) developed in tunnel 1 during the installation of each of tunnels 2 and 3. In these figures, the values of strains are expressed in units of micro-strain (10^{-6}). Negative and positive values refer to tensile and compressive strains respectively.

Overall results show that the strain in tunnel 1 varied erratically during the installation of each new tunnel. The variation trends were quite different compared with the results from the parallel tunnel model tests (see Figure 5.7 and 5.8). The variation of the strain at each of the measuring points seems to be strongly dependent on the location of the new tunnel heading as the tunnel advanced. The strains in tunnel 1 changed sign with the advance of each new tunnel. It can be also observed that the patterns of strain variation in the flexible liner case, were similar to that in the stiff liner case, at each corresponding measuring point. It is clear that the largest incremental strains occurred at the invert when tunnel 2 was installed, and at the crown when tunnel 3 was installed. In Figure 5.13 [b], it is noteworthy to point out that in the stiff liner case, the change in strain at the crown increased and then decreased significantly as the tunnel advanced. The magnitude of strain change was much larger during installation than that measured after installation was complete. This aspect means that, for the perpendicular tunnels case, there is a possibility that the interaction effects during the installation of the new tunnel may be larger than those after the new tunnel is installed.

Table 5.8 gives a summary of the incremental strains ($\Delta\varepsilon$) developed on tunnel 1 after each of tunnels 2 and 3 were completely installed.

Table 5.8 Incremental Strains on Tunnel 1 after Installation of Tunnel 2 and 3

Tunnel Installation	Test No.	C	S_F	S_F	H_F	I	H_R	S_R	S_R
		θ= 0°	45°	90°	135°	180°	225°	270°	315°
'Lower' Tunnel 2 (*S/D*=1.0)	CY1L(NF)	8	34	-190	21	257	7	-199	69
	CY2L(NS)	8	29	-96	-43	153	8	-84	-35
'Upper' Tunnel 3 (*S/D*=0.4)	CY1U(NF)	343	-142	-122	26	90	72	-118	-152
	CY2U(NS)	34	-9	-8	11	-27	-28	28	-61

(NF) = NC-caly, Flexible Liner (F=214); (NS) = NC-caly, Stiff Liner (F=75);
C = Crown, S_F = Front shoulder, SL_F = Front springline, H_F = Front haunch, I = Invert, H_R = Rear haunch, SL_R = Rear springline, S_R = Rear shoulder.

5.4.3.3 Radial Displacements of the Liner

Figures 5.14 [a] and [b] show the variation of the incremental radial displacements (Δr) of tunnel 1 during the installation of each of tunnels 2 and 3. In these figures, the negative and positive values are outward and inward radial displacements, respectively.

Different trends were observed in each of the cases of the installation of tunnel 2 and 3. For the tunnel 2 installation case ('lower' tunnel tests of CY1L and CY2L), the variation pattern was similar to that from the parallel tunnels cases. The crown and invert of tunnel 1 moved downward due to the installation of tunnel 2 (see Figure 5,14 [a]). In addition, the centreline shaft of tunnel 1 moved downward.

For the tunnel 3 installation case ('upper' tunnel tests of CY1U and CY2U), the radial displacements of tunnel 1 varied cyclically with the advance of tunnel 3 (see Figure 5.14 [b]).

Table 5.9 gives a summary of the incremental radial displacements (Δr) of tunnel 1

measured after each of tunnels 2 and 3 was completely installed.

Table 5.9 The values of Δr of tunnel 1 after installation of tunnel 2 and 3

Tunnel Installation	Test No.	Crown	SL_F	Invert	SL_R	Remarks
		$\theta = 0°$	90°	180°	270°	
'Lower' Tunnel 2 (*S/D*=1.0)	CY1L(NF)	1.820	-0.580	-1.300	0.120	*S/D* = Clearance ratio between tunnels.
	CY2L(NS)	1.127	0.059	-0.793	-0.131	
'Upper' Tunnel 3 (*S/D*=0.4)	CY1U(NF)	0.397	-0.410	0.170	-0.139	SL_F = Front springline SL_R = Rear springline. Units = mm
	CY2U(NS)	0.070	-0.044	0.027	0.063	

(NF) = Normally consolidated clay, Flexible liner;
(NS) = Normally consolidated clay, Stiff liner.

5.5 Repeatability

Repeatability is a major concern in this type of model testing. If a series of tests is conducted in which the effect of changing various parameter is being studied, it is important to establish the amount of agreement that is obtainable between results of two tests which were similar. In this section, the repeatability is described and evaluated for the model tests.

For the samples themselves, good repeatability was achieved in preparing the kaolin samples, as shown by consistent values of clay strength (Figures 4.15 and 4.16). The strengths of all any samples were within ±5 % of a common mean.

For the tunnelling process, a model tunnelling machine was developed to allow repeatable tunnel installation procedures to be adopted (refer to Section 4.5).

In order to ascertain the repeatability of the model tunnel test procedures, test $PS3^R$ was carried out as a repeat of test PS3. As shown in Figure 5.1, 5.3 and 5.4, the results of radial stresses observed in both tests PS3 and $PS3^R$ show a similar pattern. However, the results of $PS3^R$ were slightly above that of PS3. Figure 5.15 shows the distributions of radial pressure acting on Tunnel 1 observed from PS3 and $PS3^R$ after the installation of each of the tunnels. The total stress differences between the two sets of tests were ± 8% of overburden pressure (93 kPa). The results also show that these differences increased as the additional tunnels were installed. It is thought that these differences may relate to small variations in the set-up of the tunnelling machine.

For the radial displacements, It is observed from Figure 5.9 and 5.10 that both tests results show a similar pattern during the installation of tunnels. Figure 5.16 shows the comparison between incremental displacement for both tests after the installation of Tunnel 2 and 3. The average radial displacement differences between the tests were ± 0.08 mm from a common mean.

For the strain values developed on Tunnel 1 during installation of tunnels, a similar results were obtained between PS3 and $PS3^R$ as shown in Figure 5.2 to 5.4. During installation of Tunnel 1, however, the magnitudes of strain values were slightly different, although variations patterns between them were similar (Figure 5.2). This may also relate to small variation in the set-up of the tunnelling machine during the installation of tunnel 1. It is, however, observed that even though the corresponding strain values between both tests were different during the installation of Tunnel 1, each of the strain values developed on the liner converged to the same value after the installation of Tunnel 1. Figure 5.17 shows a set of strain distributions developed on Tunnel 1 after the installation of each of Tunnel 1, 2 and 3 for PS3 and $PS3^R$. The results show that the strain differences between both tests increased

as the additional tunnels were installed. This may also be due to tunnel set-up problems. Overall results indicated that the average strain differences between the tests were less than ± 20 $\mu\varepsilon$, from a common mean.

In conclusion, the exercise in repeatability between test PS3 and $PS3^R$ gives credibility to the test results obtained from all other tests.

5.6 Measurements of Total Stress, Pore Pressure and Liner Strain

In the previous sections, the results of the various tunnel interaction tests are presented and discussed in terms of total stress, pore pressure, liner strain and displacement. In this section, consideration is given to the total stress, pore pressure and liner strain responses measured at one point on the instrumented liner for two typical tests (PS3 for a normally consolidated sample and PS4 for an overconsolidated sample) during, and after, installation of the close tunnel (W=0.4D). This exercise illustrates the interaction mechanisms that were observed to act at a local level for both normally consolidated and overconsolidated samples.

Total stress, pore pressure, and incremental strain results for tests PS3 and PS4 are plotted in Figure 5.18 and 5.19, respectively. In all of these plots time t=0 corresponds to the start of the installation of tunnel 3. The data were all recorded at the springline of tunnel 1 adjacent to tunnel 3.

Figure 5.18 and 5.19 indicate that the total stresses acting on tunnel 1 starts to reduce as tunnel 3 is installed, reaching a minimum of slightly less than zero when the face of the new tunnel is approximately alongside the instrumented section of tunnel 1. In both normally consolidated and overconsolidated samples, this response clearly indicates the horizontal stress relief that would be expected to occur when a new, parallel, tunnel is constructed. As tunnel

installation continues, however, the horizontal stresses are seen to increase. This is thought to reflect the additional vertical stresses developed in the pillar of soil between the two tunnels due to arching within the soil above tunnel 3. As soon as tunnel construction is complete the total stress in the normally consolidated clay is seen to remain constant in the short term with a small decay occurring during the subsequent 24 hour period as consolidation takes place. However, in the overconsolidated clay, the total stress is seen to increase during the 24 hours after tunnel installation.

The measured pore pressure responses plotted in Figures 5.18 and 5.19 shows several distinct stages. It can be also observed from these figures that the response of the pore pressure is different in the normally consolidated and overconsolidated clay. In normally consolidated clay (Figure 5.18), the pressure is seen to rise at the start of tunnel installation. This response is thought to be caused by the additional stresses applied to the soil at the face of the tunnelling machine. After tunnel installation is about 20% complete, the pore pressure starts to reduce. From this point, until tunnel installation is complete, the pore pressure response is similar to that of the total stress and is presumably linked to the same mechanisms of lateral stress relief followed by arching. At the end of tunnel installation, however, the pore pressure continues to rise although the total stress remains approximately constant. This feature is thought to be associated with the equalisation of non-uniform pore pressures developed between tunnels 1 and 3 as a result of arching above tunnel 3. In overconsolidated clay (Figure 5.19), until the face of the new tunnel is approximately alongside the instrumented section of tunnel 1, the pore pressure response is similar to that in normally consolidated clay. From this point, however, the pore pressure response is seen to rise continuously even after tunnel installation is complete. A possible explanation of this feature is that negative pore pressure induced by the lateral stress relief is dissipated. This feature

can be linked to the fact that total stress response is seen to increase continuously. It may also be thought that the arching effect associated with the lateral stress relief is smaller in the overconsolidated clay.

Figure 5.18 and 5.19 shows that installation of tunnel 3 leads to reductions in horizontal stress acting on tunnel 1 in both normally consolidated and overconsolidated clay, respectively. Other experimental data show that, at the same time, the vertical stresses on the existing tunnel tend to increase. These stress changes lead to additional bending moments in the liner as indicated by the incremental strain response plotted in Figure 5.18 and 5.19. This response was similar in both normally consolidated and overconsolidated clay and was typical in that the incremental strains that occurred during tunnel installation were substantially larger than the additional strains that developed as subsequent consolidation processes took place.

CHAPTER 6

ANALYSIS OF INTERACTIONS BETWEEN CLOSELY SPACED TUNNELS

6.1 Introduction

The raw data obtained from the model tests is presented in Chapter 5. These data provide important information about the mechanisms of interaction between tunnels in clay. The purpose of this chapter is to interpret the model tests data and to provide a discussion of various interaction mechanisms that are mobilised. The discussion is focused on the influences of tunnel spacing, liner stiffness, and overconsolidation ratio (*OCR*) of clay on the nature of the interaction mechanisms.

In this analysis, the bending moments in the liner were estimated from the measured strain values given in Chapter 5 using elastic beam theory. Details of the application of elastic beam theory are described in the first part of this chapter. These calculated values were also used to estimate the displacements of the liner using a virtual work approach. These estimated values were used to check the displacement data that were actually measured in the model tests. The results of this virtual work analysis are presented in the final part of the chapter.

6.2 Application of Elastic Beam Theory

The bending moments developed within a tunnel liner can be calculated from the values of strains of the outside liner surface using elastic beam theory. In order to do this it is necessary to assume that the bending stresses are significantly larger than the stresses associated with ring forces. Since the tunnel liner is curved, it is necessary to adopt a curved beam theory in order to calculate the bending moments from the measured strains. This theory is developed below. It is shown that, because in this case the liner thickness is small compared with the radius of curvature, conventional beam theory may be adopted with little loss of accuracy.

For the case of a straight beam, the longitudinal strain (ε) is given by:-

$$\varepsilon = \frac{y}{R} \tag{6.1}$$

where y and R are the distance from the neutral axis and the radius of curvature of the neutral axis respectively (see Figure 6.1 [a]).

For a curved beam, however, the strain does not vary linearly with distance from the neutral axis. As shown in Figure 6.1[b], $\Delta\phi$ is the angle between two plane cross sections, *a-b* and *c-d*, before bending. During the application of pure bending moments, these two planes rotate relative to one another through a small angle $\Delta\theta$, as indicated by the dotted line *c'-d'*. The distances r and R are measured from the undeformed centre of curvature to the centroidal axis and the neutral axis, respectively.

The longitudinal strain (ε) in the curved beam may be shown to be:-

$$\varepsilon = \frac{y\ \Delta\theta}{(R-y)\ \Delta\phi} \tag{6.2}$$

where y is the distance from the neutral axis. The maximum compressive strain ε_c occurs at the innermost concave side, and the maximum tensile strain ε_t occurs at the outermost convex side.

The location of the neutral axis may be found by assuming that net hoop force is zero. In this case, the stress distribution must satisfy the equation:-

$$\int_A \sigma \, dA = 0 \qquad (\sigma = E \, \varepsilon) \tag{6.3}$$

From Equation 6.2 and 6.3, the location of the neutral axis (R) can be determined using the equation:-

$$R = \frac{\int_A da}{\int_A \frac{da}{r}} \tag{6.4}$$

where r is the distance from the centre of curvature to any location in the beam.

The bending moment is given by:-

$$M = \int_A \sigma \, y \, dA \tag{6.5}$$

Combining equations 6.2 and 6.5 gives:-

$$M = E \int_A \frac{\Delta\theta}{\Delta\phi} \frac{y^2}{R - y} \, dA \tag{6.6}$$

In the straight beam case, since the initial curvature is infinite, $\Delta\phi$ is equal to $\Delta\theta R/(R\text{-}y)$. This equation, therefore, reduces to:-

$$M = \frac{E\,I}{R} = \frac{E\,\varepsilon\,I}{y} \tag{6.7}$$

where I is the second moment of area.

For the curved beam, Equations 6.2, 6.3 and 6.6 show that the bending moment is given by:-

$$M = \frac{E\,\varepsilon\,(R-y)\,A\,y'}{y} \tag{6.8}$$

where A is the area of the cross section of beam, and y' is the distance between the neutral and centroidal axes of the beam.

For the values of thickness and radius of the liner used in the model tests, equations 6.7 and 6.8 differ by between 0.2 and 0.3 percent. It is clear, therefore, that conventional beam theory is adequate to model the behaviour of the liner.

6.3 Interactions Between Parallel Tunnels

The analysis of interactions between parallel tunnels are described in this section. All analyses were performed based on the results obtained from five sets of the parallel tunnel model tests. Although two interaction experiments were carried out using each clay sample, it is assumed that interactions between tunnels installed in position 2 and 3 were negligible. This assumption is discussed further in Chapter 7.

6.3.1 Radial Stresses Acting on the Liner

Figure 6.2 shows five sets of the normal stresses acting on tunnel 1 after the installation of each of the tunnels 1, 2 and 3 at various stages during the tests. Each set of

plots also includes the theoretical *in-situ* stress before installation of tunnel 1, which were estimated using the ideal K_o (see Equation 7.2) value for each of the model conditions.

The distributions of normal stresses acting on the clay obtained from the assumed K_o values are elliptical. However, it is clear that after tunnel 1 is installed, the pressure distribution follows a near circular pattern. This pattern was also obtained after tunnel 2 and 3 were installed. This feature of the results is associated with the fact that the liner is relatively flexible in bending and so it is only able to support stresses that are approximately hydrostatic. These results are also consistent with the observation made by Peck (1969) that a circular, flexible, liner can be in equilibrium only if the radial stresses are everywhere equal. The magnitudes of the stresses after installation of tunnel 1 vary according to the liner stiffness. The stresses for the stiff liner cases were all slightly greater than those obtained for the flexible liner. In addition, in the case of the overconsolidated clay and a flexible liner, a relatively small radial stress was measured at the crown. It is thought that this result may be anomalous and caused by cavitation within the sample.

For the interaction between tunnels, overall results indicated that radial stresses acting on tunnel 1 decreased after installation of each of the tunnels 2 and 3. It is clear that the stresses at the pillar springline were reduced by a larger amount when tunnels 2 and 3 were installed, compared with other points on the liner. As would be expected, the changes in stress at the pillar springline was larger when the tunnel were more closely spaced (tunnel 3). That is, the interaction effects of the stress acting on tunnel 1 were strongly influenced by the pillar width (W).

Figures 6.3 [a] to [d] show the variations of normalized stresses acting at the crown, invert and two springlines of the tunnel 1 plotted as a function of the pillar width ratio (W/D). In these figures, the stresses (p) developed at each of four points after installation of each of

tunnels 2 and 3 were normalized by the corresponding initial stresses (p_i), to disassociate them from the model test conditions. The initial stresses (p_i) correspond to the stresses after installation of tunnel 1.

As pointed out above, these results show that the changes in stress on the pillar springline depended strongly on the pillar width, and the stresses at the other three points do not show any clear interaction effects. In addition, at the pillar springline, it is clearly observed that the interaction effects increase as the pillar width ratio decreases (see Figure 6.3 [d]).

In all the results, although the interaction effects of the stress acting on tunnel 1 for other parameters (flexibility ratio and *OCR*) are not so clear, by the grouping of the data associated with these parameters, it, however, can be observed that:

i) the crown and pillar springline seem to be influenced by the flexibility ratio (F) and at these points, the interaction effects are slightly larger in the flexible liner cases (see Figure 6.3 [a] and [d]),

ii) the overconsolidation ratio has a clear significance in the stiff liner cases and the interaction effects for this parameter are relatively greater in the overconsolidated clay (see Figure 6.3 [b] and [c]).

From the results described above, it can be concluded that:

i) the pillar width ratio (W/D) is an important parameter governing the interaction of the normal stresses acting on the existing tunnel,

ii) the flexibility ratio (F) and overconsolidation ratio (OCR) appear to be less important,

iii) although for stiff liners at close spacing the interaction effects for the

overconsolidated sample are considerably greater than those observed for the normally consolidated sample,

iv) the largest interaction effects of the normal stresses are observed at the pillar springline,

v) the largest changes in stresses acting on the existing tunnel occur when the new tunnel has a stiff liner with a small pillar width and is installed in overconsolidated clay.

6.3.2 Bending moments in the Liner

The values of the bending moments used in this analysis were calculated from the measured strains data using conventional beam theory (see Section 6.2).

Figure 6.4 shows five sets of plots of the distributions of the bending moments developed in tunnel 1 after the installation of tunnels 1, 2, and 3. In each plot, the bending moments obtained after installation of tunnel 1 can be considered as relevant to the case of a single tunnel, since no other tunnel is present in the ground.

During the tests it was discovered that changes in temperature associated with installation of the instrumented tunnel caused adjustments to zero level of the strain gauges. In order to correct for this effect (which was assumed to be of the same magnitude for each gauge) the offset was calculated on the basis that the bending moments around the liner should, from virtual work considerations, integrate to zero. The appropriate offset was computed by integrating a cubic spline fitted to eight bending moment values calculated from the strain gauge data (see Section 6.6). The bending moment data after installation of tunnel 1 plotted in Figure 6.4 are corrected for this effect. The incremental moments were all entirely

consistent in that the incremental bending moments were all found to integrate to zero.

The results show that the maximum bending moments for the each of the tunnel installations occur at springline levels (θ = 90° and 270°) in all cases. It is clear that for the installations of tunnels 2 and 3, the tunnel interactions led to considerably larger bending moments values in the vicinity of the pillar springline side of tunnel 1 (θ=270° for tunnel 2 installation, θ=90° for tunnel 3 installation). The changes in bending moments were larger when the tunnels were more closely spaced. In addition, for the same type of clay sample, the induced bending moments were slightly larger for the stiff liner cases than for the flexible liner. This aspect may be associated with the fact that the bending moments developed in the tunnel are dependent on the flexibility of the liner (Peck, 1969) with flexible liners attracting smaller bending moments than stiff liners. A further feature of these results is that the bending moments are slightly greater for the normally consolidated clay case than for the overconsolidated clay case. This result may be associated with the fact that the surcharge pressure was lower for the overconsolidated clays than the normally consolidated clays (refer to Chapter 4).

Figures 6.5 [a] to [e] show the normalized incremental bending moments ($\Delta M/\gamma HR^2$) in tunnel 1 due to the installations of tunnels 2 and 3. In each of these figures, the incremental bending moments (ΔM) were normalized by the variable γHR^2, where γH is the overburden pressure estimated to act at the tunnel axis and R is tunnel radius.

The results show clear interaction effects due to the installation of tunnel 2 and 3. It is clear that the incremental bending moments (ΔM) were considerably larger in the vicinity of the pillar springline side and also the magnitudes of ΔM were significantly influenced by the spacing between the tunnels. For example, in the close tunnel case, as shown in Figure 6.5 [d], the normalized incremental maximum bending moments (ΔM_m) in tunnel 1 were

increased by approximately 0.03. This value corresponds to about 600 per cent of the maximum bending moments (M_{max}) measured in tunnel 1 before tunnel 2 and 3 were installed. Table 6.1 shows values of $\Delta M_m/M_{max}$ for all of the parallel tunnel tests.

Table 6.1 Summary of $\Delta M_m/M_{max}$ (%)

Tests	Clay	Liner	W=1.0D (Distant)	W=0.4D (Close)
PS1	NC	Flexible	155 %	436 %
PS2	OC		116 %	608 %
PS3	NC	Stiff	237 %	314 %
PS3r			188 %	340 %
PS4	OC		228 %	626 %

The results given in Table 6.1 indicate that for W=1.0D cases, the induced maximum incremental bending moments (ΔM_m) were a factor of about 2 greater than the maximum liner moment before the new tunnel was installed whereas for W=0.4D cases, the values of ΔM_m were a factor of between 3 and 6 greater than the maximum initial liner moments. This result provides important practical information about the additional moments applied to an existing tunnel structure when a new tunnel installed nearby. The existing tunnel liner may require strengthening in order to support the additional bending moments.

Figures 6.6 [a] to [d] show the normalized incremental bending moments ($\Delta M/\gamma HR^2$) for four representative points on the liner plotted against the pillar width ratio (W/D). The results show that the interaction effects occurred at all points of the liner except the springline opposite the new tunnel. It is clear that the largest interaction effects occur at the pillar springline (see Figure 6.6 [d]). For the three points of the crown, invert and pillar springline,

the magnitude of the incremental bending moments (ΔM) increases as the pillar width ratio (W/D) decreases.

It is clear that the flexibility ratio (F) and overconsolidation ratio (OCR) also influence the moment interaction effects as described below:-

At the pillar springline, the influence of OCR tends to increase as the pillar width ratio (W/D) decreases (see Figure 6.6 [d]). In addition, the bending moment interactions were larger for the overconsolidated clay than the normally consolidated clay. A possible explanation for this result is that as OCR increases, and W/D decreases, the horizontal stresses released by the new tunnel installation are relatively higher and the larger displacements lead to the larger incremental bending moments. For the influence of the liner flexibility, the results show that the interaction effects at the pillar springline were relatively greater for the stiff liner cases.

At the crown and invert, the results show that the interaction effects are influenced by the flexibility ratio (F) rather than OCR. The bending moment interaction effects were larger for the stiff liner cases than for the flexible liner cases (see Figure 6.6 [a] and [b]).

These results suggested that:-

i) the largest interaction effects of the bending moment occur at the pillar springline,

ii) at the pillar springline, the influence of overconsolidation ratio increases as pillar width is decreased,

iii) the interaction effects for the bending moment would be expected to be small for values of pillar width in excess of about 1.5 diameters,

iv) relatively large bending moment interaction effects are developed when a close new tunnel is installed in overconsolidated clay.

v) the magnitude of the incremental bending moments induced by new tunnel installation, were generally founded to increase a factor between two and six greater

than the maximum bending moment developed in a existing tunnel liner.

6.3.3 Liner Displacements

Figure 6.7 show the five sets of the incremental displacements (Δr) measured after installations of tunnel 2 and 3 at various stages during the model tests. The results show that the liner was distorted with a similar pattern after the installation of tunnel 2 and 3. It is also clear that the incremental displacements were concentrated mainly at the pillar springline and crown of tunnel 1. After installation of tunnels 2 and 3, the pillar springline moved outwards (i.e. towards the tunnel 2 or 3) and the crown moved downwards. Also, the magnitude of the incremental displacements tends to increase with reducing pillar width. It is also clear that the incremental displacements reduced in magnitude with increasing liner stiffness.

In particular, after tunnel 3 was installed, it is clear that in all cases both springlines of tunnel 1 moved toward the tunnel 3. That is, the centreline of tunnel 1 translated slightly towards tunnel 3.

Figures 6.8 [a] to [d] show the normalized incremental displacements measured at the crown, invert, and two springlines of tunnel 1 after the installations of tunnel 2 and 3 plotted against the pillar width ratio (W/D). In these figures, the values of the incremental displacements (Δr) were characterized by the variable $(\Delta r/D)/(p_o/s_u)$, where $\Delta r/D$ is the ratio between the incremental radial displacements and the initial tunnel diameter and p_o/s_u is the ratio between overburden stress (p_o) and undrained shear strength (s_u), which corresponds to the overload factor (N) (see Chapter 2).

These results show that displacement interaction effects occurred at each of four points of tunnel 1. It is clear that the interaction effects were larger at the pillar springline and the

crown and were very small at the invert and opposite springline. The largest interaction effects occurred at the pillar springline.

At the crown and pillar springline, the displacement interaction effects increase as the pillar width ratio is reduced. The displacements at these two points provide a significant contribution to the diameter changes of the liner resulting in a decrease of the vertical diameter and an increase in the horizontal diameter. By the grouping of the data related to F and OCR, the interaction effects at these points are seen to be larger in the overconsolidated clay than in the normally consolidated clay, and are slightly larger for the flexible liner cases than for the stiff liner cases.

It can be concluded that:

i) relatively large incremental radial displacements occur in the vicinity of the pillar springline and crown of the liner,

ii) the largest interaction effects occur at the pillar springline,

iii) the displacement interaction effects increase as the pillar width ratio (W/D) is reduced,

iv) these effects seem to increase with increasing flexibility ratio (F) and overconsolidation ratio (OCR),

v) the worst case for interaction effects of the liner displacements occurs when the pillar width is small, the liner is flexible and the value of OCR is large.

6.4 Interactions Between Perpendicular Tunnels

The analysis of interactions between perpendicular tunnels is described in this section. The purpose of this analysis is to investigate the interactions between perpendicular tunnels

in order to compare them with the parallel tunnel cases (see Section 6.5).

This analysis is carried out based on the limited data obtained from two sets of perpendicular tunnel model tests performed in normally consolidated clay in which the liner stiffness was varied.

6.4.1 Radial Stresses Acting on the Liner

Figure 6.9 shows two sets of distributions of the normal stresses acting on tunnel 1 after the installations of tunnels 1, 2 and 3. Each of these plots includes the theoretical *in-situ* stress before installation of tunnel 1 (refer to Section 6.3.1).

The results show that the initial distribution of total radial stresses acting on tunnel 1 was similar to the parallel tunnel case (refer to Figure 6.2). However, the magnitude of the radial stresses were larger in this case compared with in the parallel tunnel case, especially at both springlines. It is thought that this aspect may be associated with the K_o effect for the test tank dimensions. The value of K_o may be greater in the cylindrical tank than in the plane strain tank.

With regard to the installation of tunnel 2 and 3, the results clearly show that the largest decrease in stresses acting on tunnel 1 occurred at the invert due to the installation of tunnel 2 and at the crown due to the installation of tunnel 3.

Figure 6.10 [a] to [d] shows the normalized normal stresses acting at each of the crown, invert and two springlines after the installations of tunnel 2 and 3, plotted to the function of the clearance ratio (S/D) which corresponds to the pillar width ratio (W/D). In these figures, the normal stresses (p) were also normalized by the corresponding initial radial stresses (p_i) to disassociate them from the two model test conditions. The p_i is the measured

radial stress at each of four points when tunnel 1, alone, had been installed.

The results show that the greatest radial stress interaction effects occurred at the crown and the invert. It is clear that at the crown and invert, the trends of the stress interaction effects as the clearance ratio (S/D) was varied. At the crown, the changes in stress were larger when the clearance ratio was 0.4 corresponding to the installation of tunnel 3 (upper tunnel). In contrast, at the invert, the changes in stress were larger when the clearance ratio was 1.0 corresponding to the installation of tunnel 2 (lower tunnel). This means that the interaction effects depend strongly on the new tunnel position rather than the clearance ratio. In both cases, the stress interaction effects were larger for the stiff liner case than the flexible liner case.

In comparison with the parallel tunnel case (lower with distant tunnel, and upper with close tunnel), overall stress interaction effects were relatively smaller in this case than in the parallel tunnel case (see Figure 6.3).

In addition, at the invert and front springline, it is noteworthy to point out that in the case of the flexible liner, the radial stresses were larger than the initial radial pressure (p_i) when the clearance ratio was 0.4. A possible explanation for this aspect is that as the liner is flexible, the existing tunnel 2 may supports the tunnel 1 settled by the installation of tunnel 3 and therefore the normal stress at the invert of tunnel 1 may be increased.

As described above, it can be concluded that:

i) the radial interaction effects are dependent on the new tunnel positions.

ii) the largest interaction effects occur at the crown for upper tunnel case and at invert for lower tunnel case, respectively,

iii) in both upper and lower cases, these effects are much larger in the stiff liner than in the flexible liner,

iv) the stress interaction effects were relatively smaller in the perpendicular tunnel case than the parallel tunnel case.

6.4.2 Bending moments in the Liner

Figure 6.11 [a] shows the bending moments (M) in tunnel 1 after the installations of each of the tunnels 1, 2 and 3. The results clearly show that significant bending moments for each of the tunnel installations occur at crown, invert and springline levels ($\theta = 90°$ and $270°$) in both cases of the flexible and stiff liner. It is clear that the magnitudes of the bending moments (M) were relatively larger for the stiff liner case than for the flexible liner case.

In addition, for the bending moments after the installation of tunnel 1, it can be observed that these values were relatively larger than that for the parallel tunnel cases (see Figure 6.4). This may be because the radial stresses were relatively larger than in the parallel tunnel case as mentioned in Section 6.4.1.

Figure 6.11 [b] shows the normalized incremental bending moments ($\Delta M/\gamma HR^2$) after installation of tunnels 2 and 3. In this figure, the incremental bending moments (ΔM) were normalized by the variable γHR^2, where γH is the overburden pressure estimated to act at the tunnel axis and R is tunnel radius. It is clear that the value of $\Delta M/\gamma HR^2$ was larger at the invert ($\theta = 90°$) for the installation of tunnel 2 and crown ($\theta = 0°$ or $360°$) for the installation of tunnel 3 respectively. In case of the installation of tunnel 2 (lower tunnel), this value at the invert was slightly larger for the case of the stiff liner than the flexible liner. In case of the installation tunnel 3 (upper tunnel), however, this value at the crown was much greater for the flexible liner case.

In comparison with the parallel tunnel case, the maximum values of $\Delta M/\gamma HR^2$ were

smaller in the perpendicular tunnel case (see Figure 6.11[b]) than the parallel tunnel case (see Figure 6.5). Details of comparison are given in Section 6.5.

Figure 6.12 [a] to [d] show the normalized incremental bending moments ($\Delta M/\gamma HR^2$) at the crown, invert and two springlines, plotted against the clearance ratio (S/D). As would expected, the results show that the bending moment interaction effects seem to be dependent on the geometry condition rather than the tunnel spacing. It is also clear that at the crown, the interaction effects were greater in the flexible liner case than in the stiff liner case. At the invert and two springlines, however, these effects were similar in both the flexible liner and stiff liner cases. Details of influence of the liner flexibility are given in Section 6.5.

It can be concluded that;-

i) the bending moments were larger for the stiff liner case than for the flexible liner case.

ii) the bending moment interaction effects were larger at the invert for the installation of the lower tunnel and at the crown for the installation of the upper tunnel respectively.

iii) the interaction effects are smaller than for the parallel tunnel case.

6.4.3 Liner Displacements

Figures 6.13 shows two sets of the distributions of the incremental displacements of tunnel 1 after the installation of tunnel 2 and 3. The results show that the liner was distorted with quite different patterns following the installation of each of tunnels 2 and 3. In the case of the tunnel 2 installation (lower tunnel case), the distortion of the liner is significant. The crown and invert move downwards causing a downward movement of the centreline shaft of

the tunnel (towards the tunnel 2 side). In the case of the tunnel 3 installation (upper tunnel installation case), however, the distortion of the liner is less and the pattern is similar to the parallel tunnel case. In this case, the largest incremental displacements occur at the crown. The incremental displacement magnitudes are relatively greater in the case of the flexible liner than the stiff liner. For the flexible liner, the front springline moves outwards causing an increase in the horizontal diameter.

Figures 6.14 [a] to [d] show the normalized incremental displacements measured at the crown, invert, and two springlines of tunnel 1 after the installations of tunnel 2 and 3 plotted against the clearance ratio (S/D). In these figures, the values of the incremental displacements (Δr) were also characterized by the variable $(\Delta r/D)/(p_o/s_u)$ (see Section 6.3.3). These results show that the displacement interactions were larger at the crown and the invert and were very small at the springlines. It is clear that the displacement interaction effects were larger for the installation of tunnel 2 (lower tunnel) case even though the clearance was greater than for tunnel 3.

The displacement interaction mechanisms were different to those observed in the parallel tests. For the installation of tunnel 3 (upper tunnel), the displacements interaction effects were much smaller than the corresponding parallel tunnel case (i.e. distant tunnel installation case). However, for the installation of tunnel 2 (lower tunnel), the movement of the centreline shaft of tunnel 1 was significant even if the stress and moment interaction effects were much smaller than the corresponding parallel tunnel case (i.e. close tunnel installation case).

It can be concluded that:-

i) the interaction effects of the displacements seems to be much larger for the installation of lower tunnel case than that of upper tunnel case, in spite of the fact that

the upper tunnel was more closely spaced than the lower tunnel,

ii) the interaction effects seem to increase with increasing liner flexibility,

iii) the displacement interaction effects are relatively smaller than for the parallel tunnel case, however, in the case of the lower tunnel installation, the centreline of the existing tunnel tends to move downwards as a result of settlement induced by the installation of the lower tunnel.

6.5 Comparison Between Parallel and Perpendicular Tunnel Tests

In the previous sections, the interaction mechanisms for parallel tunnels and perpendicular tunnels are discussed. This section provides a further discussion of these interaction mechanisms by comparison between the parallel and perpendicular tunnel results. A further discussion of the influence of flexibility ratio is also given in this section.

As described in Section 6.4, three-dimensional considerations suggest that the magnitude of any interaction effects between perpendicular tunnels might be expected to be less than those developed between similar parallel tunnels. Comparisons between the two series of results, however, indicate that this is not generally the case.

Figure 6.15 shows the normalized largest incremental bending moments ($\Delta M_m/\gamma HR^2$) in tunnel 1 plotted against flexibility ratio (F) for both the parallel and perpendicular tests. In this figure, the largest incremental bending moments (ΔM_m) were generated in tunnel 1 due to the installation of tunnel 2 and 3 (i.e. at the pillar springline for parallel tunnels and at the crown and invert for perpendicular tunnels) and were normalized by the variable γHR^2, where γH is the overburden pressure estimated to act at the tunnel axis and R is tunnel radius. In the parallel tunnel case, the results show that the moment interaction effects generally

decrease with increasing the liner flexibility. It is clear that the influence of the liner flexibility is much larger in overconsolidated clay than in normally consolidated clay. By comparison between parallel and perpendicular tests, the results show quite different trends. The construction of tunnel 2 in the parallel and perpendicular tests leads to similar values of induced moment. In this case, it is thought that the three-dimensional effect associated with the construction of a perpendicular tunnel is approximately offset by additional induced moments associated with settlements above tunnel 2.

Figure 6.16 shows the normalized diameter changes ($[\Delta D/D]/[\gamma H/s_u]$) of tunnel 1 after installation of the new tunnels, plotted against flexibility ratio (F) for both the parallel and perpendicular tests. In the parallel tunnel case, the results indicated that the influences of liner flexibility were much larger in the close tunnel case. In this case, it is clear that the diameter change effects were much larger in overconsolidated clay then in normally consolidated clay and increased with increasing flexibility ratio. Similar trends were also observed in the perpendicular tunnel case. However, in the perpendicular tunnel case, the interaction observed after installation of the upper tunnel is less significant than that measured in the corresponding parallel test. For the lower tunnel, the parallel and perpendicular data are seen to be similar in magnitude; this is presumably due to the additional settlement mechanism developed in the perpendicular tunnel test.

6.6 Virtual work analysis

The purpose of this analysis is to evaluate the consistency of measured displacements of the liner. A distribution of bending moment estimated from the measured strains was used in this analysis. The diameter change was then calculated using a virtual work approach for

comparison with measured values. The analysis is limited to compute horizontal diameter change for the parallel tunnels and vertical diameter change for the perpendicular tunnels.

In structural analysis, the method of virtual work is normally applied in one of two ways:

i) by considering the movements of a real force system through a selected pattern of (virtual) displacements,

ii) by considering the movements of a selected system of (virtual) forces through the real displacement pattern.

The latter approach was adopted in this virtual work analysis. Details of the procedures adopted are given below.

A typical pattern of real displacements due to new tunnel installation is shown in Figure 6.17 [a]. The shape of displacements of the liner can be assumed as symmetric about the horizontal axis (for the parallel tunnel case). Each half of the liner can therefore be analyzed separately as shown in Figure 6.17 [b].

For the real system, the unknown displacement (δ) at the springline and the known bending moments (M) are shown in Figure 6.17 [c]. The values of the bending moments were calculated from the strain values measured in the model tests using the straight beam theory (see Section 6.2).

In order to determine a specified displacement of the liner, a unit force is applied at the point corresponding to the unknown displacement in the actual liner structure, acting in the same direction as the real displacement. A set of virtual moments M^* are then developed as shown in Figure 6.17 [d]

Using both systems, the external and internal virtual work can be written as:-

$$\text{External virtual work} = 1 \cdot \delta \tag{6.9}$$

$$\text{Internal virtual work} = \int^{L} M^{*} \left(\frac{M}{EI}\right) dx \tag{6.10}$$

where M^{*} is the bending moments in equilibrium with the applied virtual force. M is the moment distribution calculated from the strain values (see Section 6.2). The following approach was adopted to obtain the functional form of M :-

i) find a continuous function for $M(\theta)$ using cubic splines.

ii) evaluate analytically the values between each strain gauge position.

iii) each value of $M(\theta)$ with the corresponding value of $M^{*}$is used to calculate the internal virtual work.

The two expressions of virtual work should be equal, and so the unknown displacement can be determined.

Based on the procedures described above, the virtual work analyses for the diameter changes were carried out in both cases of the parallel and perpendicular tunnel. For the parallel tunnel case, the horizontal diameter changes and for the perpendicular tunnel case, the vertical diameter changes were analyzed in order to examine the predominant values of displacements in each of the cases, respectively. A summary of the results is presented in Table 6.1. The diameter changes measured directly using the diameter change device in each of the model tests, are also given in the table for comparison.

Table 6.1 The estimated and measured diameter changes (mm)

Tunnel Model	Specifications			Measured		Estimated	
	Test	Liner	Clay	$1.0D^*$	$0.4D^*$	$1.0D^*$	$0.4D^*$
Parallel (ΔD_h)	PS1	Flexible	NC	0.531	0.967	0.557 (4%)	1.094 (13%)
	PS2		OC	0.201	0.646	0.139 (31%)	0.727 (12%)
	PS3	Stiff	NC	0.370	0.525	0.400 (8%)	0.540 (2%)
	PS3r			0.372	0.731	0.389 (4%)	0.797 (9%)
	PS4		OC	0.219	0.472	0.207 (5%)	0.504 (6%)
Perpendicular (ΔD_v)	CY1	Flexible	NC	-0.520	-0.567	-0.608 (17%)	-0.727 (28%)
	CY2	Stiff		-0.333	-0.097	-0.841 (152%)	-0.055 (53%)

ΔD_h and ΔD_v are horizontal and vertical diameter change, respectively.
$1.0D^*$ = Distant tunnel for parallel tunnel, Lower tunnel for perpendicular tunnel.
$0.4D^*$ = Close tunnel for parallel tunnel, Upper tunnel for perpendicular tunnel.
(%) = Per cent of differences between measured and estimated values.

For the parallel tunnel case, the results show that the values estimated using the virtual work analysis are in good agreement with the measured values. In this case, overall differences between measured and estimated values were less than about 10 per cent (except PS2). The differences in the stiff liner were smaller than that in the flexible liner.

For the perpendicular tunnel case, however, agreement was less marked. For the flexible liner, the estimated values were relatively close to the measured values. The values from the virtual work analysis were slightly larger than the measured values. Whereas, for the stiff liner, the difference between both values was quite large. This is because the deformation

mechanism in the perpendicular tunnels case differs from the parallel tunnels case.

It is concluded that, even though the difference between the values was quite large in the perpendicular tunnel cases, this approach provided some confidence in the consistency of the measurements from the model tests.

CHAPTER 7

NUMERICAL ANALYSIS AND COMPARISON WITH MODEL TESTS

7.1 Introduction

The results of the physical model tests were presented and interpreted in Chapter 5 and Chapter 6, respectively. The mechanics of the interaction between adjacent tunnels is clearly complex and cannot be fully studied using physical model testing because of the large number of parameters involved. A parametric study could be carried out using finite element analysis but, in order to have confidence in the results, it is first necessary to develop realistic modelling procedures. A limited amount of finite element analysis was carried out during this project in order to develop some conclusions as to how this soil-structure interaction problem might best be modelled. The finite element analysis has also been used to investigate some of the modelling assumptions inherent in the physical tests. Special numerical procedures were used to model the ground loss associated with tunnel installation (Kim *et al*, 1996). Further studies could be carried out to investigate possible scaling errors or boundary effects although this aspect is beyond the scope of this research. The analysis is limited to the case of undrained loading to model interaction behaviour immediately after tunnel construction.

This chapter is concerned only with the use of two dimensional finite element analysis to model the behaviour of the parallel tunnel tests. Computed values of incremental displacement and bending moment associated with new tunnel construction are presented and

compared with the corresponding physical model test data.

7.2 Specification of Analysis

7.2.1 Numerical Modelling

The numerical analyses were all restricted to two-dimensional, plane-strain conditions using the finite element program, OXFEM which has been developed by the soil mechanics group at Oxford University. The OXMESH program was used to generate the finite element meshes. The analyses were all performed using a linear elastic soil model. Although this is a crude model it gave good results and is easy to use.

7.2.1.1 Mesh Generation

Six-noded continuum elements and three-noded linear beam elements were used to model the ground and the tunnel liners respectively. Figure 7.1 shows a typical finite element mesh used in these analyses (note that the beam elements used in the analyses were based on a formulation that required them to be straight). As shown in Figure 7.1, the following boundary conditions were applied to the model:-

i) the base of the finite element model was restrained in both vertical and horizontal directions,

ii) roller restraints were applied to the sides of the finite element mesh.

A total of five separate finite element meshes were generated to model each of the

sample dimensions adopted in the physical model tests.

7.2.1.2 Simulation of Tunnel Excavation

The excavation of the tunnel was simulated by numerical removal of the soil elements inside the tunnel (Augarde *et al.*,1995). Consideration was given to the choice of numerical procedure to model the overcut that occurred during tunnel construction and the consequent radial movement of the clay as it swells onto the tunnel liner. The approach selected was to apply a suitable hydrostatic suction to the inside of the tunnel liner in order to reduce its circumference. The value of hydrostatic suction (F_{hu}) needed to model a specified amount of overcut may be obtain from elastic ring compression theory and is given by:-

$$F_{hu} = E_l A \frac{\delta_g}{R} \tag{7.1}$$

where δ_g and R are the specified gap and tunnel radius respectively.

This procedure would be expected to produce spurious values of hoop force, but this is not significant since structural behaviour is determined primarily by the bending moments.

7.2.1.3 Modelling and Calculation Procedures

The following modelling procedures were used for the construction of each tunnel in the analyses.

General = Apply initial stresses to the soil with beam elements switched off.

Step 1 = Remove excavated elements within tunnel.

Step 2 = Switch on beam elements to model tunnel liner in the tunnel position to be installed.

Step 3 = Apply internal pressure to simulate ground loss.

Using these modelling procedures, the analyses were carried out for four separate cases in order to model the conditions that occurred in the model tests. Details of these calculation procedures are given below (refer to Figure 7.2).

Case 1 = Single tunnel construction in position 1 (Instrumented tunnel case)

Case 2 = Tunnel construction in position 2 after installation of tunnel in position 1 (Two parallel tunnels case).

Case 3 = Tunnel construction in position 3 after tunnel installation in positions 1 and 2 (Three parallel tunnels case)

Case 4 = Tunnel construction in position 3 after tunnel installation in position 1. (Two parallel tunnels case)

Cases 1,2 and 3 were intended to represent the procedures adopted in the physical model tests. Case 4 was intended to investigate the possibility of interactions between tunnels installed in positions 2 and 3 by comparing the results of Cases 3 and 4.

7.2.2 Specification of Parameters

The parameters listed in Table 7.1 are required for the finite element analysis. The procedures by which these parameters were obtained are described below.

Table 7.1 The list of parameters for finite element analysis

Items	Parameters	
Soil (Clay)	- Shear modulus (G) - Poisson's ratio (υ_s)	
Tunnel Liner	- Young's modulus (E) - Sectional area (A) - Second moment of area (I)	to calculate EI and EA
Initial Stresses	- Earth pressure coefficient at rest (K_o) - Overconsolidation ratio (OCR) - Unit weight (γ_t)	

7.2.2.1 Clay Parameters

The values of shear modulus (G) adopted in the finite element analysis were obtained the procedures described in Section 3.4.3. The values used in the analyses are given in Table 4.1. A clay Poisson's ratio of 0.49 was adopted in order to approximate undrained behaviour. The values of clay unit weight (γ_t) measured during each of the physical model tests were used in each of the computations.

7.2.2.2 Tunnel Liner Parameters

A Young's modulus (E) of 210 kN/mm^2 was adopted for all of the analyses. This value was used to calculate the values of EI and EA of the liner, where I and A are the area moments of inertia and section area of the liner respectively.

7.2.2.3 Initial Stresses

The initial stresses corresponding to each of the physical model tests were estimated using a specified value of the earth pressure coefficient at rest (K_o). The values of K_o adopted in the analyses were obtained from the following expression proposed by Schmidt (1966):-

$$K_o = K_{o(nc)}\, OCR^{0.5} \tag{7.2}$$

where $K_{o(nc)}$ is the coefficient of earth pressure for normally consolidated clay.

A value of $K_{o(nc)}$ of 0.64 was adopted for all of the analyses (Fannin, 1986). Values of *OCR* were obtained directly from the model test data and used to find values of K_o for each of the finite element analyses.

7.3 Results of Back-Analyses

The results of the numerical back-analysis calculations, grouped according to the new tunnel positions, are shown in Figures 7.3 to 7.8. In each of these figures, these results are also compared with the corresponding data obtained from each of the model tests.

7.3.1 Displacements and Diameter Changes

The results of the incremental displacements of the tunnel 1 (instrumented tunnel) due to the installation of each of two new tunnels in positions 2 and 3, are shown in Figures 7.3 and 7.4 respectively. In these figures, the numerical results clearly reproduced the important trend observed from the physical model tests that relatively large displacements occur at the

pillar springline and crown due to new tunnel installation. A further feature of both the numerical and model test results was that the magnitudes of the displacements at these points were influenced considerably by the pillar width (W), especially at the springline. It is also clear that overall results of these back-analysis calculations were in good agreement with the model tests data.

Model test data and finite element results for the case where a tunnel is installed in position 2 are shown in Figure 7.3. For the normally consolidated clay cases (i.e. NS, NF and NS1), the numerical back-analysis agreed well with the model tests results. For the overconsolidated clay cases (i.e. OF and OS), the displacements obtained from the numerical analyses were generally greater than those measured in the model tests. It is thought that this discrepancy is associated with errors in the estimation of K_o for use in the finite element analysis with Equation 7.2 giving values that are too high.

Corresponding results for the close tunnel cases are plotted in Figure 7.4. In this case, agreement is excellent for both the normally and overconsolidated clay. The results also indicate that even though cases 3 and 4 were slightly different for the flexible liner cases (i.e. NF and OF), the calculated behaviour for cases 3 and 4 were generally similar which suggests that the tunnels placed in positions 2 and 3 do not interact significantly. This important result provides some confidence that in the approach adopted in the model tests of using one clay sample to perform two interaction experiments is a reasonable one.

Figures 7.5 [a] to [e] show five sets of results for the horizontal and vertical diameter changes plotted against the pillar width (W). Each of these plots consists of three sets of the data reproduced from the results of the numerical analysis, displacements measured directly in the model tests and displacements estimated from the strain measurements using a virtual work approach. In all these plots, the results are characterized by the variable $(\Delta D/D)/(p_o/s_u)$,

where $\Delta D/D$ is the ratio of diameter change and p_o/s_u is the overload factor (N), in order to disassociate the conditions between them. The parameter p_o is the estimated overburden pressure at the tunnel axis level.

These figures show that the finite element data confirm the trend observed in the model test results that the displacement interactions are a strong function of pillar width. These data would suggest, by extrapolation, that interaction effects would be expected to be small for values of tunnel spacing in excess of about 1.5 D. The results also indicate that the magnitude of displacement interaction effects tends to increase with increasing OCR and with increasing flexibility of the liner.

7.3.2 Bending Moments

Figures 7.6 and 7.7 show the numerical results and model test data for the incremental bending moments in tunnel 1 (instrumented tunnel) caused by the installation of new tunnels in positions 2 and 3. Good agreement is observed in both cases between the two sets of data.

Figures 7.8 shows the magnitude of the incremental bending moments for the flexible and stiff liner developed at the springline where the largest bending moment interaction effects occur. In this figure, all data were normalized by the variable (p_oR^2) where p_o and R are the overburden pressure at the tunnel axis and the tunnel radius, respectively. The data were plotted against pillar width (W) normalized by tunnel diameter (D). The trends indicated by the numerical analysis confirm those that are observed in the model test results.

7.3.3 Conclusions

According to the comparison of results between model tests and numerical analyses described above, it can be concluded that:-

i) elastic finite element analysis with a hydrostatic gap modelling procedure gives results that appear to be in good agreement with the results of the physical model tests,

ii) based on the results of finite element analyses performed to verify experimental procedure, it is suggested that the procedure adopted in the model tests of using one clay sample to carry out two interaction experiments is reasonable,

iii) the numerical approach used in this analysis is a reasonable approach to estimate the liner behaviour of existing tunnel liners due to the construction of new, nearby, parallel tunnels.

7.4 Additional Results

This section describes some additional results relating of the magnitude of the shear strains caused by new tunnel installation. Typical results of maximum shear strains obtained from the analyses corresponding to PS1 and PS3 are plotted in Figure 7.9. The results show that, although the local strains around tunnel 1 are relatively large (> 1%), overall values of shear strains around tunnel 1 lied in a wide range. The averaged maximum shear strains against distance from the new tunnel are plotted in Figure 7.10. These plots indicate that the incremental shear strains developed around adjacent tunnels are of the under of 0.5-1%. This

confirms the previous assumption made in the selection of a suitable value of shear modulus (Section 3.4.3).

CHAPTER 8

CONCLUDING REMARKS

8.1 Introduction

This research programme has investigated the interaction between closely spaced tunnels during shield tunnel construction, concentrating on the study of the short-term incremental behaviour of the liner. This study was carried out because an ability to predict interactions of this kind is necessary to assess the possibility of damage to an existing tunnel caused by new, nearby, tunnelling activities. Carefully controlled physical model tests were carried out and the test results were complemented by a limited amount of numerical analysis.

Physical model testing of this sort is still a relatively new area of research. In the physical model tests described in this dissertation, two groups of tests were carried out at laboratory scale; one set of tests studied closely spaced parallel tunnels and the other set investigated perpendicular tunnels. An important feature of the study was that a novel model tunnelling machine was designed and developed as part of the research.

8.2 Experimental Procedures

8.2.1 Preparation of Clay Samples

The experimental technique adopted in the preparation of clay samples (which is a

well-established procedure) was found to produce high quality samples. Good repeatability was achieved in preparing the kaolin samples, as shown by consistent values of clay strength (Section 4.6.4). The clay strength of all samples were within ±5 % of a common mean. The measured strength of each sample agreed well with theoretical predictions based on a critical state model.

It was discovered, however, that at the end of K_o consolidation the horizontal total stresses were slightly smaller in the plane strain tank than the cylindrical tank. It is thought that this might be due to the stiffer nature of the cylindrical tank (Section 5.2).

8.2.2 Design of Tunnelling Machine

A novel model tunnelling machine was designed and constructed during the project. This machine allowed tunnel liners to be installed using similar procedures to those adopted in the construction of full scale shield tunnels using an earth pressure balance approach. It became clear during commissioning of the model tunnelling machine it was necessary to ensure that the machine was aligned correctly to a high accuracy in order to achieve accurate and repeatable tunnel installation procedures.

The main difficulties encountered during the tunnelling process were; i) during the installation of tunnels, alignment errors in the set-up of the tunnelling machine tended to lead to small differences of radial stresses acting on the liner, and ii) the water jet system adopted to remove the clay gave rise to the possibility of water coming into contact with the strain gauges and reducing the accuracy of the measurements. In order to minimize the first difficulty, a guide shaft was installed before tunnelling work (Section 4.3.2). This shaft was installed to a high accuracy using a specially designed jig bolted to the side of the test tank

(see Figure 3.7). In order to avoid water affecting the accuracy of the measurements, all strain gauges wires were enclosed in small-diameter steel tubes that were welded to the inside of the liner to ensure that the tube remained water tight (Section 3.7.3). The gauges and connections were also protected by a silicon coating.

8.2.3 Measurement Systems

During the model tests measurements were made of liner strains, pore water pressures and total stresses acting on the liner. These data were logged using a translog 500 data logger. Errors in the data logging system were shown to be very small (of the order of less than 2% of peak values). It was found that all instruments were relatively stable over a 4 day period (Section 3.8). Short-term incremental effects were measured in the model tests over a period of about 1 hour. It may be assumed, therefore, that these measurements are not subjected to errors associated with long-term drift, noise and temperature.

8.3 Interaction Between Tunnels

8.3.1 Parallel Tunnels

Interaction effects between parallel tunnels are discussed in Section 6.3. The results generally indicate that new tunnel construction reduces the total stress acting on the pillar springline of an existing tunnel. This lateral stress relief is presumably associated with the ground loss developed by construction of the adjacent tunnel. In addition, arching effects lead to an increase in vertical stress acting on the crown of the existing tunnel. This redistribution

of stress leads in turn to the development of additional bending moments. The magnitude of these additional bending moments were greatest at the pillar springline of the existing tunnel. The magnitude of the induced bending moments were generally found to be a factor of between two and six greater than the maximum liner moment before the new tunnel was installed (see Table 4.1 in Section 6.3.2). These bending moments, in turn, led to an increase in the horizontal diameter and a decrease in vertical diameter of the existing tunnel.

These results highlight the deficiencies of some of the early attempts to model this problem by finite element analysis. Ghaboussi and Ranken (1977), for example, published results that suggest that tunnel interaction effects tend to reduce the tunnel diameter (Section 2.3.2) whereas intuition (and also these test results) suggest the opposite trend. More realistic analysis in which the effects of ground loss are included (e.g. Addenbrook and Potts, 1996) give results that show the same trends as those observed in the tests.

The pillar width ratio (W/D) is an important parameter governing the magnitude of the interaction effects. As might be expected, the interaction effects increase as the pillar width ratio is reduced. Increasing the liner flexibility was found to reduce the induced bending moments but to increase the induced displacements. It is interesting to note that although the flexibility number (F) for the stiff and flexible liners adopted in the tests differed by about a factor of 3, the induced displacements were different only by a factor of about 1.5 (Section 6.3.3). This suggests that displacement interaction effects are not particularly sensitive to the value of flexibility ratio.

The results also indicate that the overconsolidation ratio has an influence on the interaction effects. Figure 6.7, for example, indicates the rather surprising result that induced displacements are larger in the normally consolidated clay samples than in the overconsolidated samples. However, it should be noted that the stress levels in the

overconsolidated clay were less than the normally consolidated sample and so the magnitude of the changes induced by new tunnel construction will be correspondingly less. Overall results suggest that the worst case for interaction effects occurs when the pillar width is small, the liner is flexible and the value of *OCR* is large.

The research project specifically considered short-term effects. However, long-term interaction effects were also measured and were generally found to be of the order of 20% greater than the corresponding short-term values.

8.3.2 Perpendicular Tunnels

The interaction mechanisms developed in the perpendicular tests are thought to be different from those operating in the parallel tests (Section 6.5). In particular a settlement mechanism is thought to act when a new tunnel is constructed below an existing tunnel. When a new tunnel is constructed above an existing liner, then vertical stress relief occurs in the existing tunnel liner leading to an increase in vertical diameter. Three-dimensional considerations suggest that interaction between parallel tunnels may be more severe than those measured in the corresponding perpendicular tunnel tests. However, the different nature of the mechanisms in the two cases appear to be more significant than this geometric effect.

An attempt was made to compare both sets of tests but the interaction mechanisms involved were sufficiently different for this comparison to be difficult. Figure 6.15 and 6.16 indicate that these two sets of data show quite different trends. These data suggest that the interaction induced by perpendicular tunnels constructed above an existing tunnel is less significant than that induced in the corresponding parallel tunnel test. For a perpendicular tunnel constructed beneath an existing tunnel, however, the data suggest that the interactions

in both the parallel and perpendicular tunnels may be similar in magnitude. It is thought, however, that in this case the additional settlement mechanism has an important influence on the results.

The additional complexities in the behaviour of perpendicular tunnels suggest that it may not be appropriate to use two-dimensional methods for design.

8.4 Mechanisms of Interaction

The mechanisms governing the structural interaction between closely spaced tunnels are highly complex. It is, for example, clear that the nature of the interaction mechanisms depends on the geometry configuration of the tunnels (e.g. side-by-side, vertically stacked, and perpendicular tunnels). For tunnels that are parallel and side-by-side, for example, construction of a new tunnel will lead to adjustments in the lateral stresses acting on the existing tunnel. In addition, arching effects within the soil may increase the vertical stresses acting on the existing tunnel. When the tunnel liners are relatively flexible, these two mechanisms will tend to interact. Additional mechanisms may come into play for tunnels that are located one above the other. For example, if a new excavation is constructed beneath an existing tunnel, then this may induce settlements in the upper tunnel. Further interaction mechanism have been proposed; for example Hansmire *et al* (1981) suggest that, for shield tunnelling, the stresses developed between the shield and the ground may lead to significant effects in any nearby tunnels. It is clear that the problem of interaction between adjacent tunnels is highly complex, and that the magnitude of any structural interaction will depend on geometry of the tunnels, the properties of the liner and soil and the method of tunnel installation.

It is of interest to consider the speed of tunnel installation adopted in the tests and the observed speed of response of the soil. It is presumed that the time-dependent response of the soil is determined by its consolidation behaviour. It may then be appropriate to consider the time scales adopted in the test in terms of the non-dimensional parameter $c_v t/D^2$ where t is time and c_v is coefficient of consolidation. A simple example may then be considered of a full-scale tunnel of diameter (say) 5m installed in a soil with identical value of c_v to that of the clay used in the tests. In this case the prototype and model time scales will be related by a factor of about 500, although the geometric scale is approximately 70. In the model test, a tunnel of length 300mm was installed in about 50 minutes; this corresponds to the installation of a 21m length of full scale tunnel in about 7 months. This rate of construction is slower than might be expected in practice. The model test data were recorded about 15 minutes after installation was complete corresponding to a period of about 2 months at full scale. It is clear then that the short-term measurements recorded in these tests may correspond to behaviour several months after tunnel completion at full scale. In the model tests, long-term effects were observed to be developed after a period of 1-2 days corresponding to a period of 15-30 years in the example full scale case. Issues relating to consolidation around the tunnels are beyond the scope of this research. This simple example is included, however, to provide a rough indication of the relationship between time scale in the model and prototype tunnels. The correlation is, of course, approximate, and the assumption of identical values of c_v is somewhat arbitrary.

8.5 Practical Applications

This research has indicated the highly complex nature of this problem. Tunnel

interaction effects have been shown to depend on tunnel spacing and alignment, liner properties, and overconsolidation ratio. In addition, interaction effects are likely to depend on tunnel installation method and the magnitude of the ground loss.

This project consisted of 8 independent plane strain interaction tests and 4 independent perpendicular tests. It is clearly not possible to extend these test results to all cases of practical interest. The results have been presented in non-dimensional format, however, and so could be used for full-scale design for cases when the range of parameters tested match those that are under consideration in practical design.

A set of simplified finite element analyses were carried and the results were shown to agree reasonably well with those obtained from the model tests. This suggests that it should be possible to use numerical methods with some confidence to carry out design calculations. Any numerical model used in this way could first be calibrated against the data presented in this thesis. It should be noted that many of the previously published finite element studies of this problem do not include the effects of ground loss. This leads to solutions that are inconsistent with field experience and also with the results of this study. However, numerical models in which ground loss is included (e.g. Addenbooke and Potts, 1996) appear to give realistic results. This suggest that currently available numerical models may be used to obtain high-quality solutions to design problems involving parallel tunnels. Satisfactory analysis of perpendicular tunnels, however, may require the use of three-dimensional numerical models.

The test results lead further weight to current understanding that interactions are not significant when the pillar width is greater than the tunnel diameter ($W>D$). Although tests were not carried out for $W>D$, the results indicate that interaction effects decay strongly as pillar width is increased. This suggests that special consideration of interaction effects in design may not be necessary for cases where $W>D$.

The model tests show that for $W<D$, induced bending moments may be substantially greater than those initially existing in the original tunnel liner. Two important practical cases would appear to exist. If a new tunnel is constructed in close proximity to a tunnel built some time previously then, presumably, the original tunnel would not have been designed to withstand the resulting interaction effects. In this case, the additional bending moments induced by adjacent tunnel construction could lead to structural damage of the liner. It may, therefore, be necessary to strengthen the existing tunnel liner. However, the existing tunnel liner may be able to support the additional loads applied to it by ring compression even if the bending moment capacity is exceeded. Although in these cases collapse may not occur, it is possible that visible cracking may occur in the original liner and that this may lead to further problems such as loss of water tightness and, for the case of reinforced concrete liner, corrosion of the reinforcement. The second case concerns the construction of two new closely spaced tunnels. In this case the liners may be designed specifically to support the additional bending moments induced by the interaction effects and the practical difficulties of dealing with interaction effects are, perhaps, less severe. It is clear that interaction effects between adjacent tunnels may be minimized by careful choice of construction procedures. The mechanisms observed in the model tests suggest, for example, that if tunnels are to be constructed one above the other then interaction effects are minimized if the lower tunnel is constructed first. The research described in this thesis is concerned entirely with shield tunnelling. However, it is possible that the use of NATM technique could lead to a reduction in interaction effects. For example, the use of NATM allows tunnels to be constructed by progressive bench cutting. It is thought that careful selection of construction procedures lead to the reduction in interaction effects.

The model test results suggest that short-term interaction effects are more significant

than the additional effects that develop over the long-term. This has important implications for the long-term behaviour of closely spaced tunnels. If, immediately after construction, interaction effects are found to be minimal, then this may provide a reasonably reliable indication that significant interaction effects will not develop in the long term.

8.6 Future Research

Based on the results of this research, future work is suggested as follows.

The model tunnelling machine used in this model tests was designed to produce a ground loss of about 6 % (Section 3.6.1). Even though this relatively large amount of overcut, it was chosen to ensure that the experiments modelled the worst case that might be expected in practice. Practical tunnelling works produce varying amounts of ground loss depending on the tunnelling methods (less than 3 % in general). It would be of interest to investigate the dependency of the interaction effects on the magnitude of the ground loss.

As mentioned above, the model tests were necessarily performed using limited values of the parameters defining the problem. The results of these investigations, however, indicated that tunnel proximity and alignment were important parameters governing the interaction behaviour. However, the case of parallel tunnels with pillar depth (vertically above or under) was not included in this research programme. The results of the perpendicular tunnel tests suggest that the interaction mechanisms in parallel, stacked tunnels may be different to those acting in side-by-side tunnels. It would be of great interest, therefore, to carried out further tests in which the stacked configuration is studied.

It is suggested that further experimental investigations for interactions between tunnels in sand could be fruitful. Comparison of interaction behaviour between the clay and sand

would be of interest.

In this dissertation, the two-dimensional elastic finite elements back-analyses were carried out with the aim of modelling the experimentally observed events (Chapter 7). Further work in this area would benefit from the use of a soil model in which a non-linear variation of shear modulus with strain is included. It is thought that three-dimensional finite element analysis using recently developed non-linear soil models could provides good solutions to this interaction problem, and the results of perpendicular tunnel tests given in this dissertation could be useful to verify the numerical modelling. It is clear that model testing and the collection of field data can only be used to study limited features of the problem. The use of numerical procedures would seem to be a promising way to extend the range of parameters that can be studied.

REFERENCES

Adachi, T. and Kojima, K (1989). *Estimation of design parameters for earth tunnels.* Proc. of the 12th ICSMFE, Rio de Janeiro, Vol.2, pp 771-774.

Addenbrooke, T.I. and Potts, D.M. (1996). *Twin tunnel construction - ground movements and lining behaviour.* Int. Symp. on Geotechnical Aspects of Underground Construction in Soft Ground, City University, London, 15-17 April.

Airey, D.W. (1984). *Clays in the circular simple shear apparatus.* Ph.D. Thesis, University of Cambridge.

Al-Tabbaa, A. (1987). *Permeability and stress-strain response of Speswhite kaolin.* Ph.D. University of Cambridge.

Anderson, W.F., Pyrah, I.C. and Fryer, S.J. (1989). *Clay calibration chamber-Specification and clay bed preparation procedures.* Report No. 50996/4, University of Sheffield.

Assadi, A and Sloan, S.W. (1991). *Undrained stability of shallow square tunnel.* J. Geotech. Div., ASCE, 117, pp 1152-1173.

Atkinson, J.H. (1993). *An introduction to the mechanics of soils and foundations.* McGraw-Hill International Series in Civil Engineering.

Atkinson, J.H., Cairncross, A.M. and James, R.G. (1974). *Model tests on shallow tunnels in sands and clay.* Tunnels and Tunnelling, 6(3), pp 28-32.

Atkinson, J.H. and Mair, R.J. (1981). *Soil mechanics aspects of soft ground tunnelling.* Ground Engineering, Vol.14, No.5, pp 20-26,38.

Atkinson, J.H. and Potts, D.M. (1977). *Stability of a shallow circular tunnel in cohesionless soil.* Géotechnique 27, No. 2, pp 203-215.

Atkinson, J.H. and Orr, T.L.L. (1976). *Experiments on model tunnels in stiff clay.* Proc. 6th European Conf. Soil Mech. Found. Eng., Vienna, 1.1, pp 227-280.

Attewell, P.B. (1977). *Ground movements caused by tunnelling in soil.* Proc. Int. Conf. Large Ground Movements and Structures, Cardiff, Pentech Press, London, pp 812-948.

Attewell, P.B. and Yeates, J. (1984). *Tunnelling in soil.* Ground movements and their effect on structure (Attewell, P.B. and Tayor, R.K., ed.), Surrey Univ. Press.

Attewell, P.B., Yeates, J. and Selby, A.R. (1986). *Soil movements induced by tunnelling and their effects on pipelines and structures.* Blackie and Son Ltd., Bishopbriggs, Glasgow.

Augarde, C.E., Burd, H.J. and Houlsby, G.T. (1995). *A three-dimensional finite element model of tunnelling.* Numerical Models in Geomechanics - NUMOG V, Pande & Pietruszczak (eds), pp 457-462.

Baligh, M.M. (1985). *Stress path method.* ASCE, J. Geotech. Engng. Div., 111, GT9, pp 1108-1136.

Balthaus, H.(1989). *Tunnel face stability in slurry shield tunnelling.* Proc. of the 12th ICSMFE, Rio de Janeiro, Vol.2, pp 775-778.

Barla, G. and Ottoviani, M.(1974). *Stresses and displacements around two adjacent circular openings near to the ground surface.* Proc. 3rd Congress, ISRM, Vol.2, Part B, pp 975-980.

Barratt, D.A., O'Reilly, M.P. and Temporal, J. (1994). *Long-term measurements of loads on tunnel linings in overconsolidated clay.* Tunnelling '94, Institution of Mining & Metallurgy and BTS, Chapman & Hall, pp. 469-481.

Brand, E.W. and Premchitt, J. (1982). *Response characteristics of cylindrical piezometers.* Géotechnique, Vol.32, No.3, pp 203-216.

Britto, A.M. (1979) *Thin walled buried pipes.* Ph.D. Thesis, University of Cambridge.

Broms, B.B. and Bennermark, H. (1967). *Stability of clays at vertical openings.* ASCE, J. SMFD, 93, SM1, pp 71-94.

Burns, J.Q. and Richard, R.M. (1964). *Attenuation of stresses for buried cylinders.* Proc. Sym. on Soil-Structure Interaction, Tucson, pp 378-392.

Casarin, C. (1977). *Soil deformations around tunnel headings in clay.* M.Sc. Thesis, University of Cambridge.

Cairncross, A.M. (1973). *Deformations around model tunnels in stiff clay.* Ph.D. Thesis, University of Cambridge.

Clegg, D. (1981). *Model piles in stiff clay.* Rh.D. Thesis, University of Cambridge.

Clough, G.W. (1981). *Innovations in tunnel construction and support techniques.* Bulletin Association of Engrg. Geologists, XVIII (2), pp 151-167.

Clough, G.W. and Finno, R.J. (1983). *Measured soil response to EPB shield tunneling.* Journal of Geotechnical Engineering, Vol.109, No.2, pp 131-149.

Clough, G.W. and Schmidt, B. (1981). *Design and performance of excavation and tunnels in soft clay.* Chapter 8, Soft Clay Engineering, Elsevier Scientific Publishing Co.

Cooley, P. (1982). *Wedge-block tunnels in water supply.* Journal of Water Engineers and Scientists, Vol.36, Feb, pp 9-26.

Cooling, L.F. and Ward, W.H. (1953). *Measurements of load and strain in earth supporting structures.* Proc. 3rd Int. Conf. Soil Mech. Fndn Engng, Zurich, Vol.2, pp 162-166.

Cording, E.J. and Hansmire, J.B. (1975). *Displacements around soft ground tunnels.* Proc. 5th Panam. Conf. Soil Mech. found. Eng., Buenos Aires, 4, pp 571-633.

Craig, W.H. and Chua, K. (1990). *Deep penetration of spud-can foundations on sand and clay.* Géotechnique 40, No.4, pp 541-556.

Davis, E.H., Gunn, M.J., Mair, R.J. and Seneviratne, H.N. (1980). *The stability of shallow tunnels and underground openings in cohesive material.* Géotechnique 30, No.4, pp 397-416.

Davidson, C.S. (1980). *The shear modulus of clays.* Part II project, University of Cambridge.

Deere, D.U., Peck, R.B., Monsees, J.E. & Schmidt, B. (1969). *Design of tunnel liners and support systems.* Report for U.S. Dept. of Trans., Office of High Speed Ground Trans., Contract No. 3-0152.

Duffaut, P. and Panet, M. (1989). *Convergence-confinement method for tunnels in ground.* Proc. of the 12th ICSMFE, Vol.2,Rio de Janeiro,pp783-784.

Einstein, H.H. and Schwartz, C.W.(1979). *Simplified analysis for tunnel support.* Journal of Geotechnical Engineering Div., ASCE, Vol.105, No. GT4, pp 499-518.

Eisenstein, Z. and Branco, P. (1985). *Convergence-confinement method in shallow tunnels.* Proc. of the 11th ICSMFE, Vol.4, San Francisco, pp 2067-2071.

Elmes, D. (1985). *Creep and viscosity in two kaolin clays.* Ph.D. Thesis, University of Cambridge.

Fang, Y.S., Lin, J.S. and Su, C.S. (1994). *An estimation of ground settlement due to shield tunnelling by the Peck-Fujita method.* Canadian Geotechnical Journal, Vol. 31, No. 3, pp 431-443.

Fernández-Moya, J., Oteo, C.S. and Sagaseta, C. (1981). *Predicción de asientos producidos por la excavación de túneles.* Simp. Uso Industrial del Subsuelo. Vol. 1, paper 2-3, Madrid.

Fannin, R.J. (1986). *Geogrid reinforcement of granular layers on soft clay - a study at model and full scale.* D.Phil. Thesis, University of Oxford.

Fotieva, N.N. and Sheinin, V.I. (1966). *Distribution of stresses in the lining of a circular tunnel when driving a parallel tunnel.* Soil Mech. Found. Engng, 6,pp 417-422.

Fujita, K. (1989). *Underground construction, tunnel, underground transportation.* Proc. of the 12th ICSMFE, Rio de Janeiro, Vol.4, pp 2159-2176.

Ghaboussi, J.and Ranken, R.E.(1977). *Interaction between two parallel tunnels.* International Journal for Numerical and Analytical Methods in Geomechanics, Vol.1, pp 75-103.

George K.P.and Yusuf M.J.B.(1981). *Tunnel liner subjected to excavation loading.* Proc. of the 10th ICSMFE, Stockholmn, Vol.1, pp 297-300.

Gesta, P. (1986). *Recommendations for use of the convergence-confinement method.* Tunnels Ouvrages Souterrains 73, pp 18-39.

Gioda, G.and Jurina, L.(1981). *Identification of earth pressure on tunnel liners.* Proc. of the 10th ICSMFE, Stockholmn, Vol.1, pp 301-304.

Glossop, N.H. (1977). *Soil deformation caused by soft ground tunnelling.* PhD thesis, Univ. of Durham.

Grant, R.J. and Taylor, R.N. (1996). *Centrifuge modelling of ground movements due to tunnelling in layered ground.* Int. Symp. on Geotechnical Aspects of Underground Construction in Soft Ground, City University, London, 15-17 April.

Gue, S.S. (1984). *Ground heave around driven piles in clay.* D.Phil. Thesis, University of Oxford.

Hansmire, W.H., Parker, H.W., Ghaboussi, J., Casey, E.F. and Lentell, R.L. (1981). *Effects of shield tunneling over subways.* Proc. 3rd Rapid Exca. and Tunneling Conf., pp.254-276.

Henkel, D.J. (1960). *The shear strength of saturated remoulded clays.* Proc. Research Conf. Shear Strength of Cohesive Soils, Boulder, Colo., pp 533-560.

Hisatake, M. (1994). *Ground surface settlements due to shield tunnels.* Soil Structure Interaction: Numerical Analysis and Modelling, Edited by John W. Bull, Published by E&FN Spon, pp 647-672.

Höeg, K.(1968). *Stresses against underground structural cylinder.* Journal of the Soil Mechanics and Foundation Division, ASCE, Vol.94, No. SM4, pp 833-858.

Houlsby, G.T. (1993). *In lecture notes for reinforced soil: Mechanics and Design.* Short course at Oxford University, 19-21 April.

Imamura,S., Nomoto,T., Mito,K., Ueno,K. and Kusakabe,O. (1996). *Design and development of underground construction equipment in a centrifuge.* pp.453-458.

ITA Working Group. (1988). *Guidelines for the design of tunnels.* Tunnelling and Underground Space Technology, Vol.3, No.3, pp 237-249.

Jardine, R.J., Potts, D.M., Foutie, A.B. and Burland, J.B. (1986). *Studies of the influence of non-linear stress-strain characteristics in soil-structure interaction.* Geotéchnique, Vol. 36, No.3, pp 377-396.

Kanzkai, Y., Yamada, Y. and Asai, K. (1992). *Construction of main tunnel entrance of two crossing tunnels subject to unsymmetrical earth pressures.* In Towards New Worlds in Tunnelling, Utesa, V. and Cararaxo, M. (eds), Balkema, Rotterdam, pp 373-380.

Kim, S.H. (1993). *Model testing of the interactions between closely spaced tunnels in clay.* First Year report, University of Oxford.

Kim, S.H., Burd, H.J. and Milligan, G.W.E. (1996). *Interaction between closely spaced tunnels in clay.* Int. Symp. on Geotechnical Aspects of Underground Construction in Soft Ground, City University, London, 15-17 April.

Kimmance, J.P., Lawrence, S., Hassan, O., Purchase, N.J. and Tollinger, G. (1996). *Observations of deformations created in existing tunnels by adjacent and cross cutting excavations.* pp.617-622.

Kimura T.and Mair R.J.(1981). *Centrifugal testing of model tunnels in soft clay.* Proc. of the 10th ICSMFE, Stockholmn, Vol.1, pp 319-322.

Kitamura, M., Ito, S. and Fugiwara, T. (1981). *Shield tunneling performance and behaviour of soft ground.* Proc. Rapid Exca. and Tunneling Conf., Vol.1, pp 201-220.

Ladd, C.C. and Foott, R., Ishihara, K., Schlosser, F. and Poulos, H.G. (1977). *Stress-deformation and strength characteristics*: state of the art report. Proc. 9th Int. Conf. Soil Mech. Fndn Engng, Tokyo, 2, pp 421-494.

Leca, E. (1989). *Analysis of NATM and shield tunneling in soft ground.* D.Phil. Thesis, Virginia Polytechnic Institute and State University.

Leca, E. and Dormieux, L. (1990). *Upper and lower bound solutions for the face stability of shallow circular tunnels in frictional material.* Géotechnique 40, No.4, pp 581-606.

Ledesma, A., Gens, A. and Alonso, E.E. (1987). *Identification of parameters in a tunnel excavation problem.* Proc. 2nd Int. Conf. Num. Models in Geomechanics, Ghent, pp 333-344.

Lee, K.M. and Rowe, R.K. (1988). *Effects of undrained strength anisotropy on surface subsidence induced by the construction of shallow tunnels.* Geotech. Research Centre Report, GEOT-11-88, Faculty of Engineering Science, The Univ. of Western Ontario, London.

Lee, K.M. and Rowe, R.K. (1989). *Deformations caused by surface loading and tunnelling: the role of elastic anisotropy.* Géotechnique 39, No.1, pp125-140.

Lombardi, G. (1974). *Nociones generales sobro la estática de los túneles.* 1er Simposio Nacional sobro Túneles, Madrid, Vol. 2, pp 125-141.

Lo, K.W., Lee, S.L., Makino, H., Chang, L.K., Leung, C.F. and Mihara, T. (1987). *Tunnels in close proximity.* Proc. Singapore MRT Conf., Singapore, pp 275-281.

Love, J.P. (1984). *Model testing of geogrids in unpaved roads.* D.Phil. thesis, University of Oxford.

Mair, R.J. (1979). *Centrifugal modelling of tunnel construction in soft clay.* Ph.D. Thesis, University of Cambridge.

Mair, R.J. (1983). *Geotechnical aspects of soft ground tunnelling.* Proc. Int. Seminar on Construction Problems in Soft Soils, Singapore, Nanyang Technological Institute, Singapore.

Mair, R.J. (1987). *Tunnel face pressure, Soft clay.* Proc. 8th Asian regional conference on SMFE. JSSMFE, Tokyo. Vol.2, pp 290.

Mair,R.J., Taylor,R.N. and Bracegirdle ,A. (1993). *Surface settlement profiles above tunnels in clays.* Geotéchnique, Vol.43, No.2, pp.315-320.

Martin, C.M. (1994). *Physical and numerical modelling of offshore foundation under combined loads.* D.Phil. Thesis, University of Oxford.

Martins, J.P. (1983). *Shaft resistance of axially loaded piles in clay.* Ph.D. Thesis, Imperial College, University of London.

Matsushita, H. (1979). *Earth pressure balanced shield method - A new developed tunneling method for loose subaqueous sandy soil.* Proc. Rapid Exca. and Tunneling Conf., Vol. 1, pp 521-530.

May, R.E. (1987). *A study of the piezocone penetrometer in normally consolidated clay.* D.Phil. Thesis, University of Oxford.

Mitchell, J.K. (1976). *Fundamentals of soil behaviour.* New York: John Wiley & Sons.

Mitchell, R.J. (1983). *Earth structures engineering.* Allen and Unwin., Boston.

Mori, A., Tamura, M., Kurihara, K. and Shibata, H. (1991). *A suitable slurry pressure in slurry-type shield tunnelling.* Tunnelling 91, Institution of Mining & Metallurgy, Elsevier Applied Science, pp 361-369.

Muir Wood, D. (1990). *Soil behaviour and critical state soil mechanics.* Cambridge University Press.

Murayama, S. (1979). *Development and future trend of shield tunnelling in Asian area.* Report to Research Working Group of the ITA, Atlanta, Ga.

Ng, R.M.C. and Lo, K.T. (1985). *The measurements of soil parameters relevant to tunnelling in clays.* Canadian Geotechnical Journal, Vol.22, No.3, pp 375-391.

Nishimura, M., Wadabayashi, M., Wanatabe, K., Daikoku, A. and Iai, Y. (1994). *The excavation of effects by motorway tunnel excavation on nearby railway tunnel in operation and the supervising system to maintain the tunnel stability.* In Tunnelling and Ground Conditions, Salem, A. (ed.), Balkema, Rotterdam, pp 67-74.

Nyirenda, Z.M. (1989). *The piezocone in lightly overconsolidated clay.* D.Phil. thesis, University of Oxford.

O'Reilly, M.P. and New, B.M. (1982). *Settlements above tunnels in the United Kingdom - their magnitude and prediction.* Tunnelling '82, pp 173-181.

Orr, T.L.L. (1976). *The behaviour of lined and unlined model tunnels in stiff clay.* Ph.D. Thesis, University of Cambridge.

Oteo, C.S.and Sagaseta, C. (1982). *Prediction of settlements due to underground openings.* Int. Sym. on Numerical Methods in Geomechanics, Zurich, pp 653-659.

Perri, G. (1994). *Analysis of the effects of the two new twin tunnels excavation very close to a big diameter tunnel of the Caracas subway.* In Tunnelling and Ground Conditions, Salem, A. (ed.), Balkema, Rotterdam, pp 523-530.

Peck, R.B.(1969). *Deep excavations and tunneling in soft ground.* Proc. of the 7th ICSMFE, Mexico, State-of-the-Art Report Volume, pp 225-290.

Peck, R.B., Deere, D.U., Moness, J.E., Parker, H.W. and Schmidt, B. (1969). *Some design considerations in the selection of underground support system.* Report for Us Dept. of Transportation, Office of High Speed Ground Transpotation, Contract 3-0152.

Peck, R.B., Hendron, A.J. and Mohraz, B.(1972). *State of the art of soft ground.* Proc. 1st Rapid Excavation and Tunneling Conference, AIME, (1), pp 259-286.

Penman, A.D.M. (1960). *A study of the response time of various types of piezometers.* Proc. of the Conf. on Pore Pressure and Suction in Soils, Butterworths, London, pp 53-58.

Potts, D.M. (1976). *Behaviour of lined and unlined tunnels in sand.* Ph.D. Thesis, University of Cambridge.

Randolph, M.F., Steenfelt, J.S. and Wroth, C.P. (1979). *The effect of pile type on design parameters for driven piles.* Proc. 7th European Conf. Soil Mech. Fndn Engng, Brighton, 2, pp 107-114.

Rankin, W.J. (1988). *Ground movements resulting from urban tunnelling.* Proc. Conf. Engng Geol. Underground Movements, Nottingham, pp 79-92.

Roscoe, K.H. and Burland, J.B. (1968). *On the generalised stress-strain behaviour of 'wet' clay.* In Engineering Plasticity, Eds. J. Heyman and F.A. Leckie, Cambridge University Press, pp 535-609.

Sagaseta, C. (1987). *Analysis of undrained soil deformation due to ground loss.* Géotechnique 37, No.3, pp 301-320.

Saitoh, A., Gomi, K. and Shiraishi, T. (1994). *Influence forecasts and field measurement of a tunnel excavation crossing right above existing tunnels.* In Tunnelling and Ground Conditions, Salem, A. (ed.), Balkema, Rotterdam, pp 83-90.

Santa Maria, P.E.L. de (1988). *Behaviour of footings for offshore structures under combined loads*. D.Phil. Thesis, University of Oxford.

Sauer, G. and Jonuscheit, P. (1976). *Kräfteumlagerungen in der zwischenwand eines deppelröhrentunnels im zuge eines synchronvortriebes*. Rock Mechanics, 8, No.1, pp 1-22.

Schmidt, B. (1966). Discussion on, *Earth pressures at rest related to stress history*, by Brooker, E.W. & Ireland, H.O. Can. Geotech. J., 3, pp 239-242.

Schmidt, B. (1969). *Settlements and ground movements associated with tunnelling in soil.* PhD. thesis, University of Illinois.

Schmidt, B. (1988). Discussion on: Sagaseta,C.: *Analysis of undrained soil deformation due to ground loss*, Author's reply to B. Schmidt. Géotechnique 38, No.4, pp 647.

Seneviratne, H.N. (1979). *Deformation and pore pressure dissipation around shallow tunnels in soft clay*. Ph.D. Thesis, University of Cambridge.

Sheeran, D.E. and Krizek, R.J. (1971). *Preparation of homogeneous soil samples by slurry consolidation*. Jour. of Materials, Vol.6, No. 2, pp 356-373.

Sinha, R.S. (1989). *Underground structures*. Development in Geotechnical Engineering, 59 A, Elsevier, pp 200.

Sloan, S.W. and Assadi, A. (1993). *Stability of shallow tunnels in soft ground.* Predictive Soil Mechanics, Wroth Symposium, pp 644-663.

Smith, M.G. (1993). *A laboratory study of the Marchetti dilatometer.* D.Phil. Thesis, University of Oxford.

Smith, O.R. (1970). *Discussion on the Victoria Line.* Proc. Instn Civ. Engrs, Supplement xiii, Paper 7270s, pp 319-322.

Soliman, E., Duddeck, H, and Ahrens, H. (1993). *Two-and three-dimensional analysis of closely spaced double-tube tunnels*. Tunnelling and Underground Space Technology, Vol.8, No. 1, pp 13-18.

Stallebrass, S.E. (1990). *Modelling the effects of recent stress history on the deformation of overconsolidated clays.* Ph.D. thesis, City University, London.

Stallebrass, S.E., Grant, R.J. and Taylor, R.N. (1996). *A finite element study of ground movements measured in centrifuge model tests of tunnels*. Int. Symp. on Geotechnical Aspects of Underground Construction in Soft Ground, City University, London, 15-17 April.

Steenfelt, J.S., Randolph, M.F. and Wroth, C.P. (1981). *Instrumented model piles jacked into clay*. Proc. 10th Int. Conf. Soil Mech. Fndn Engng, Stockholm, 2, pp 857-864.

Stein, D., Möllers, K. and Bielecki, R. (1989). *Microtunnelling.* Ernst and Shon, pp 119-120.

Széchy, K. (1961). *The art of tunnelling.* Akademiai Kiado, Budapest.

Tattersall, F., Wakeling, T.R.M. and Ward, W.H. (1955). *Investigations into the design of pressure tunnels in London Clay.* Proc. Instn Civ. Engrs, Vol.4, No.4, pp 400-455.

Taylor, R.N.(1984). *Ground movements associated with tunnels and trenches.* Ph.D.thesis, University of Cambridge.

Terzaghi, H. (1942). *Liner-plate tunnels on the Chicago subway.* Proc. ASCE, 68, No.6, pp 862-899.

Uriel, A.O. and Sagaseta, C.(1989). *Selection of design parameters for underground construction.* Proc. of the 12th ICSMFE, Rio de Janeiro, Vol.4, pp 2521-2551.

Viggiani, G. and Atkinson, J.H. (1995). *Stiffness of fine-grained soil at very small strains.* Geotéchnique 45, No. 2, pp 249-265.

Wang, J.J. and Chang, C.T. (1992). *Numerical method in analysis of staked tunnels.* In Towards New Worlds in Tunnelling, Utesa, V. and Cararaxo, M. (eds), Balkema, Rotterdam, pp 197-202.

Ward W.H. and Pender M.J. (1981). *Tunnelling in soft ground.* Proc. of the 10th ICSMFE, Stockholmn, Vol.4, pp 216-275.

Ward, W.H. and Thomas, H.S.H. (1965). *The development of earth loading and deformation in tunnel linings in london clay.* Pro. of the 6th ICSMFE, Vol.2, Toronto, pp 432-436.

Wroth, C.P. (1984). *The interpretation of in situ soil tests.* Géotechnique 34, No.4, pp.449-489.

Wroth, C.P. and Houlsby, G.T. (1985). *Soil mechanics-property characterisation, and analysis procedures.* Proc. 11th Conf. Soil Mech., San Francisco 1, pp 1-55.

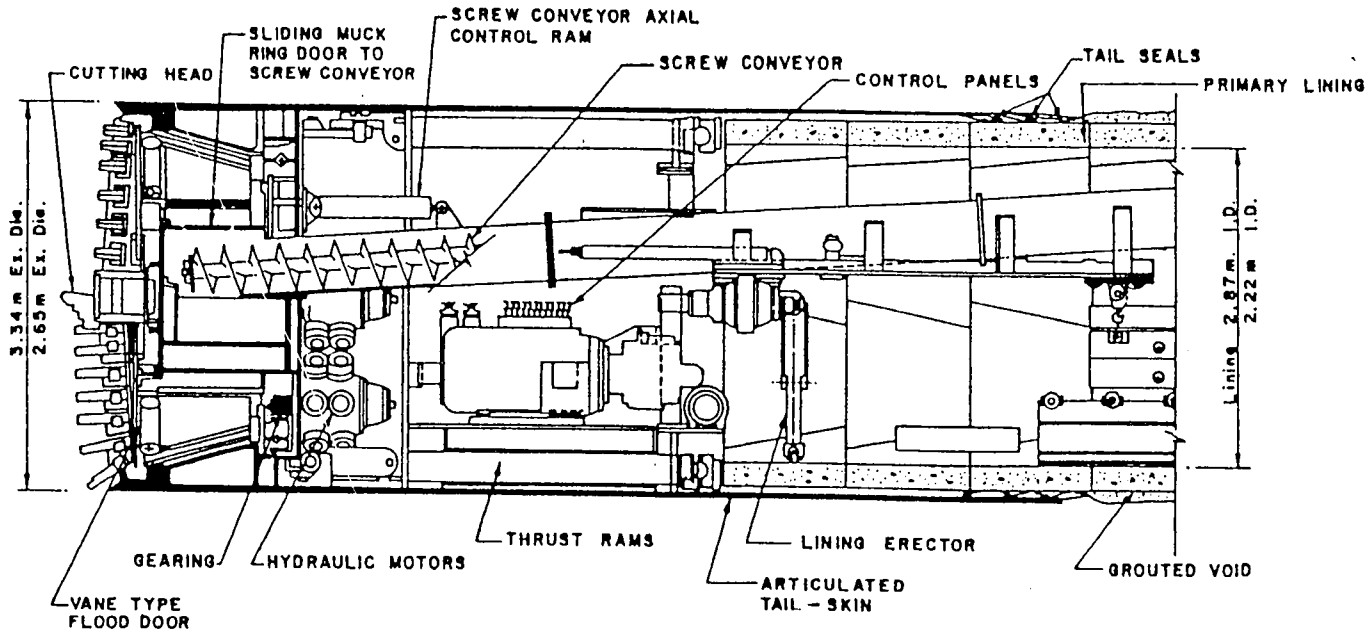


FIGURE 2.1 Earth Pressure Balance Shield Tunnelling Machine

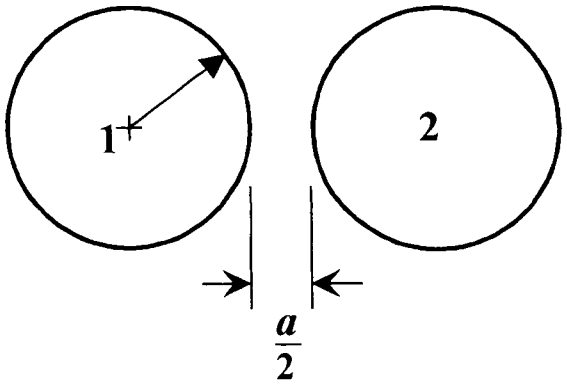
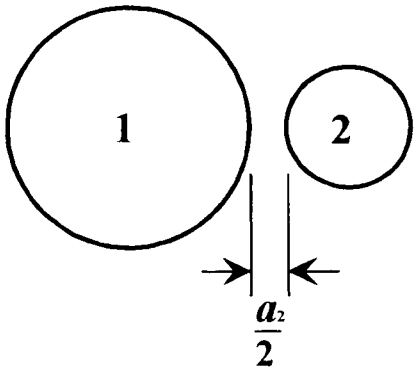
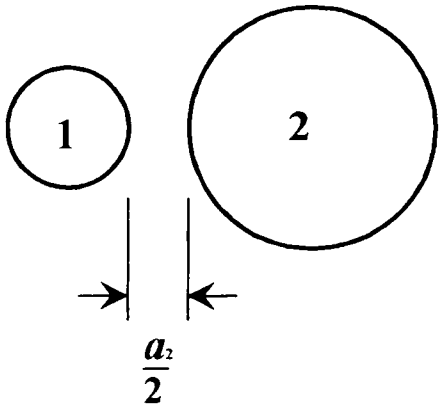
Order of Excavation	*Distortion*	
	Tunnel 1	**Tunnel 2**
	$\frac{2\Delta a}{a}$	$\frac{\Delta a}{a}$
	$\frac{\Delta a_1}{a_1}$ **With local curvature equal to twice that for the above distortion**	$\frac{\Delta a_2}{a_2}$
	$\frac{2\Delta a_1}{a_1}$	$\frac{\Delta a_2}{a_2}$

FIGURE 2.2 Increased Distortion of Adjacent Tunnels in Soft Ground (Peck *et al.*, 1969)

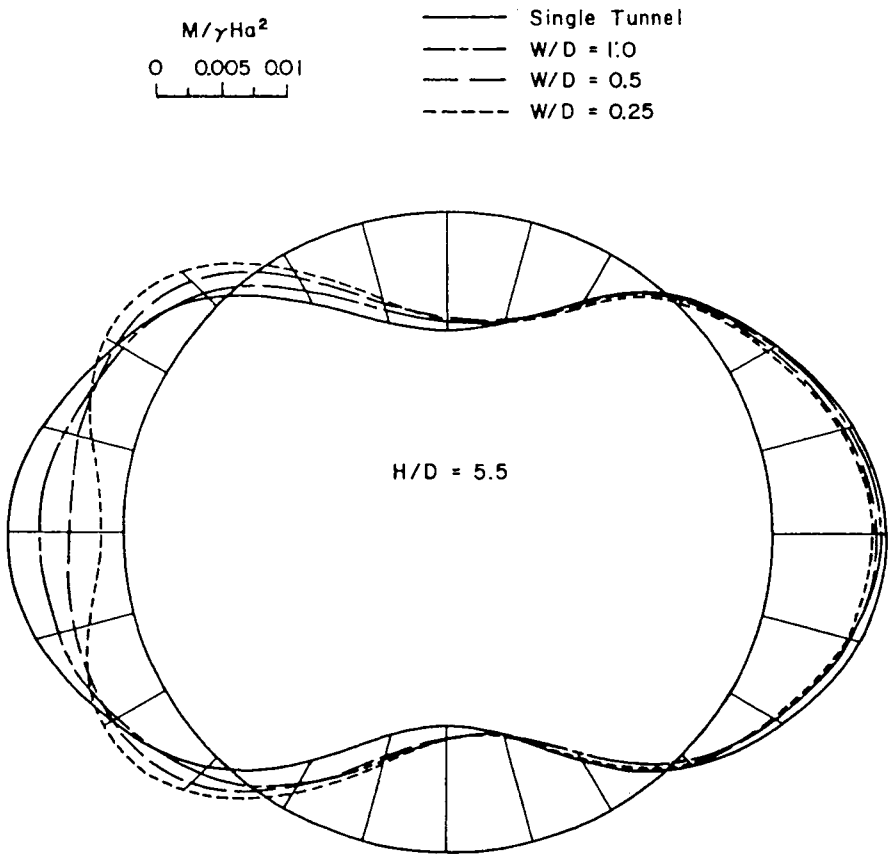


FIGURE 2.3 Moments Distribution (after Ghaboussi and Ranken, 1977)

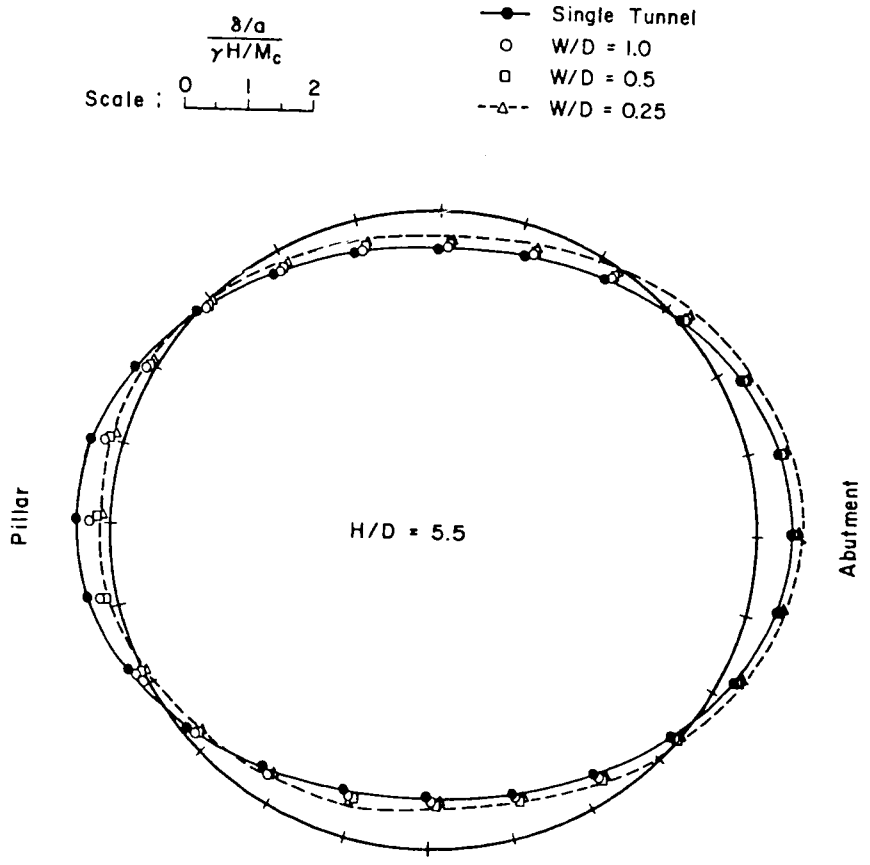


FIGURE 2.4 Displacements Distribution (after Ghaboussi and Ranken, 1977)

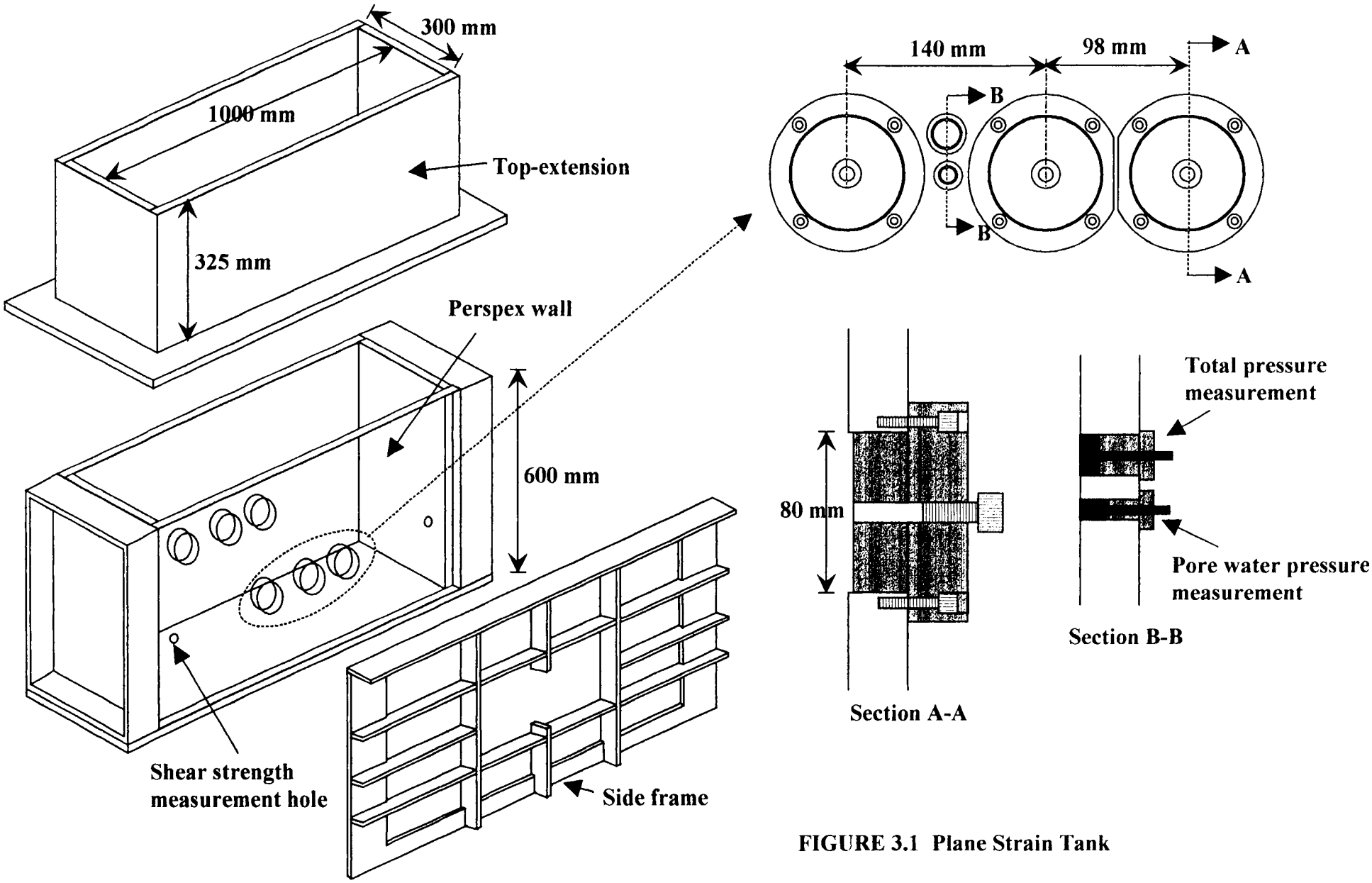


FIGURE 3.1 Plane Strain Tank

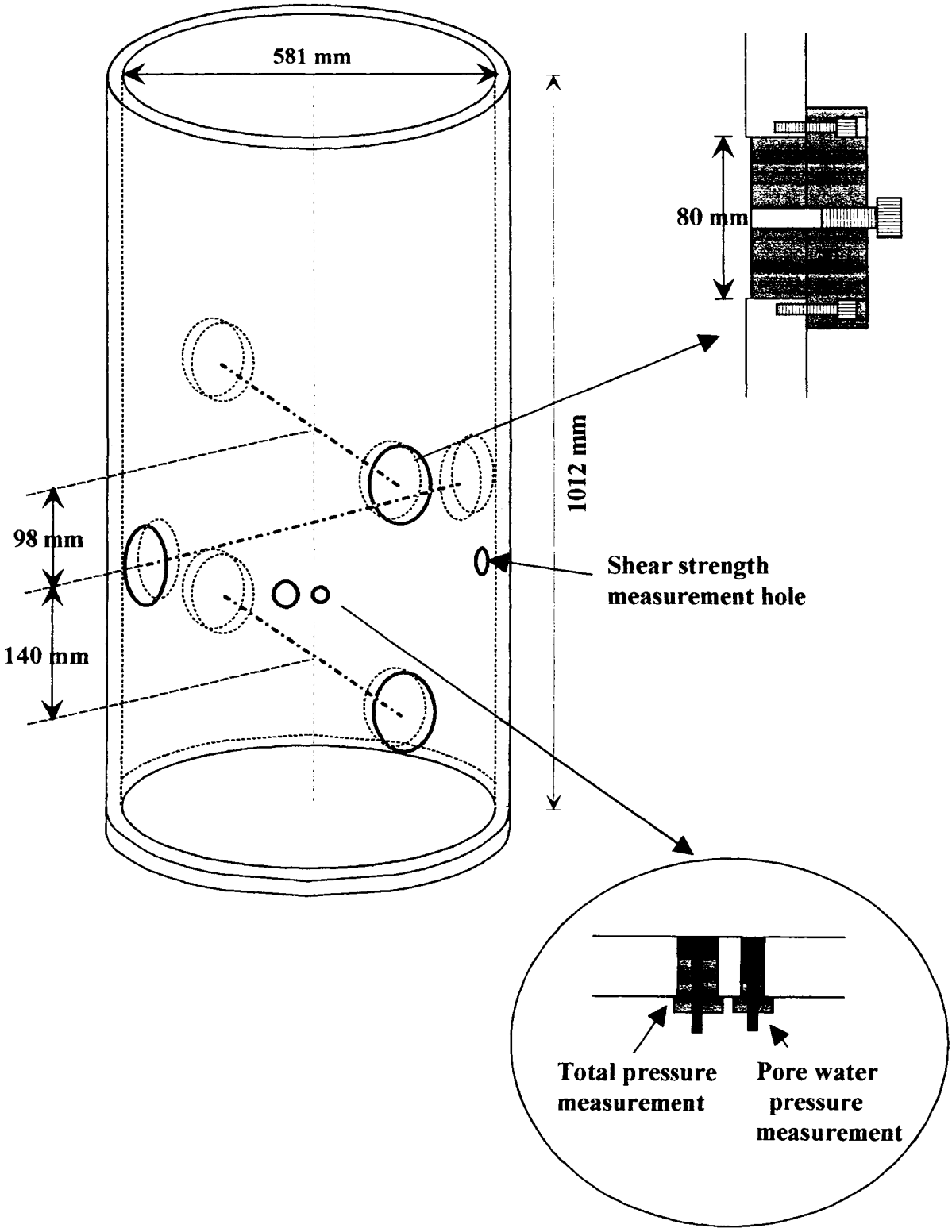


FIGURE 3.2 Cylindrical Tank

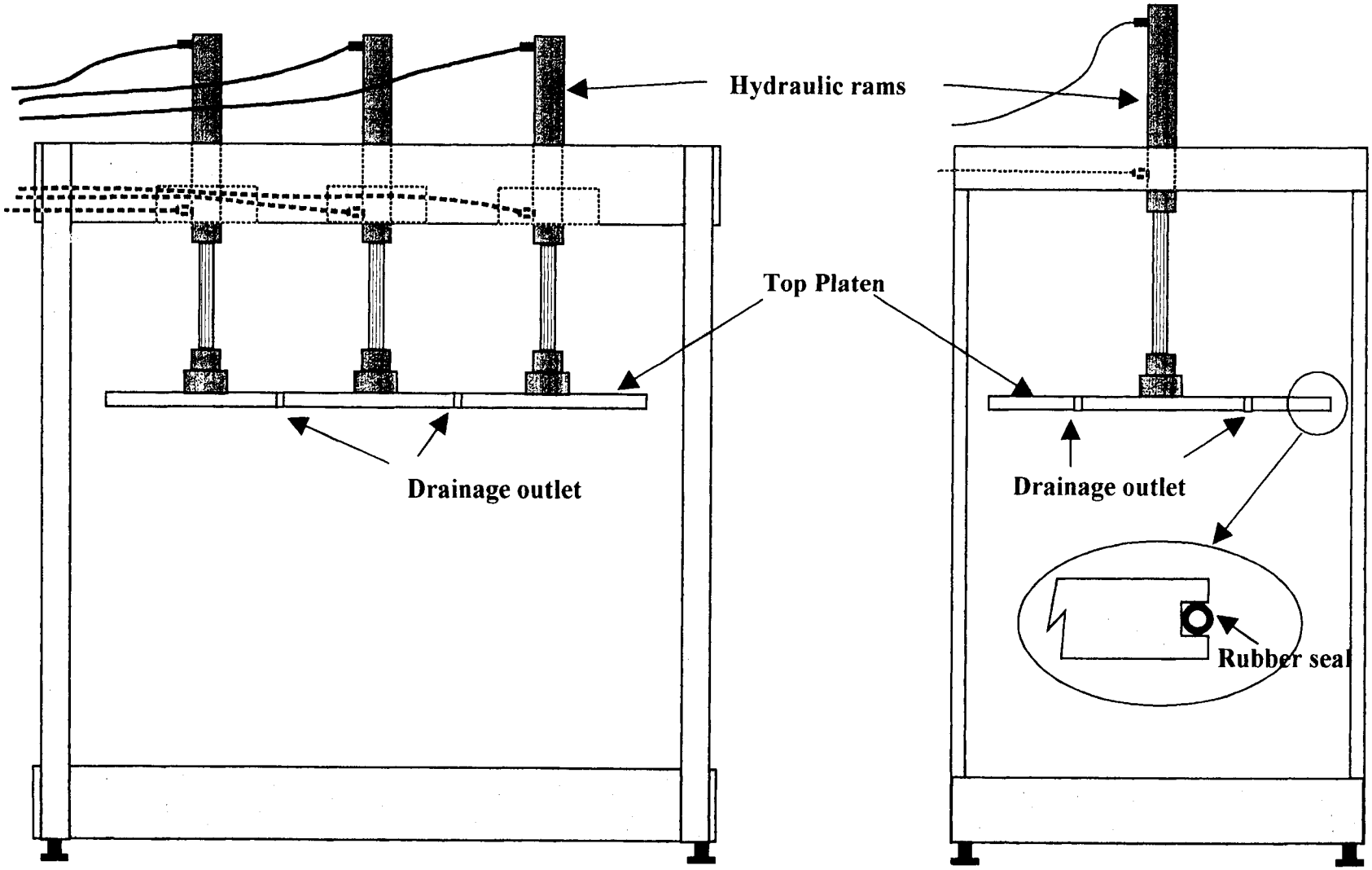


FIGURE 3.3 Reaction Frames

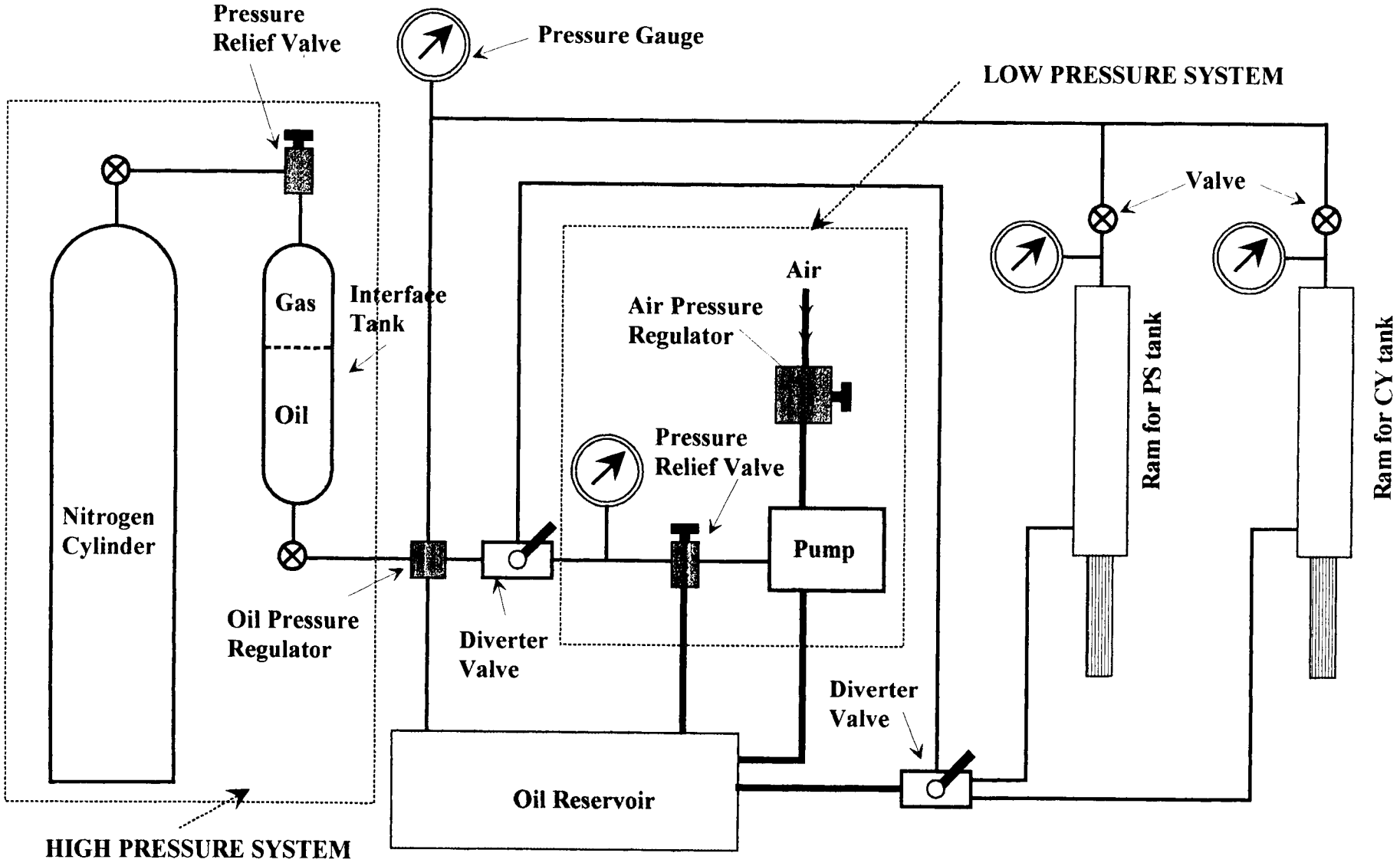


FIGURE 3.4 Pneumatic and Hydraulic Control System

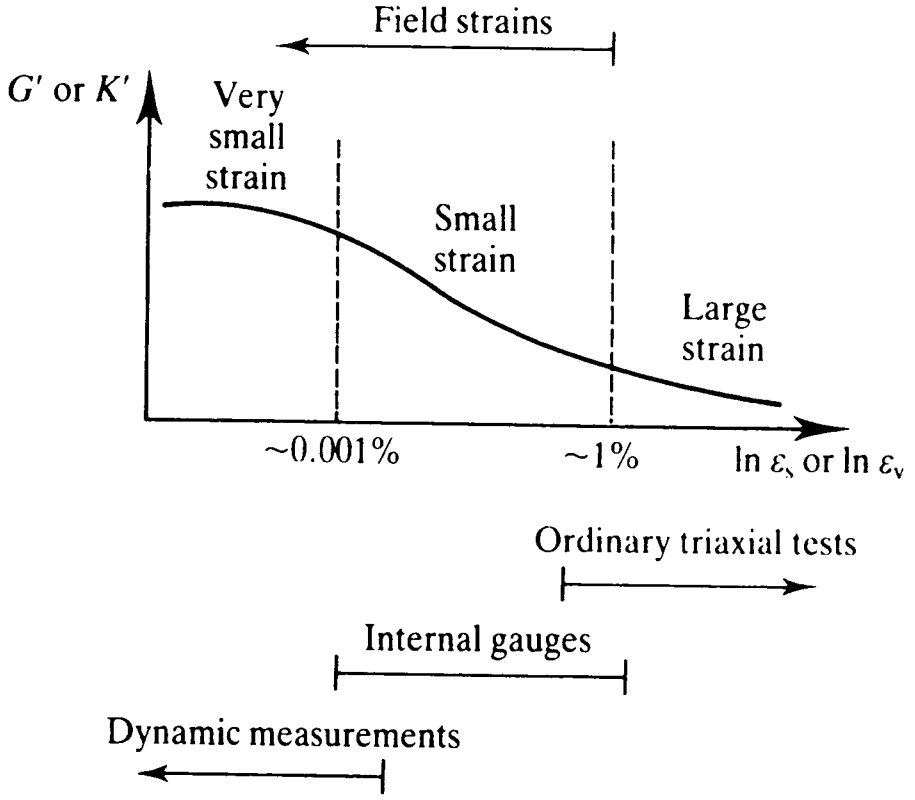


FIGURE 3.4.1 Typical Plot of Shear Modulus against Strain (after Atkinson, 1993)

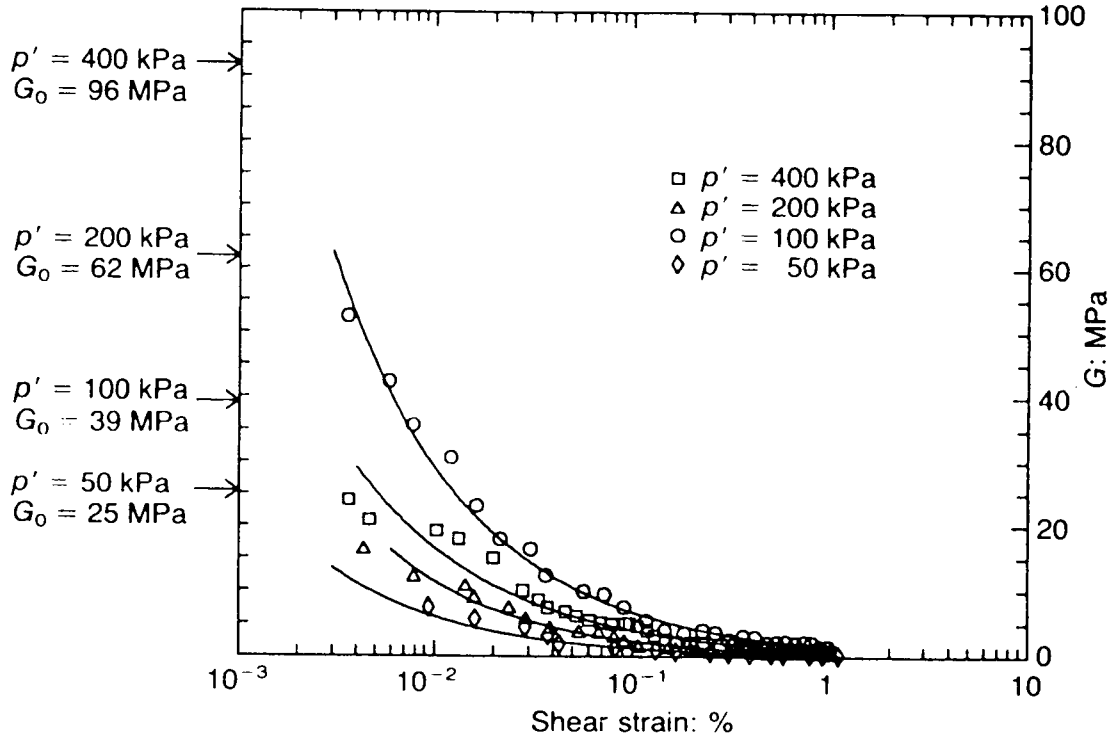
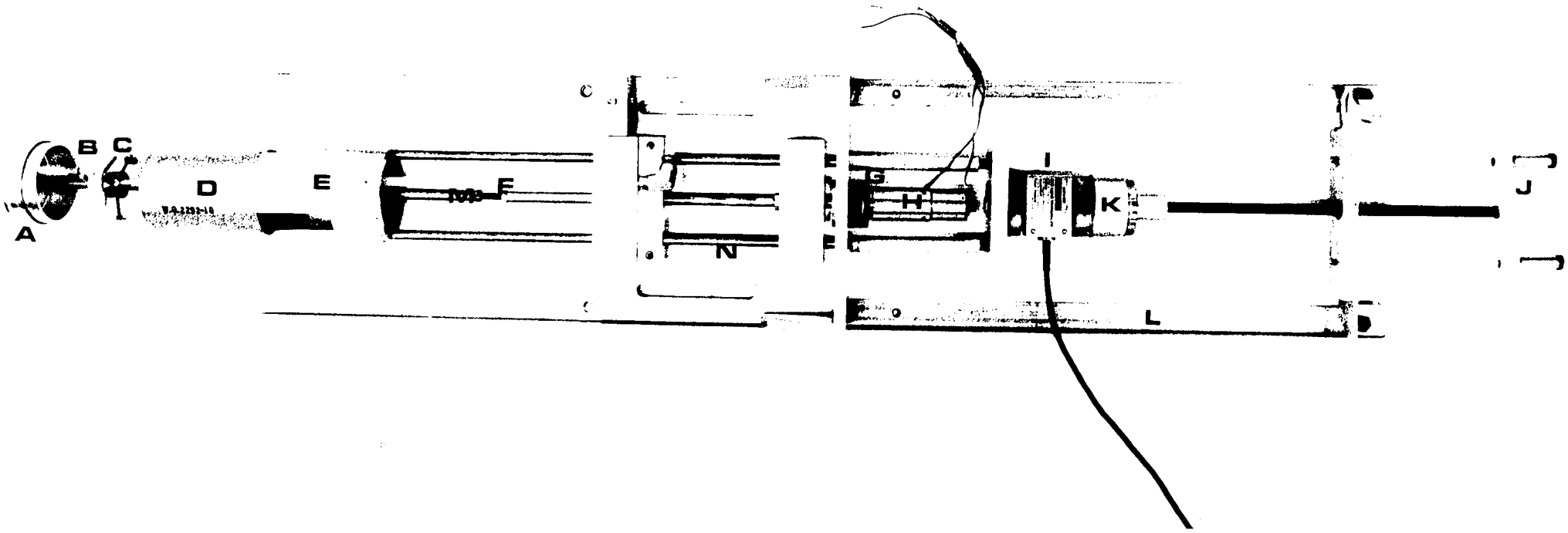


FIGURE 3.4.2 Variation of Shear Modulus with Strain for Kaolin Clay (after Viggani and Atkinson, 1995)



A: Cutting head B: Water jet nozzel C: Liner holder D: Liner E: Liner pushing head

F: Water supply hose G: Gear box H: Motor I: Load cell J: Pushing handle

K: Axial bearing L: Guide lane M: Centreline shaft N: Side shaft

FIGURE 3.5 Model Shield Tunnelling Machine

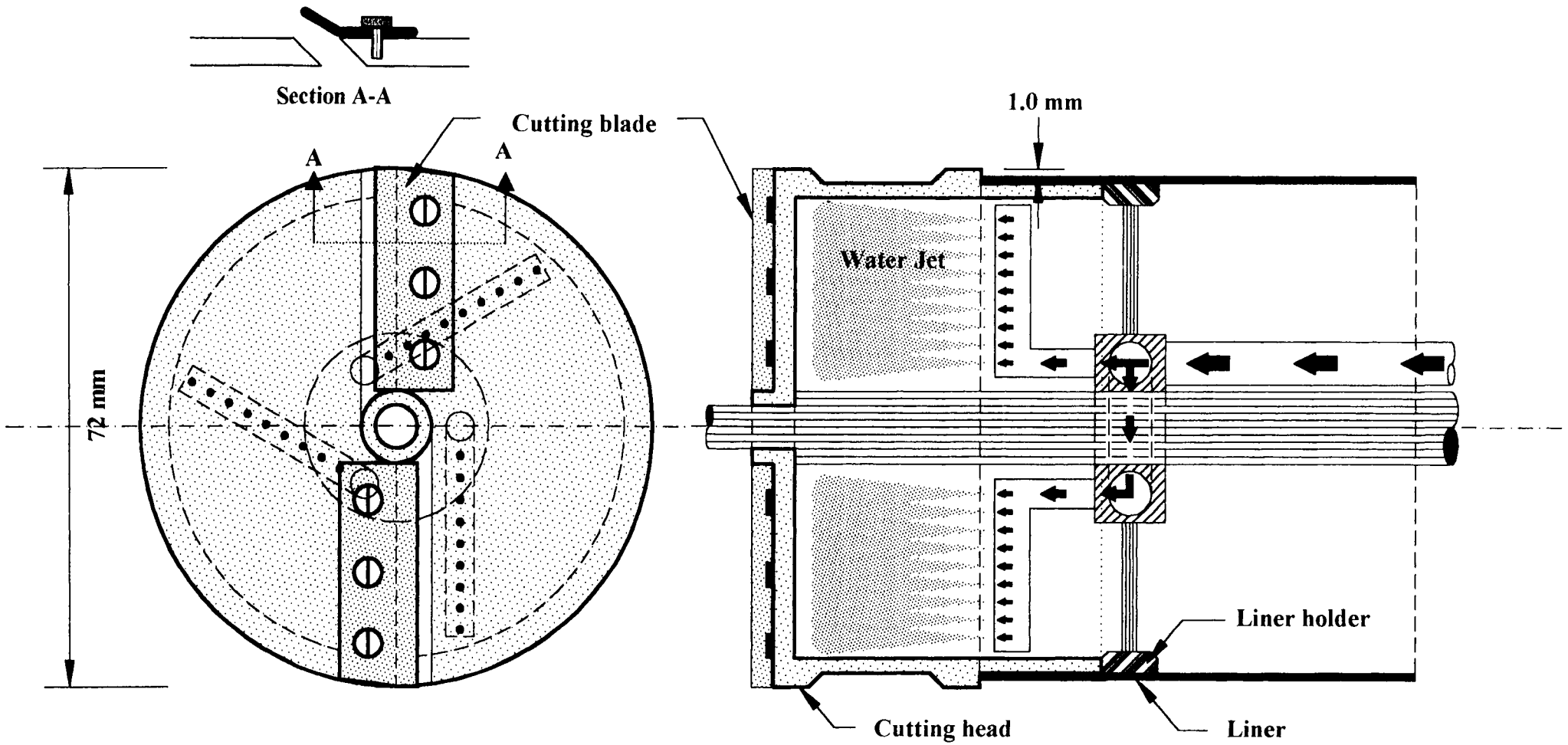


FIGURE 3.6 Cutting Head and Water Jet System

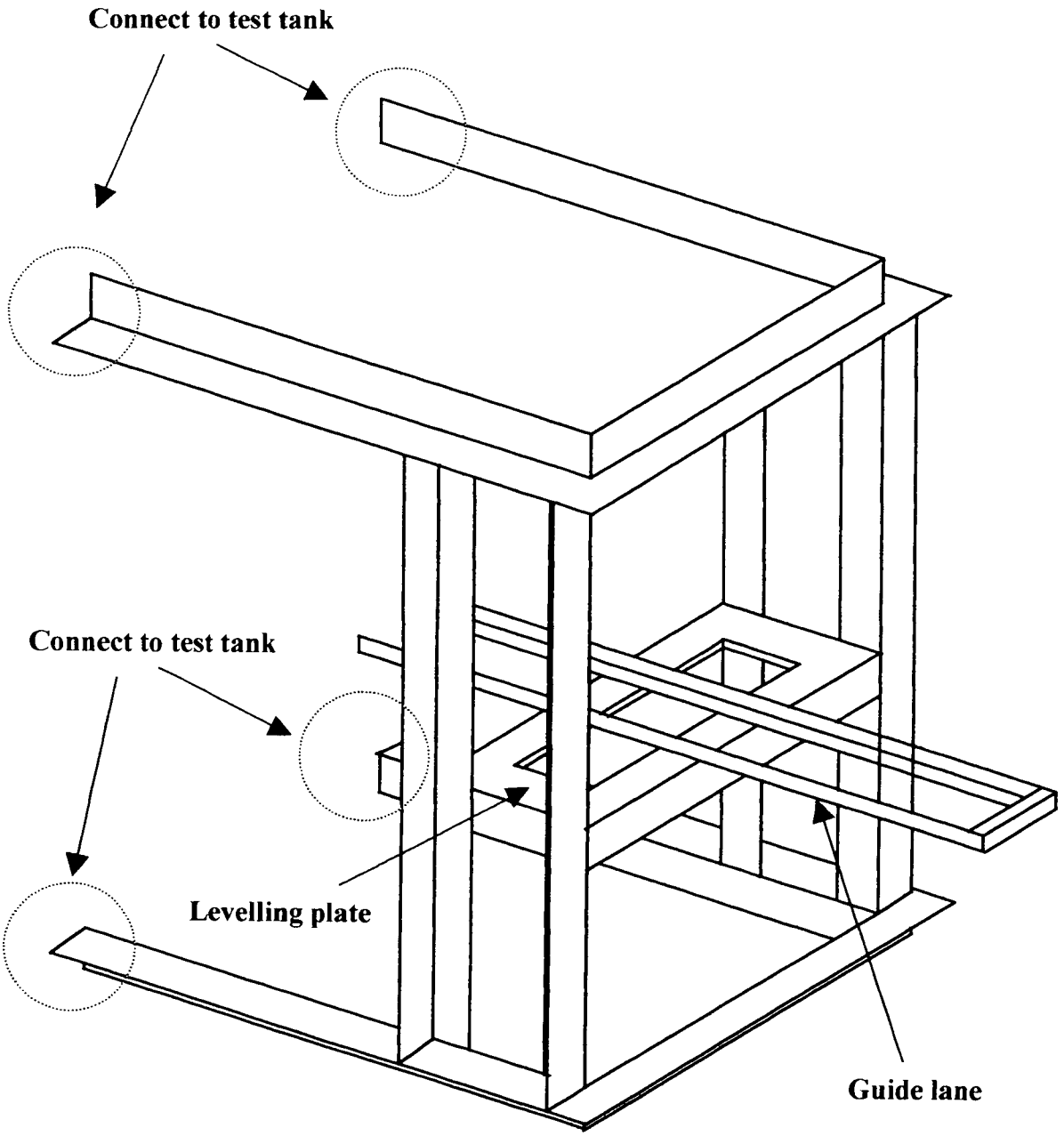


FIGURE 3.7 Reference Frame

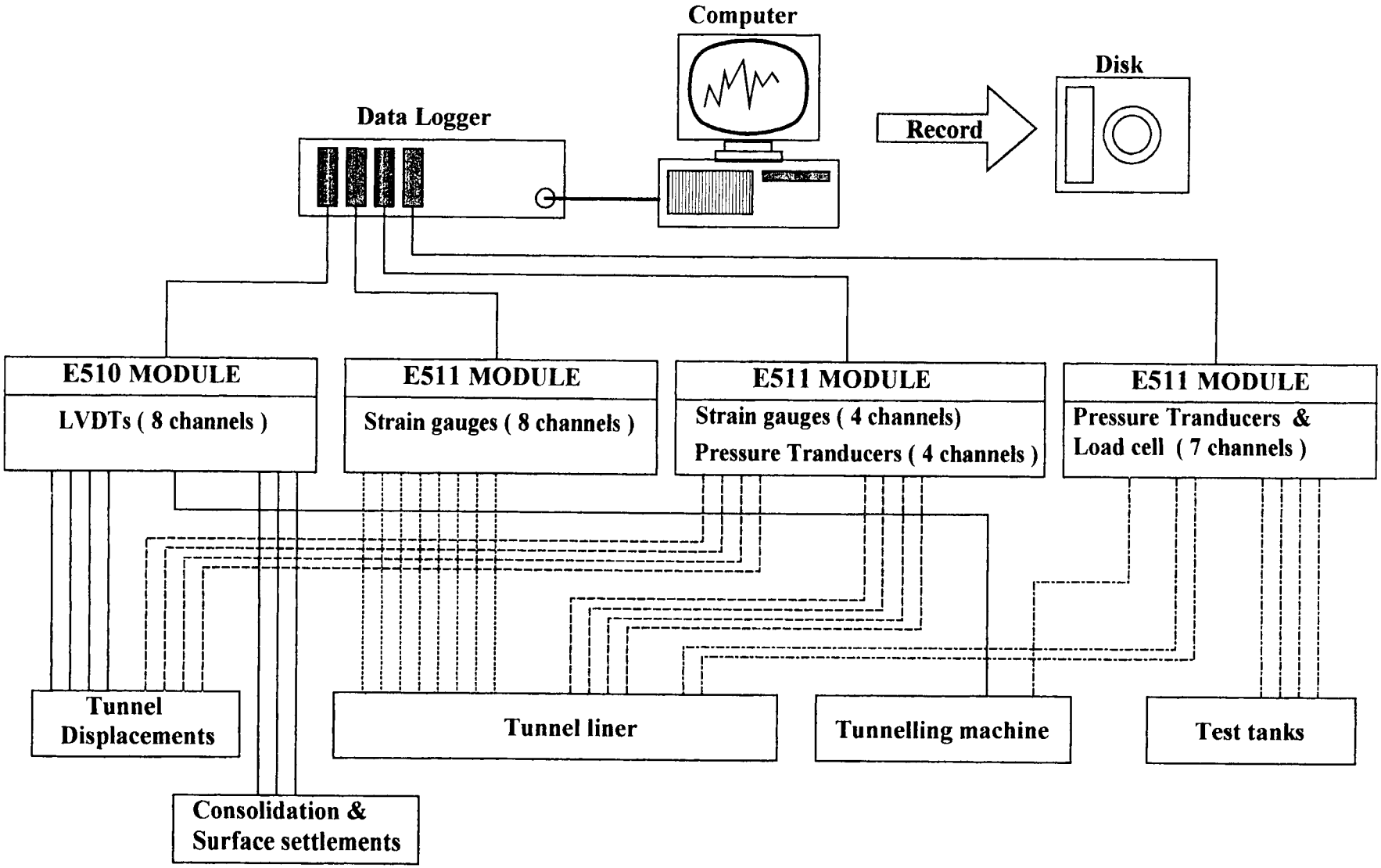


FIGURE 3.8 [a] Instrumentation Systems

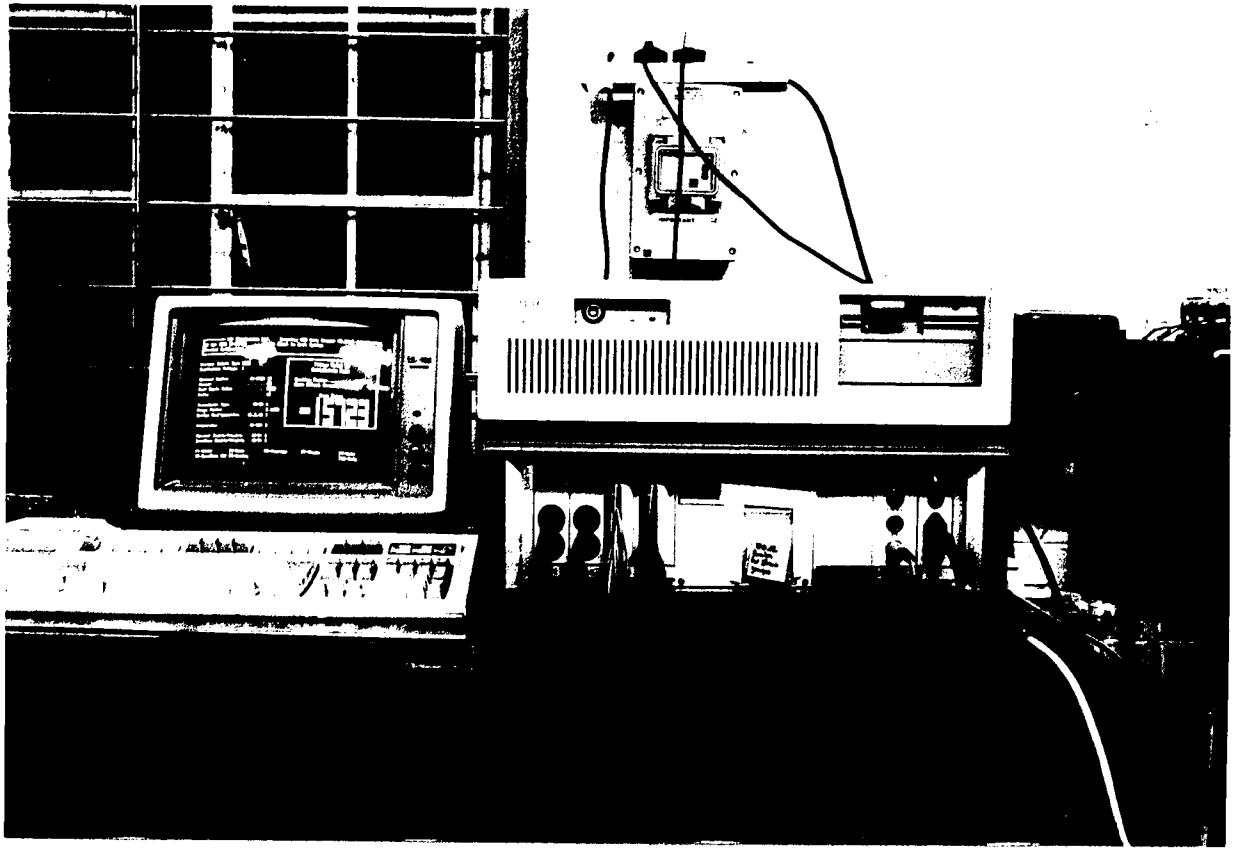


FIGURE 3.8 [b] Photograph of Datalogger and Compter

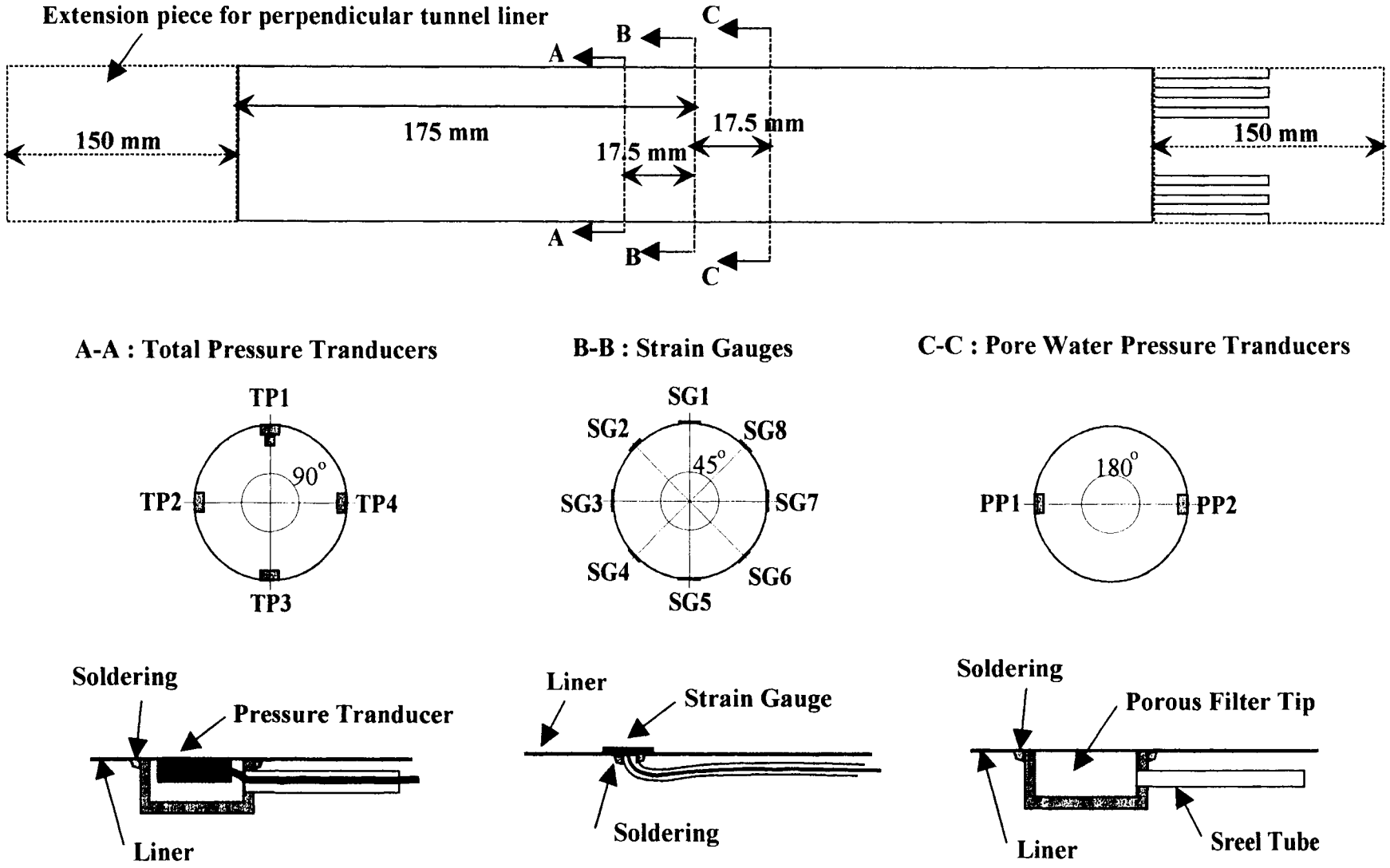


FIGURE 3.9 [a] Locations of Instruments on the Liner

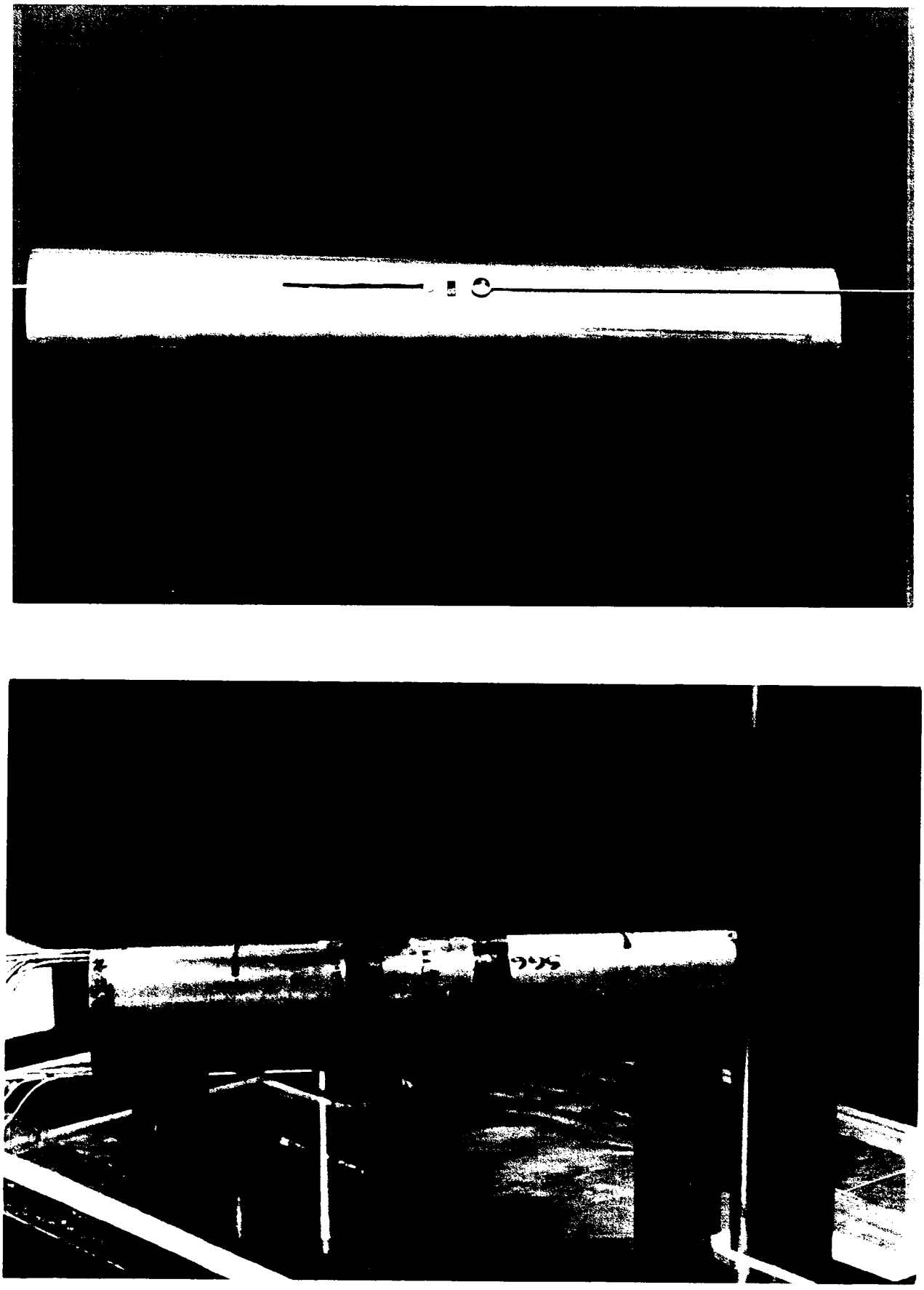
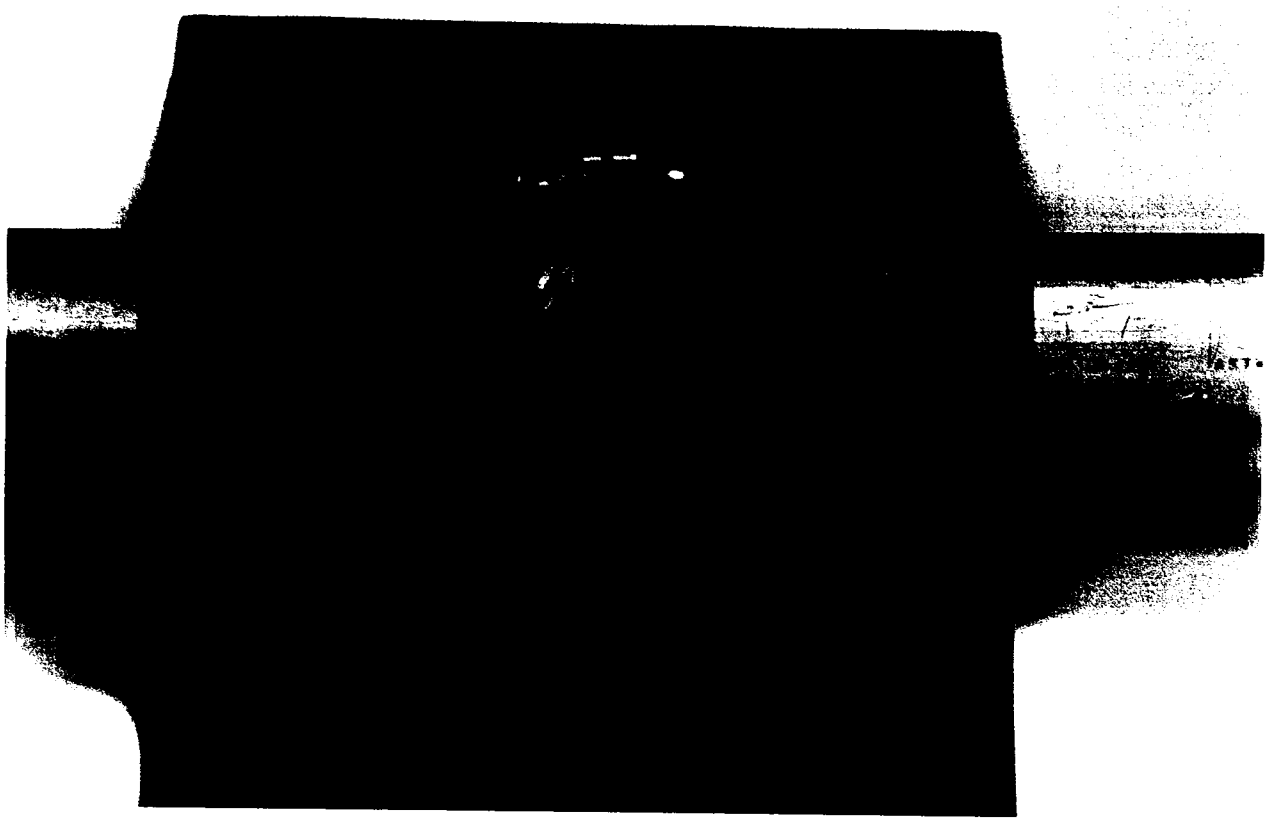


FIGURE 3.9 [b] Photograph of Instrumented Tunnel Liner



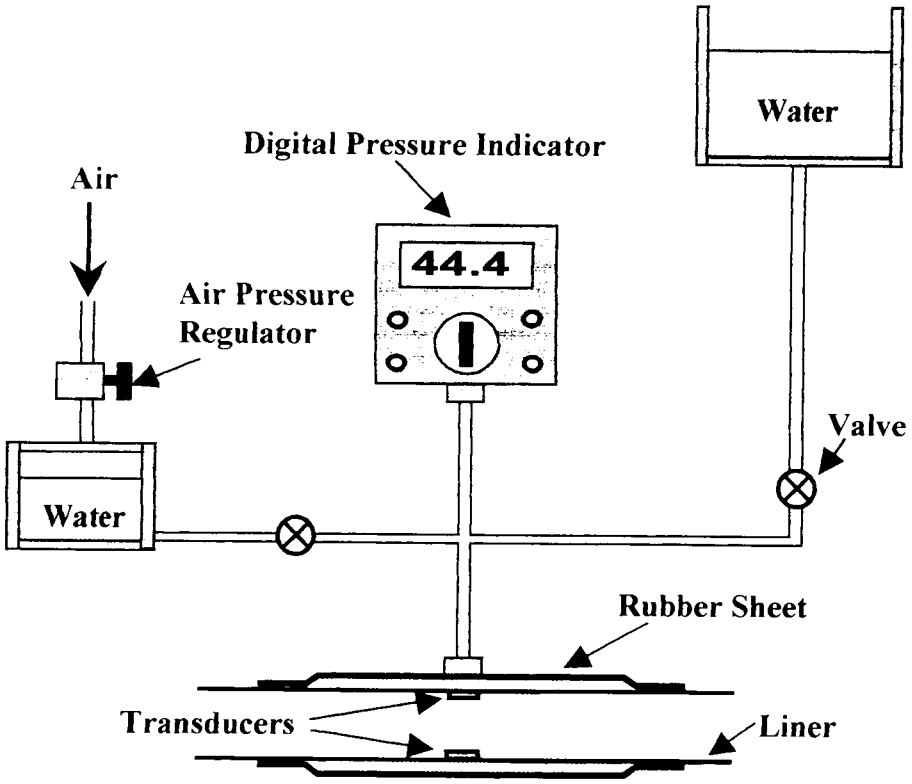


FIGURE 3.10 [a] Calibration Device and System

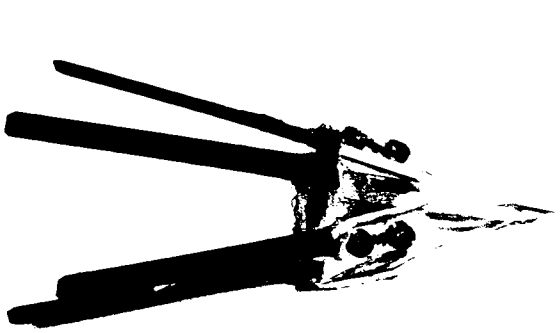


no pressure

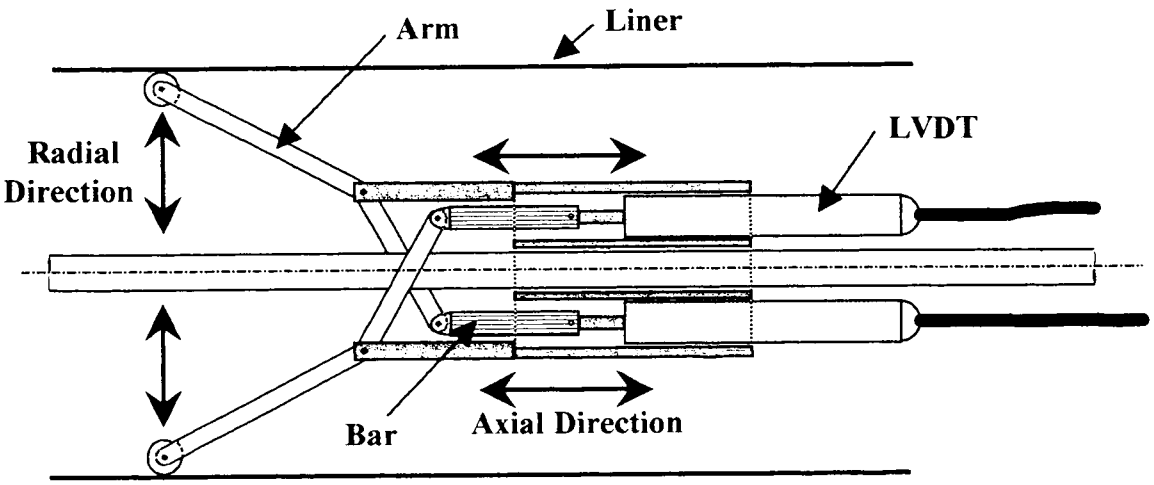


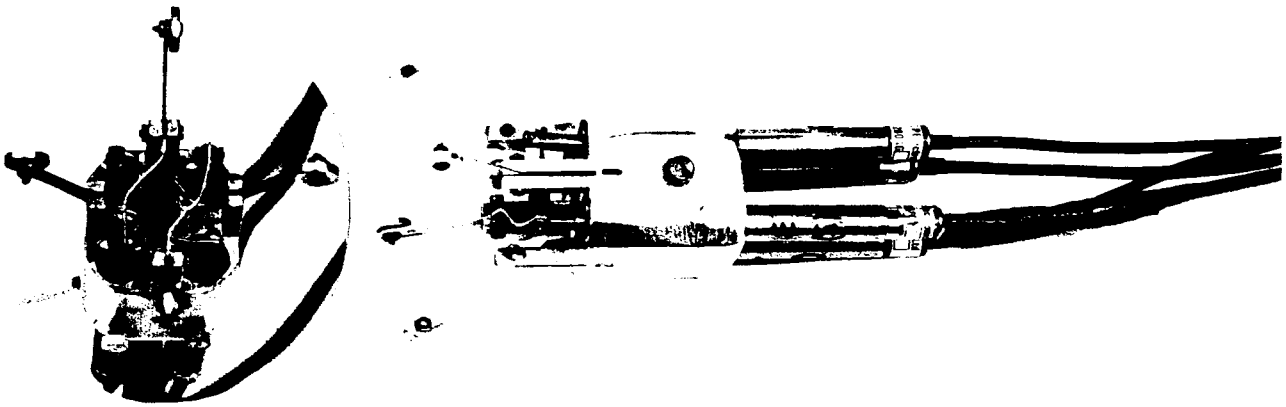
under pressure

FIGURE 3.10 [b] View of Calibration



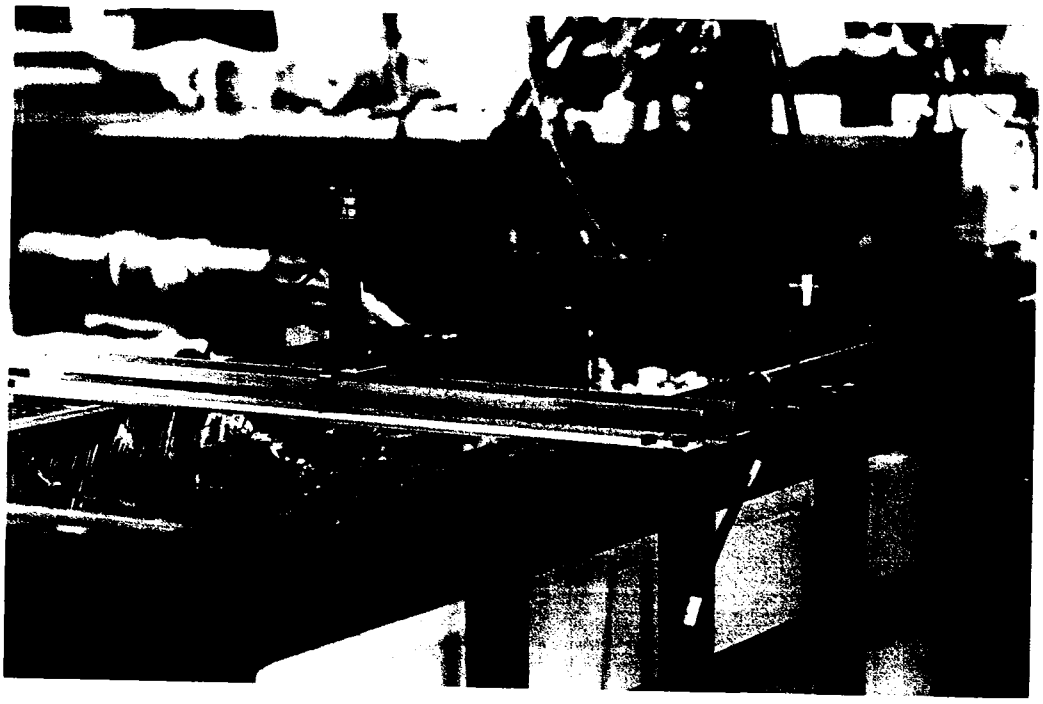
[a] RDMD1



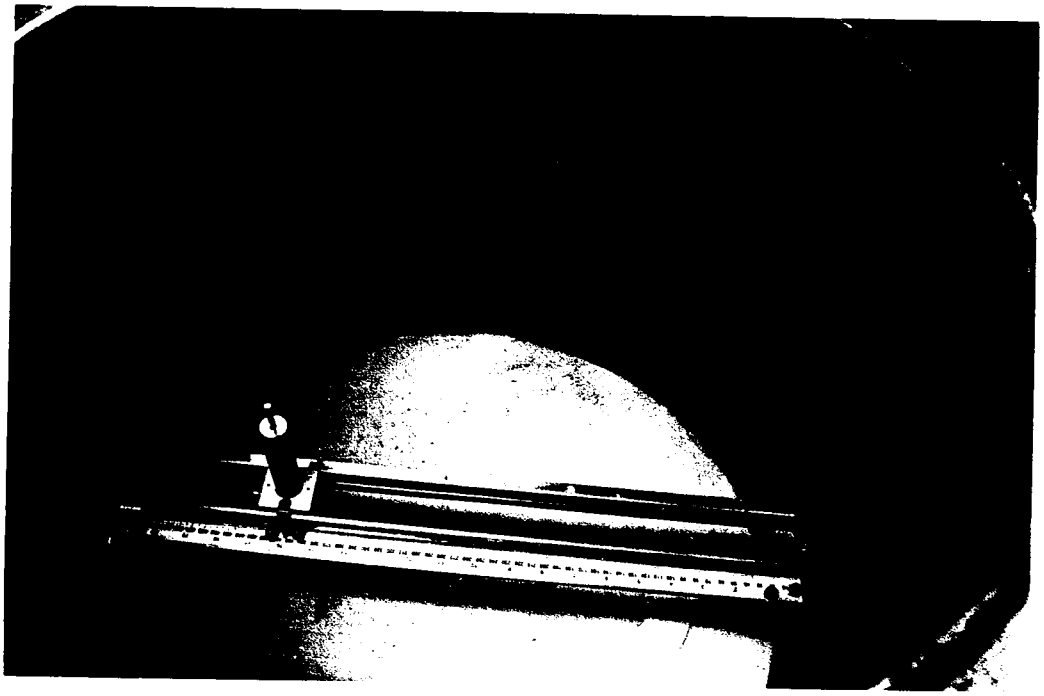


[b] RDMD2

FIGURE 3.11 Radial Displacement Measuring Devices (RDMD)



[a] In Plane Strain Tank



[b] In Cylindrical Tank

FIGURE 3.12 Surface Settlement Measuring Divice

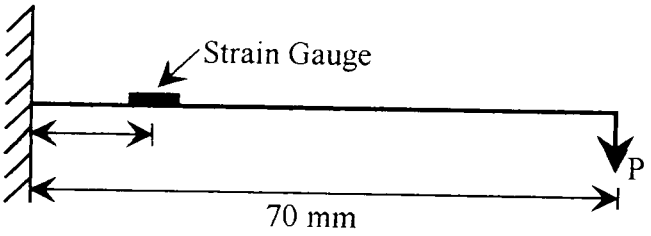


FIGURE 3.13 Calibration System of Strain Gauges

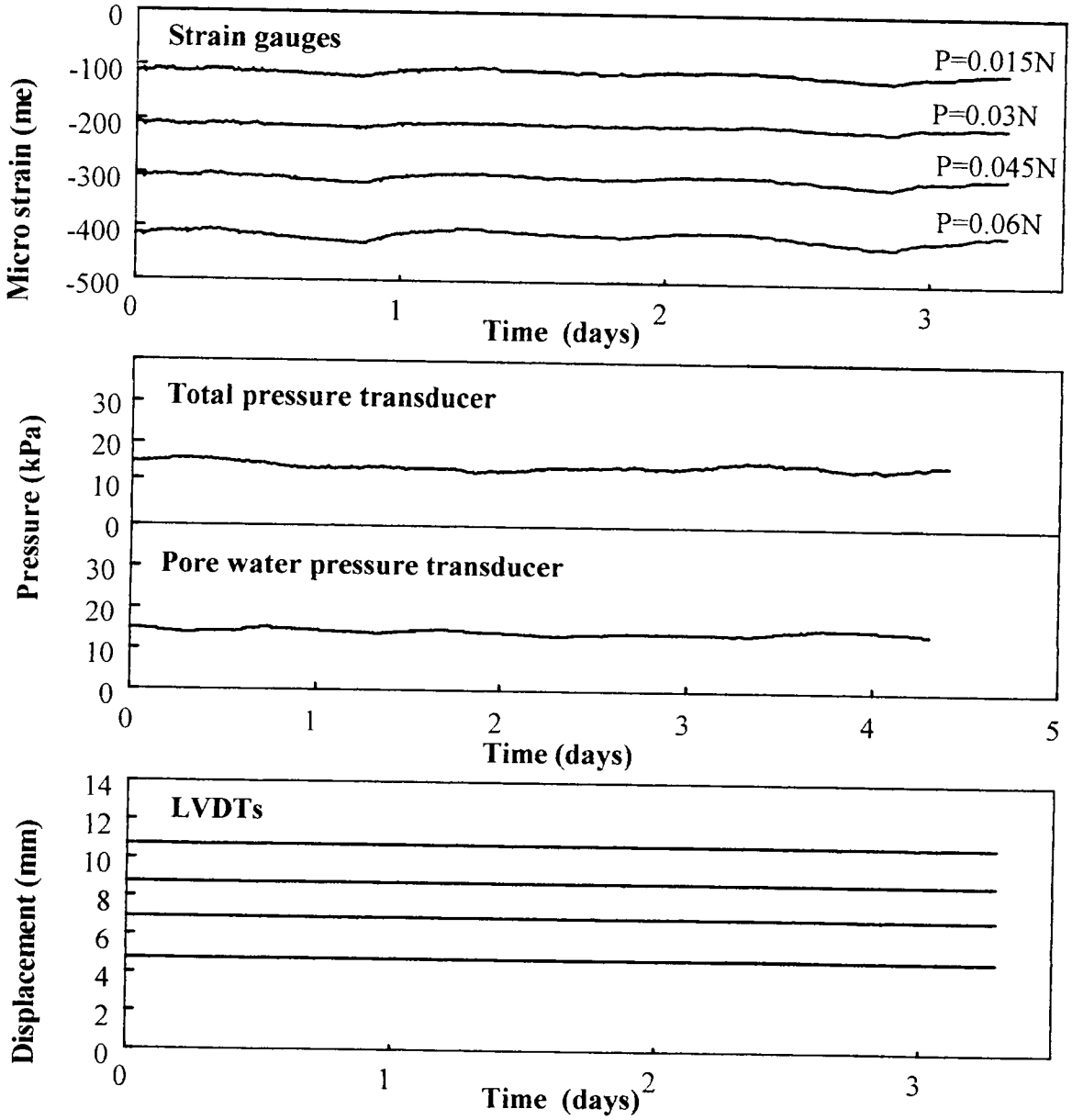


FIGURE 3.14 Measurements due to Long-term (4 day period)

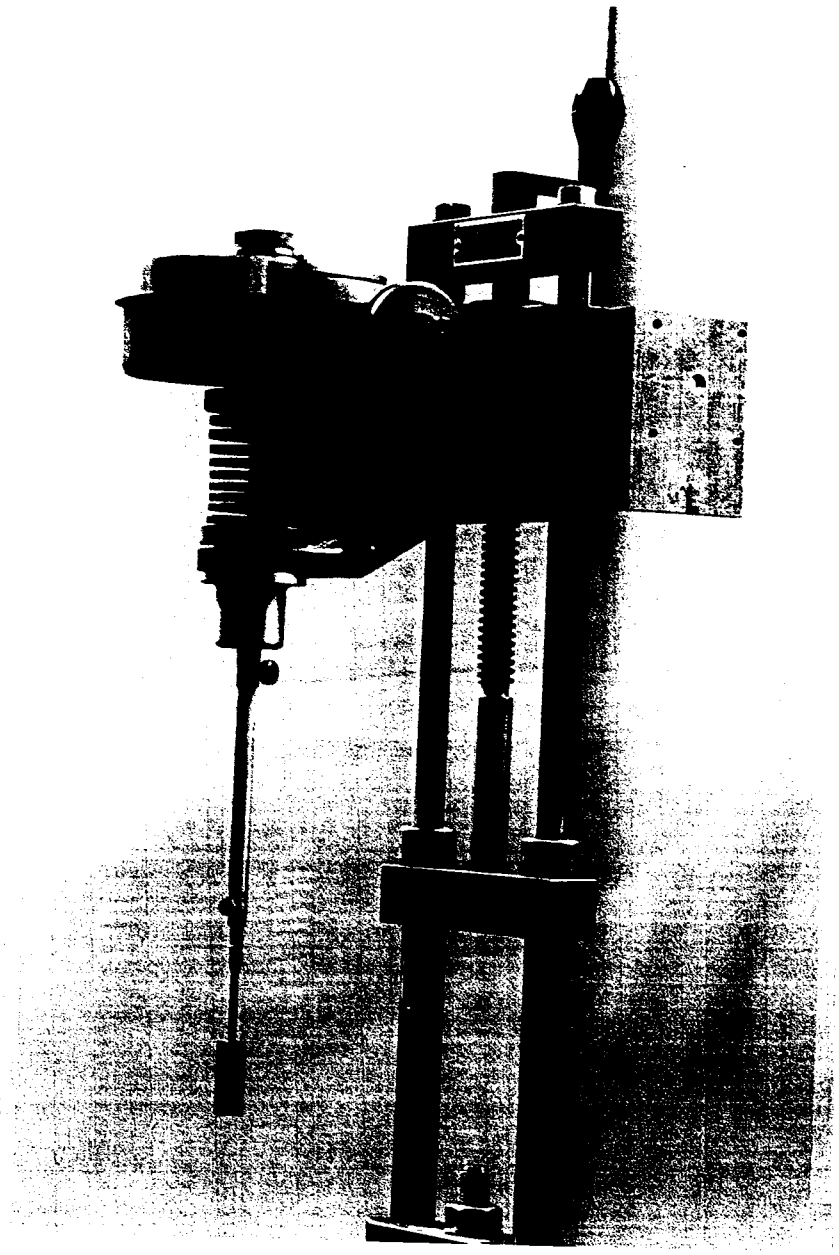
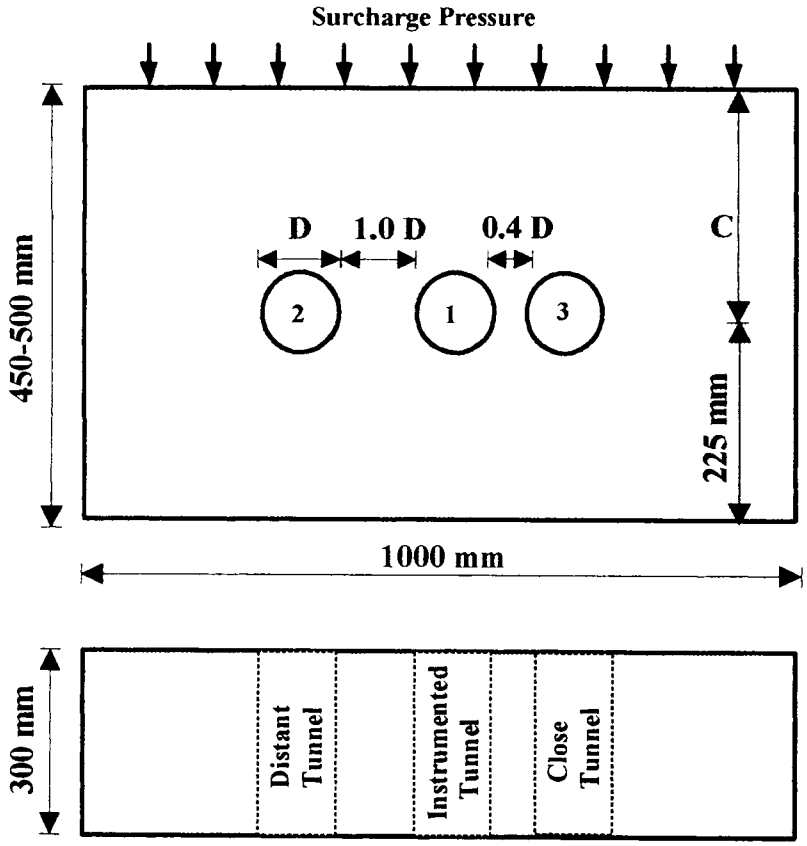


FIGURE 3.15 Laboratory Shear Vane Testing Apparatus



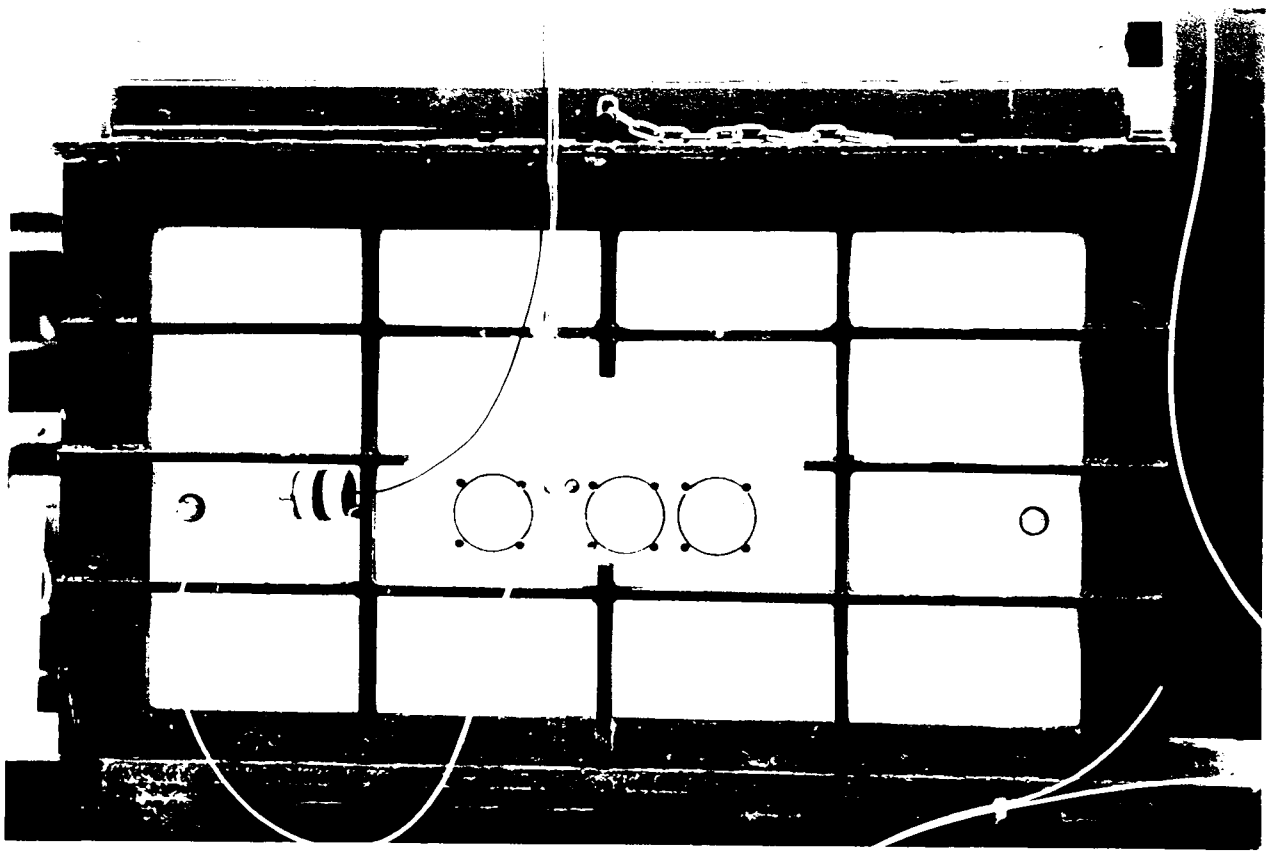


FIGURE 4.1 [a] Layout of Parallel Tunnel Models

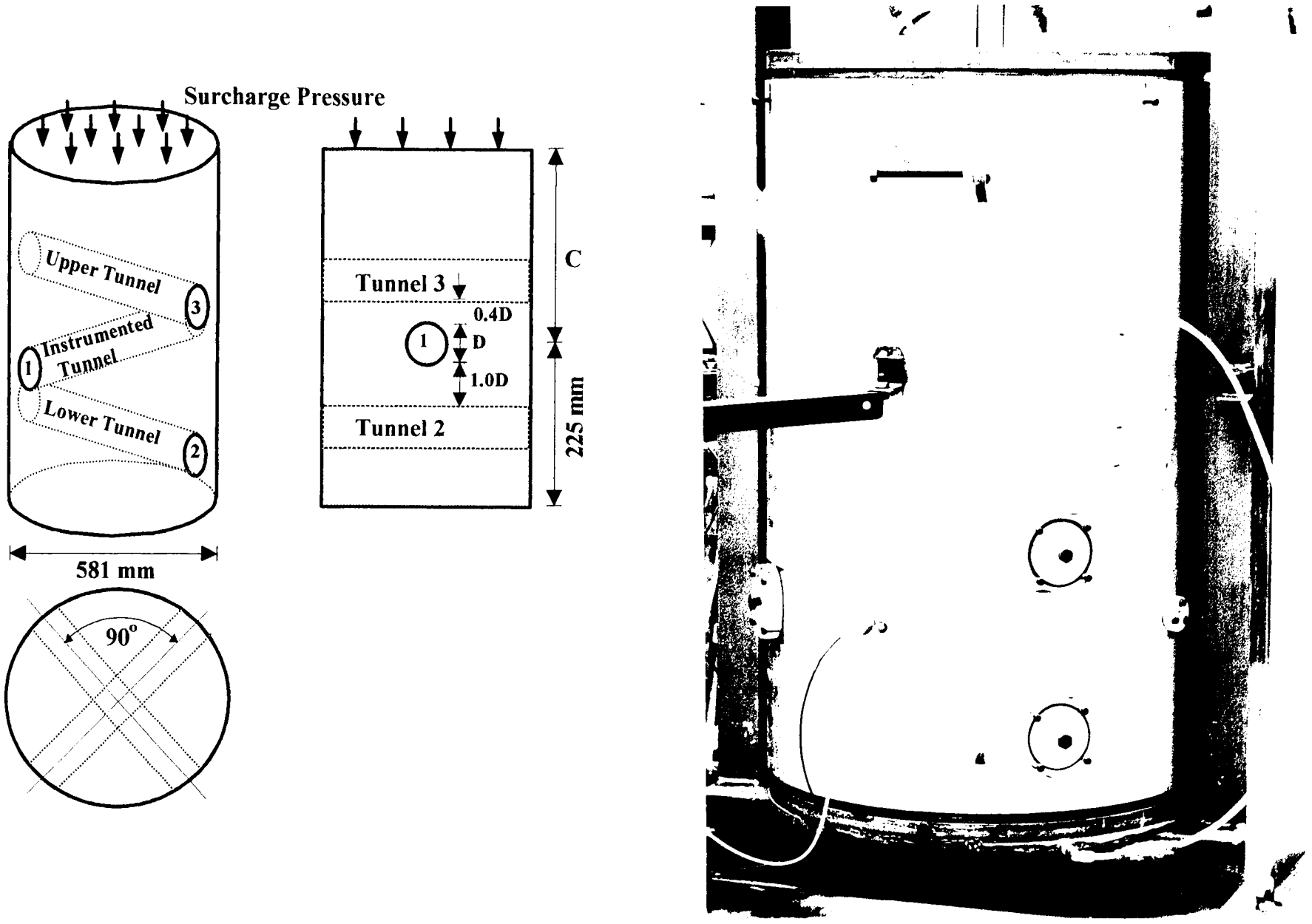


FIGURE 4.1 [b] Layout of Perpendicular Tunnel Models

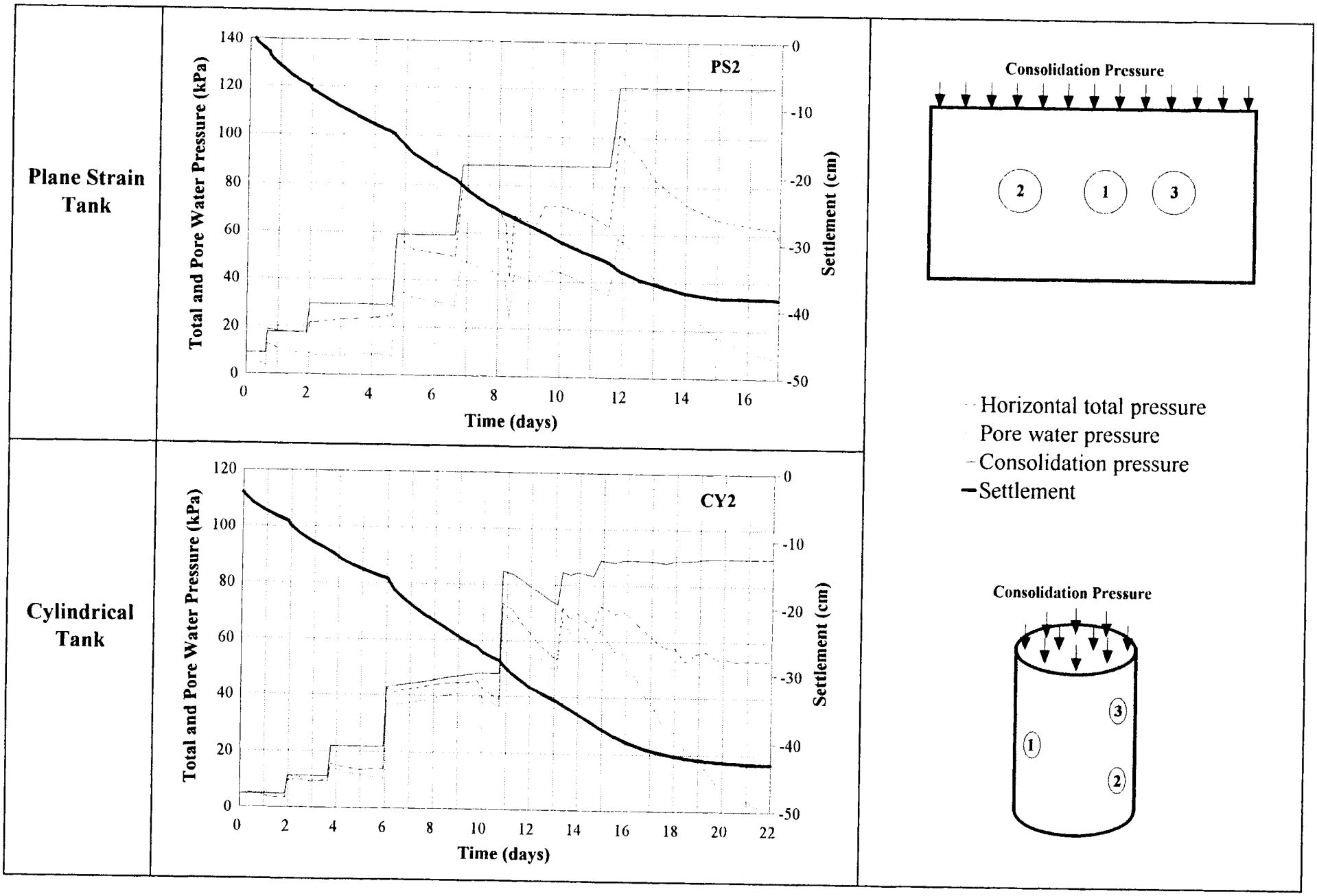
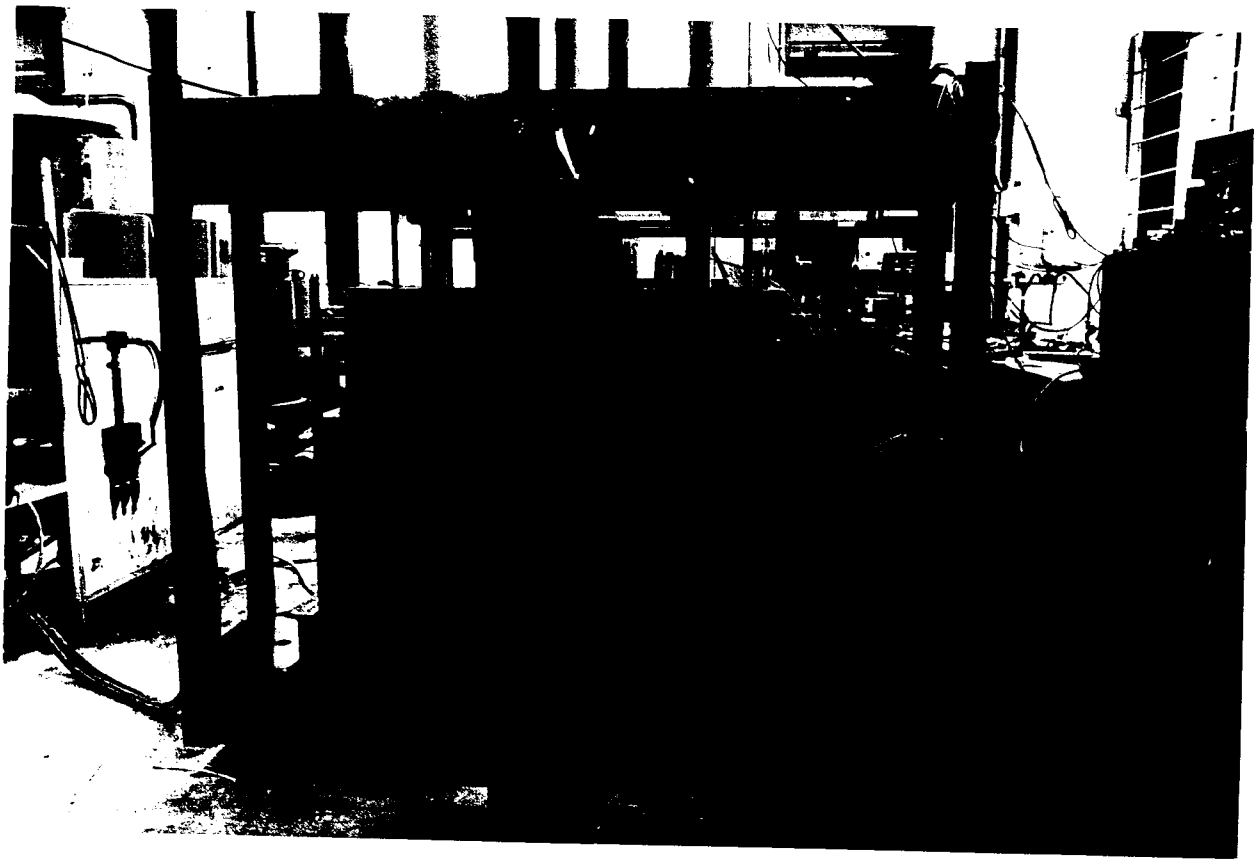
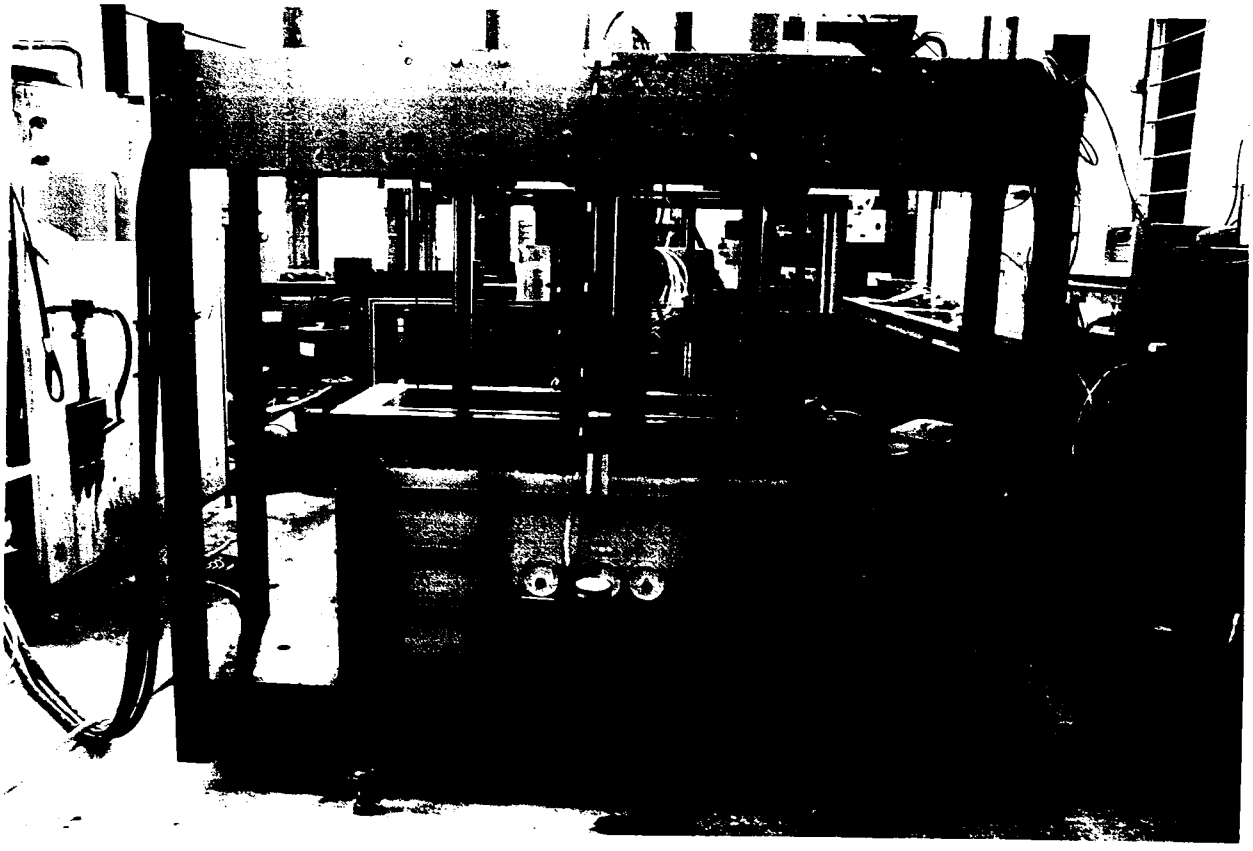


FIGURE 4.2 Typical Consolidation Curves



[a] During Consolidation



[b] Under Surcharge on the Sample

FIGURE 4.3 View of Assembled Test Tank (PS)

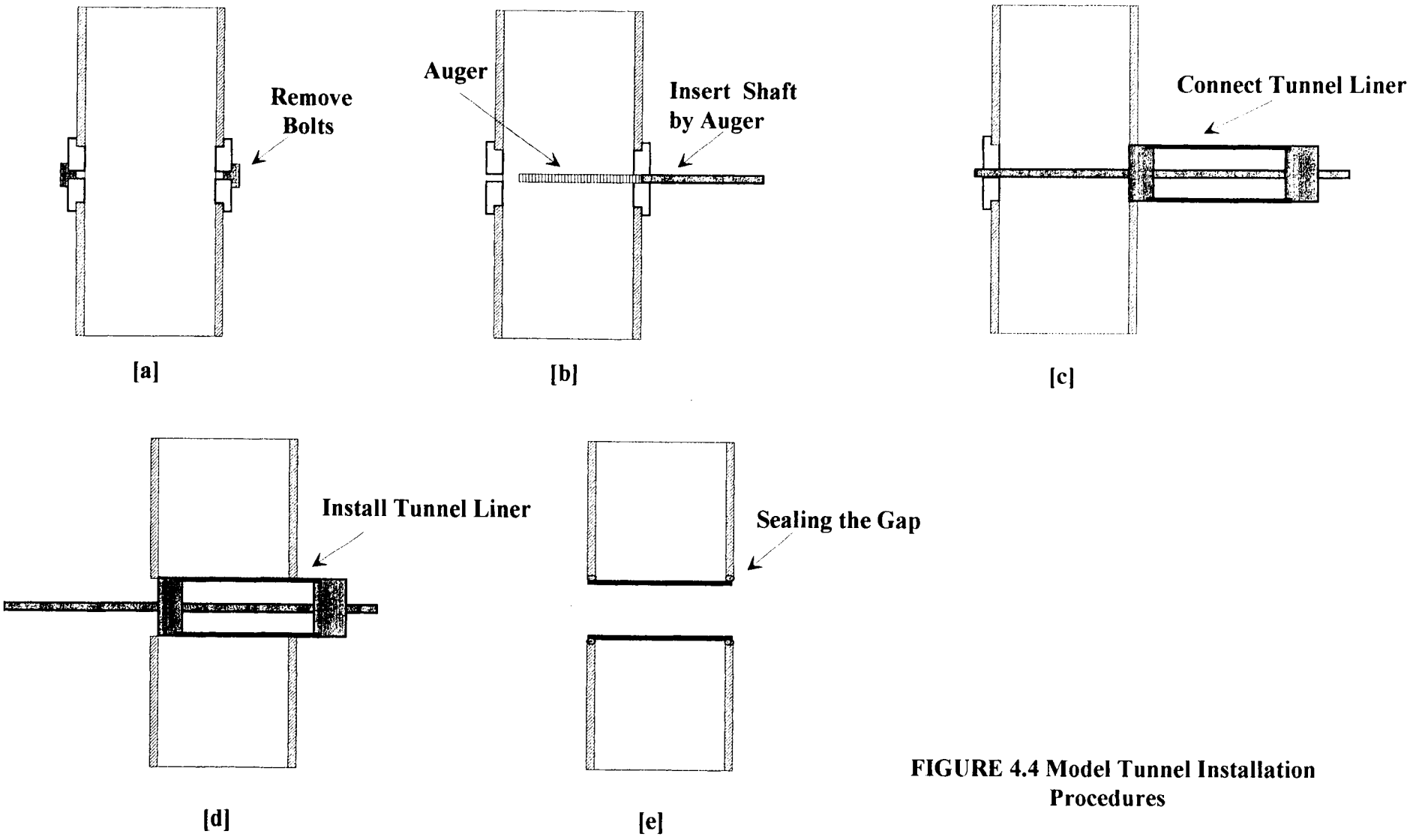


FIGURE 4.4 Model Tunnel Installation Procedures

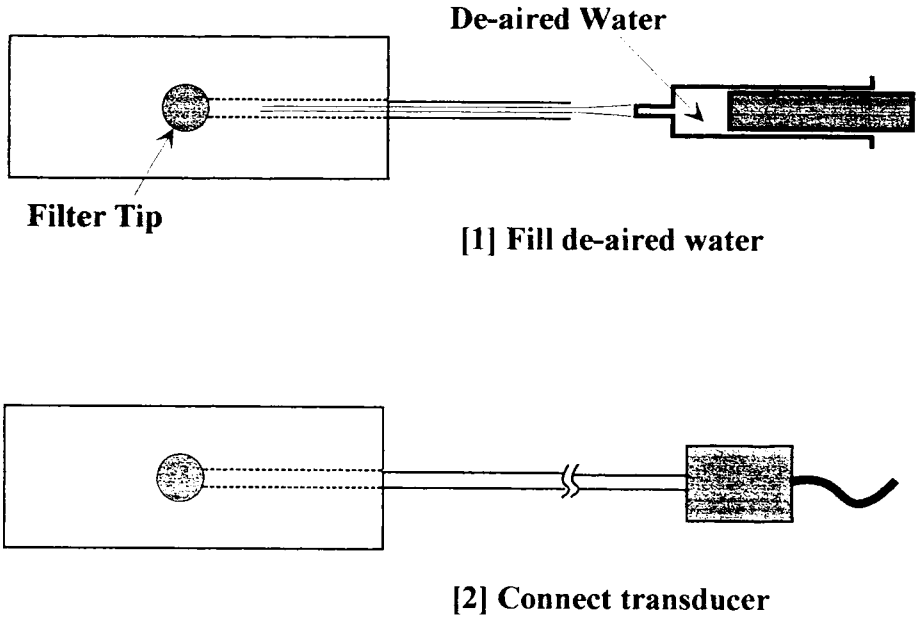


FIGURE 4.5 Connection of Pore Water Pressure Transducer

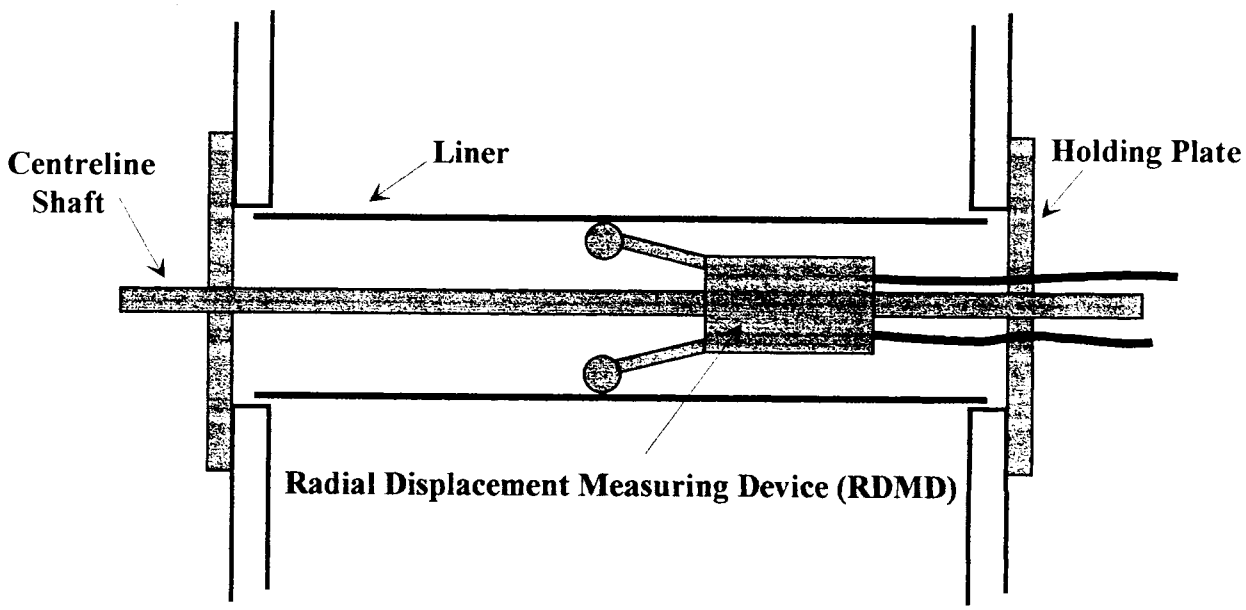
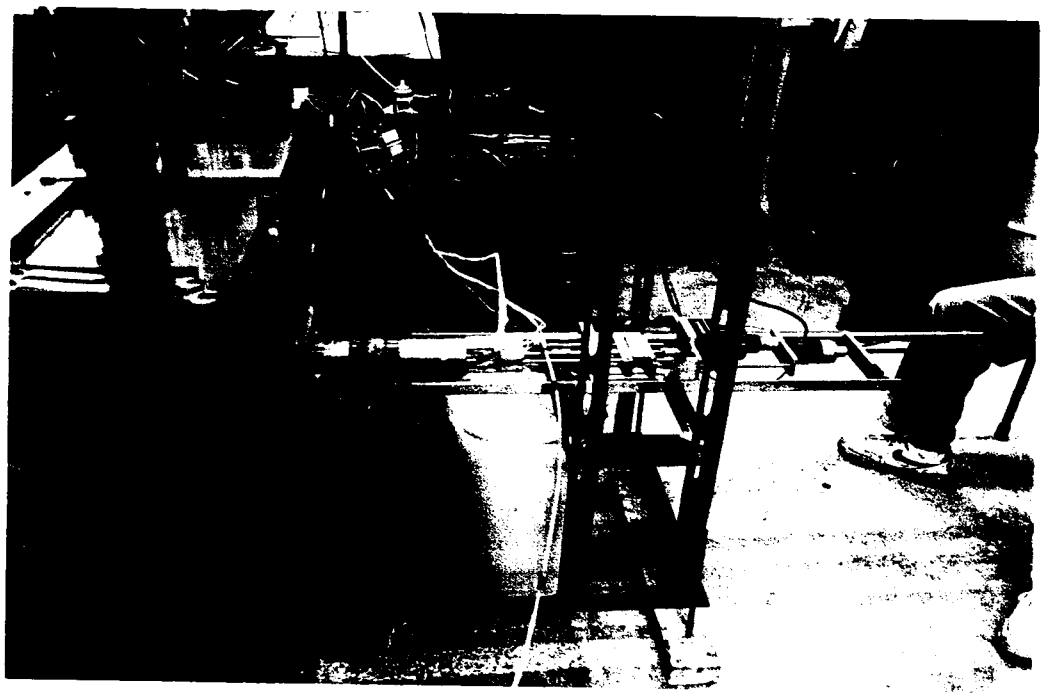
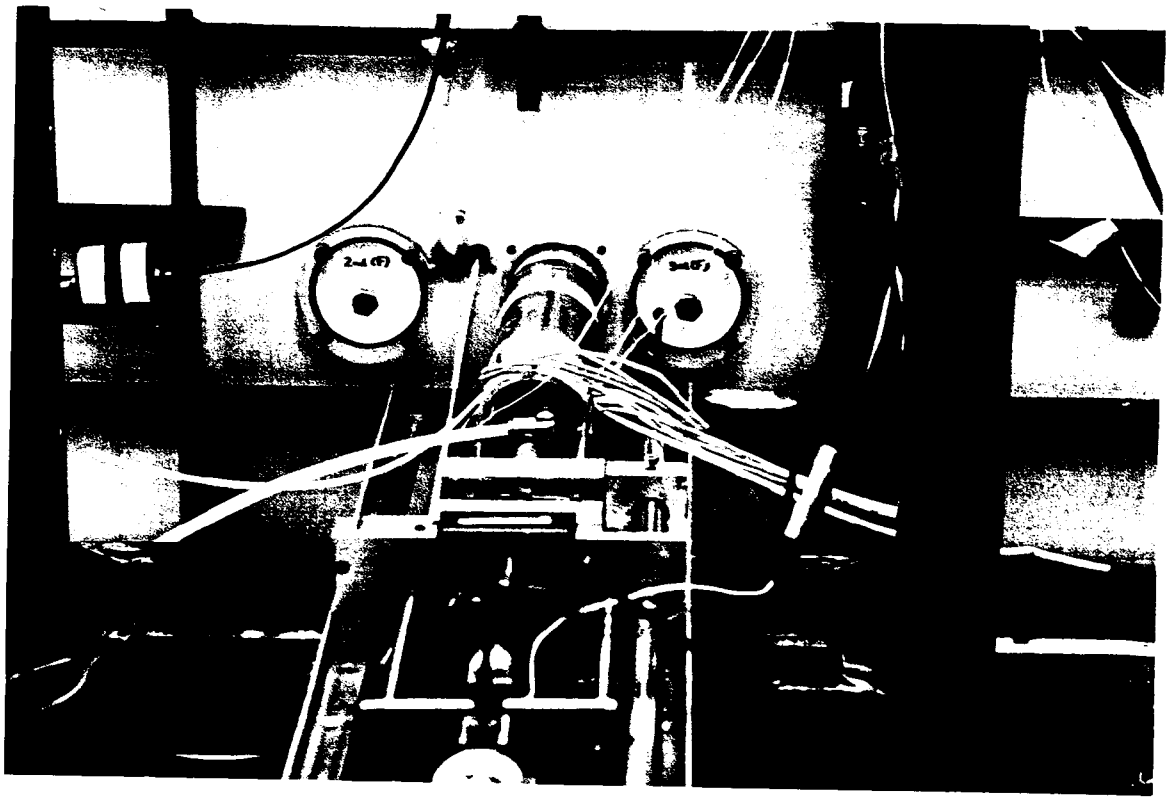


FIGURE 4.6 Installation of Radial Displacement Measuring Device

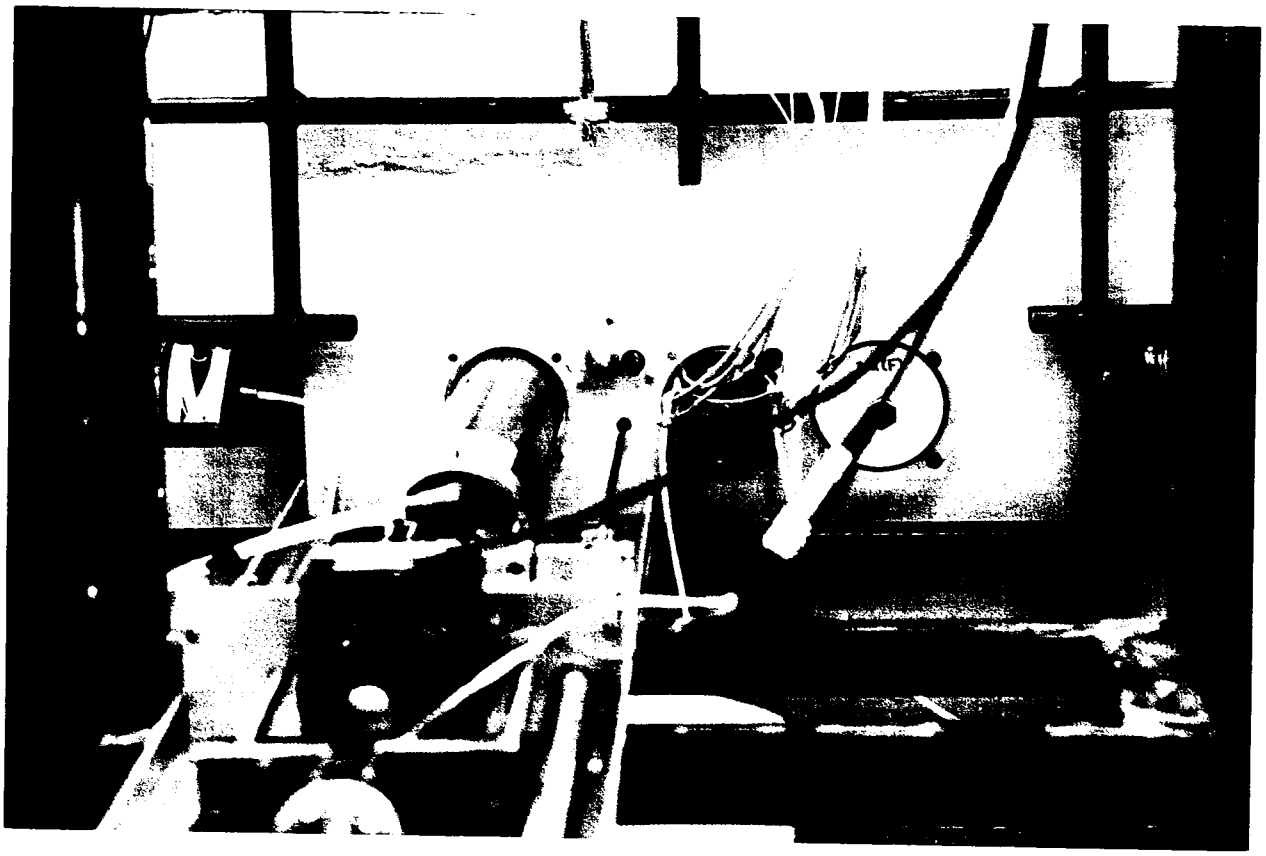


[a] General View of Tunnelling Work

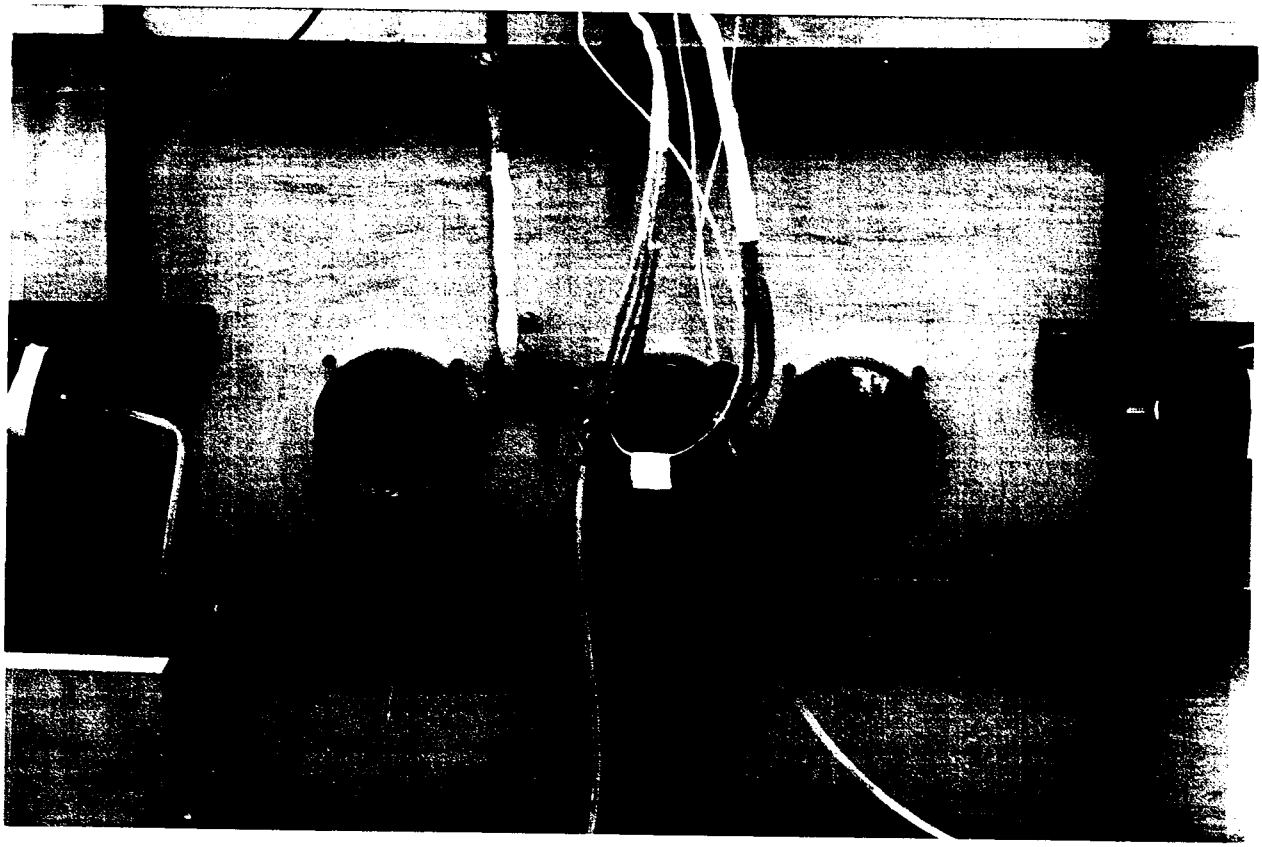


[b] Installation of Tunnel 1

continue figure 4.7



[c] Installation of Tunnel 2



[d] After Installation of Tunnel 1,2 and 3

FIGURE 4.7 Installation of Each of Tunnels

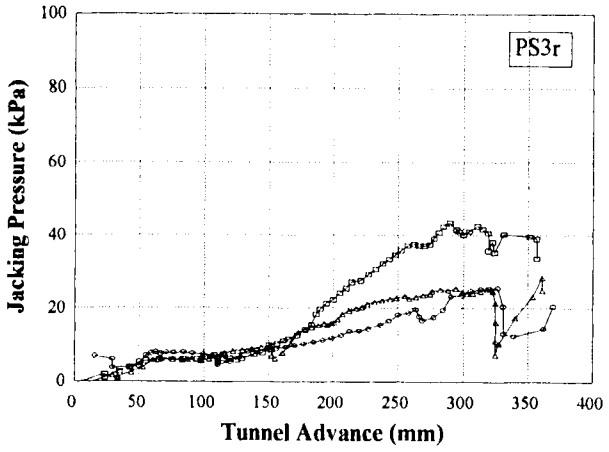
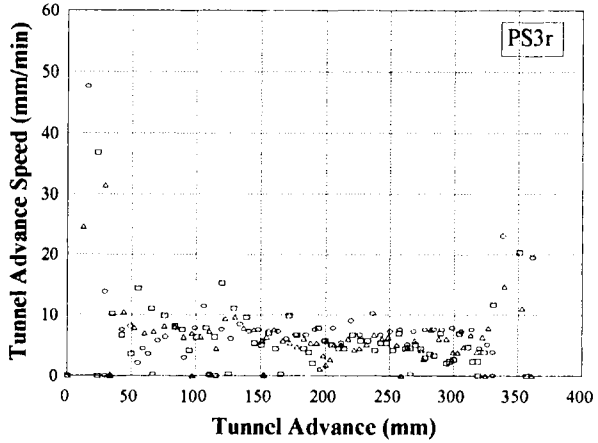
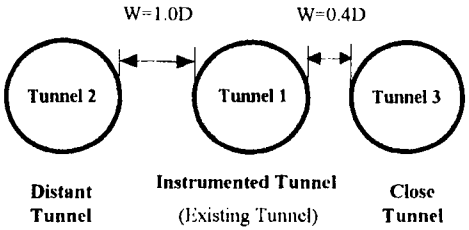
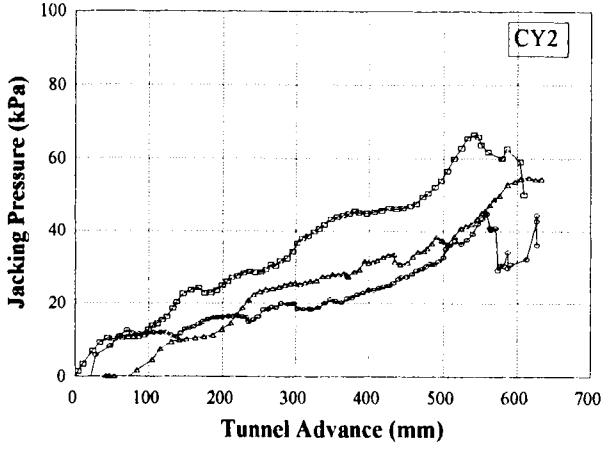
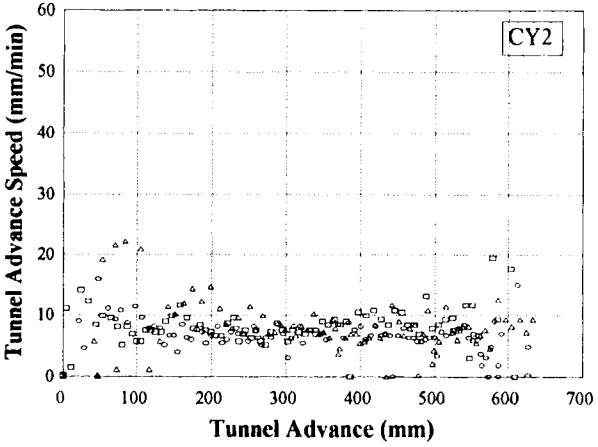
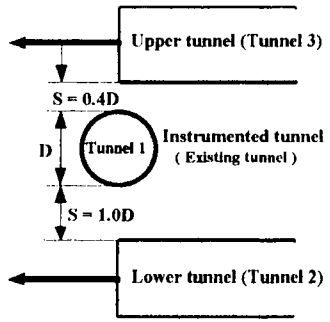
	[a] Jacking Pressure	[b] Tunnel Advance Speed	Remarks
Parallel Tunnel			 During installation of tunnel 1 During installation of tunnel 2 During installation od tunnel 3
Perpendicular Tunnel			

FIGURE 4.8 Typical Results of Jacking Pressure and Tunnel Advance Speed

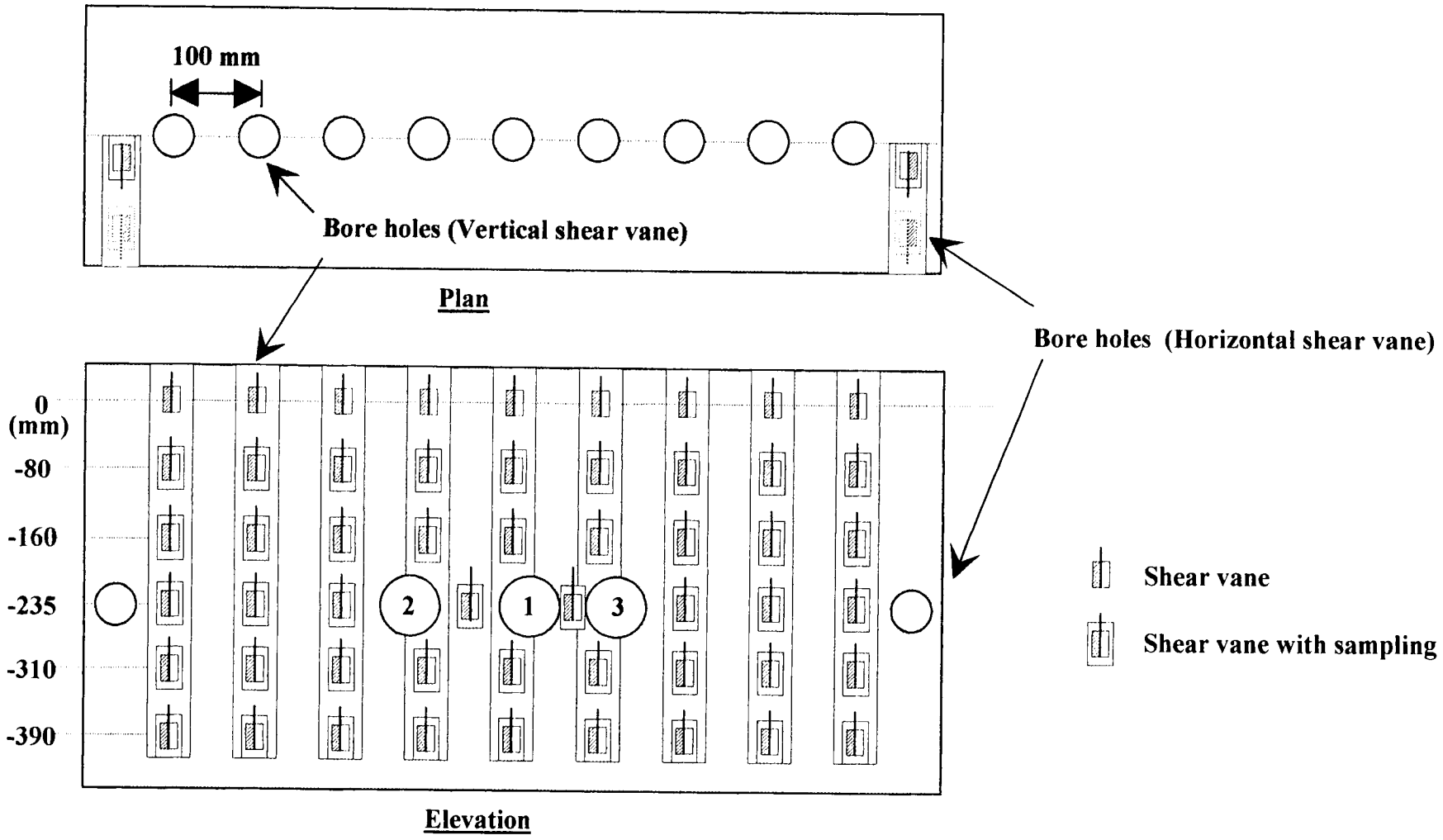


FIGURE 4.9 Location of Site Investigation in Plane Strain Tank

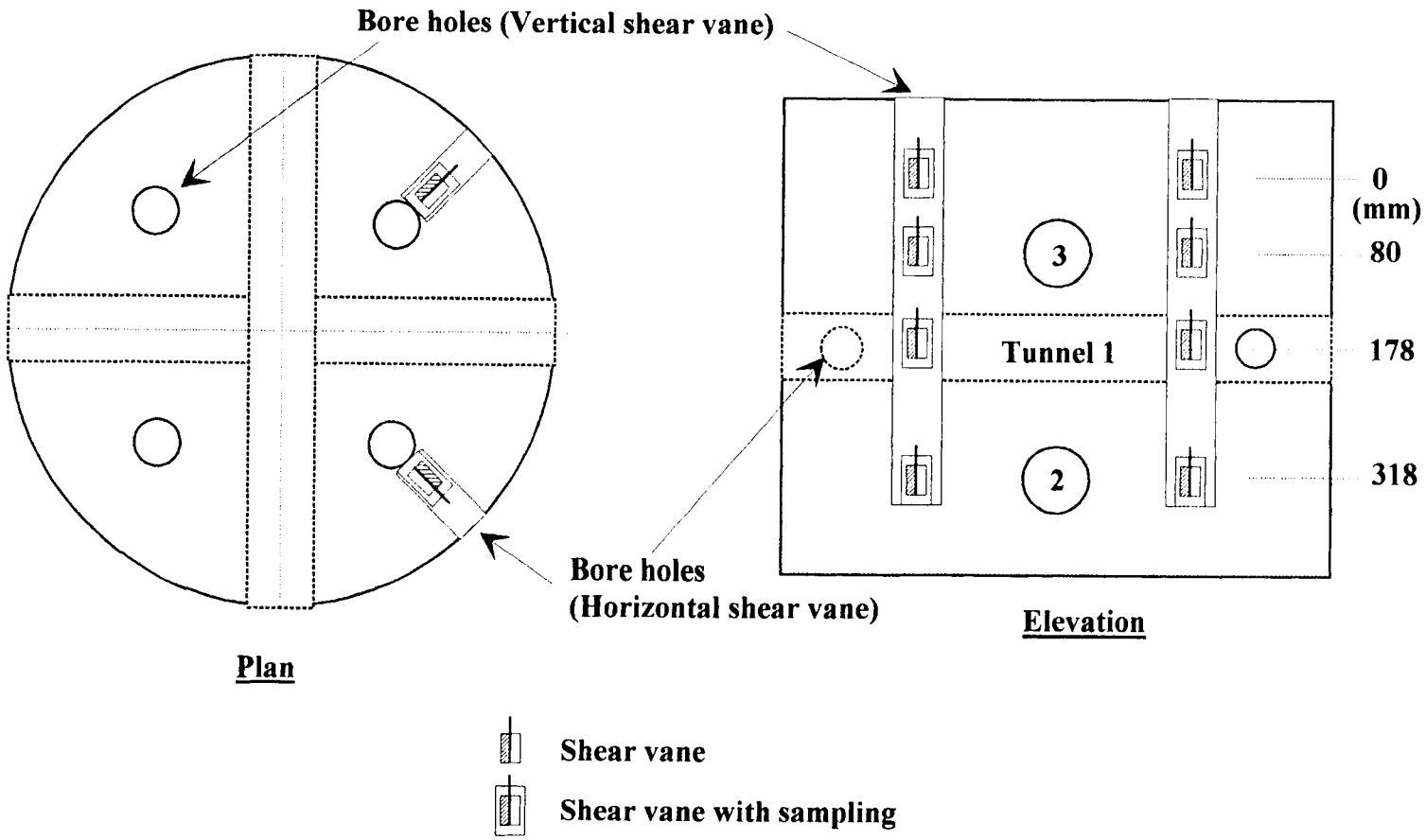
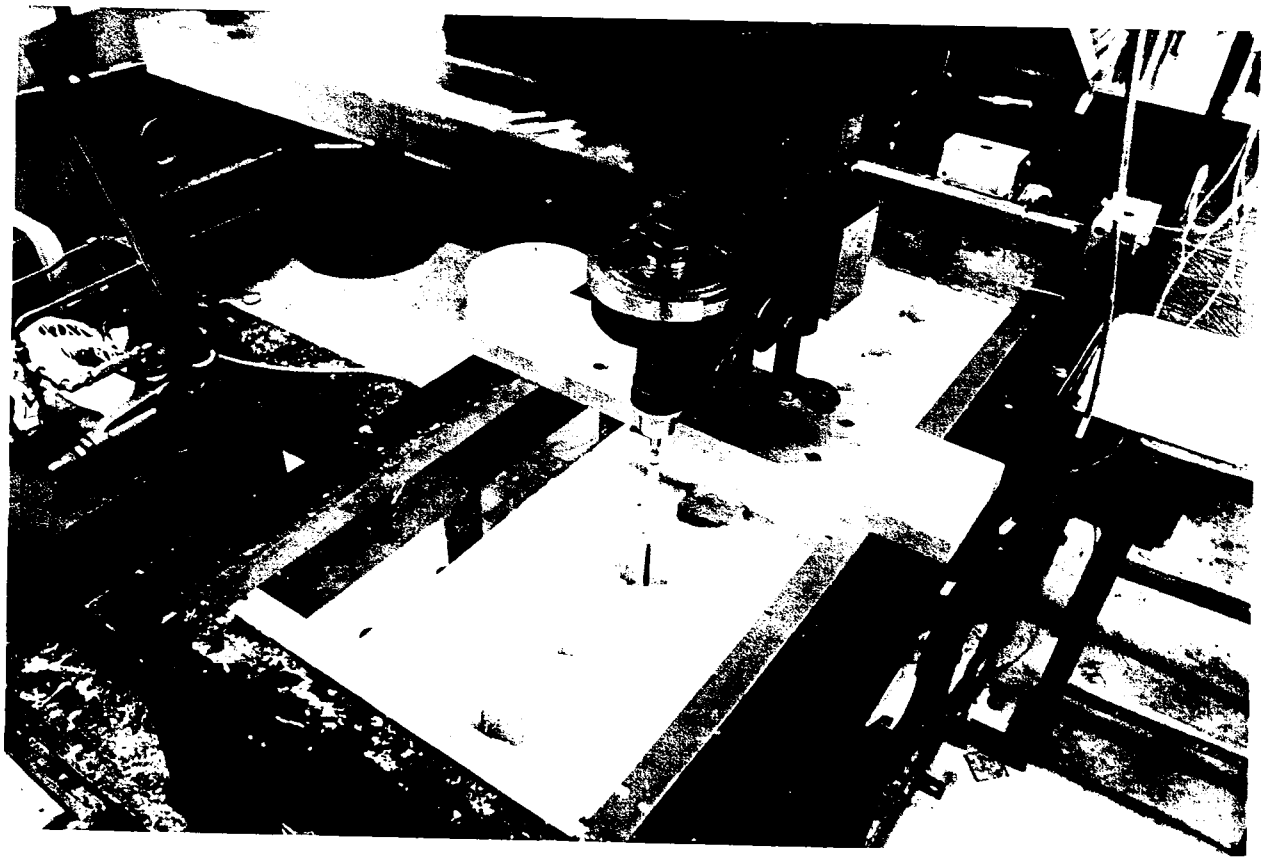
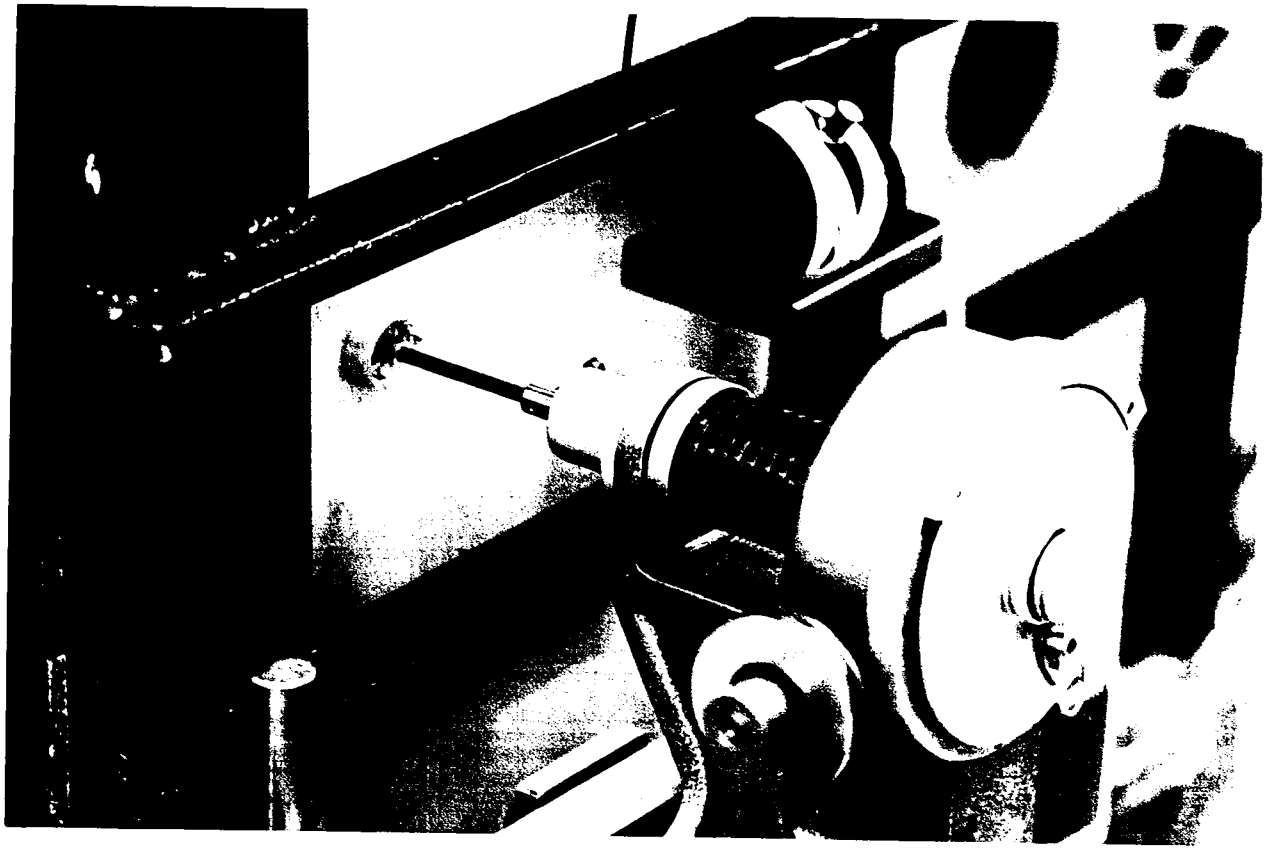


FIGURE 4. 10 Layout of Site Investigation in Cylindrical tank



[a] Vertical Shear Vane Testing (no Surcharge Pressure)



[b] Horizontal Shear Vane Testing (under Surcharge Pressure)

FIGURE 4.11 Views of Shear Vane Testing

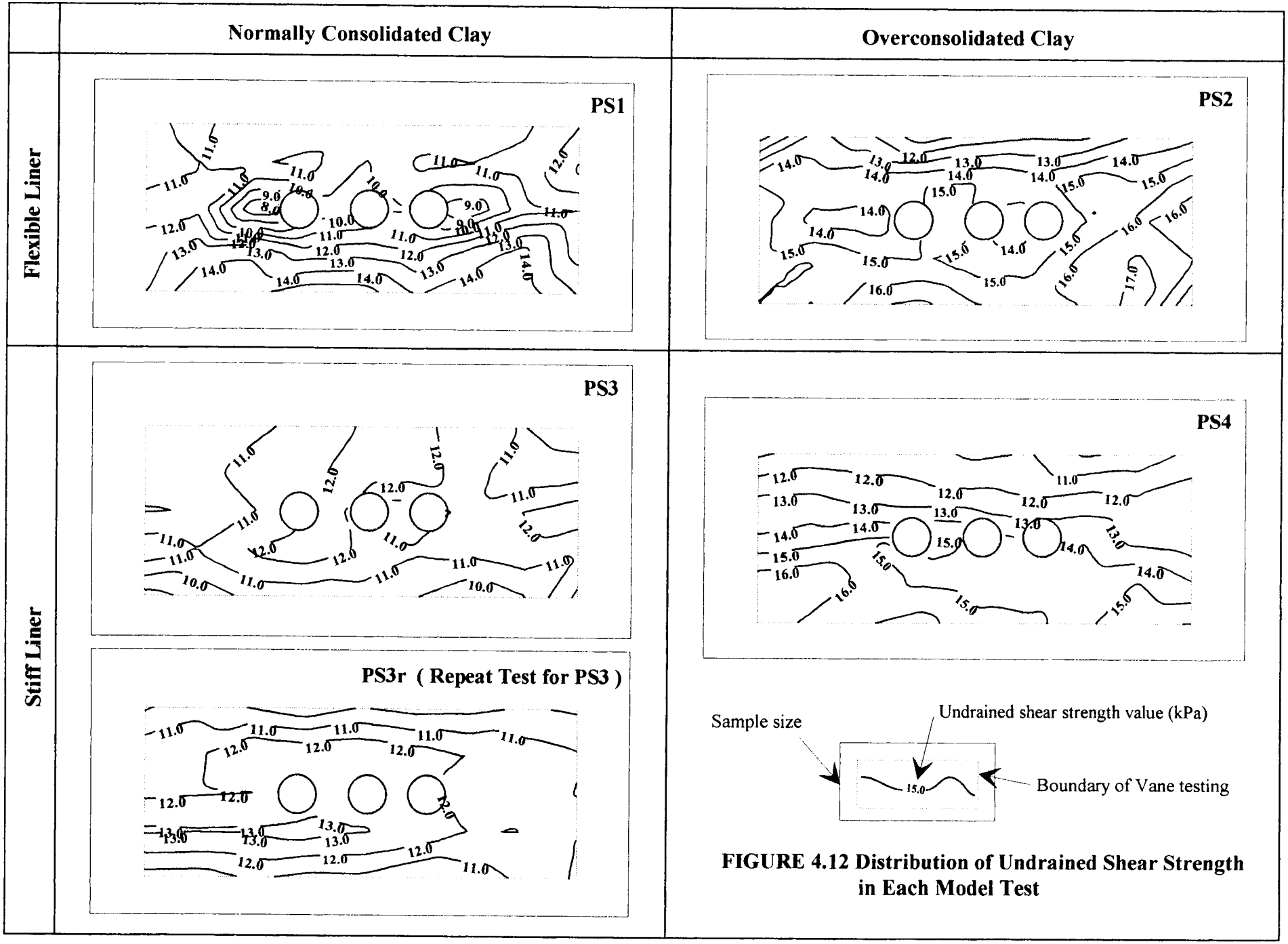


FIGURE 4.12 Distribution of Undrained Shear Strength in Each Model Test

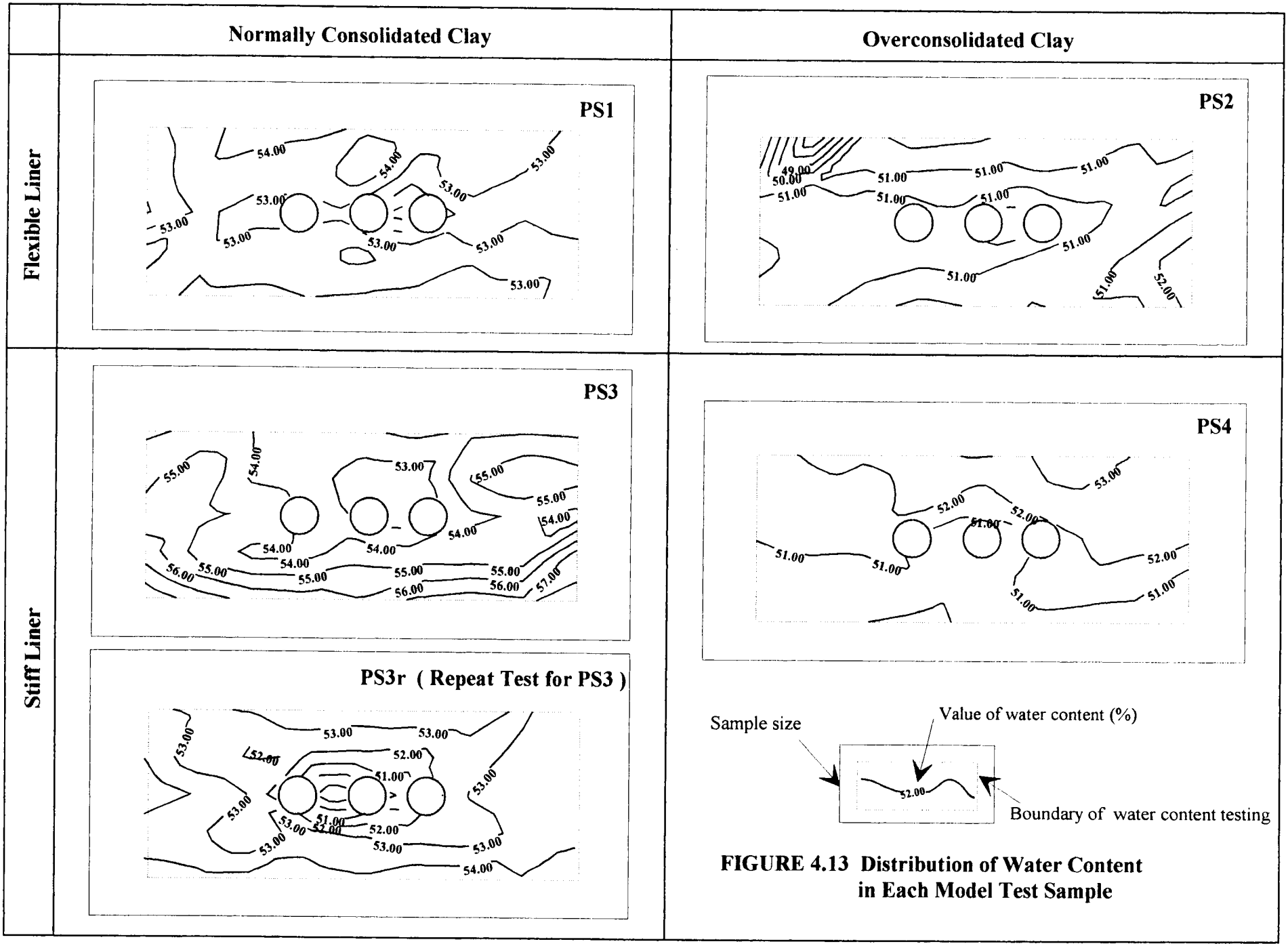


FIGURE 4.13 Distribution of Water Content in Each Model Test Sample

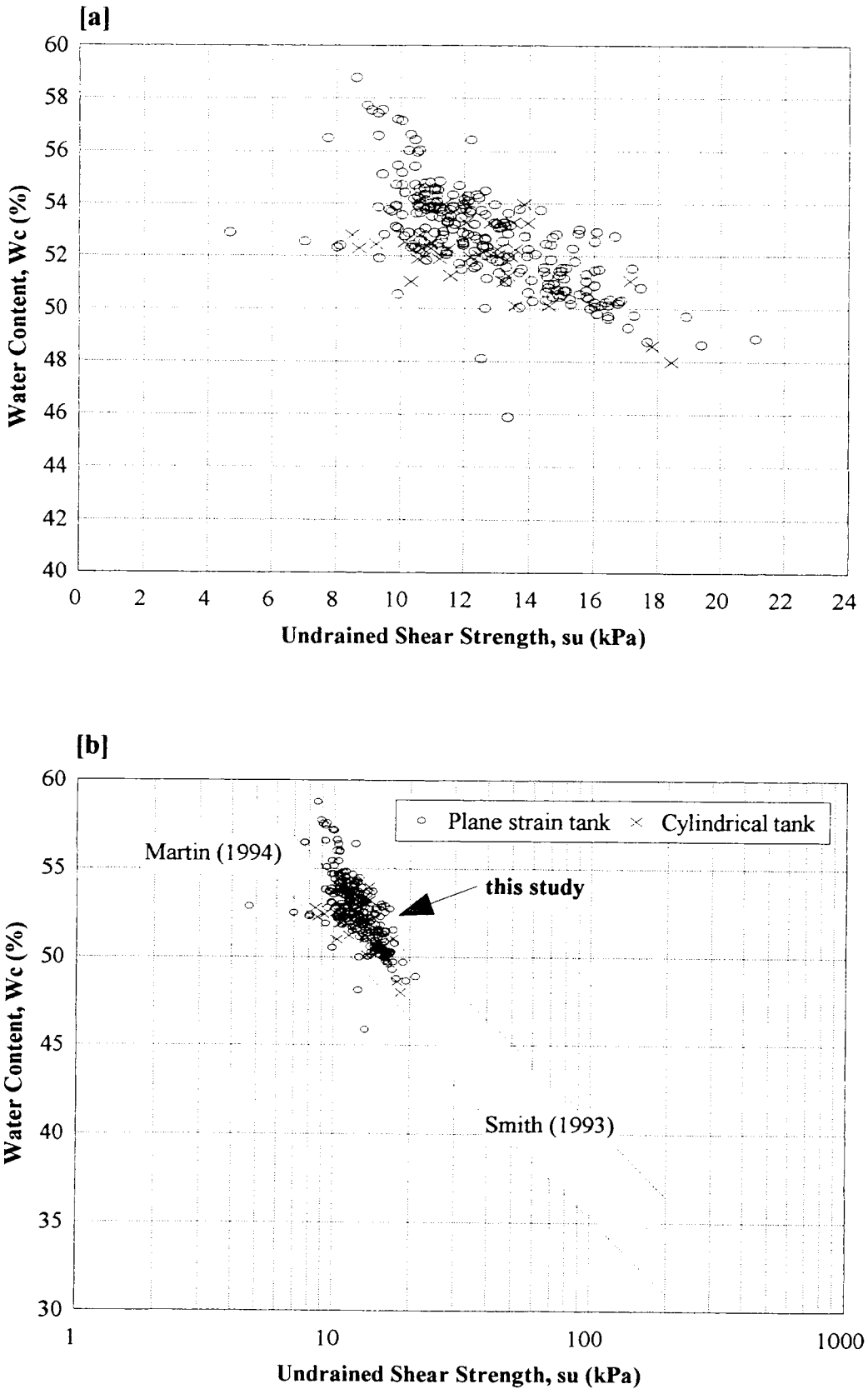


FIGURE 4.14 [a] Undrained strengths and corresponding to water contents
[b] Comparison with previous research from Martin (1994) and Smith (1993)

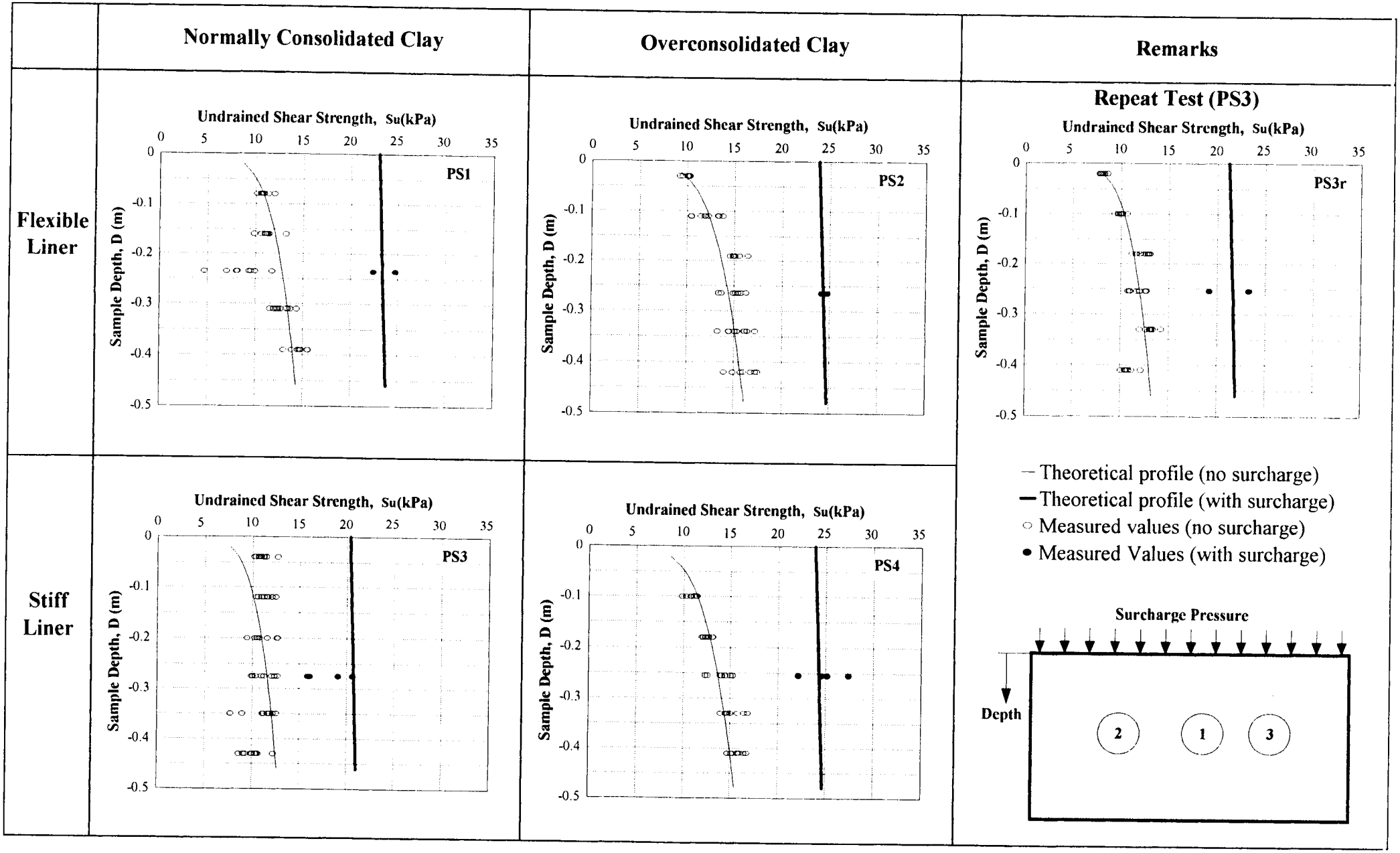


FIGURE 4.15 Undrained Shear Strength Profiles of Samples (Plane strain tank)

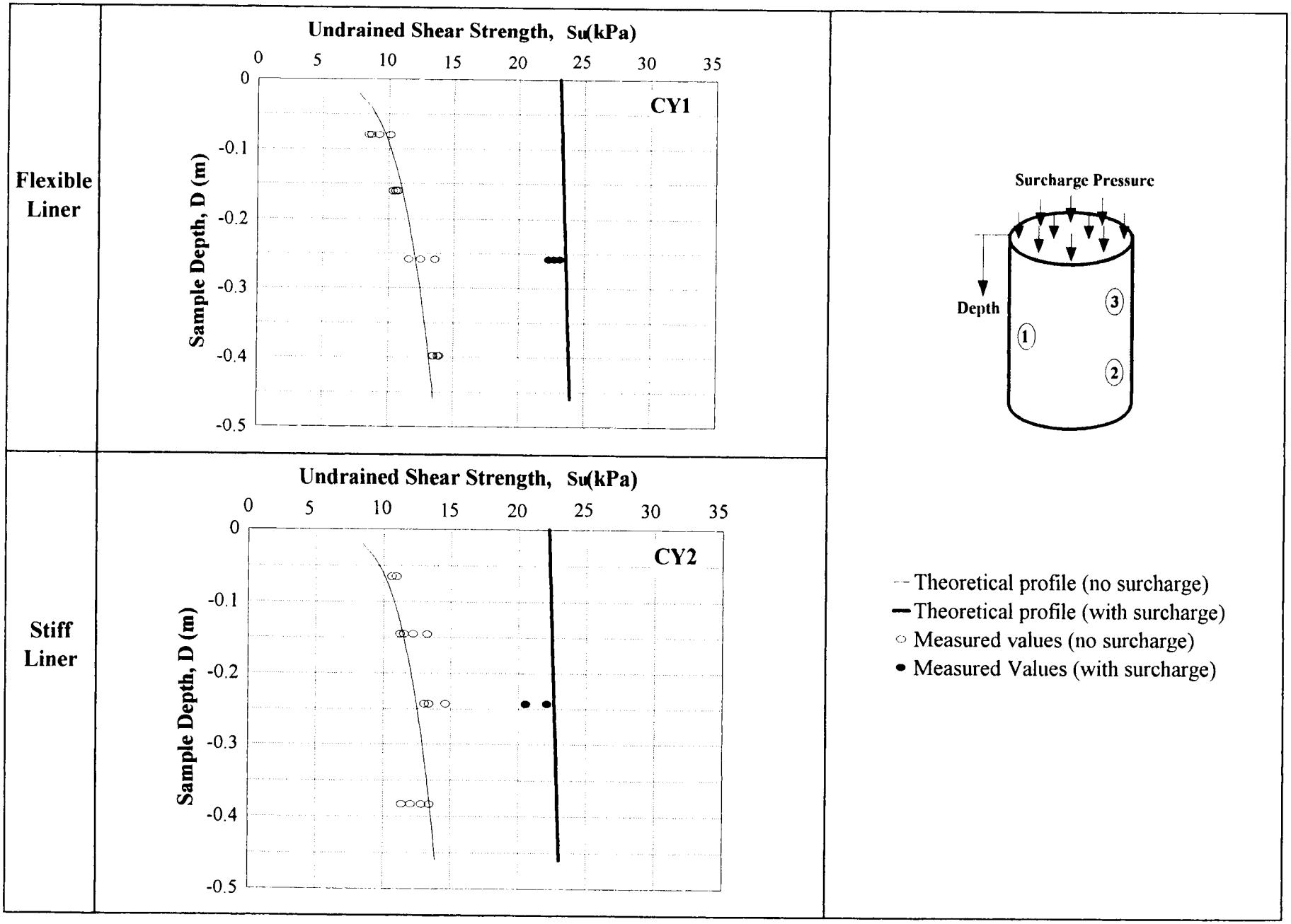


FIGURE 4.16 Undrained Shear Strength Profiles of Samples (Cylindrical tank)

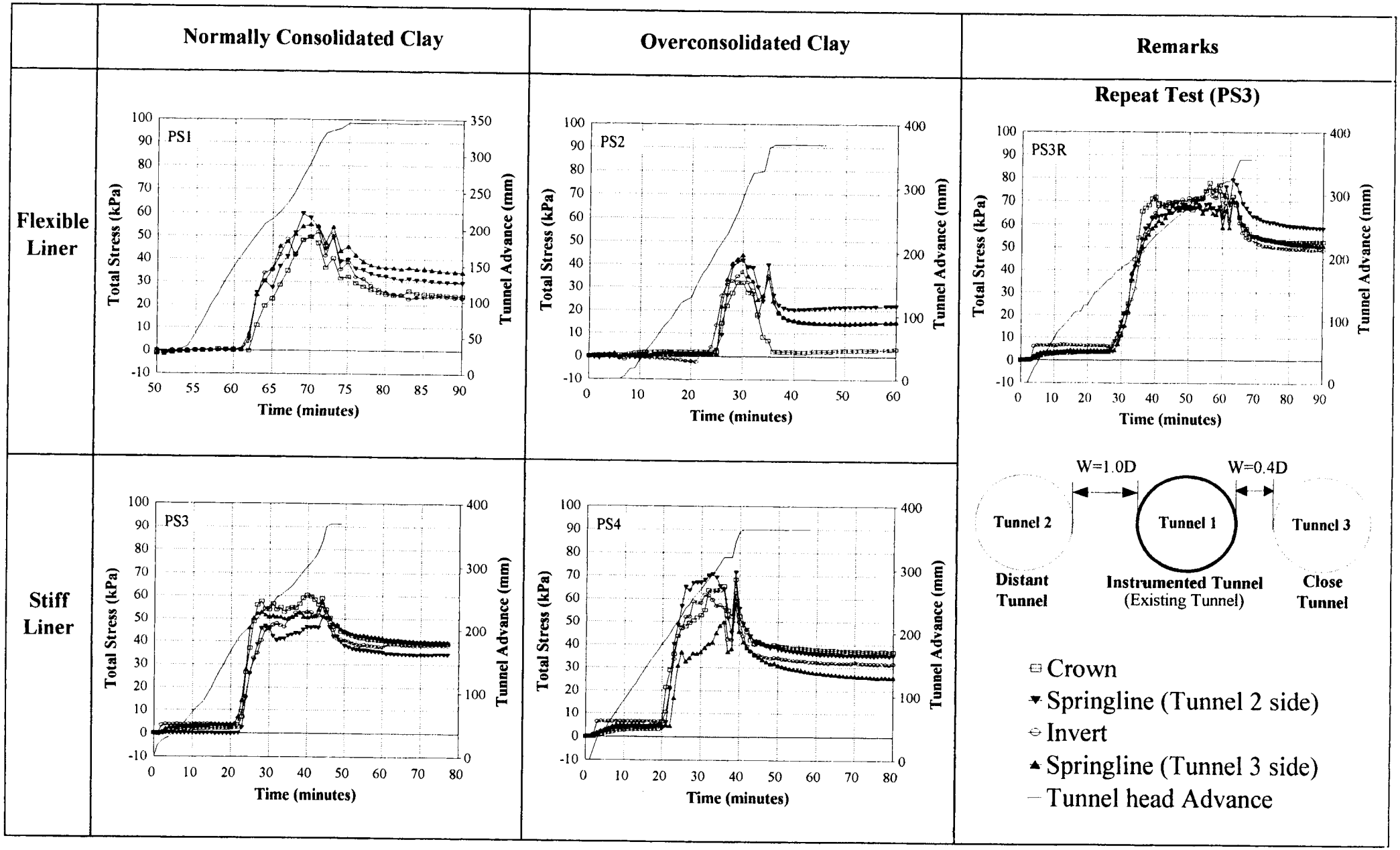


FIGURE 5.1 Variations of Total Radial Stress During Installation of Tunnel 1

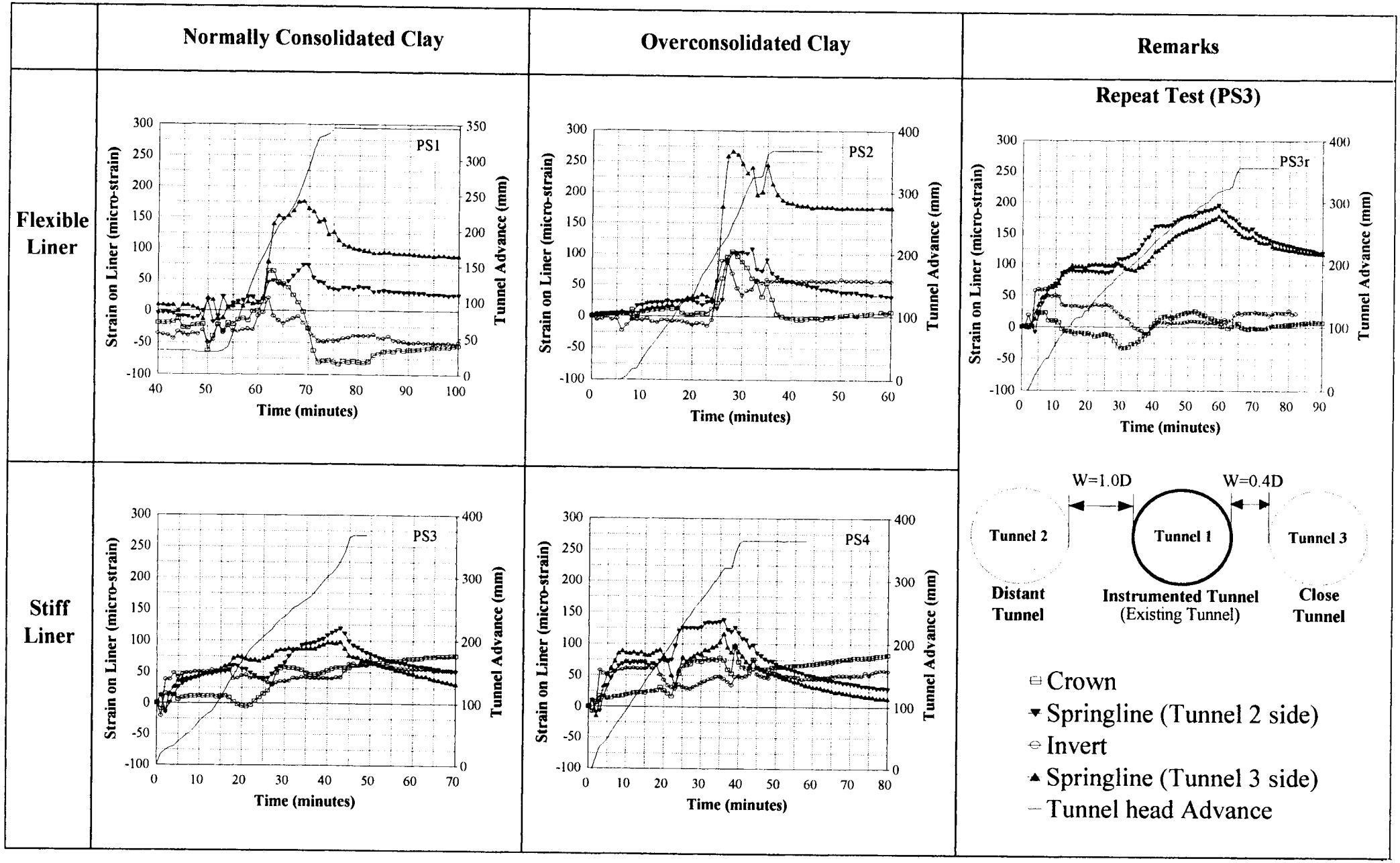


FIGURE 5.2 Variations of Strains During Installation of Tunnel 1

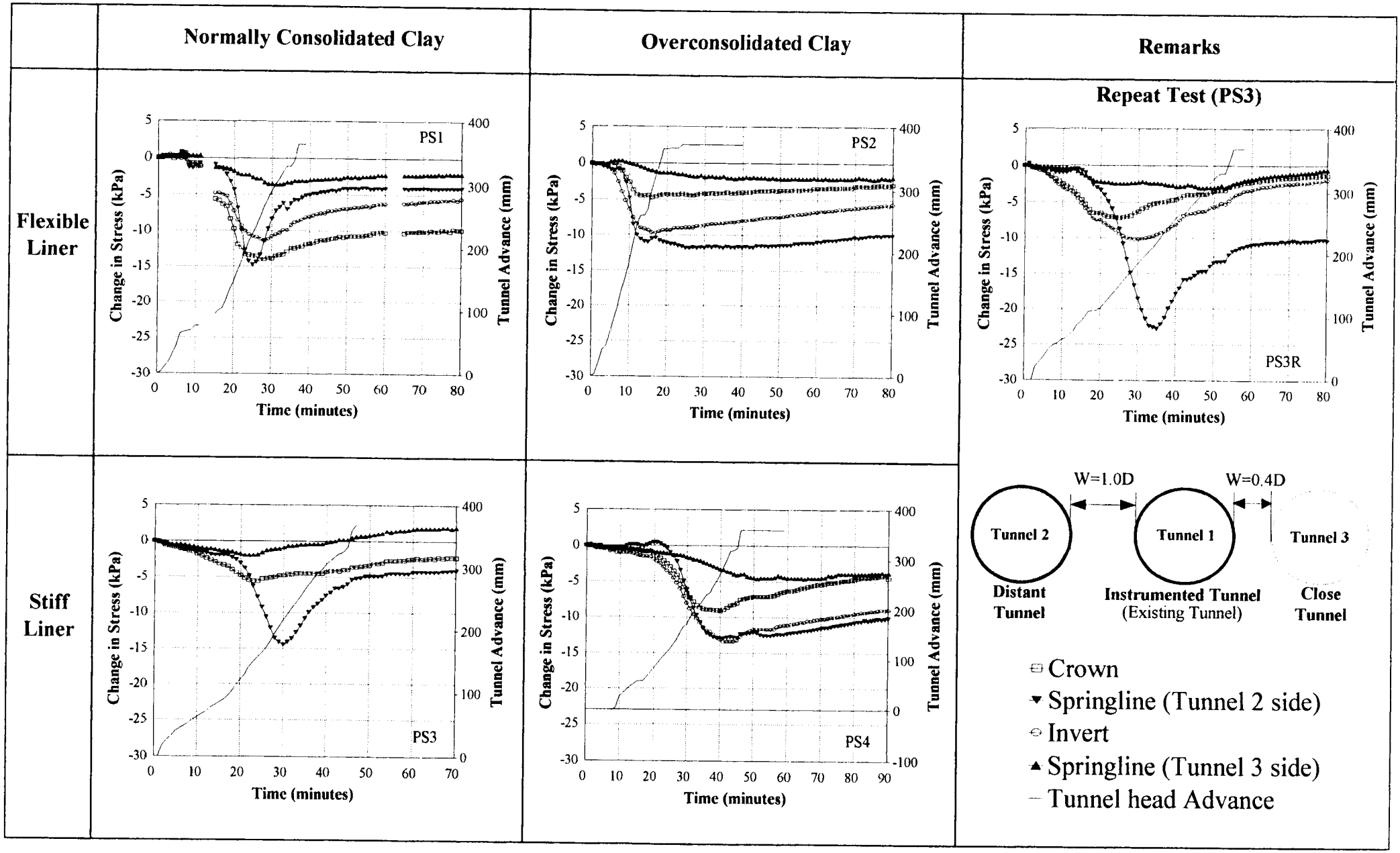


FIGURE 5.3 Change in Stress on Tunnel 1 During Installation of Tunnel 2

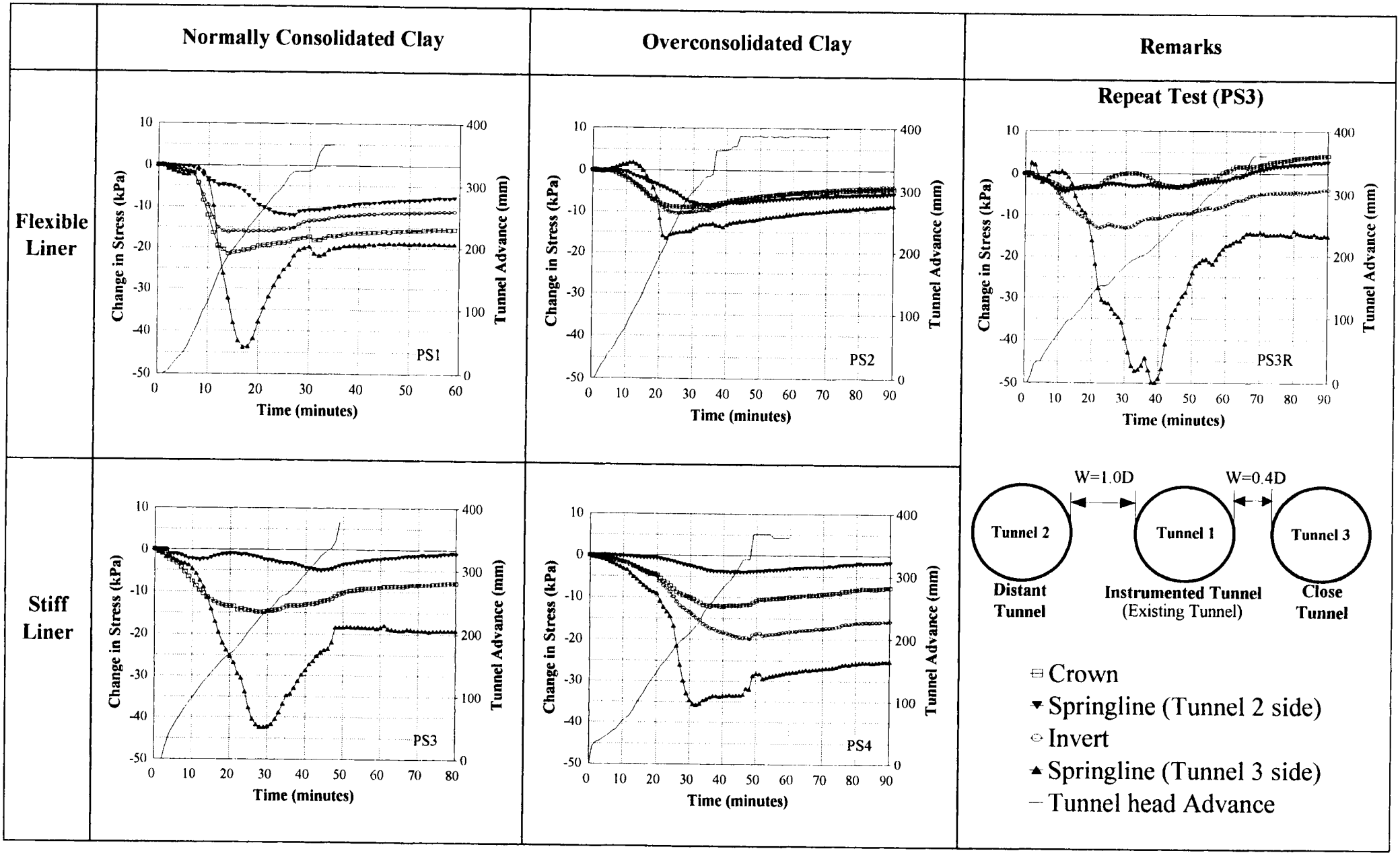


FIGURE 5. 4 Change in Stress on Tunnel 1 During Installation of Tunnel 3

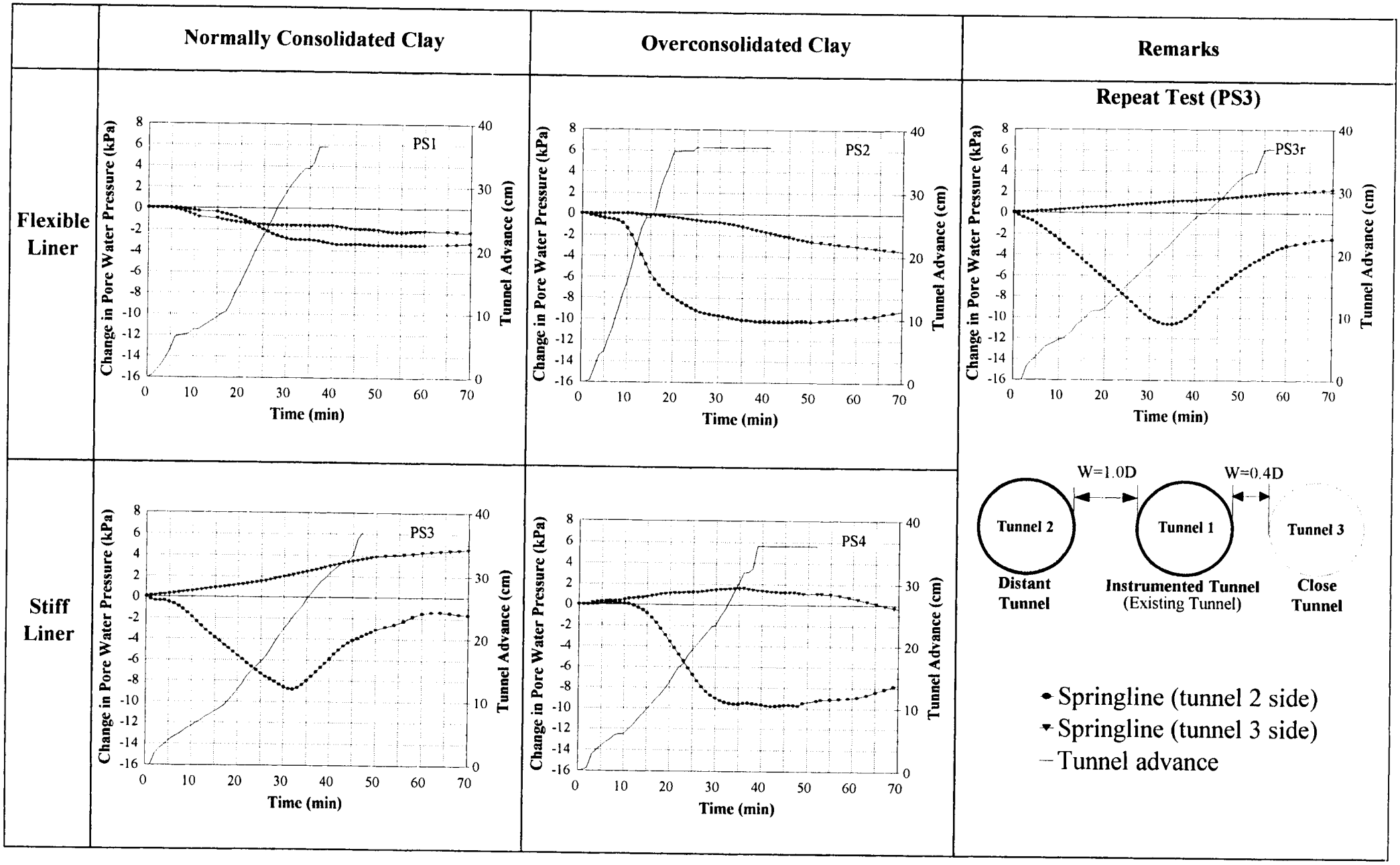


FIGURE 5.5 Change in Pore Water Pressure on Tunnel 1 During Installation of Tunnel 2

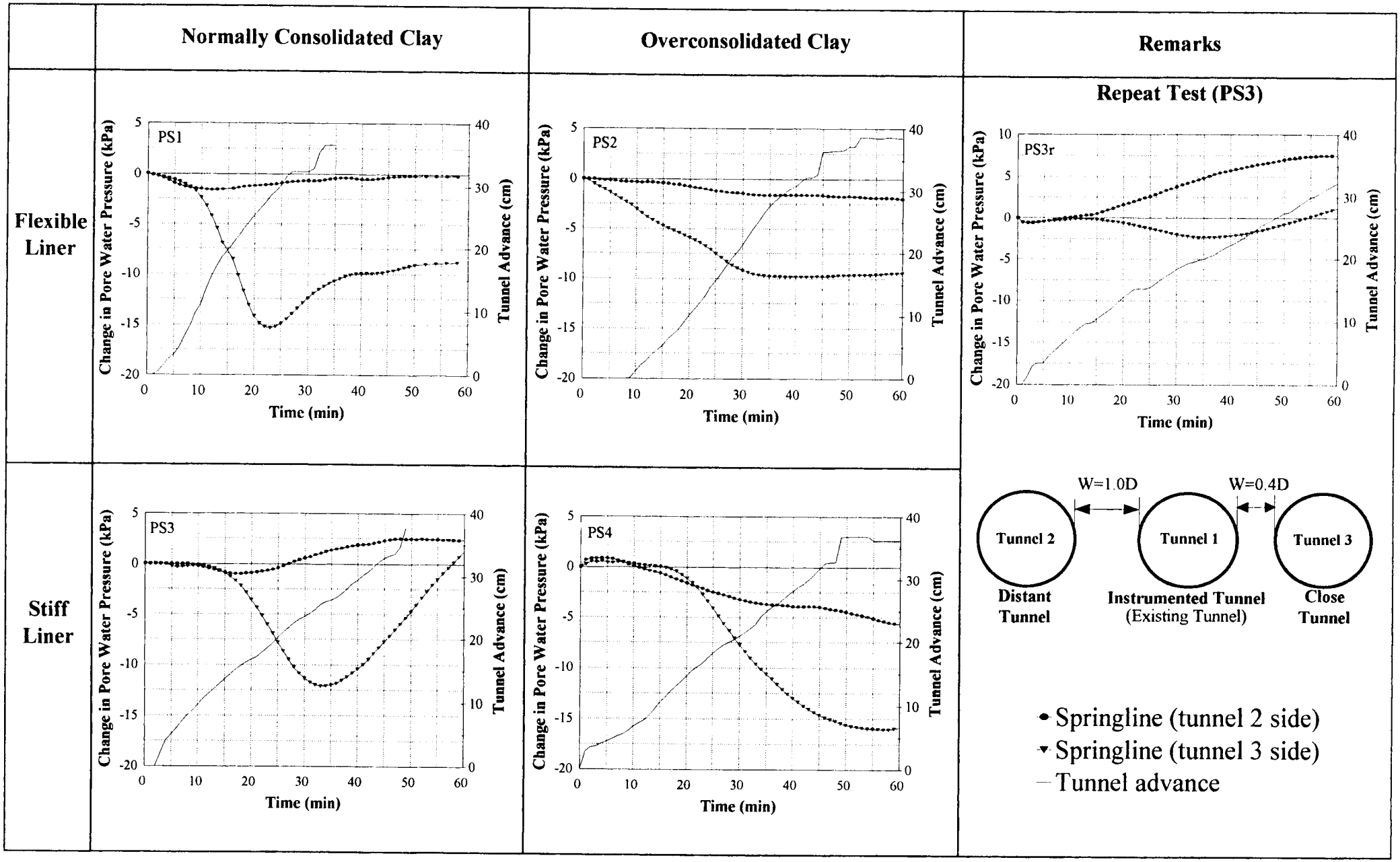


FIGURE 5.6 Change in Pore Water Pressure on Tunnel 1 During Installation of Tunnel 3

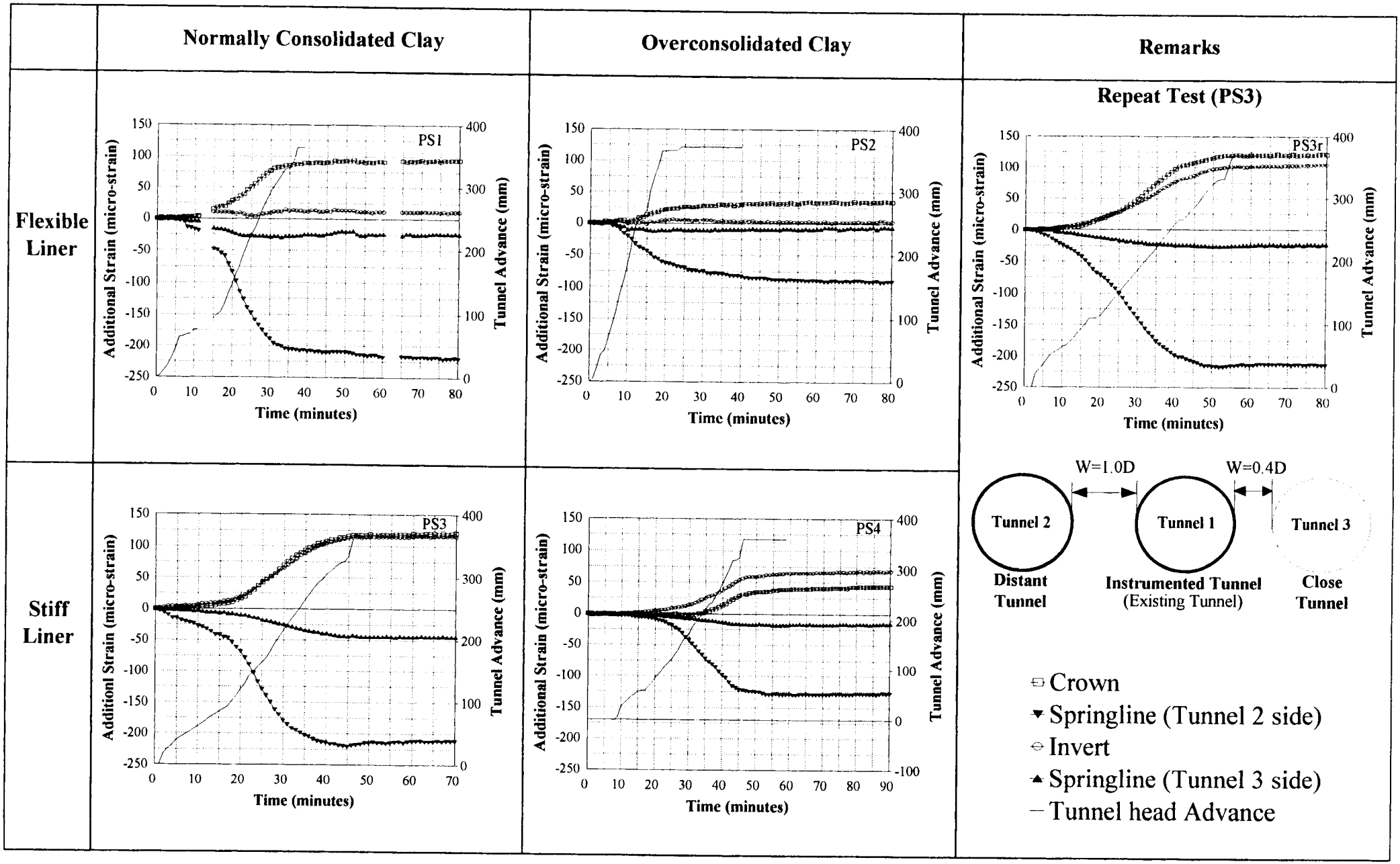


FIGURE 5.7 Incremental Strain on Tunnel 1 during Installation of Tunnel 2

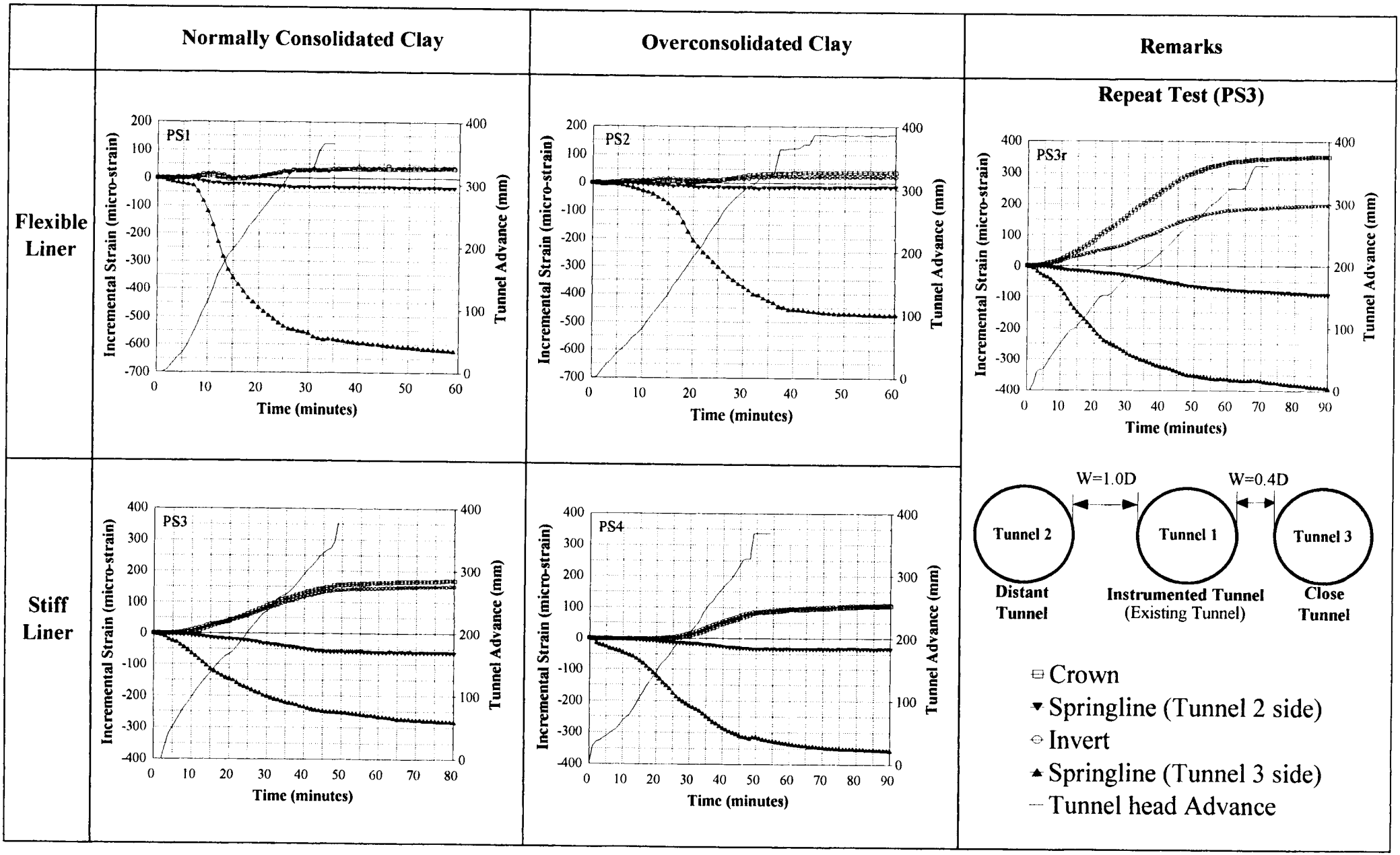


FIGURE 5.8 Incremental Strain on Tunnel 1 During Installation of Tunnel 3

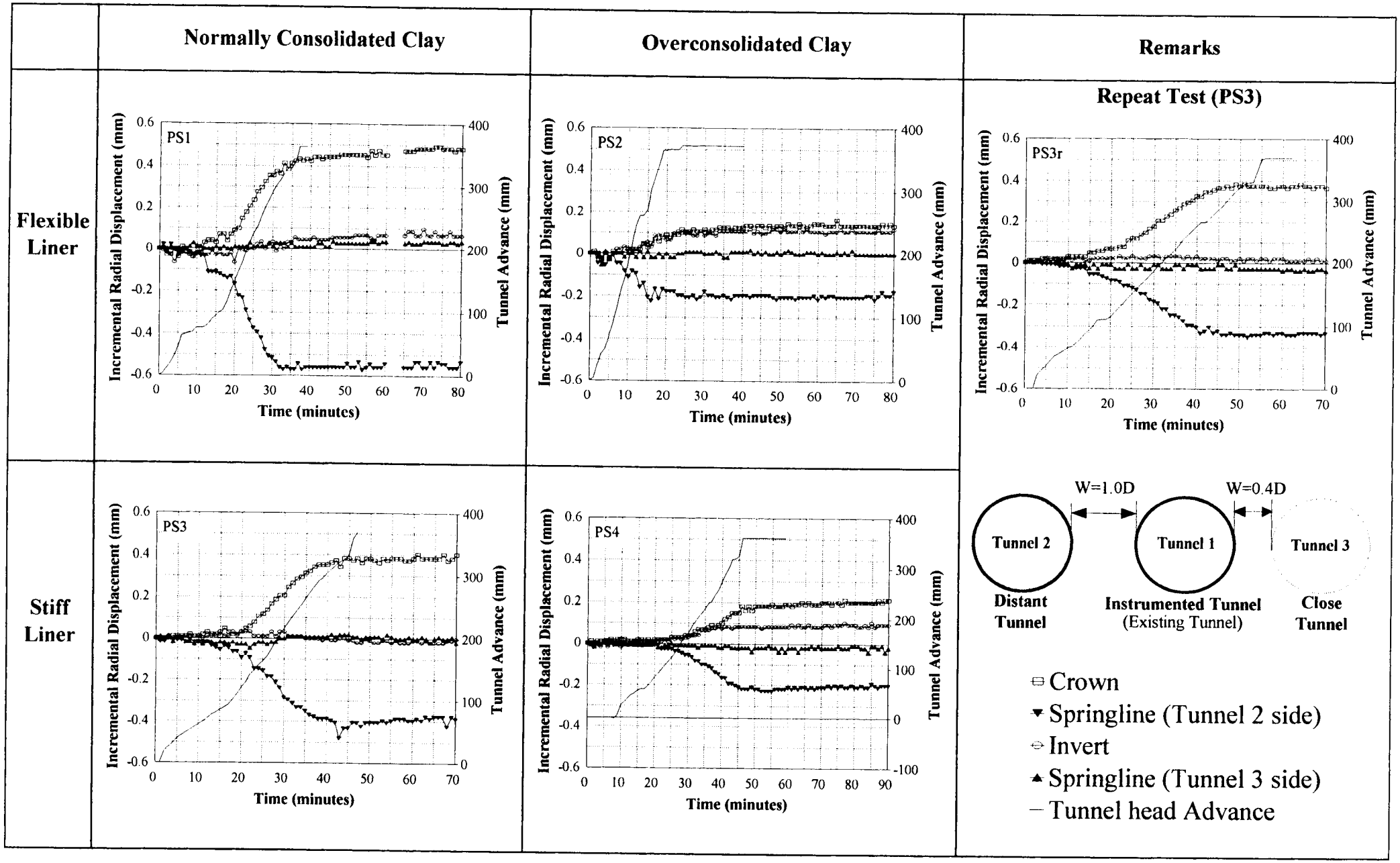


FIGURE 5. 9 Variations of Incremental Radial Displacements of Tunnel 1 During Installation of Tunnel 2

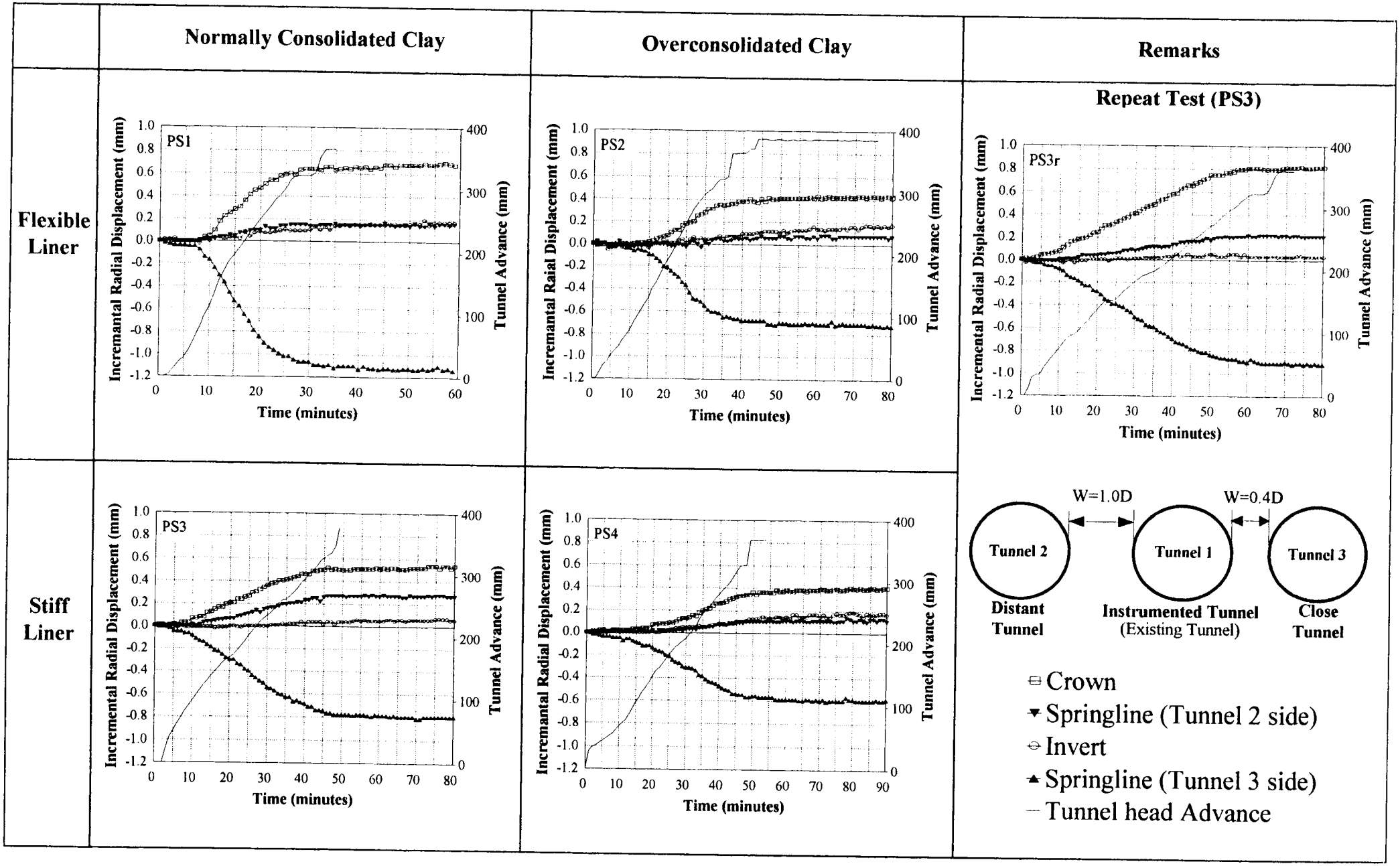


FIGURE 5. 10 Variations of Incremental Radial Displacements of Tunnel 1 During Installation of Tunnel 3

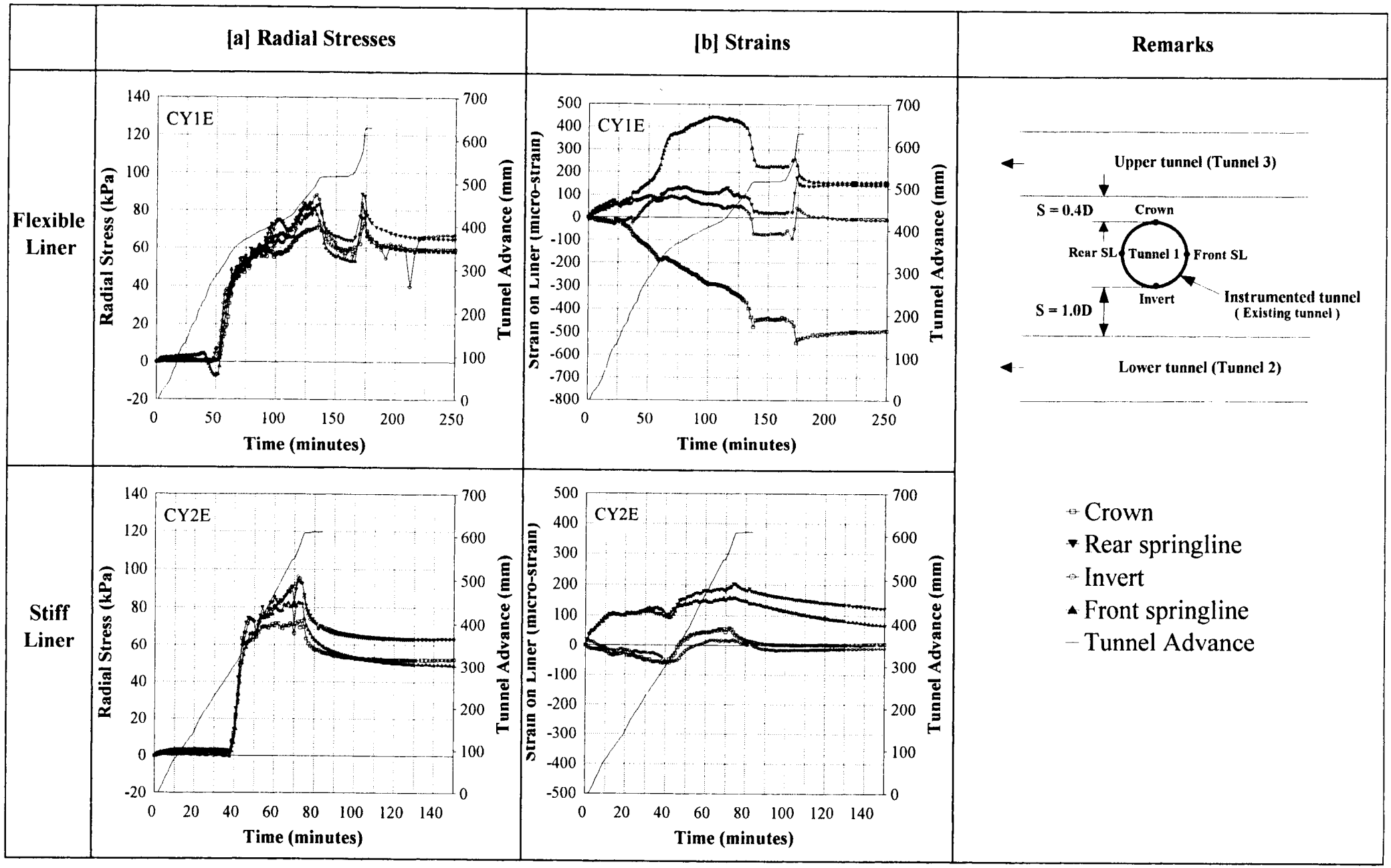


FIGURE 5.11 Variations of Total Radial Stresses and Strains during Installation of Tunnel 1

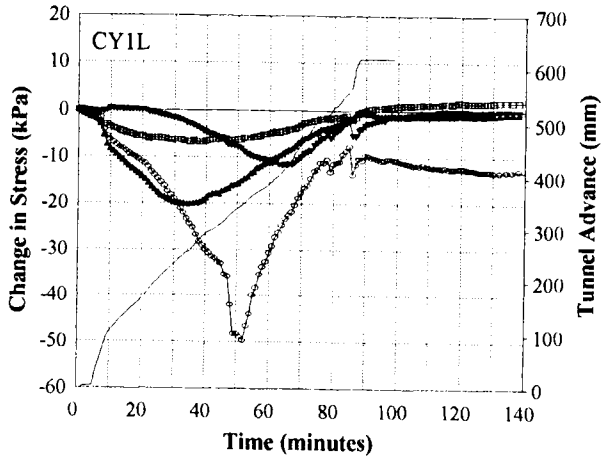
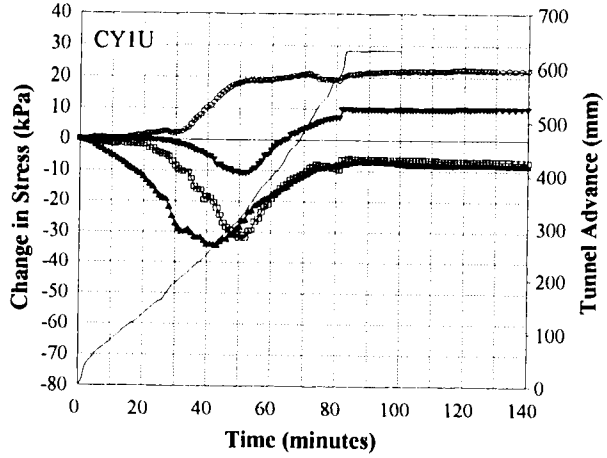
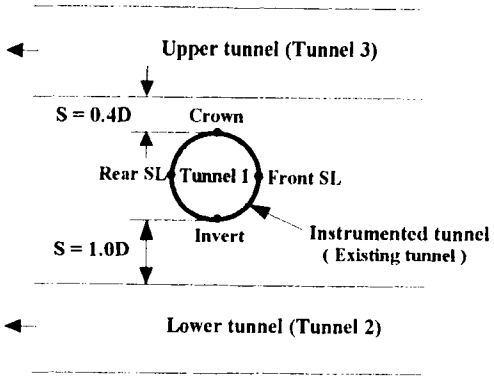
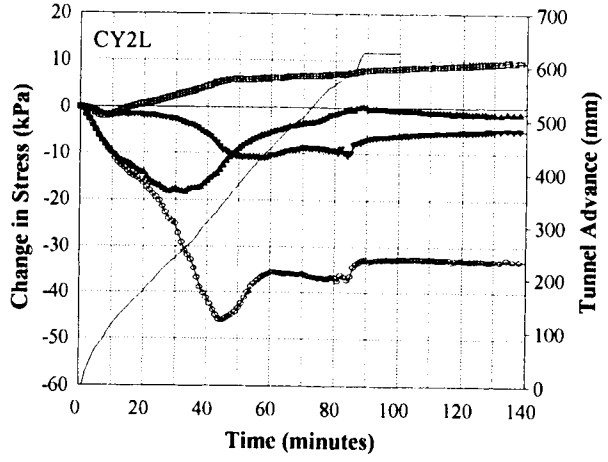
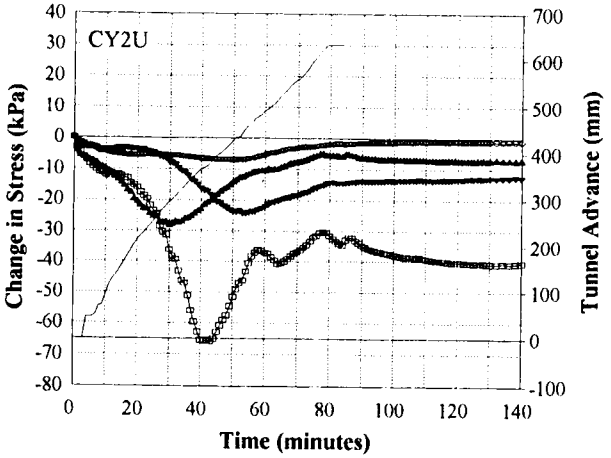
	[a] During Installation of Tunnel 2	[b] During Installation of Tunnel 3	Remarks
Flexible Liner			
Stiff Liner			Crown Rear springline Invert Front springline Tunnel Advance

FIGURE 5.12 Change in Radial Stress on Tunnel 1 during Installation of Tunnel 2 and 3

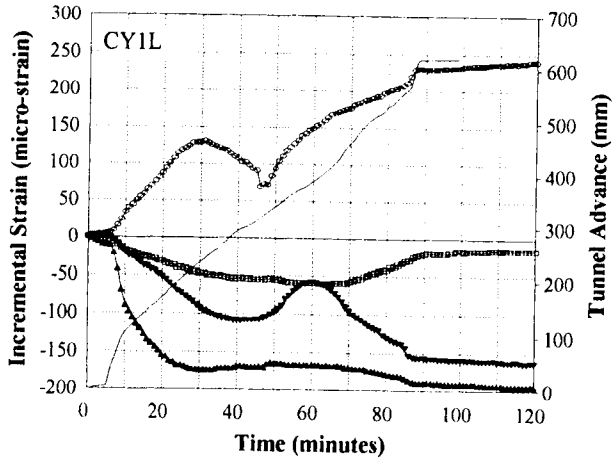
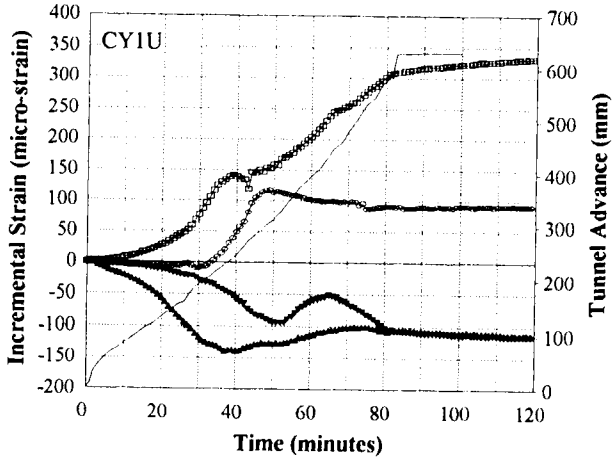
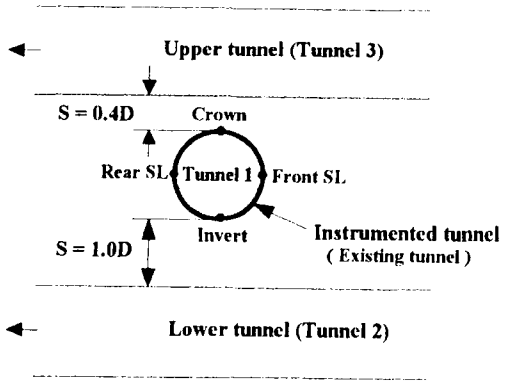
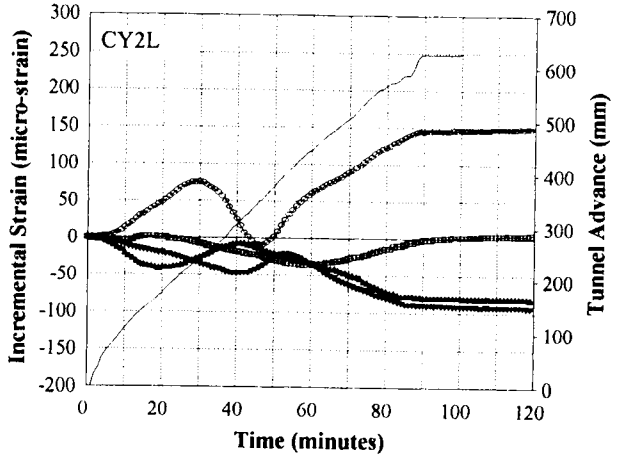
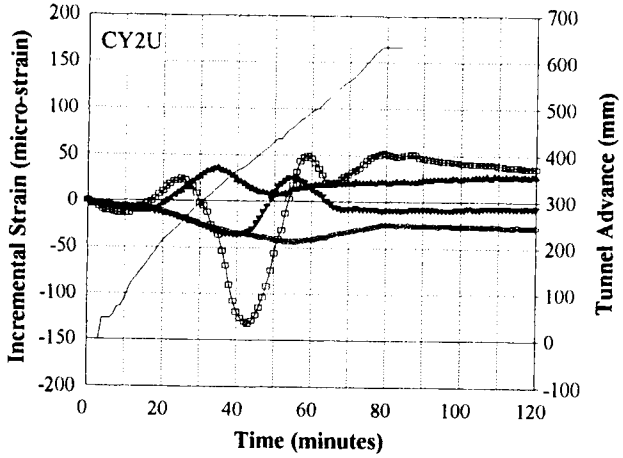
	[a] During Installation of Tunnel 2	[b] During Installation of Tunnel 3	Remarks
Flexible Liner			
Stiff Liner			Crown Rear springline Invert Front springline Tunnel Advance

FIGURE 5.13 Variations of Incremental Strains on Tunnel 1 during Installation of Tunnel 2 and 3

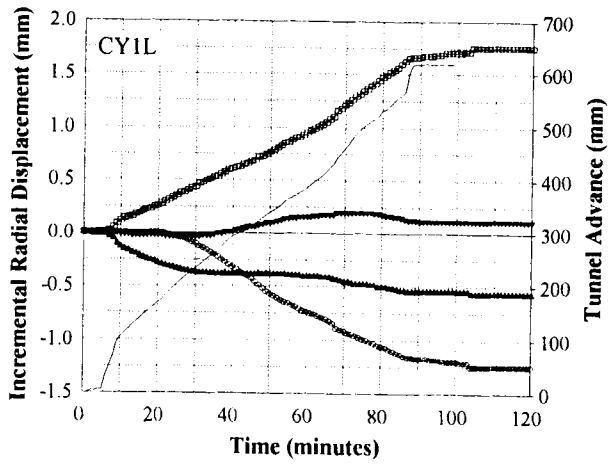
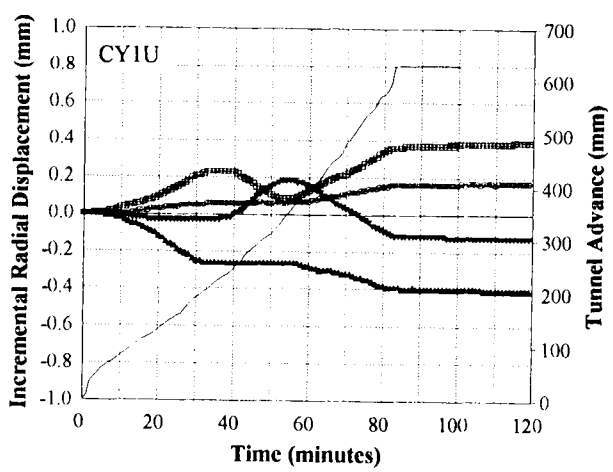
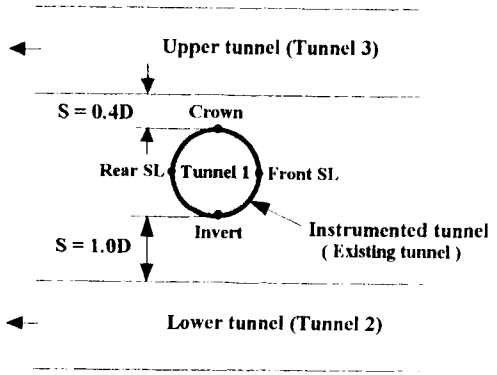
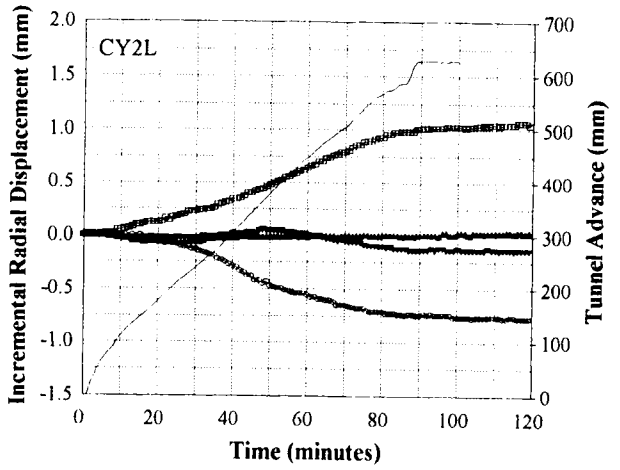
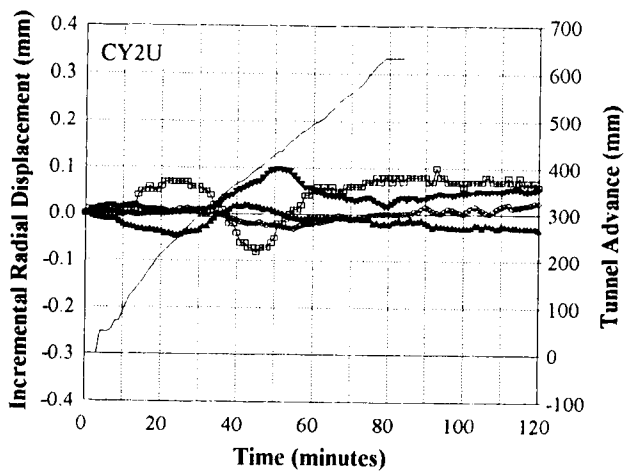
	[a] During Installation of Tunnel 2	[b] During Installation of Tunnel 3	Remarks
Flexible Liner			
Stiff Liner			Crown Rear springline Invert Front springline Tunnel Advance

FIGURE 5.14 Variations of Incremental Displacements of Tunnel 1 during Installation of Tunnel 2 and 3

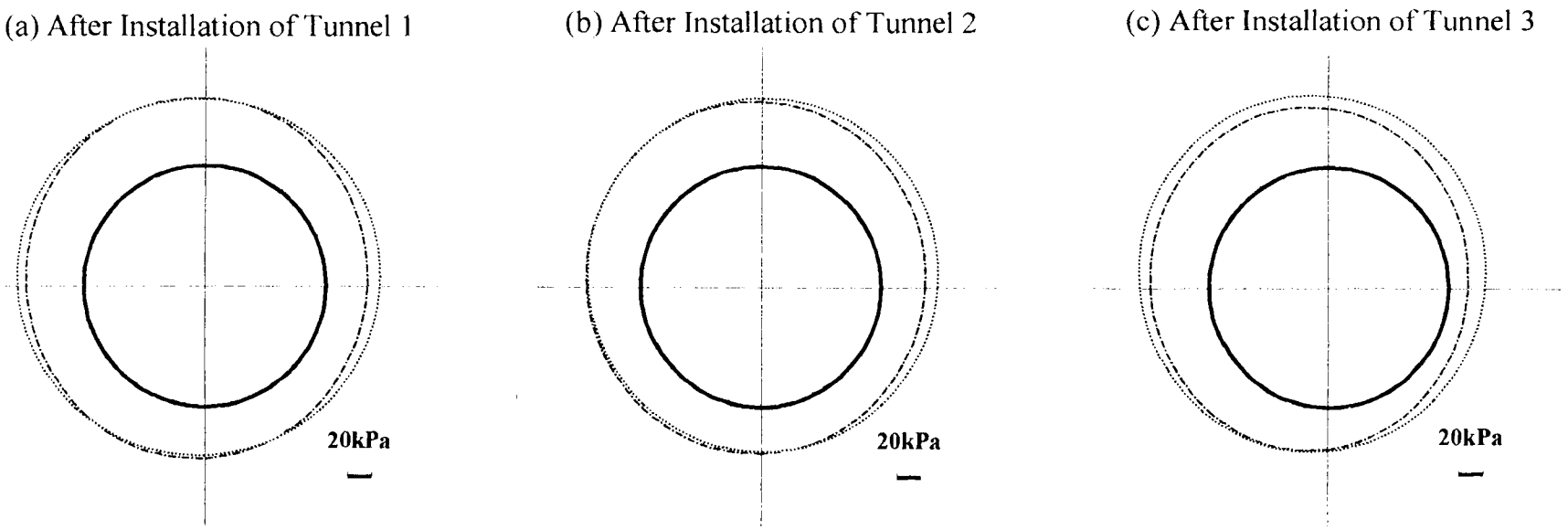


FIGURE 5.15 Comparison Between Total Radial Pressure for PS3 and PS3R

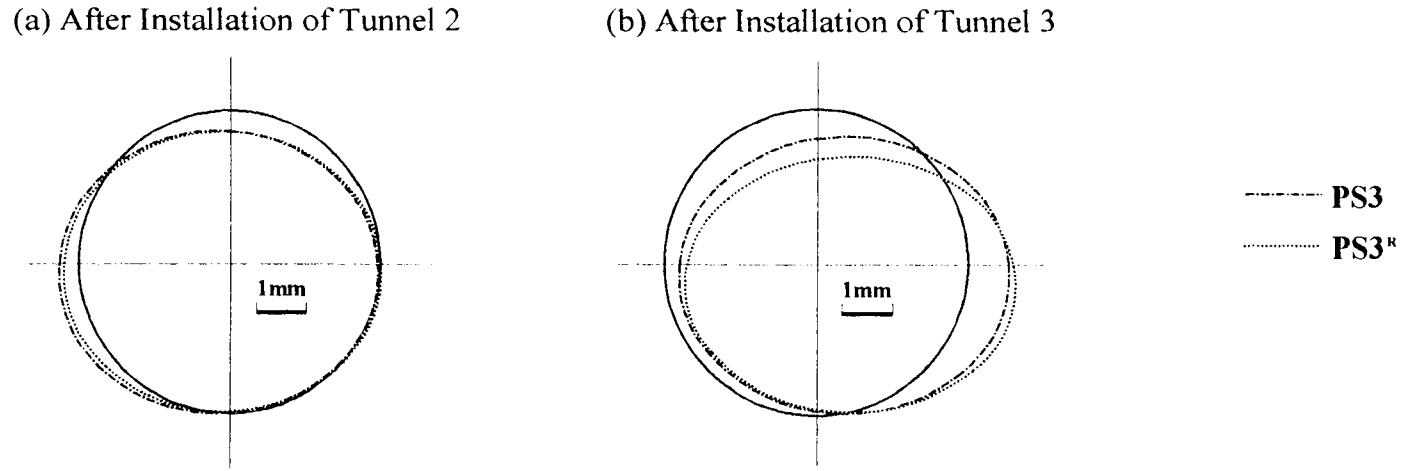
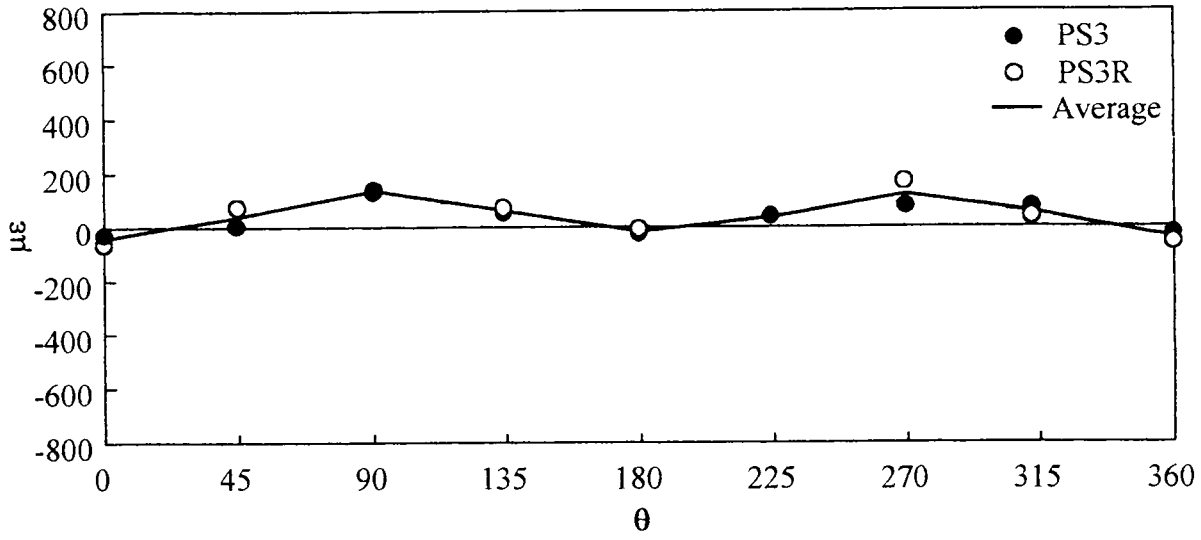
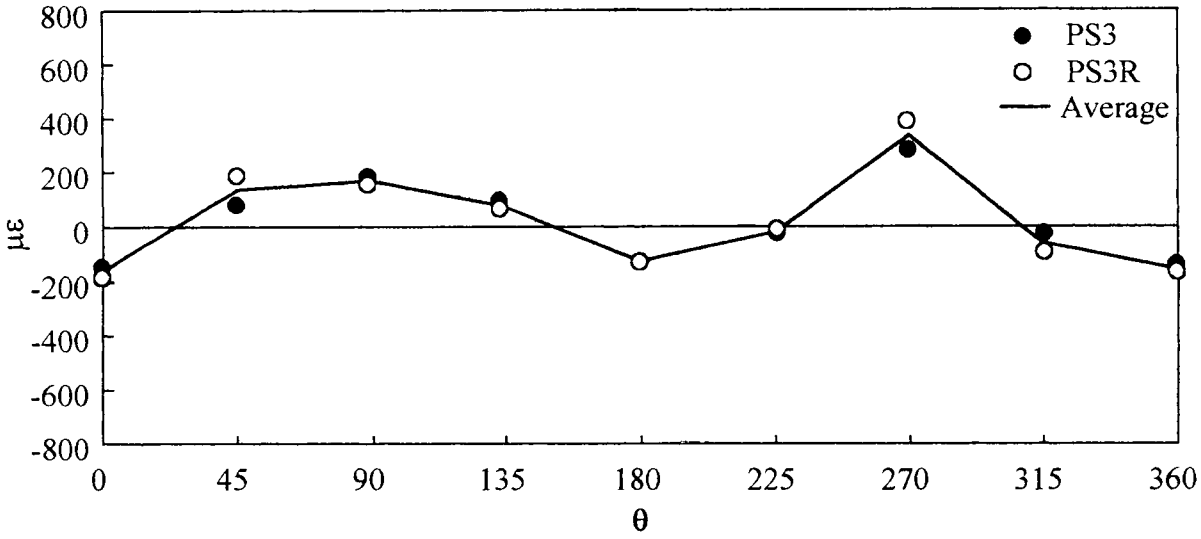


FIGURE 5.16 Comparison Between Incremental Displacement for PS3 and PS3R

(a) After Installation of tunnel 1



(b) After Installation of tunnel 2



(c) After Installation of tunnel 3

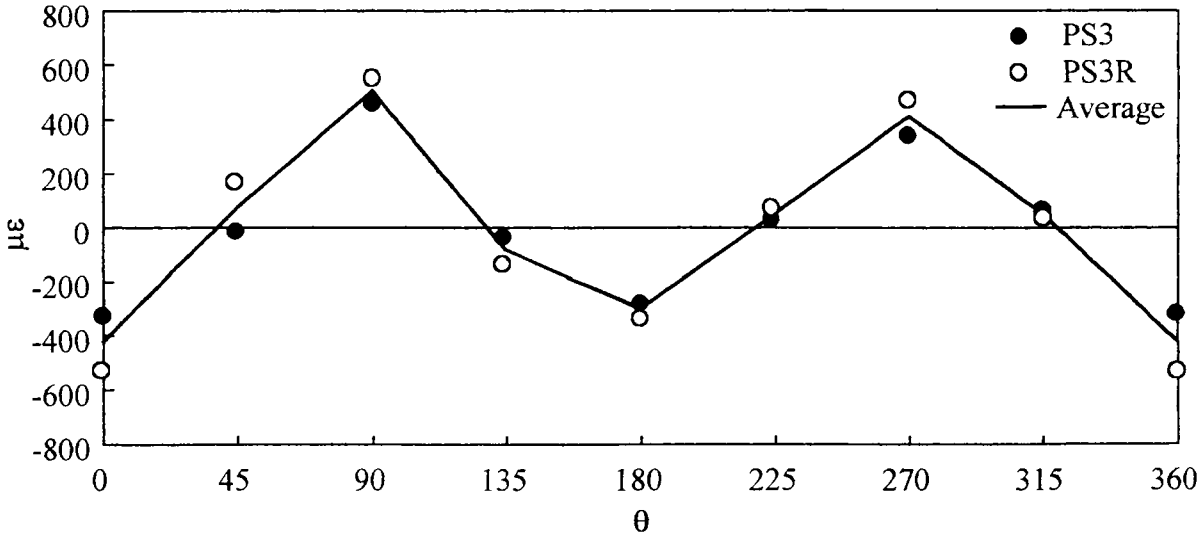


FIGURE 5.17 Comparison Between Strain on Tunnel 1 for PS3 and PS3R

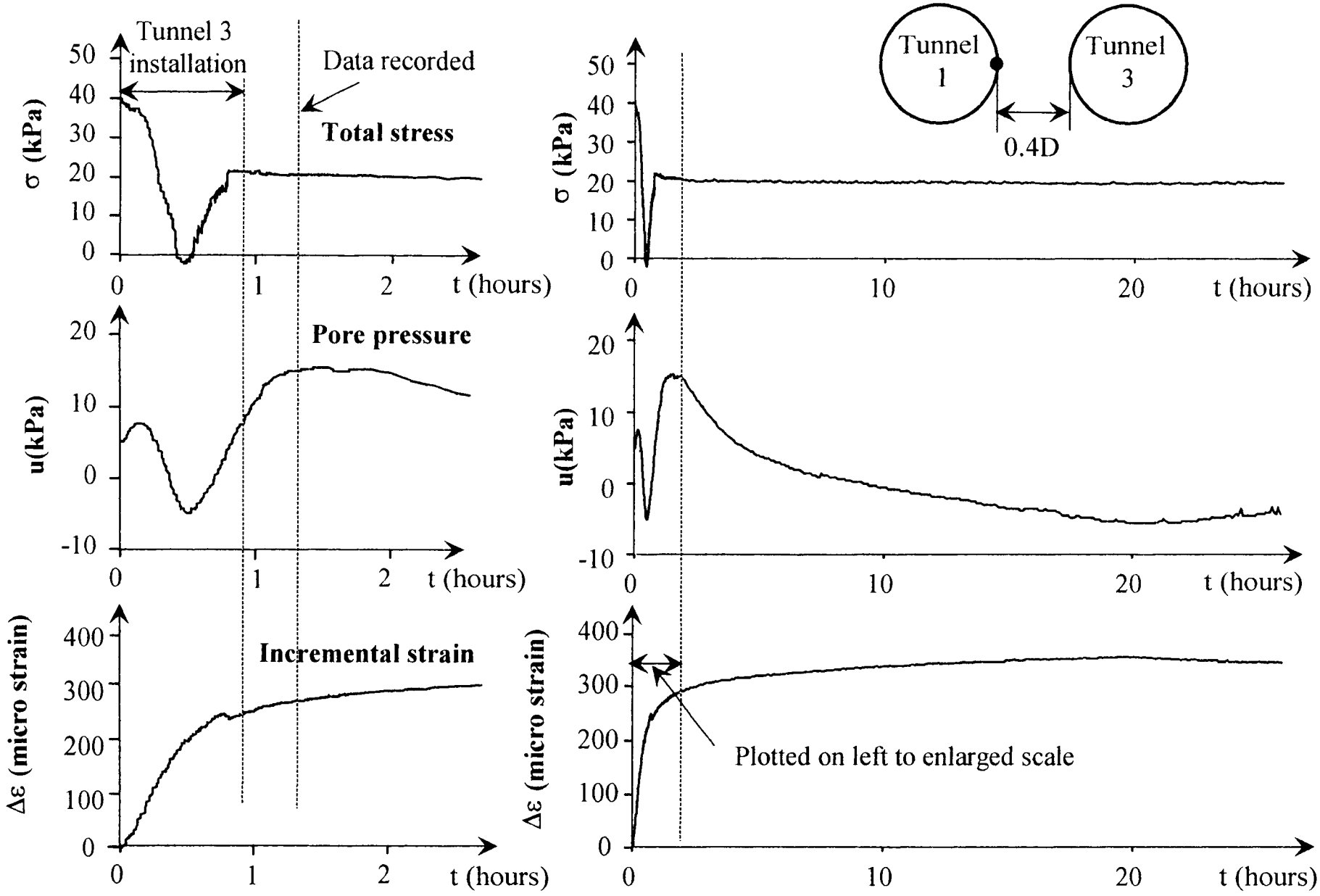


FIGURE 5.18 Pore pressure, total stress, incremental strain (PS3)

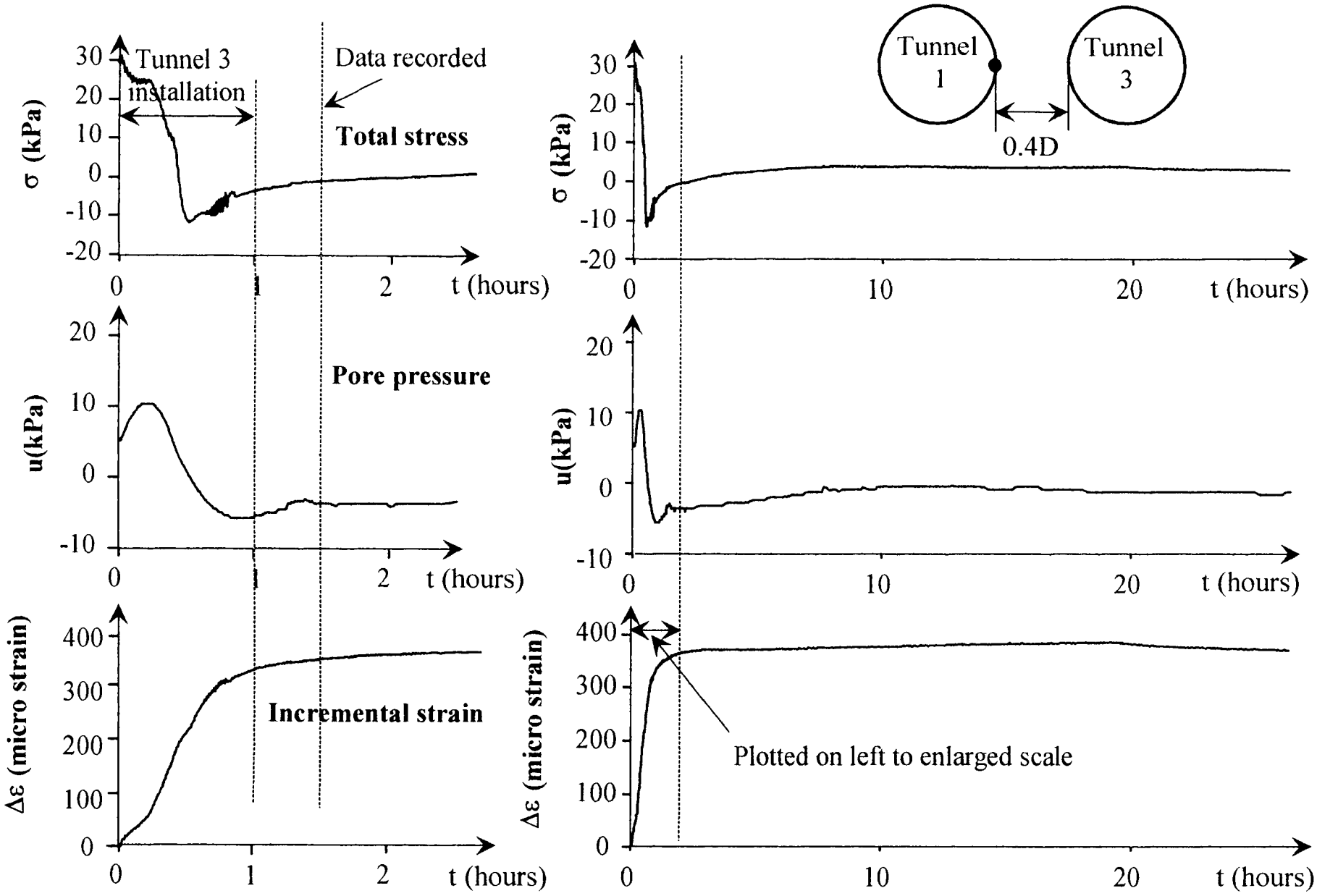
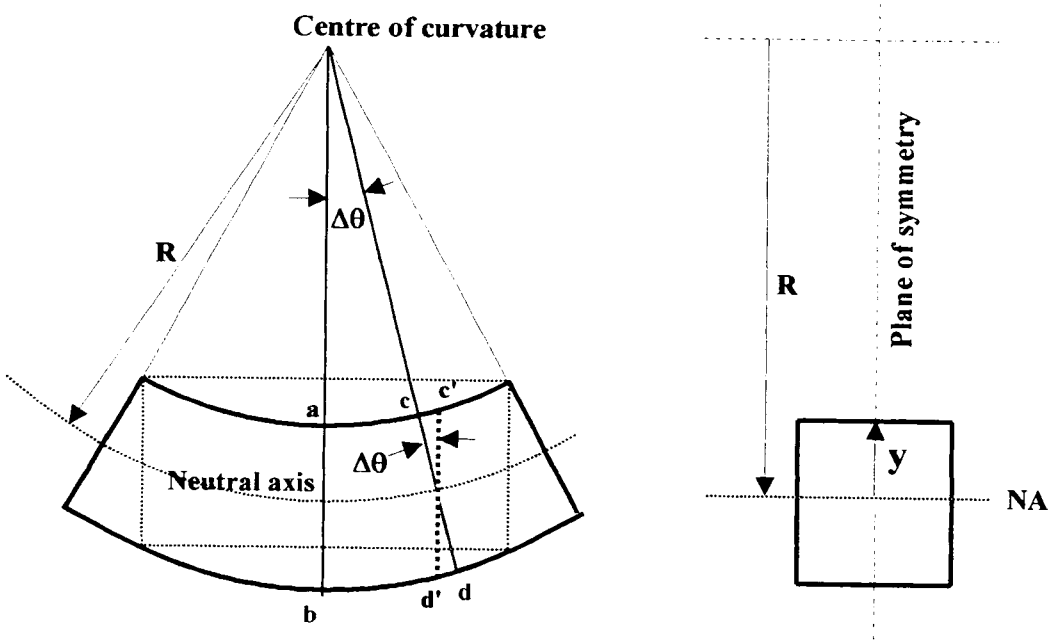
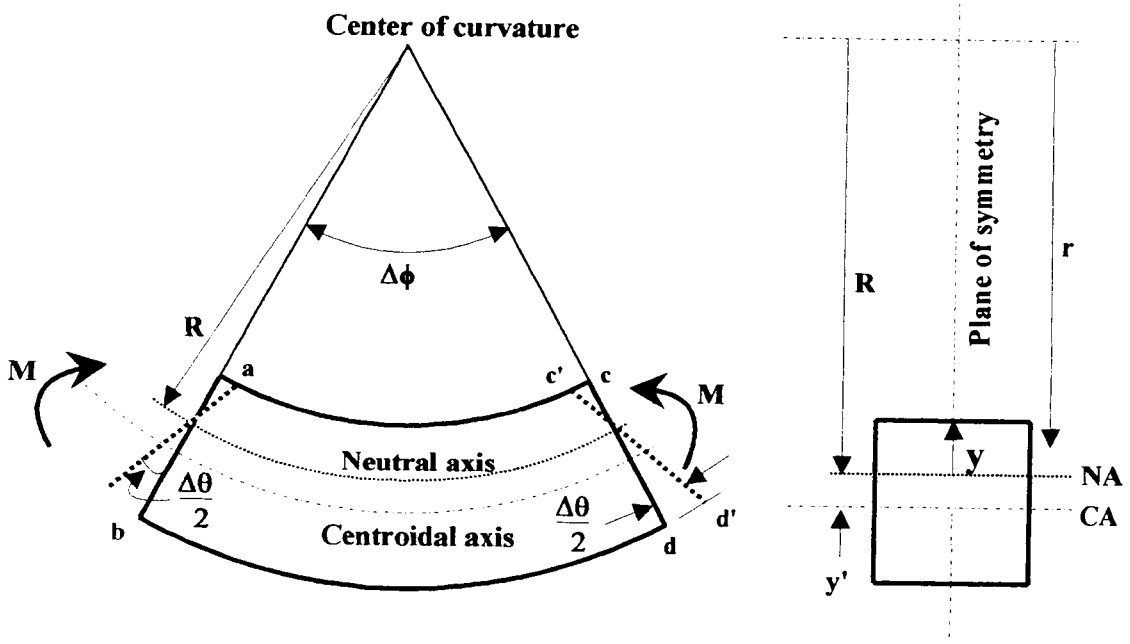


FIGURE 5.19 Pore pressure, total stress, incremental strain (PS4)



[a] Straight Beam with Longitudinal Plane of Symmetry



[b] Curved Beam with Longitudinal Plane of Symmetry

FIGURE 6.1 Summary of Elastic Beam Theory

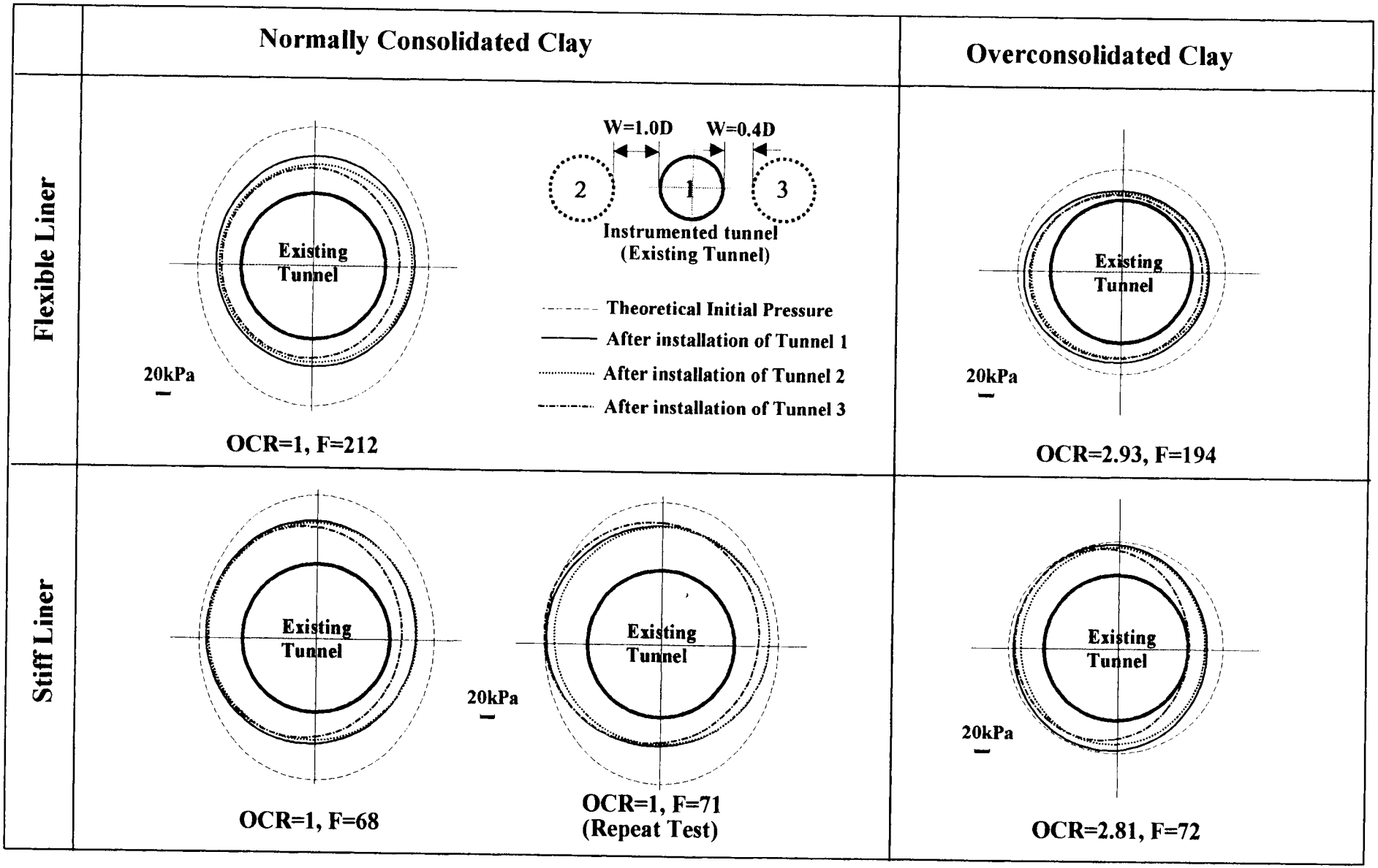


FIGURE 6.2 Total Stresses Acting on Tunnel 1

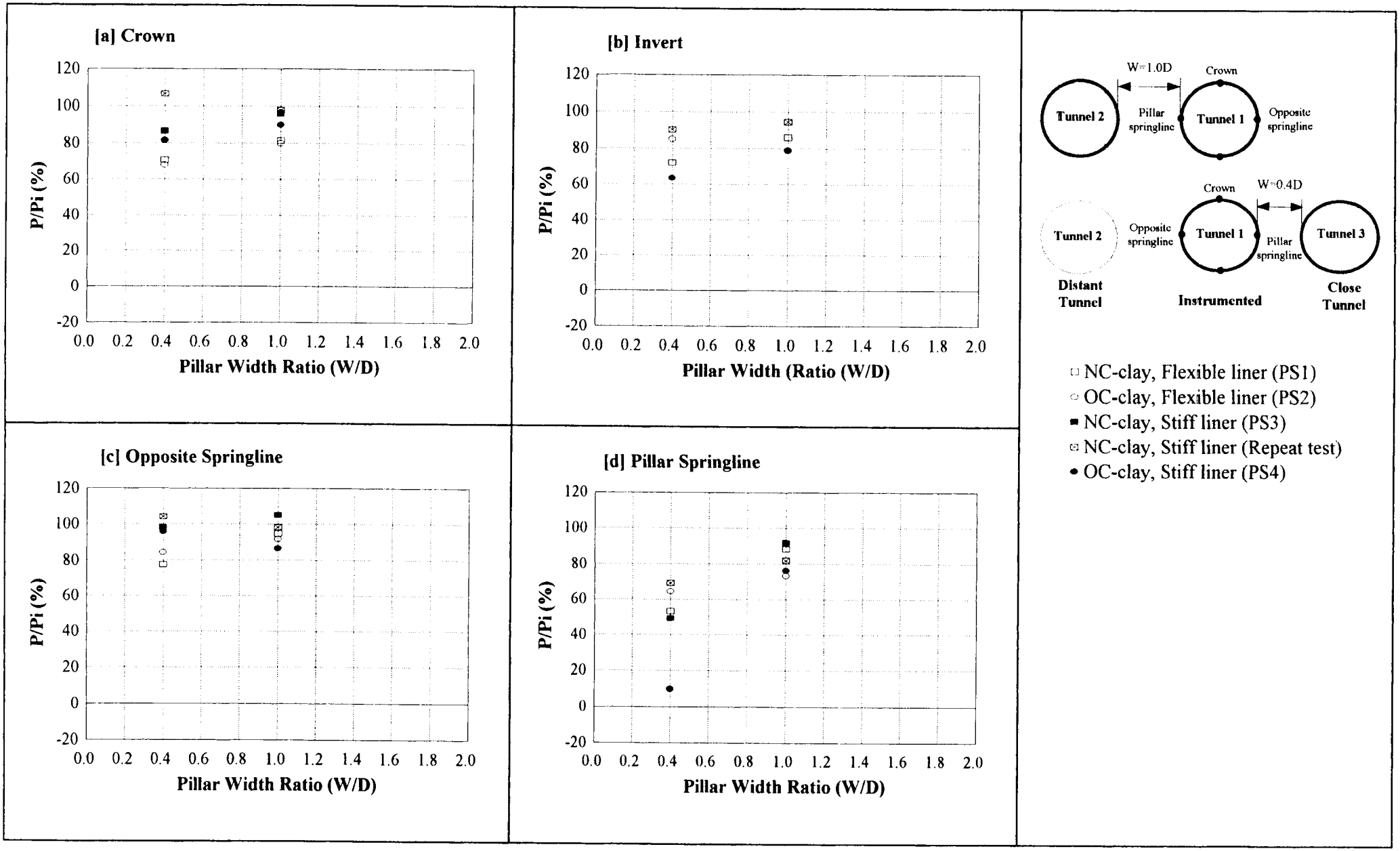


FIGURE 6.3 Normalized Stresses acting on Tunnel 1 vs. Pillar Width (W/D)

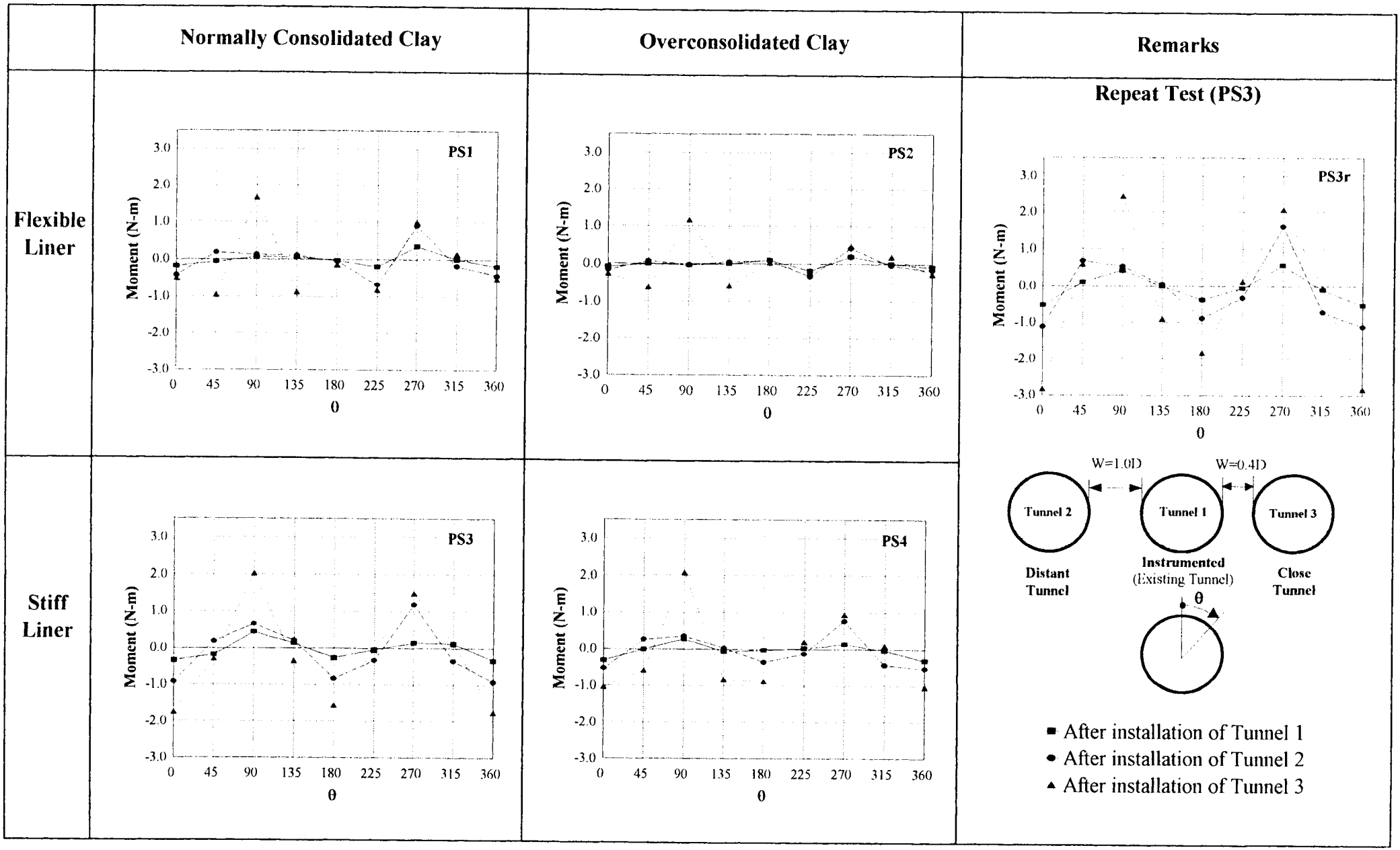


FIGURE 6.4 Bending Moment in Tunnel 1 after Installation of Tunnels 2 and 3

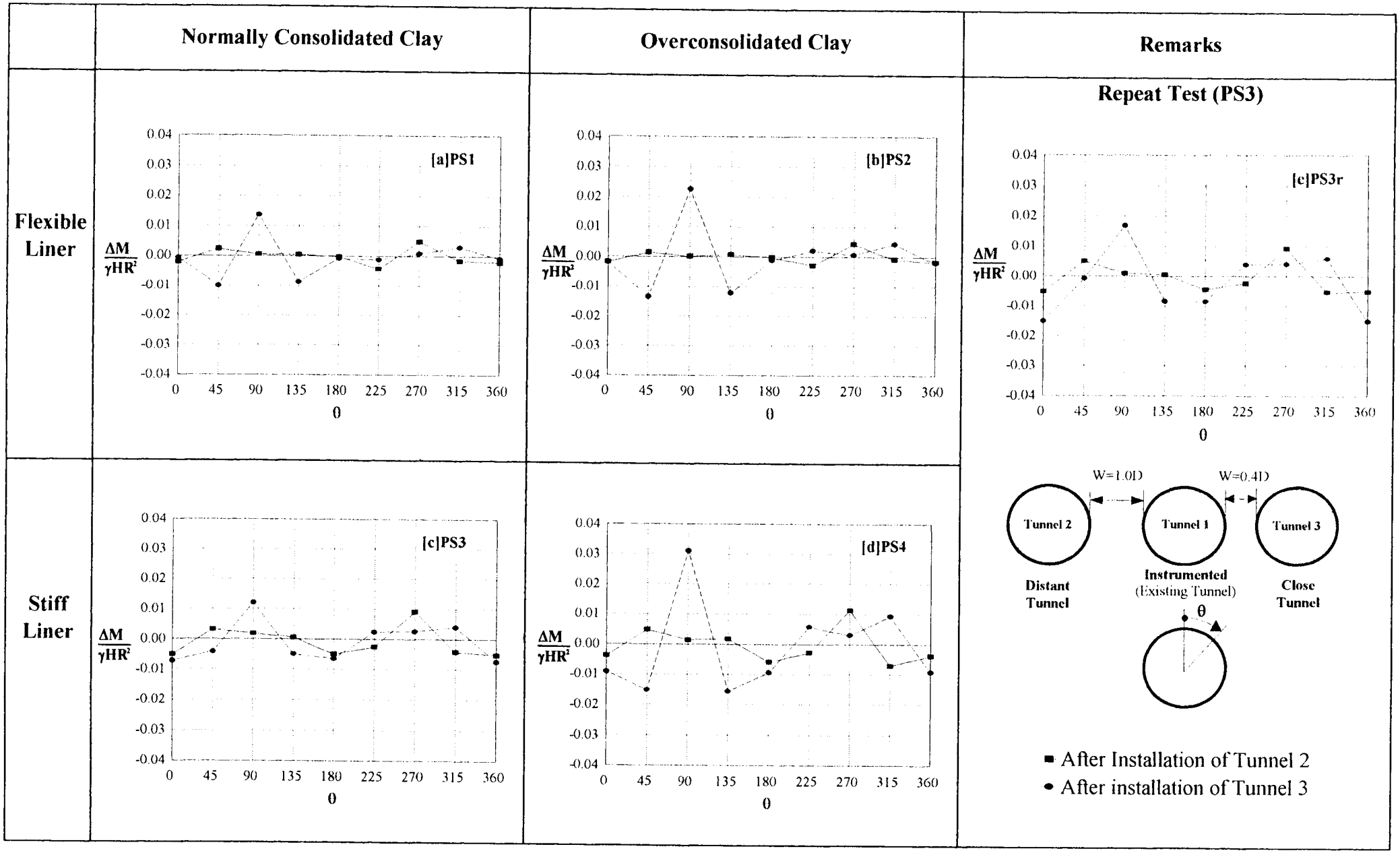


FIGURE 6.5 Normalized Incremental Bending Moment in Tunnel 1 after Installation of Tunnels 2 and 3

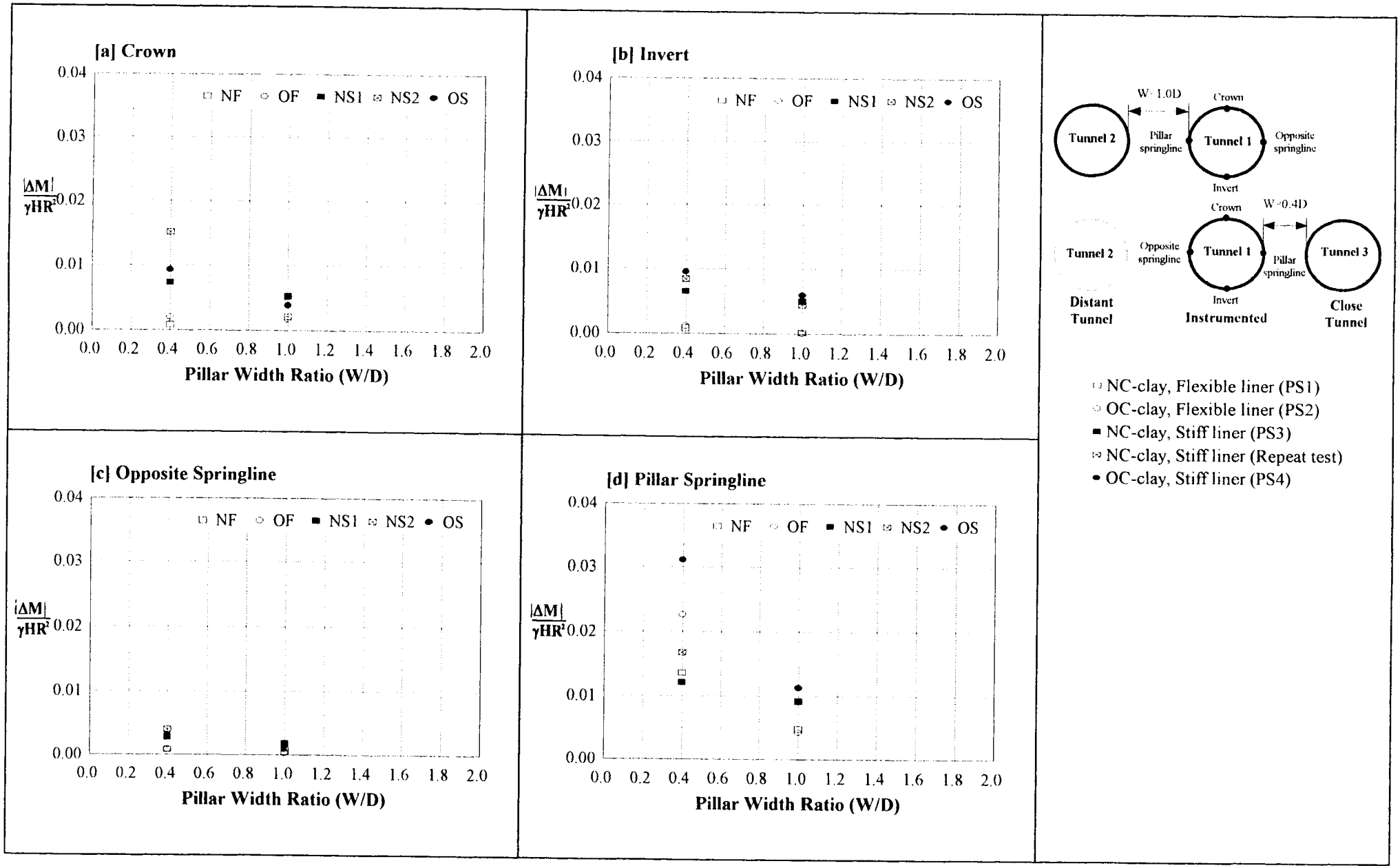


FIGURE 6.6 Normalized Incremental Bending Moment in Tunnel 1 vs. Pillar Width (W/D)

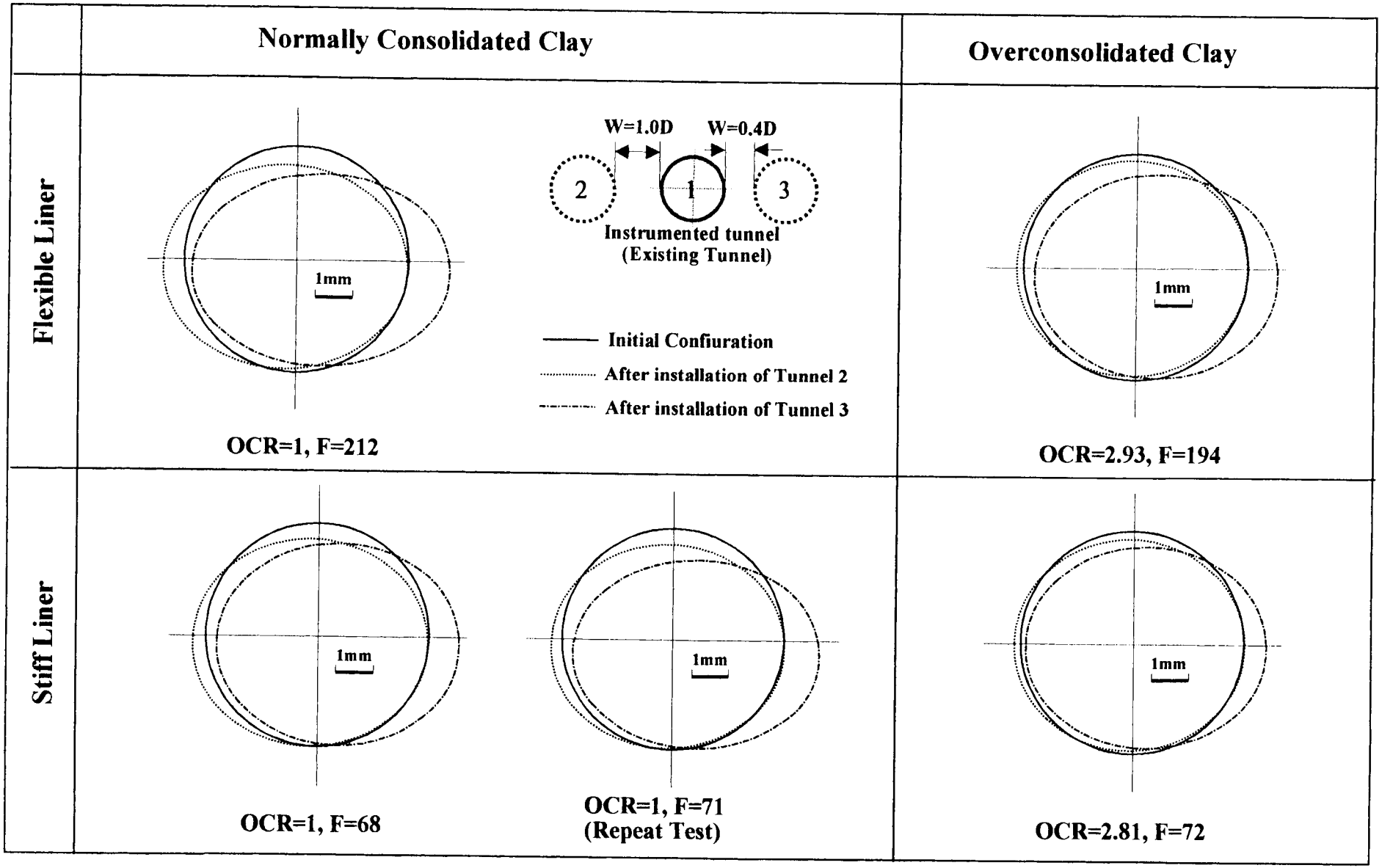


FIGURE 6.7 Incremental Displacement of Tunnel 1 after Installation of Tunnels 2 and 3

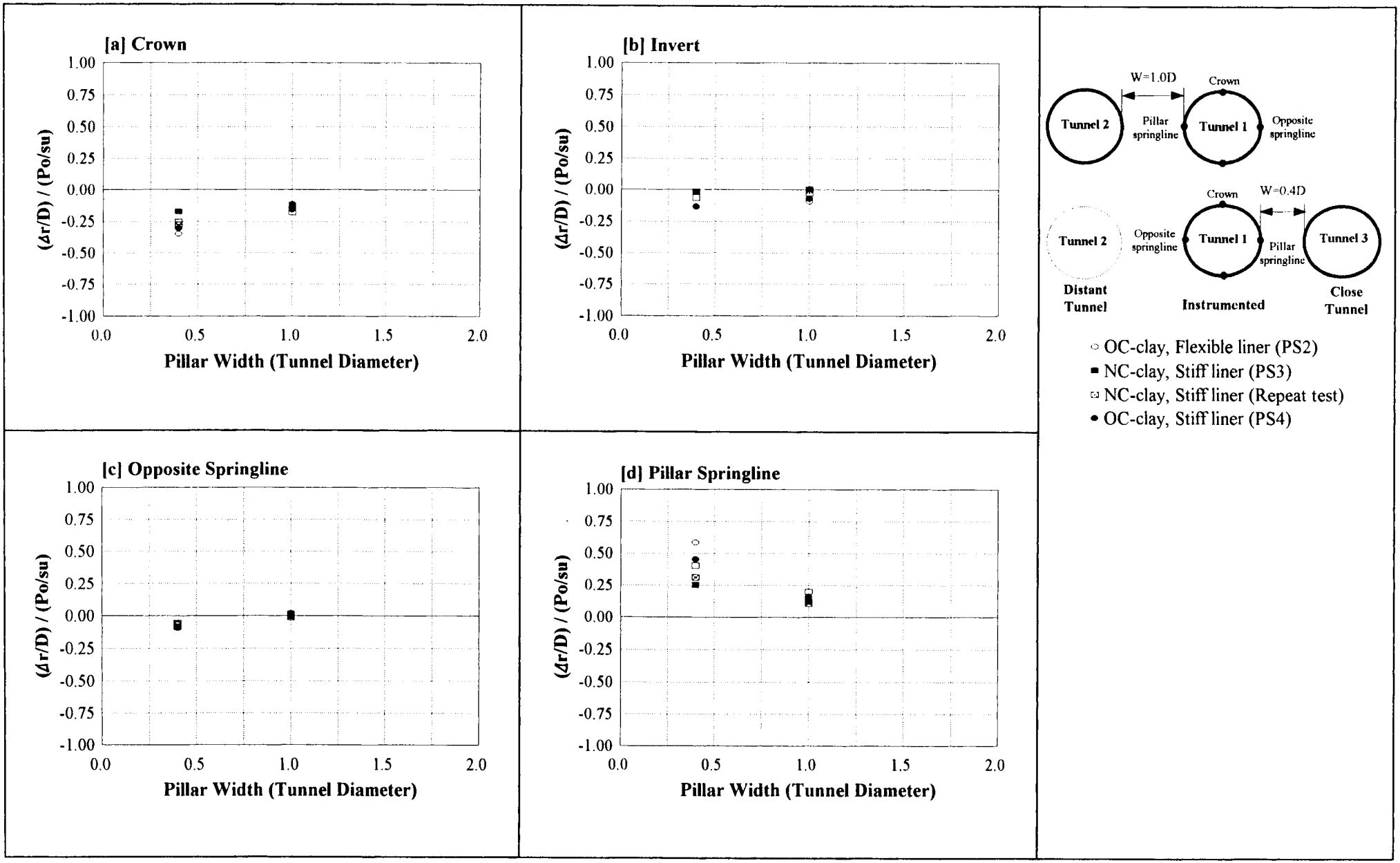


FIGURE 6.8 Normalized Incremental Displacement in Tunnel 1 vs. Pillar Width

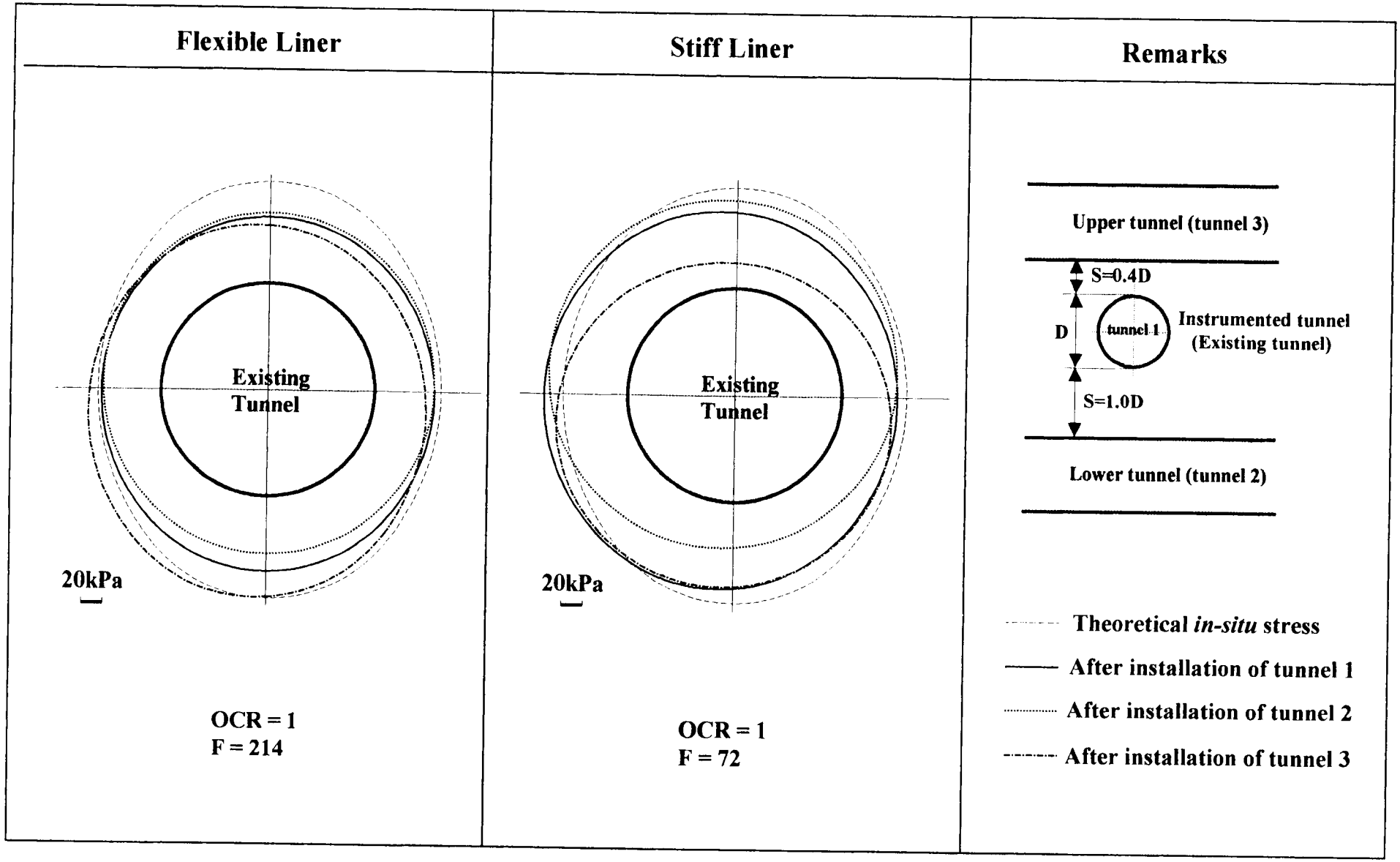


FIGURE 6.9 Stresses Acting on Tunnel 1 (Cylindrical Tank)

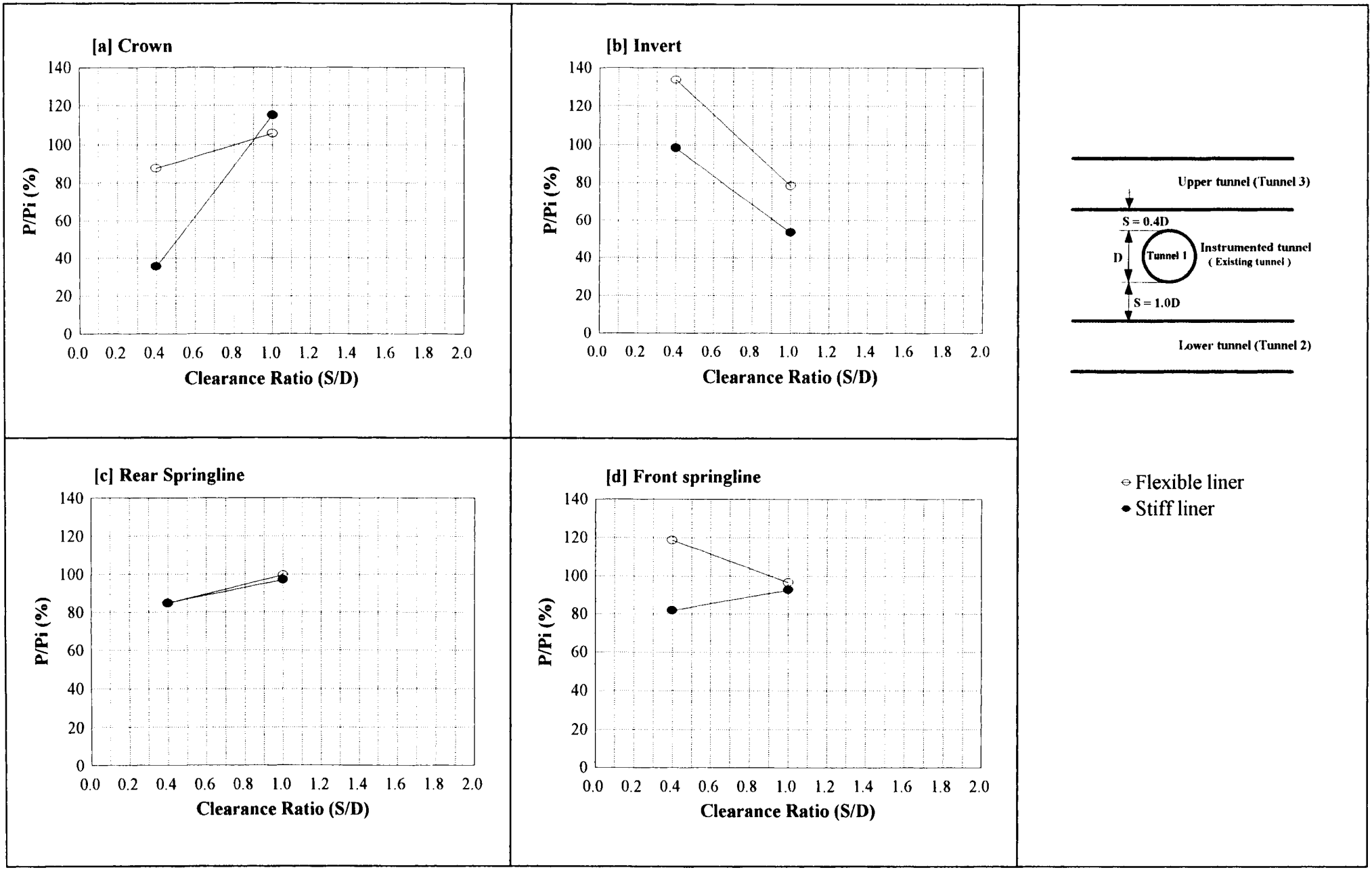


FIGURE 6.10 Normalized Liner Pressure in Tunnel 1 vs. Clearance Ratio (S/D)

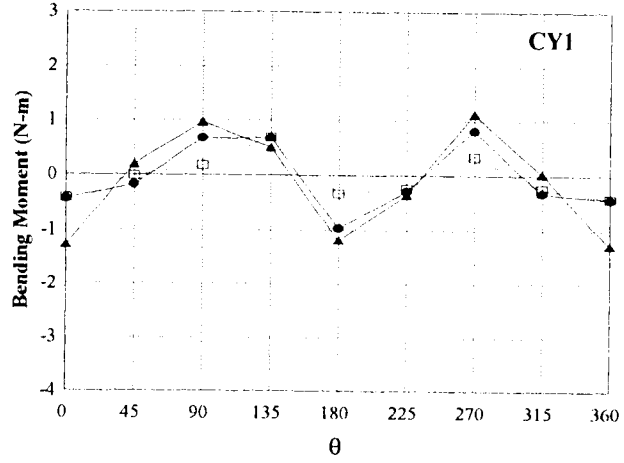
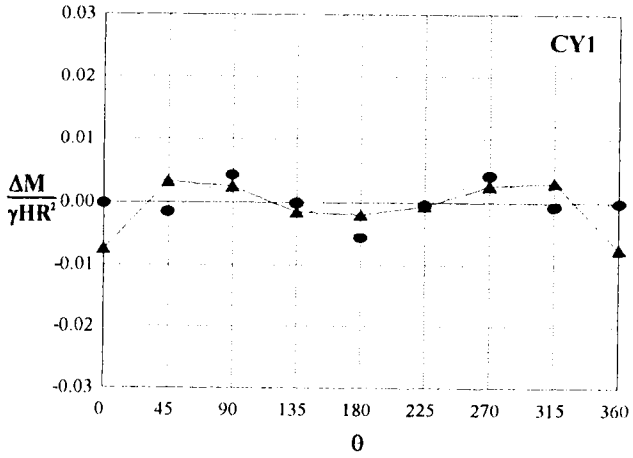
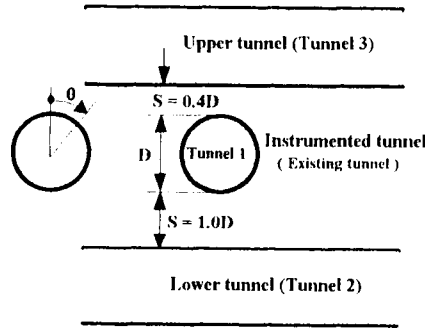
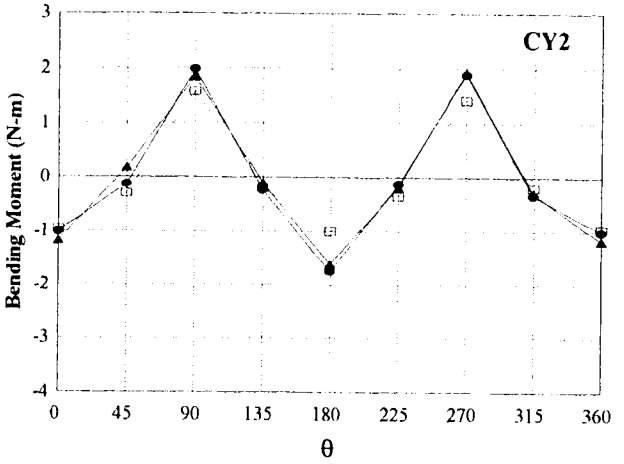
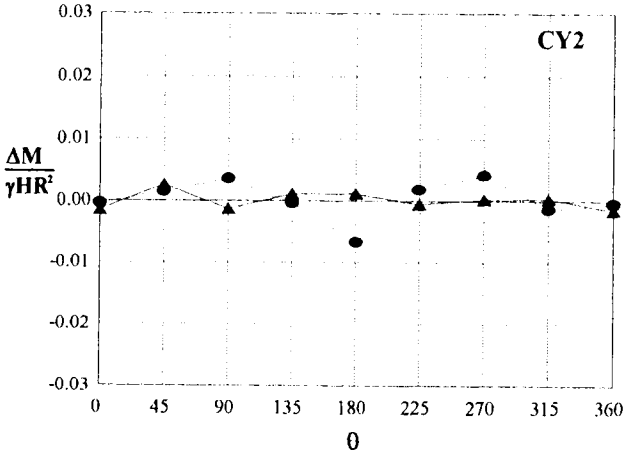
	[a] Bending Moment	[b] Normalized Incremental Bending Moment	Remarks
Flexible Liner			
Stiff Liner			□ After installation of tunnel 1 ● After installation of tunnel 2 ▲ After installation of tunnel 3

FIGURE 6.11 Bending Moment and Normalized Incremental Bending Moment in Tunnel 1

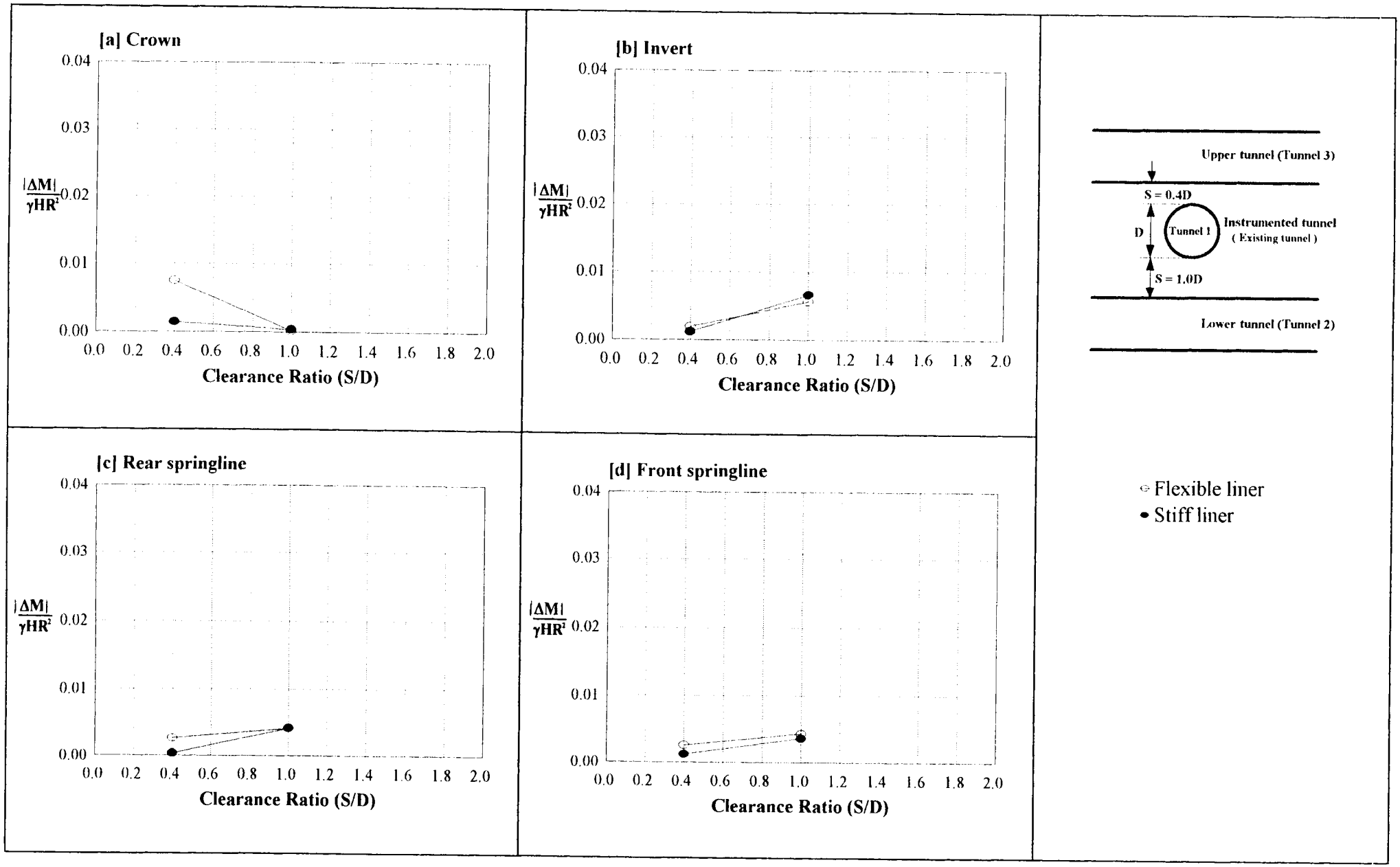


FIGURE 6.12 Normalized Additional Bending Moment in Tunnel 1 vs. Clearance Ratio (S/D)

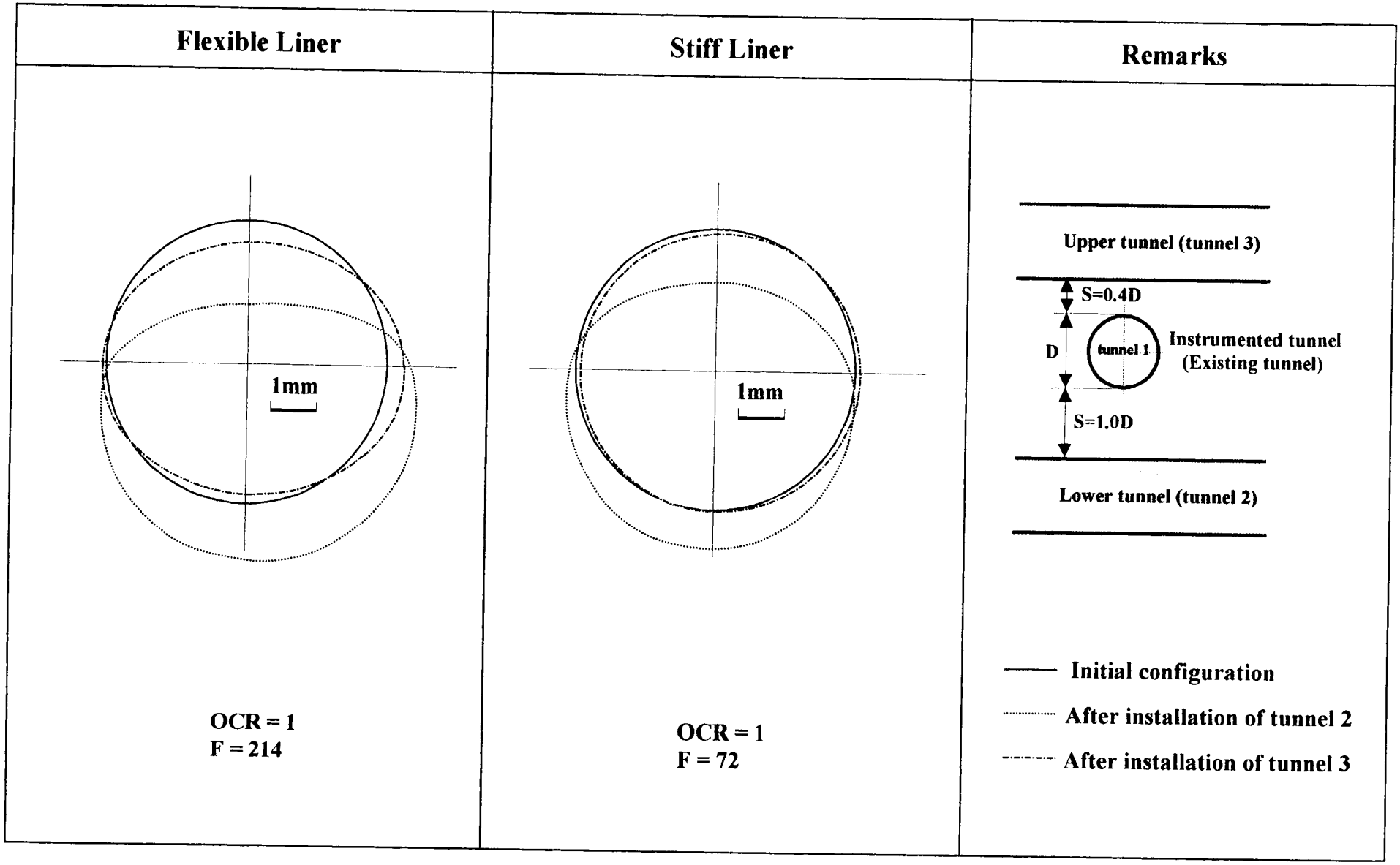


FIGURE 6.13 Distribution of Displacement of Tunnel 1 due to New Tunnel Installation

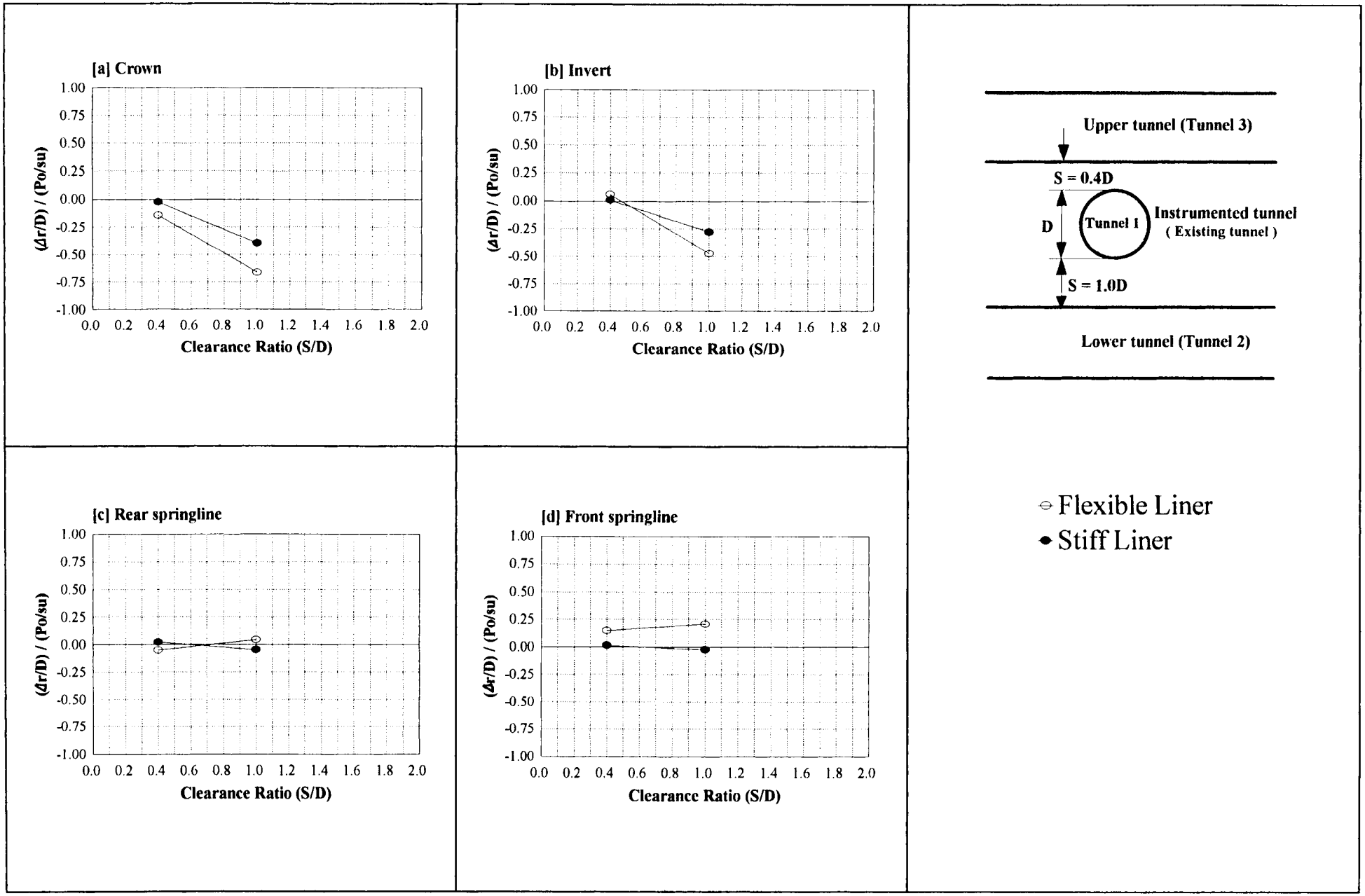


FIGURE 6.14 Normalized Additional Displacement in Tunnel 1 vs. Clearance Ratio (S/D)

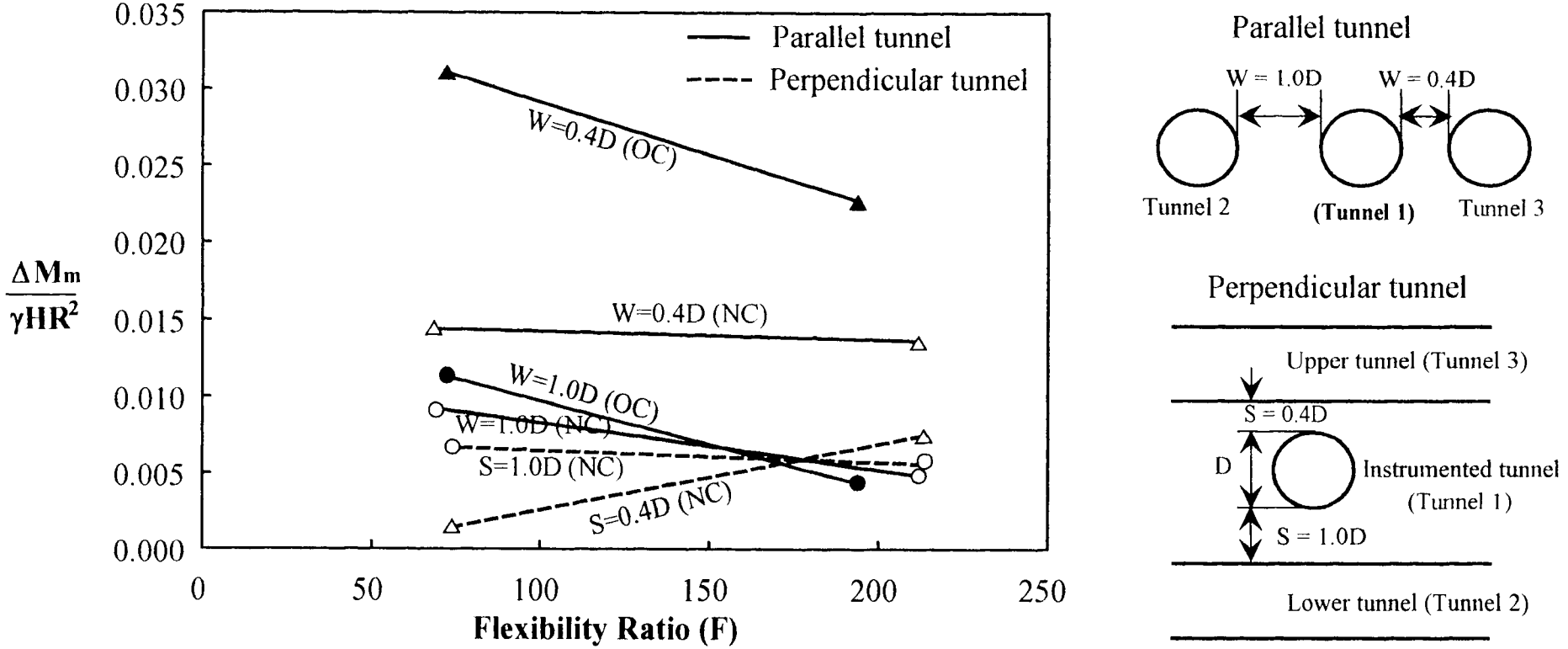


FIGURE 6.15 Comparison between incremental bending moments measured in parallel and perpendicular tests

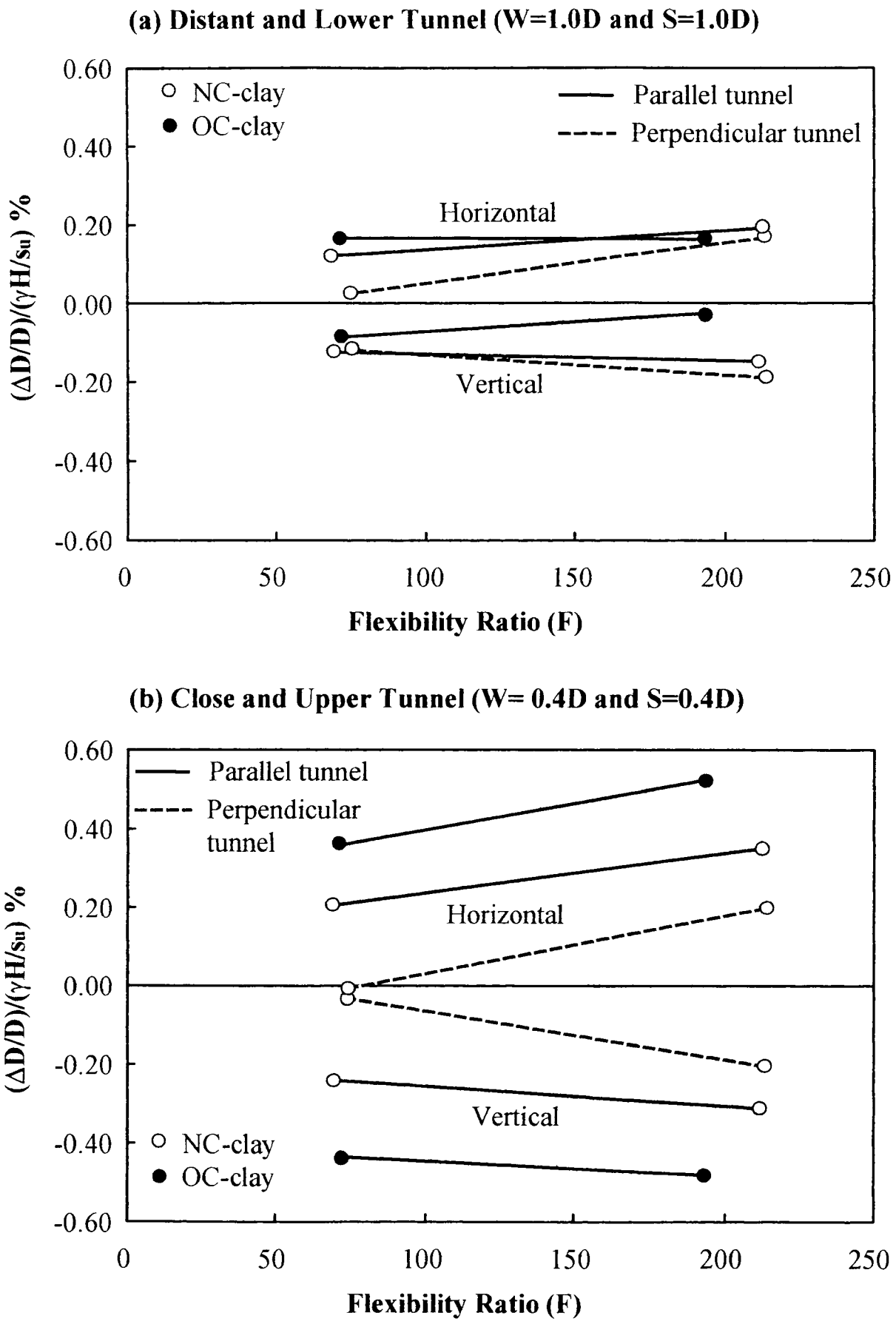
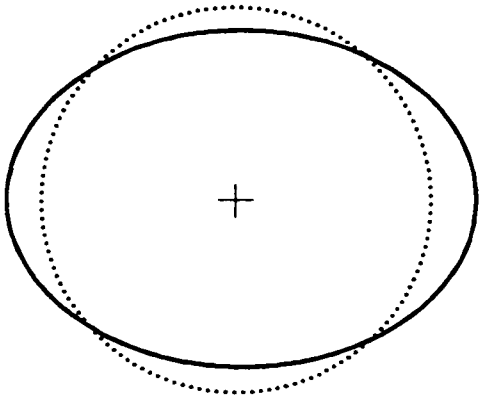
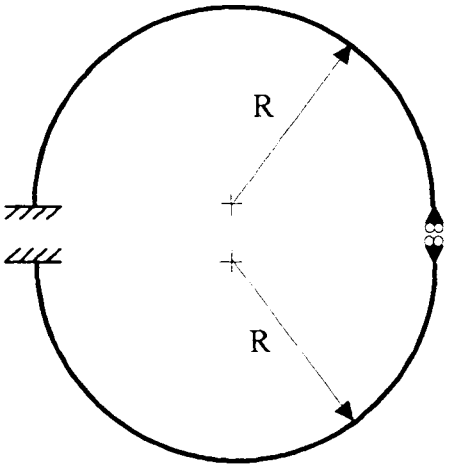


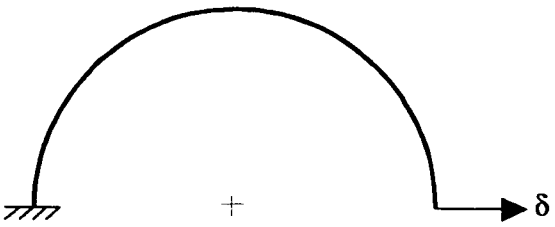
FIGURE 6.16 Comparison between incremental diameter change measured in parallel and perpendicular tests

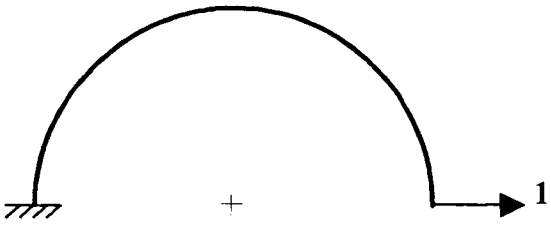


[a] Actual displacements pattern

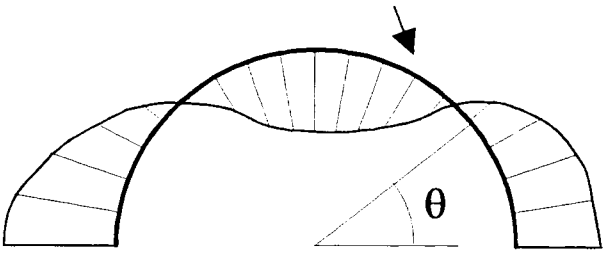


[b] Structure model



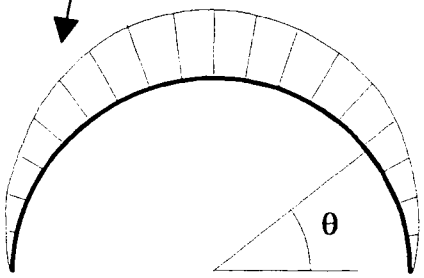


M=M (θ)



[c] Real system

M*= R sin (θ)



[d] Virtual work system

FIGURE 6.17 Summary of Virtual Work Analysis

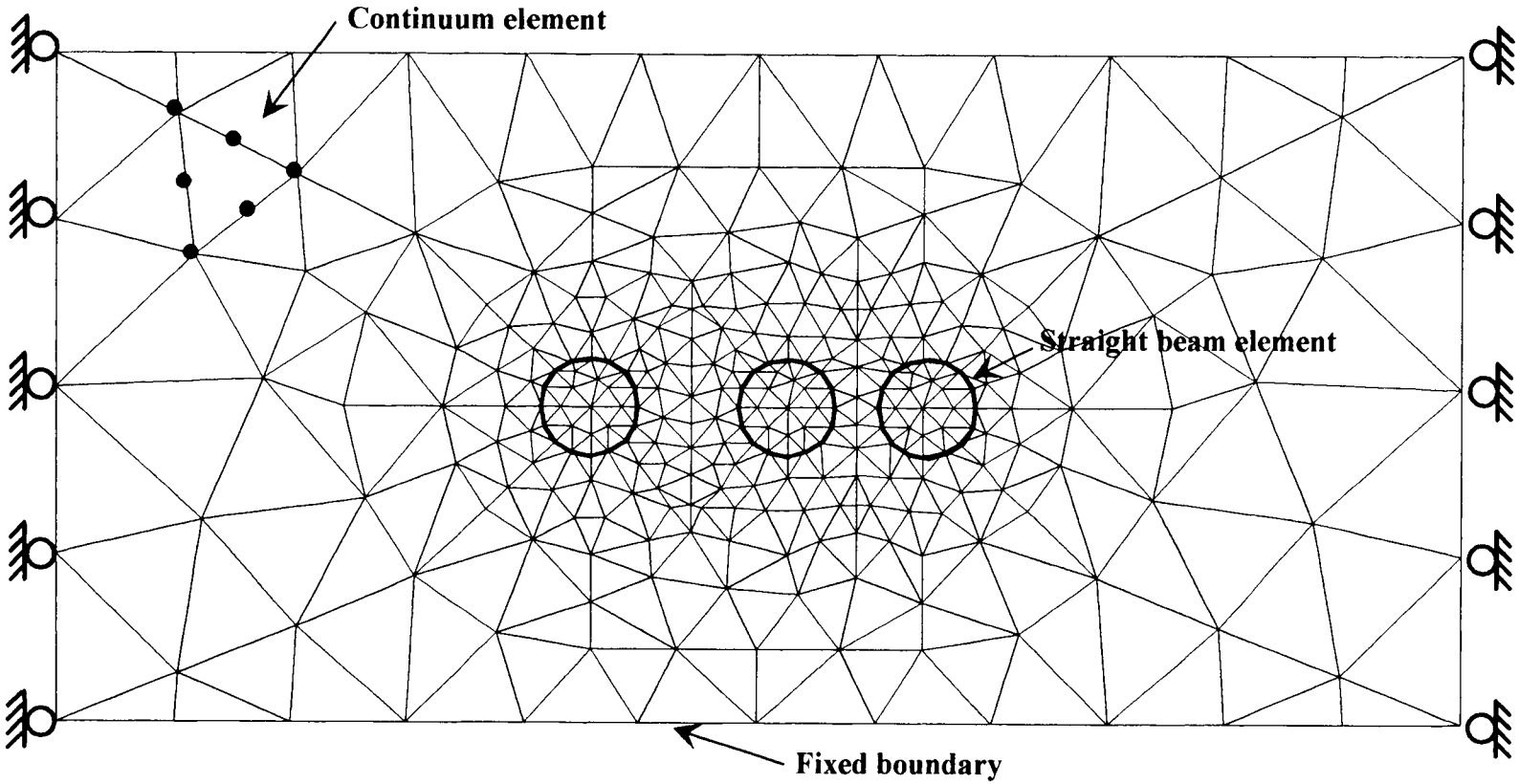


FIGURE 7.1 Finite Element Mesh

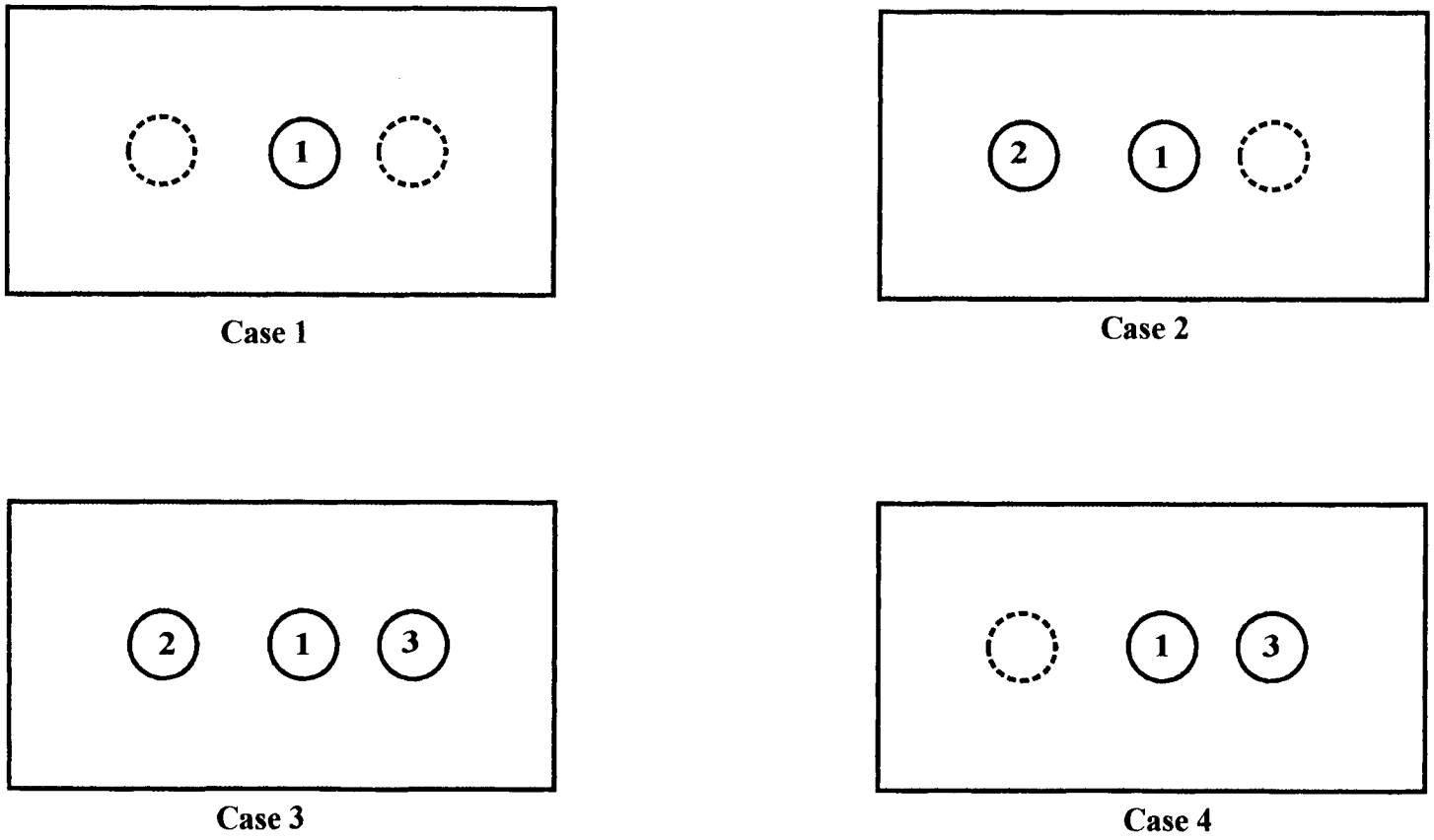


FIGURE 7.2 Numerical Analysis Procedures

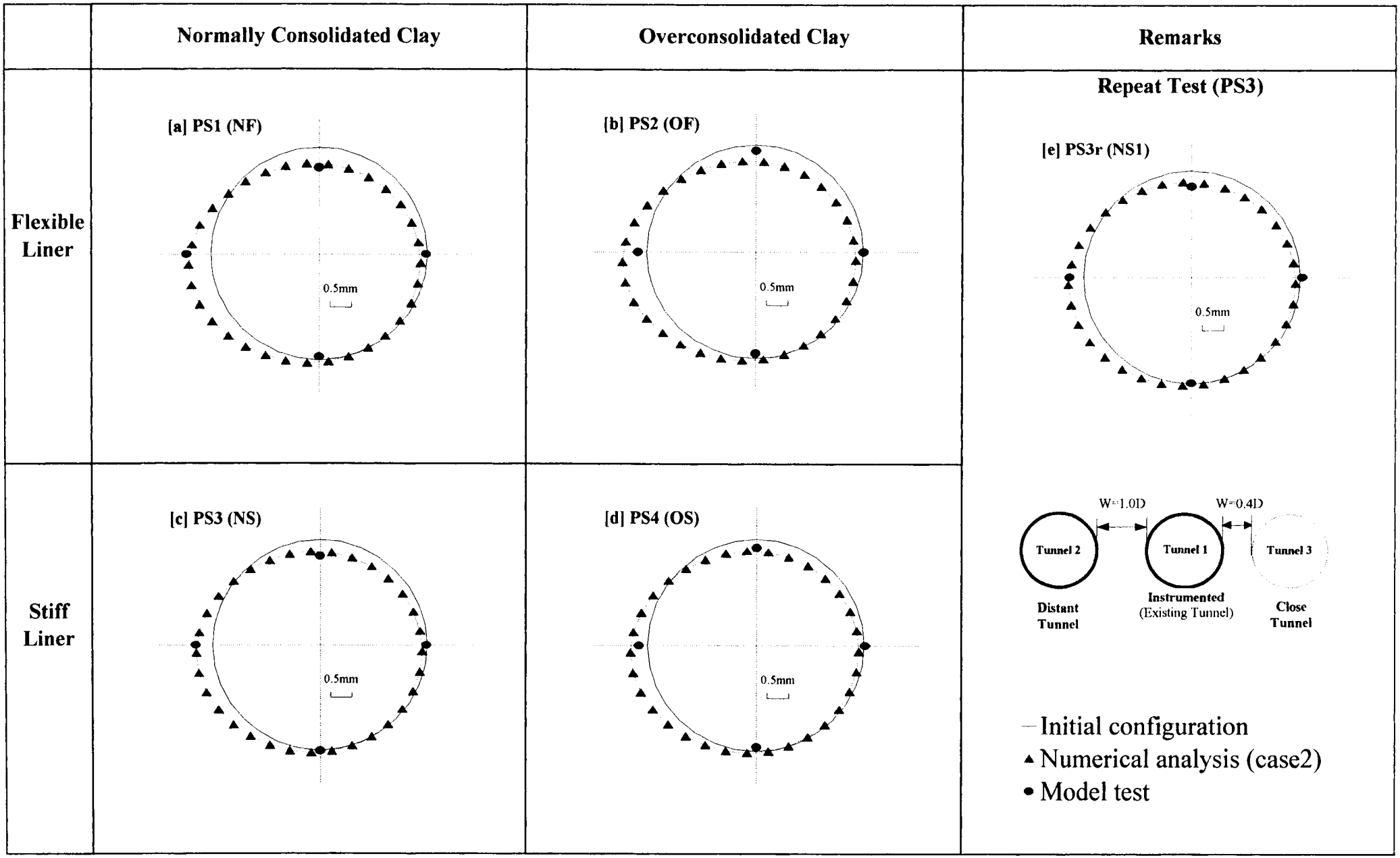


FIGURE 7.3 Incremental Displacements of Tunnel 1 due to Distant Tunnel Installation (W=1.0D)

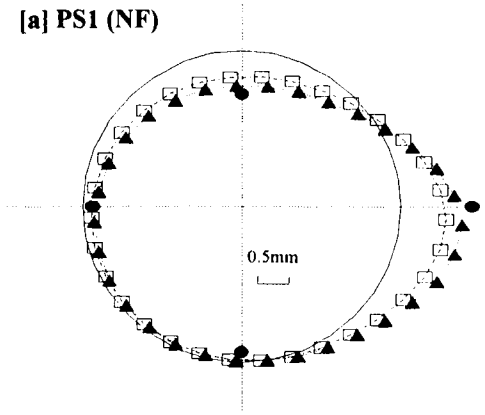
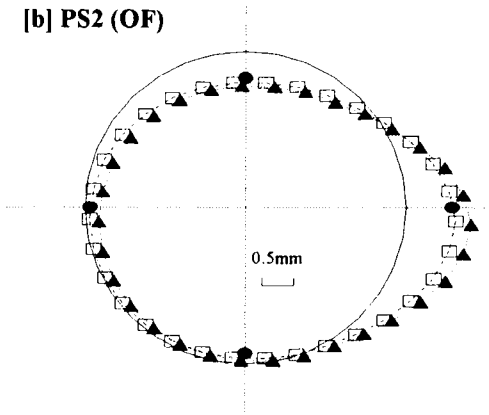
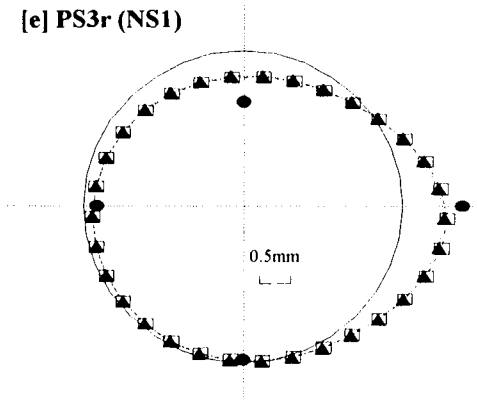
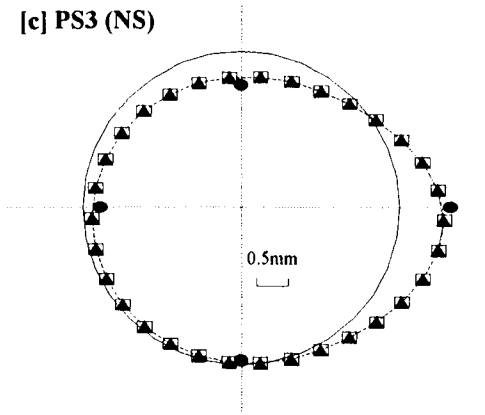
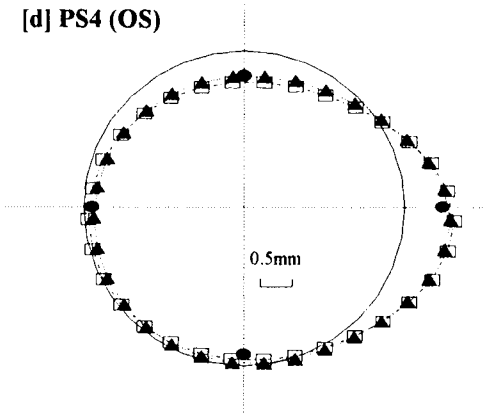
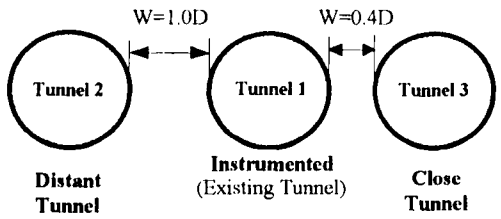
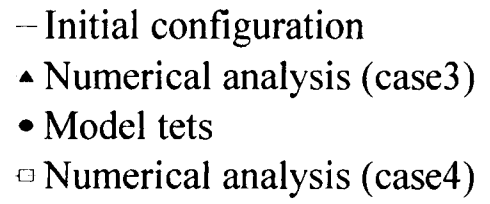
	Normally Consolidated Clay	Overconsolidated Clay	Remarks
Flexible Liner	[a] PS1 (NF) 	[b] PS2 (OF) 	Repeat Test (PS3) 
Stiff Liner	[c] PS3 (NS) 	[d] PS4 (OS) 	 

FIGURE 7.4 Incremental Displacements of Tunnel 1due to Close Tunnel Installation (W=0.4D)

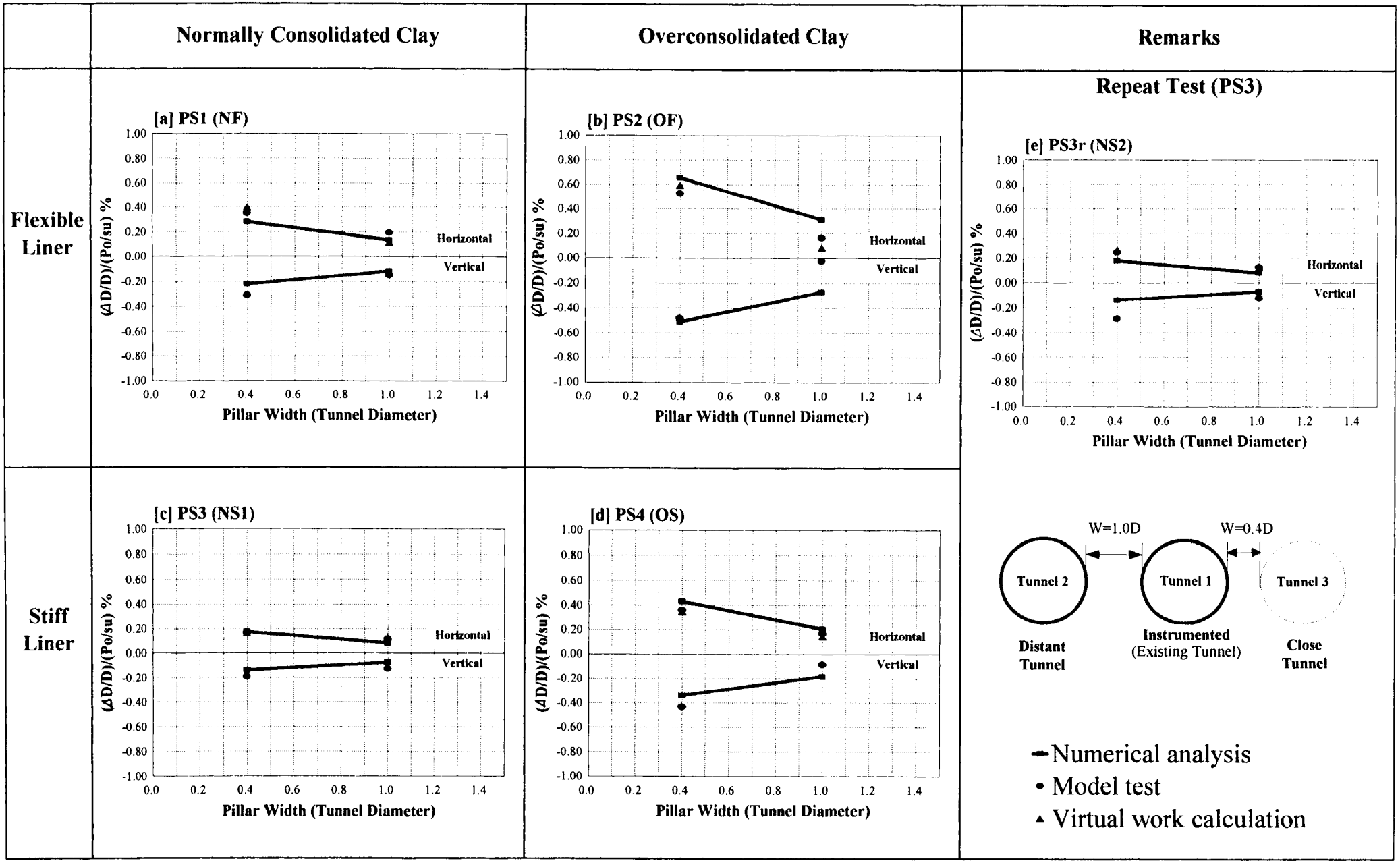


FIGURE 7.5 Comparison of Normalized Diameter Change Between Model Test and Numerical Analysis

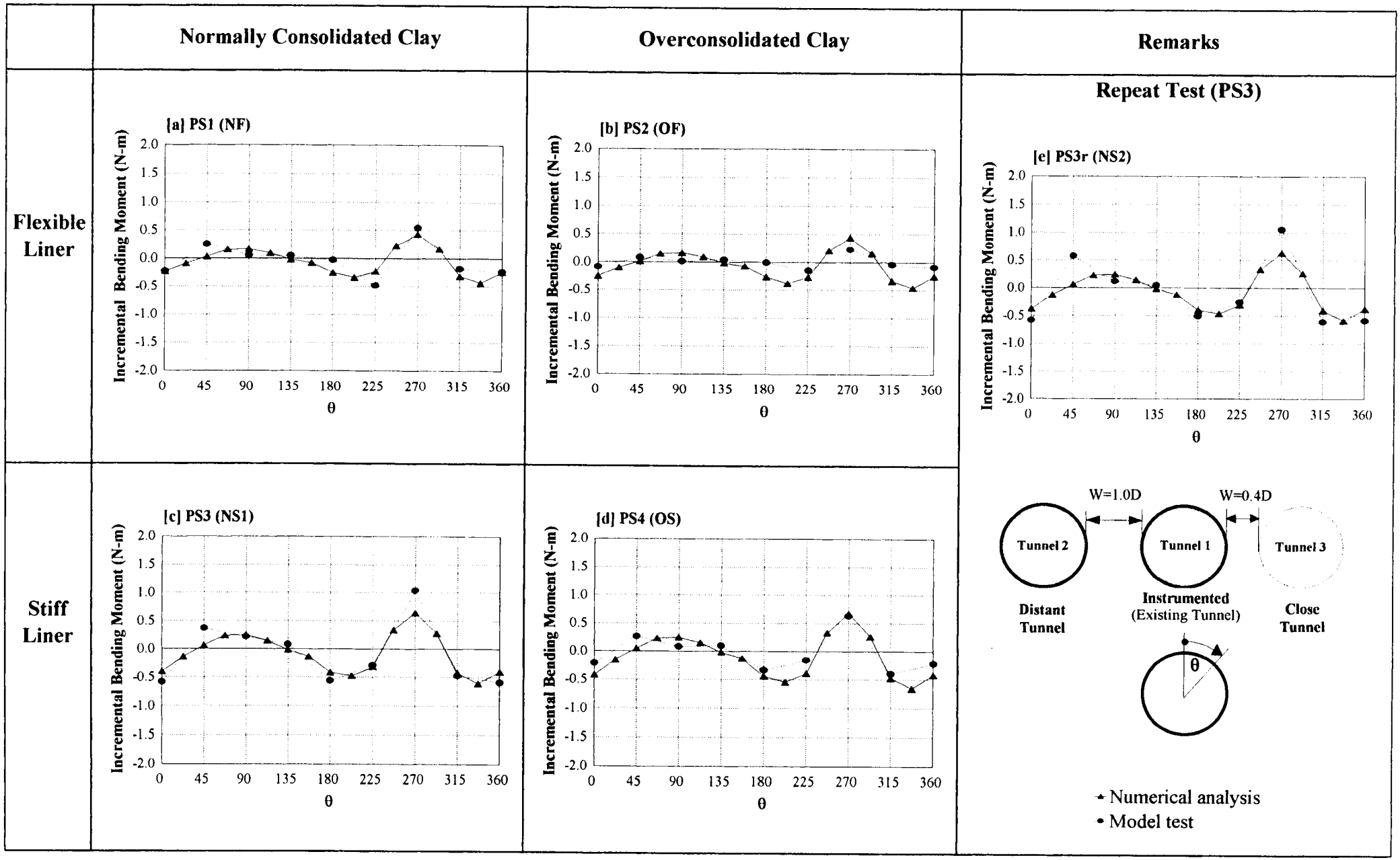


FIGURE 7.6 Incremental Bending Moment on Tunnel 1 due to Installation of Tunnel 2 (W=1.0D)

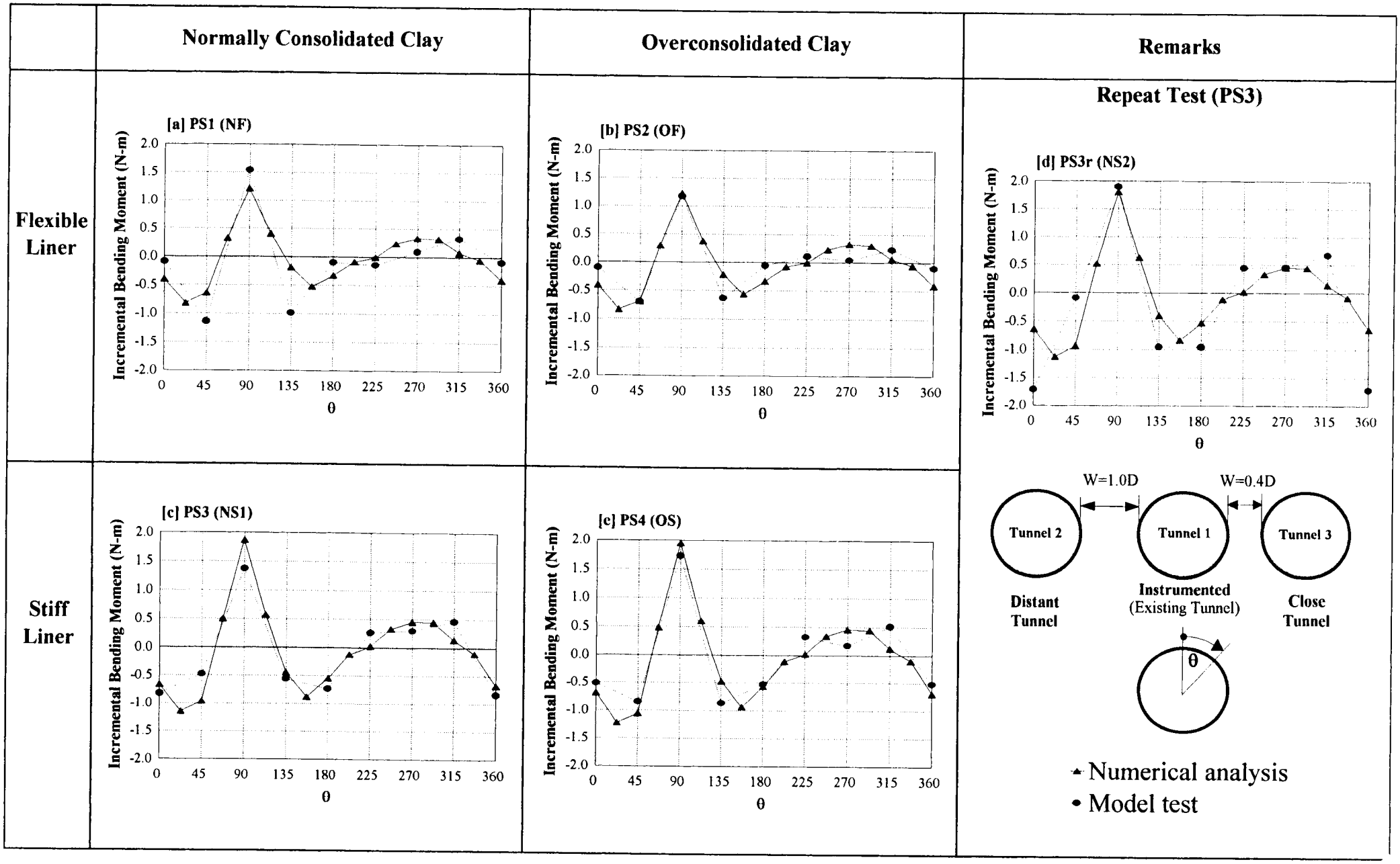


FIGURE 7.7 Incremental Bending Moment on Tunnel 1 due to Installation of Tunnel 2 (W=0.4D)

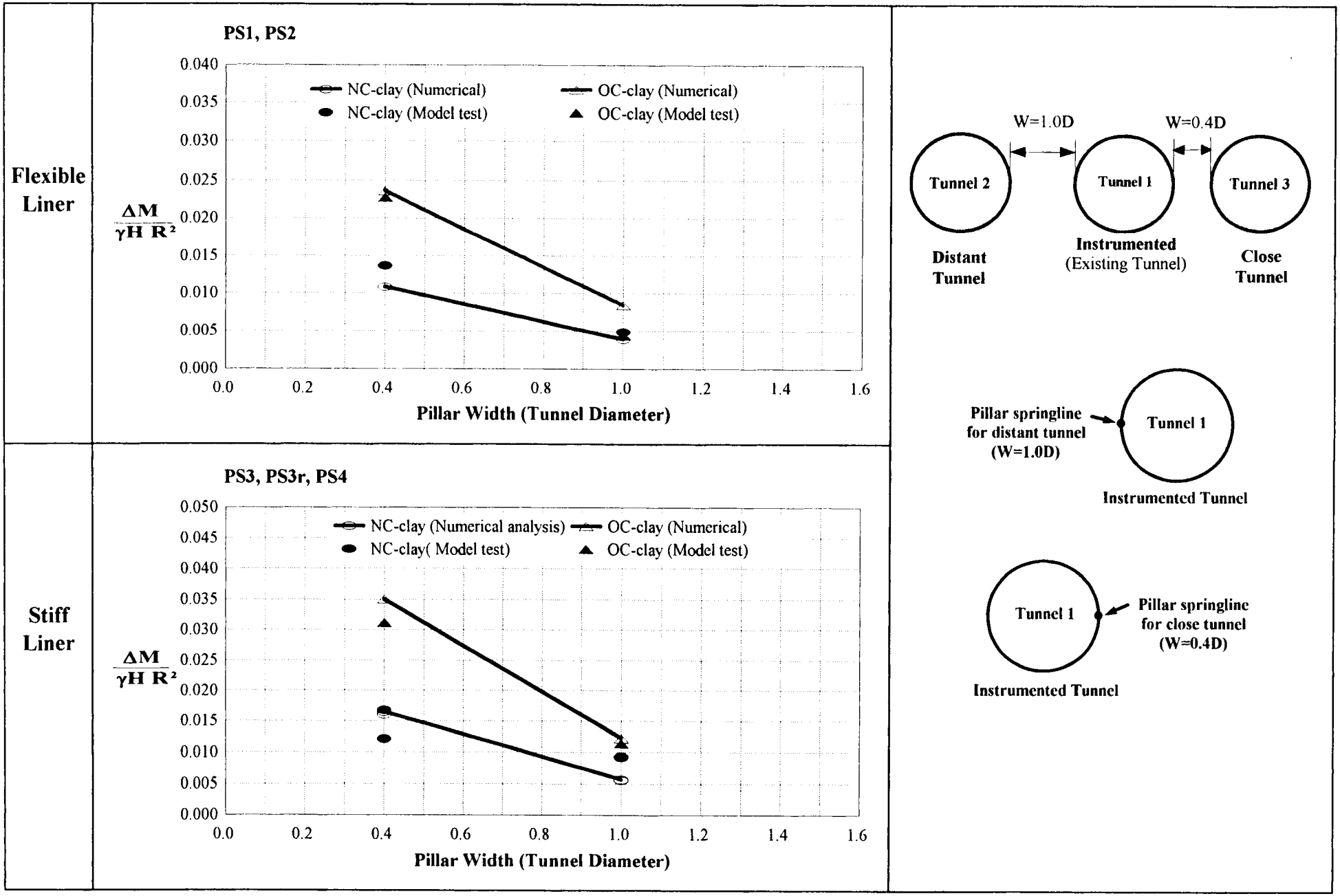
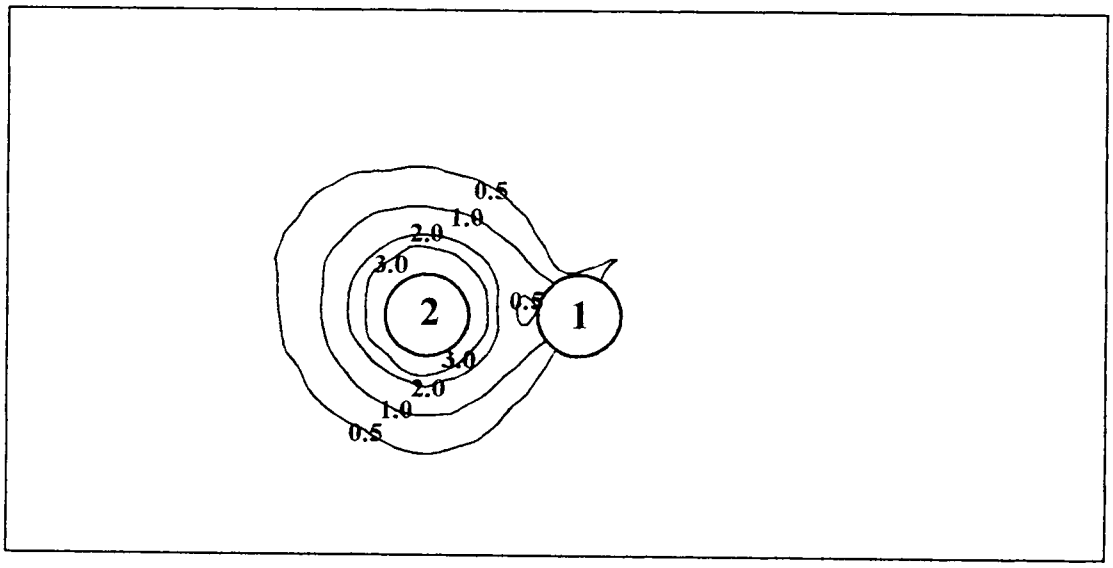


FIGURE 7.8 Normalized Maximum Incremental Bending Moments on Tunnel 1 (at Pillar Springline)

(a) PS1 (NC-clay, Flexible liner)



(b) PS3 (NC-clay, Stiff liner)

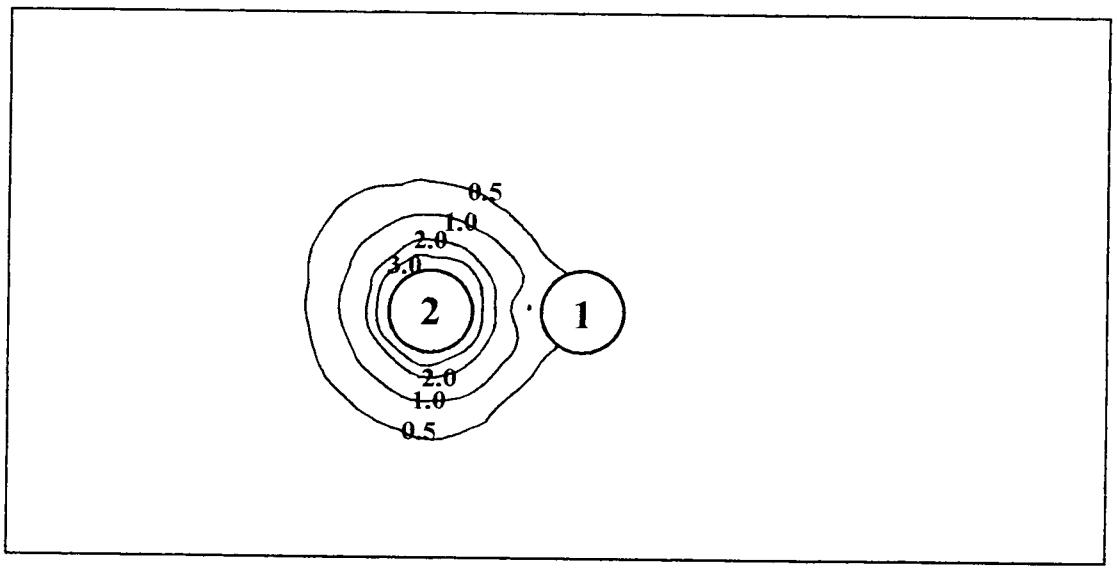


FIGURE 7.9 Incremental Maximum Shear strain (γ_{max} %) after Installation of Tunnels (PS1 and PS3)

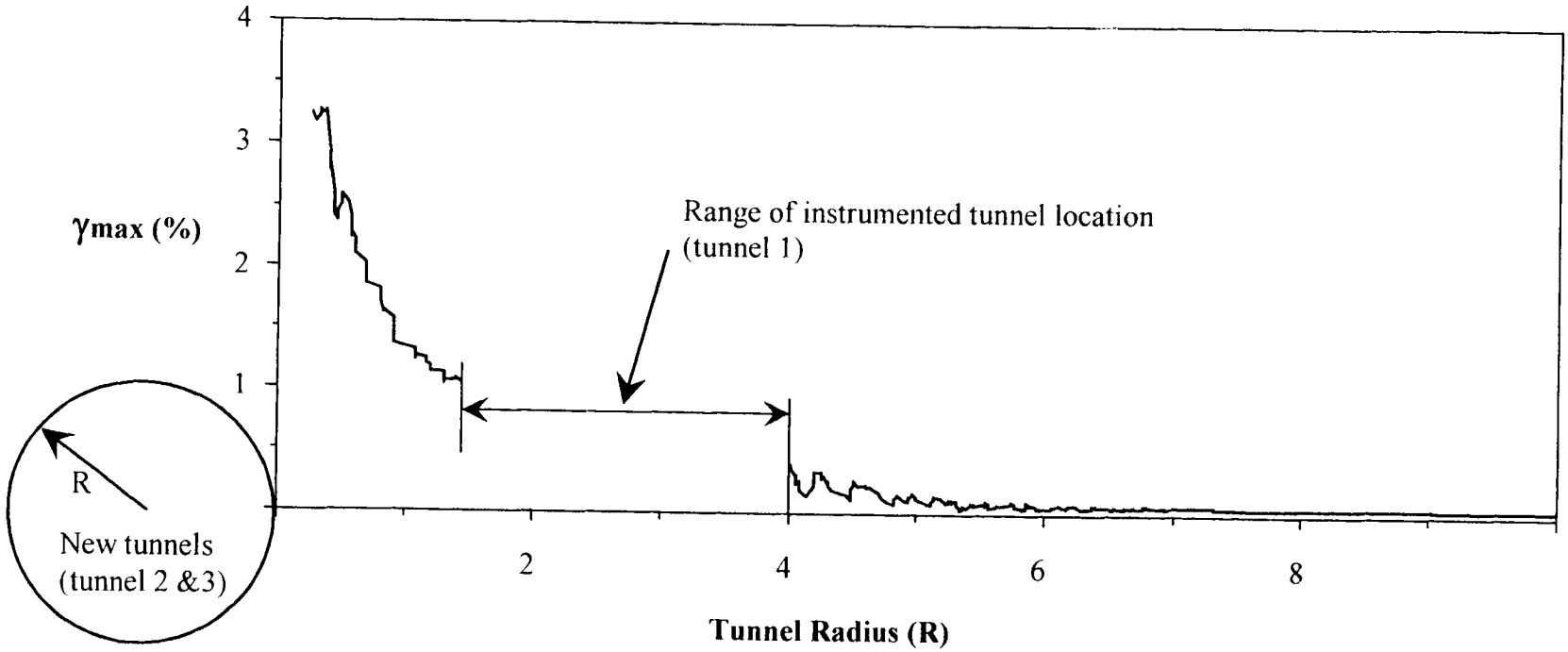


FIGURE 7.10 Averaged Incremantal Maximum Shear Strain against Distance